MOLECULAR AND CELLULAR MECHANISMS OF THE LEGUME-RHIZOBIA SYMBIOSIS

EDITED BY: Jianping Wang, Stig Uggerhøj Andersen and Pascal Ratet
PUBLISHED IN: Frontiers in Plant Science and Frontiers in Microbiology

frontiers Research Topics

frontiers

ISSN 1664-8714
ISBN 978-2-88945-757-1
DOI 10.3389/978-2-88945-757-1

About Frontiers

Frontiers is more than just an open-access publisher of scholarly articles: it is a pioneering approach to the world of academia, radically improving the way scholarly research is managed. The grand vision of Frontiers is a world where all people have an equal opportunity to seek, share and generate knowledge. Frontiers provides immediate and permanent online open access to all its publications, but this alone is not enough to realize our grand goals.

Frontiers Journal Series

The Frontiers Journal Series is a multi-tier and interdisciplinary set of open-access, online journals, promising a paradigm shift from the current review, selection and dissemination processes in academic publishing. All Frontiers journals are driven by researchers for researchers; therefore, they constitute a service to the scholarly community. At the same time, the Frontiers Journal Series operates on a revolutionary invention, the tiered publishing system, initially addressing specific communities of scholars, and gradually climbing up to broader public understanding, thus serving the interests of the lay society, too.

Dedication to Quality

Each Frontiers article is a landmark of the highest quality, thanks to genuinely collaborative interactions between authors and review editors, who include some of the world's best academicians. Research must be certified by peers before entering a stream of knowledge that may eventually reach the public - and shape society; therefore, Frontiers only applies the most rigorous and unbiased reviews.
Frontiers revolutionizes research publishing by freely delivering the most outstanding research, evaluated with no bias from both the academic and social point of view. By applying the most advanced information technologies, Frontiers is catapulting scholarly publishing into a new generation.

What are Frontiers Research Topics?

Frontiers Research Topics are very popular trademarks of the Frontiers Journals Series: they are collections of at least ten articles, all centered on a particular subject. With their unique mix of varied contributions from Original Research to Review Articles, Frontiers Research Topics unify the most influential researchers, the latest key findings and historical advances in a hot research area! Find out more on how to host your own Frontiers Research Topic or contribute to one as an author by contacting the Frontiers Editorial Office: researchtopics@frontiersin.org

MOLECULAR AND CELLULAR MECHANISMS OF THE LEGUME-RHIZOBIA SYMBIOSIS

Topic Editors:
Jianping Wang, University of Florida, United States; HIST, Fujian Agriculture and Forestry University, China
Stig Uggerhøj Andersen, Aarhus University, Denmark
Pascal Ratet, Institute of Plant Sciences Paris-Saclay IPS2, CNRS, INRA, Université Paris-Sud, Université Evry, Université Paris-Saclay, Paris Diderot, Sorbonne Paris-Cité, France

Image: Worachat Tokaew/Shutterstock.com

The legume-rhizobia symbiosis is a remarkable biological phenomena, which is critically important for sustainable agriculture. In the past decades, significant progress has been made to understand the mechanisms of the symbiotic processes. In this eBook, we present the most recent researches focusing on the molecular mechanisms of legume-rhizobia symbiosis including rhizobium characters, plant responses to different types of bacteria, phytohormones involved in the symbiosis, SYM pathway signals, and R genes and specificity of rhizobia infection. This eBook will be a great reference book highlighting the research frontiers in legume-rhizobia symbiosis.

Citation: Wang, J., Andersen, S. U., Ratet, P., eds. (2019). Molecular and Cellular Mechanisms of the Legume-Rhizobia Symbiosis. Lausanne: Frontiers Media. doi: 10.3389/978-2-88945-757-1

Table of Contents

SECTION IV

SYM PATHWAY SIGNALS

SECTION V

R GENES AND SYMBIOTIC SPECIFICITY

frontiers in Plant Science

EDITORIAL
published: 12 December 2018
doi: 10.3389/fpls.2018.01839

Editorial: Molecular and Cellular Mechanisms of the Legume-Rhizobia Symbiosis

Jianping Wang[1,2]*, *Stig Uggerhøj Andersen*[3] and *Pascal Ratet*[4,5]

[1] Key Laboratory of Genetics, Breeding and Multiple Utilization of Crops, Ministry of Education, Fujian Provincial Key Laboratory of Haixia Applied Plant Systems Biology, Center for Genomics and Biotechnology, Fujian Agriculture and Forestry University, Fuzhou, China, [2] Agronomy Department, University of Florida, Gainesville, FL, United States, [3] Department of Molecular Biology and Genetics, Aarhus University, Aarhus, Denmark, [4] Institute of Plant Sciences Paris-Saclay IPS2, CNRS, INRA, Université Paris-Sud, Université Evry, Université Paris-Saclay, Orsay, France, [5] Institute of Plant Sciences Paris-Saclay, Paris Diderot, Sorbonne Paris-Cité, Orsay, France

Keywords: legume, rhizobium, nodule, symbiosis, SYM pathway, biological nitrogen fixation

Editorial on the Research Topic

Molecular and Cellular Mechanisms of the Legume-Rhizobia Symbiosis

Legume-rhizobia symbiosis is a remarkable and mutually beneficial association between higher plants and microbes, which is extremely important for sustainable agriculture and ecology. During this association, biological nitrogen fixation occurs in the nodule, which is a specialized accessory legume organ, generally formed on roots. In mature nodules, rhizobia convert inert atmospheric N_2 into ammonia (NH_3), essential for plant growth. In return, bacteria obtain photosynthetic carbon from the plant. The biologically fixed nitrogen during symbiosis accounts for approximately 65% of nitrogen use in agriculture (Burris and Roberts, 1993).

Due to its agricultural importance and interesting biological features, the legume-rhizobia symbiosis fascinated many researchers in the past decades. It has been discovered that the legume-rhizobia symbiosis is initiated through mutual chemical communication. The plant root releases flavonoids, which induce rhizobia to produce specific lipo-chitooligosaccharides (LCOs), called nodulation factors (Nod factors, or NFs) (Dénarié et al., 1996). These NFs are specifically recognized by the host plant and trigger a sophisticated symbiotic signaling cascade in the host root cells to coordinate rhizobial infection, nodule organogenesis and later on nitrogen fixation (Oldroyd et al., 2011). The main aim of this research topic was to assemble papers addressing and discussing the fundamental science of the molecular mechanisms of legume-rhizobia symbiosis. A total of nine articles were published under this research topic related to rhizobium characters (2), plant response to different type of bacteria (1), phytohormones (3), SYM pathway signals (2), and R genes determining specificity of rhizobia infection (1).

Rhizobia have two lifestyles, a free-living state in soil and a symbiotic state in plant cells when engaged in symbiosis (Gibson et al., 2008). Rhizobia therefore have to adapt to changing conditions outside and inside the host plants. Besides LCOs, a few other bacterial components are important for a successful symbiotic interaction. Lipopolysaccharides (LPSs) are major components of the outer membrane of gram negative bacteria including rhizobia and play a central role in rhizobia infection, in adaptation to the host environment, and in facilitating symbiosis (Lerouge and Vanderleyden, 2002; Raetz and Whitfield, 2002). Busset et al. characterized a cluster of five genes presumably involved in LPS biosynthesis and investigated the specific roles of one gene (*lpxXL*) in *Bradyrhizobium* free-living and symbiotic states.

Some rhizobia can also use a type 3 secretion system (T3SS) to translocate bacterial effector proteins into host cells to trigger and facilitate symbiosis in certain legume species

Edited by:
Andrea Genre,
Università degli Studi di Torino, Italy

Reviewed by:
Beatrice Lace,
University of Freiburg, Germany
Joëlle Fournier,
UMR2594 Plant Interactions Laboratory Microorganisms (LIPM), France

****Correspondence:***
Jianping Wang
wangjp@ufl.edu

Specialty section:
This article was submitted to Plant Microbe Interactions, a section of the journal Frontiers in Plant Science

Received: *14 September 2018*
Accepted: *27 November 2018*
Published: *12 December 2018*

Citation:
Wang J, Andersen SU and Ratet P (2018) Editorial: Molecular and Cellular Mechanisms of the Legume-Rhizobia Symbiosis. Front. Plant Sci. 9:1839. doi: 10.3389/fpls.2018.01839

(Jiménez-Guerrero et al., 2015; Okazaki et al., 2016). Songwattana et al. examined the role of a T3SS present on a *Bradyrhizobium* symbiotic plasmid. The symbiotic performance of a T3SS mutant *Bradyrhizobium* strain was tested on 9 different legume species. In addition, the role of the R3SS in *Bradyrhizobium* endophytic colonization of rice roots was examined. This work confirmed that the T3SS plays significant roles in symbiosis for certain legume species.

Legume plants, when perceiving compatible NFs, respond very rapidly to rhizobial infection at the physiological and molecular levels (Desbrosses and Stougaard, 2011; Oldroyd, 2013). However, how legumes differentiate compatible from incompatible rhizobia or pathogens was not clear. Kelly et al. investigated the transcriptome profiles of *Lotus japonicus* in response to a spectrum of interacting bacteria, including compatible symbiotic *Mesorhizobium loti*, semi-compatible symbiotic *Sinorhizobium fredii*, incompatible symbiotic *Bradyrhizobium elkanii*, and pathogenic *Pseudomonas syringae* and *Ralstonia solanacearum*. This comparative analysis revealed distinct transcriptional responses of the legume plant to different types of bacteria and challenged the concept that an early defense-like response is evoked by compatible rhizobia in *L. japonicus* during the establishment of symbiosis.

Rhizobial infection and organogenesis events during legume-rhizobia symbiosis are tightly coordinated, and defects in the infection process often result in defective nodule organogenesis. The tight coordination with signaling across root layers strongly suggests the involvement of hormonal pathways. The mini review presented by Buhian and Bensmihen summarized how phytohormones, as key regulators of cellular and developmental plasticity in plants, control the symbiosis process, specifically the early symbiotic events involving NFs. New findings illustrating NF and phytohormone signaling crosstalk in controlling symbiosis establishment were summarized and synergized comprehensively in this mini review.

Cytokinins are essential phytohormones for rhizobia infection and nodule development, particularly for initiation of root cortical cell divisions and induction of critical gene expression in the NF-signaling pathway. To further investigate the role of cytokinin in controlling nodule numbers in soybean. Mens et al. evaluated and characterized the *IPT* gene family involved in cytokinin biosynthesis in soybean with respect to gene number, sequences, and expression in response to nodulation and soil nitrogen. The results illustrated the exact function of various *IPT* genes in soybean nodulation and indicated that in general low levels of cytokinins promote nodulation, whereas high levels inhibit it possibly due to toxic effects, and interestingly *IPT* genes may not play a role in the autoregulation of nodulation pathway.

Two different types of nodules, indeterminate and determinate, are generally formed by legumes. The model legume *Medicago truncatula* forms indeterminate nodules (typically elongate and maintaining an apical nodule meristem), while *L. japonicus* forms determinate nodules (typically round with no meristematic activity in mature nodules (Hirsch, 1992). What determines the difference between these two organogenesis programs is largely unknown. The phytohormone auxin is essential for cell divisions in plants and required for both indeterminate or determinate nodule development (Suzaki et al., 2012). Ng and Mathesius carried out a detailed analysis of auxin transport and localization during indeterminate and determinate nodule formation. Their results suggest that auxin response is observed in pericycle, endodermis, and inner cortex cells of the roots of indeterminate nodule-forming species**,** while increased auxin responses in outer cortex cells likely take place during determinate nodule formation. Specifically, the tissue difference correlates nicely with the fact that the initial cell divisions start in pericycle and endodermis in *M. truncatula* (indeterminate nodules) while the first cell divisions leading to determinate nodule formation initiate in the outer cortex for plants with determinate nodules.

Research on the legume-rhizobia symbiosis benefits from the advances of technologies at the cellular and molecular levels. Cellular calcium oscillations are critical for signal transduction. The analysis of Ca^{2+} signaling in different cellular compartments requires tools adapted for monitoring Ca^{2+} dynamics with high spatial and temporal resolution. Kelner et al. demonstrated the successful application of dual color sensors for simultaneously monitoring calcium signal dynamics *in vivo* in single root cell compartments during symbiosis, thus providing a powerful tool to study the signal transduction involving Ca^{2+} signaling.

CCaMK is a calcium/calmodulin-dependent protein kinase localized in the nucleus and plays a critical role downstream of symbiotic calcium spiking. Activated by Ca^{2+} and Ca^{2+}-loaded calmodulin, CCaMK phosphorylates CYCLOPS or IPD3 in *M. truncatula* (Yano et al., 2008). Jauregui et al. demonstrated that mutations in the calmodulin-binding domain of CCaMK alter its calmodulin binding capacity, generating a constitutively activated kinase that confers an altered nodulation phenotype.

Particular rhizobial species or strains normally nodulate only a narrow group of legume species or genotypes (Wang et al., 2012, 2017). Understanding the genetic and molecular basis of this symbiotic specificity is important for developing strategies to improve symbiosis. Through genetic mapping Fan et al. identified a dominant gene in soybeans that restricts nodulation with *S. fredii* USDA193. Further validation indicated that an *Rfg1* allele encoding a member of the Toll-interleukin receptor/nucleotide-binding site/leucine-rich repeat class of plant resistance proteins restricts nodulation by *S. fredii* strains USDA257 and USDA205. In combination with several previous studies, they showed that the *Rfg1* allele likely provided broad-spectrum resistance to nodulation by many *S. fredii* and *B. japonicum* strains in soybean.

AUTHOR CONTRIBUTIONS

JW prepared the first draft of the manuscript. SA and PR revised the draft critically and constructively. All authors reviewed and approved the final draft.

REFERENCES

Burris, R. H., and Roberts, G. (1993). Biological nitrogen fixation. *Annu. Rev. Nutr.* 13, 317–335. doi: 10.1146/annurev.nu.13.070193.001533

Dénarié, J., Debellé, F., and Promé, J. C. (1996). Rhizobium lipo-chitooligosaccharide nodulation factors: signaling molecules mediating recognition and morphogenesis. *Annu. Rev. Biochem.* 65, 503–535.

Desbrosses, G. J., and Stougaard, J. (2011). Root nodulation: a paradigm for how plant-microbe symbiosis influences host developmental pathways. *Cell Host Microbe* 10, 348–358. doi: 10.1016/j.chom.2011.09.005

Gibson, K. E., Kobayashi, H., and Walker, G. C. (2008). Molecular determinants of a symbiotic chronic infection. *Annu. Rev. Genet.* 42, 413–441. doi: 10.1146/annurev.genet.42.110807.091427

Hirsch, A. M. (1992). Developmental biology of legume nodulation. *New Phytol.* 122, 211–237. doi: 10.1111/j.1469-8137.1992.tb04227.x

Jiménez-Guerrero, I., Pérez-Montaño, F., Monreal, J. A., Preston, G. M., Fones, H., Vioque, B., et al. (2015). The *Sinorhizobium (Ensifer) fredii* HH103 Type 3 secretion system suppresses early defense responses to effectively nodulate soybean. *Mol. Plant Microbe Interact.* 28, 790–799. doi: 10.1094/MPMI-01-15-0020-R

Lerouge, I., and Vanderleyden, J. (2002). O-antigen structural variation: mechanisms and possible roles in animal/plant-microbe interactions. *FEMS Microbiol. Rev.* 26, 17–47. doi: 10.1111/j.1574-6976.2002.tb00597.x

Okazaki, S., Tittabutr, P., Teulet, A., Thouin, J., Fardoux, J., Chaintreuil, C., et al. (2016). *Rhizobium*-legume symbiosis in the absence of Nod factors: two possible scenarios with or without the T3SS. *ISME J.* 1, 64–74. doi: 10.1038/ismej.2015.103

Oldroyd, G. E. (2013). Speak, friend, and enter: signalling systems that promote beneficial symbiotic associations in plants. *Nat. Rev. Microbiol.* 11, 252–263. doi: 10.1038/nrmicro2990

Oldroyd, G. E., Murray, J. D., Poole, P. S., and Downie, J. A. (2011). The rules of engagement in the legume-rhizobial symbiosis. *Annu. Rev. Genet.* 45, 119–144. doi: 10.1146/annurev-genet-110410-132549

Raetz, C. R., and Whitfield, C. (2002). Lipopolysaccharide endotoxins. *Annu. Rev. Biochem.* 71, 635–700. doi: 10.1146/annurev.biochem.71.110601.135414

Suzaki, T., Yano, K., Ito, M., Umehara, Y., Suganuma, N., and Kawaguchi, M. (2012). Positive and negative regulation of cortical cell division during root nodule development in *Lotus japonicus* is accompanied by auxin response. *Development* 139, 3997–4006. doi: 10.1242/dev.084079

Wang, D., Yang, S., Tang, F., and Zhu, H. (2012). Symbiosis specificity in the legume-rhizobial mutualism. *Cell Microbiol.* 14, 334–342. doi: 10.1111/j.1462-5822.2011.01736.x

Wang, Q., Yang, S., Liu, J., Terecskei, K., Ábrahám, E., Gombár, A., et al. (2017). Host-secreted antimicrobial peptide enforces symbiotic selectivity in *Medicago truncatula*. *Proc. Natl. Acad. Sci. U.S.A.* 114, 6854–6859. doi: 10.1073/pnas.1700715114

Yano, K., Yoshida, S., Müller, J., Singh, S., Banba, M., Vickers, K., et al. (2008). CYCLOPS, a mediator of symbiotic intracellular accommodation. *Proc. Natl. Acad. Sci. U.S.A.* 105, 20540–20545. doi: 10.1073/pnas.0806858105

Conflict of Interest Statement: The authors declare that the research was conducted in the absence of any commercial or financial relationships that could be construed as a potential conflict of interest.

frontiers in Microbiology

ORIGINAL RESEARCH
published: 21 September 2017
doi: 10.3389/fmicb.2017.01821

The Very Long Chain Fatty Acid (C_{26}:25OH) Linked to the Lipid A Is Important for the Fitness of the Photosynthetic *Bradyrhizobium* Strain ORS278 and the Establishment of a Successful Symbiosis with *Aeschynomene* Legumes

*Nicolas Busset[1], Flaviana Di Lorenzo[2], Angelo Palmigiano[3], Luisa Sturiale[3], Frederic Gressent[1], Joël Fardoux[1], Djamel Gully[1], Clémence Chaintreuil[1], Antonio Molinaro[2], Alba Silipo[2] and Eric Giraud[1]**

[1] Institut de Recherche pour le Développement, LSTM, UMR IRD, SupAgro, INRA, Université de Montpellier, CIRAD, Montpellier, France, [2] Dipartimento di Scienze Chimiche, Complesso Universitario Monte Sant'Angelo, Università di Napoli Federico II, Naples, Italy, [3] Istituto per i Polimeri, Compositi e Biomateriali IPCB, Consiglio Nazionale delle Ricerche, Catania, Italy

OPEN ACCESS

Edited by:
Pascal Ratet,
Centre National de la Recherche Scientifique (CNRS), France

Reviewed by:
Christian Staehelin,
Sun Yat-sen University, China
Oswaldo Valdes-Lopez,
National Autonomous University of Mexico, Mexico

***Correspondence:**
Eric Giraud
eric.giraud@ird.fr

Specialty section:
This article was submitted to Plant Microbe Interactions, a section of the journal Frontiers in Microbiology

Received: 07 June 2017
Accepted: 06 September 2017
Published: 21 September 2017

Citation:
Busset N, Di Lorenzo F, Palmigiano A, Sturiale L, Gressent F, Fardoux J, Gully D, Chaintreuil C, Molinaro A, Silipo A and Giraud E (2017) The Very Long Chain Fatty Acid (C_{26}:25OH) Linked to the Lipid A Is Important for the Fitness of the Photosynthetic Bradyrhizobium Strain ORS278 and the Establishment of a Successful Symbiosis with Aeschynomene Legumes. Front. Microbiol. 8:1821. doi: 10.3389/fmicb.2017.01821

In rhizobium strains, the lipid A is modified by the addition of a very long-chain fatty acid (VLCFA) shown to play an important role in rigidification of the outer membrane, thereby facilitating their dual life cycle, outside and inside the plant. In *Bradyrhizobium* strains, the lipid A is more complex with the presence of at least two VLCFAs, one covalently linked to a hopanoid molecule, but the importance of these modifications is not well-understood. In this study, we identified a cluster of VLCFA genes in the photosynthetic *Bradyrhizobium* strain ORS278, which nodulates *Aeschynomene* plants in a Nod factor-independent process. We tried to mutate the different genes of the VLCFA gene cluster to prevent the synthesis of the VLCFAs, but only one mutant in the *lpxXL* gene encoding an acyltransferase was obtained. Structural analysis of the lipid A showed that LpxXL is involved in the transfer of the C_{26}:25OH VLCFA to the lipid A but not in the one of the C30:29OH VLCFA which harbors the hopanoid molecule. Despite maintaining the second VLCFA, the ability of the mutant to cope with various stresses (low pH, high temperature, high osmolarity, and antimicrobial peptides) and to establish an efficient nitrogen-fixing symbiosis was drastically reduced. In parallel, we investigated whether the BRADO0045 gene, which encodes a putative acyltransferase displaying a weak identity with the apo-lipoprotein *N*-acyltransferase Lnt, could be involved in the transfer of the C_{30}:29OH VLCFA to the lipid A. Although the mutant exhibited phenotypes similar to the *lpxXL* mutant, no difference in the lipid A structure was observed from that in the wild-type strain, indicating that this gene is not involved in the modification of lipid A. Our results advance our knowledge of the biosynthesis pathway and the role of VLCFAs-modified lipid A in free-living and symbiotic states of *Bradyrhizobium* strains.

Keywords: VLCFA, lipid A, *Bradyrhizobium*, acyltransferase, symbiosis, *Aeschynomene*

INTRODUCTION

Rhizobia are Gram-negative bacteria with two life styles, one in a free-living state in the soil where they have to cope with changing environmental conditions (hydric, acid, saline stresses, nutrient starvation, etc.) and the other in symbiosis with plants, inside an organ called a nodule, in which they reduce atmospheric nitrogen to ammonium for the benefit of the host plant. A simplistic view would be that inside the nodule, the bacteria benefit from a safe ecological niche with unlimited carbon and energy provided by the plant in exchange for ammonium. In fact, inside the host cells, bacteria also encounter stressful conditions imposed by the plant (low oxygen tension, low pH, hyperosmosis, and various oxidative stresses) (Gibson et al., 2008; Haag et al., 2013). In addition, in some host species, including in inverted repeat-lacking clade (IRLC) legumes or the *Aeschynomene* species, the bacteria have to cope with antimicrobial peptides called NCR, that are used by plants to control bacterial metabolism and can led to a marked change in the shape of the bacteria (Van de Velde et al., 2010; Czernic et al., 2015; Montiel et al., 2017; Wang et al., 2017). The life of the rhizobia therefore does not resemble that of a long peaceful river since they have to adapt to changing stressful conditions outside and inside the host plants.

The first barrier used by the bacteria against biotic and abiotic stresses is its outer membrane (OM). Lipopolysaccharides (LPSs) are major components of the OM of Gram-negative bacteria. These compounds have three components (i) the O-antigen side chain that is in direct contact with the host plant, (ii) the core oligosaccharide, and (iii) a glycolipid moiety named the lipid A that anchors the LPS to the OM. LPSs are known to play a central role in bacterial invasion and adaptation to the host environment (Lerouge and Vanderleyden, 2002; Raetz and Whitfield, 2002). The variability of the O-antigen region observed in most rhizobia species is assumed to be a strategy to modulate or suppress plant defense responses, thereby facilitating the establishment of the symbiosis (Kannenberg and Carlson, 2001; Gourion et al., 2015). In addition, the lipid A of rhizobia LPSs is characterized by the presence of a C_{26} to C_{30} very long-chain fatty acid (VLCFA) (Bhat et al., 1994; Raetz et al., 2007). A lipid A-linked VLCFA is also encountered in pathogenic or intracellular bacteria such as *Brucella* or *Legionella*, suggesting that this structure promotes intracellular life by increasing the stability of the membrane (Bhat et al., 1991; Zähringer et al., 1995; Lerouge and Vanderleyden, 2002; Becker et al., 2005). The biosynthesis of the VLCFA and its addition to the lipid A require a cluster of five genes found in all the bacteria that synthesize a VLCFA-modified lipid A (Ardissone et al., 2011). This region is composed of genes encoding an acyl carrier protein (*acpXL*), fatty acid elongation proteins (*fabF1XL* and *fabF2XL*), a beta-hydroxyacyl-acyl carrier protein (ACP) dehydratase (*fabZXL*) and an acyltransferase (*lpxXL*) (Ardissone et al., 2011; Brown et al., 2011).

Analysis of *acpXL* and *lpxXL* mutants of *Rhizobium leguminosarum* and *Sinorhizobium meliloti* showed that the VLCFA plays a major role in the resistance to various abiotic stresses (high osmolarity, detergents, and dessication) but also in the establishment of a functional symbiosis (Ferguson et al., 2005; Haag et al., 2009; Ardissone et al., 2011; Bourassa et al., 2017). The plants inoculated with the VLCFA mutants are less efficient than the WT to fix nitrogen and present a nodulation delay. In addition, the nodules elicited by the VLCFA mutants present various alterations such as a white color, a smaller size, a disorganization of the infected zone and an early senescence. Furthermore, some bacteroids of the VLCFA mutants strains are abnormally large and have aberrant forms indicating also an alteration of the bacteroid differentiation process (Ferguson et al., 2005; Haag et al., 2009; Ardissone et al., 2011; Bourassa et al., 2017). Interestingly, while mutations in *acpXL* and *lpxXL* completely abolished VLCFA attachment to lipid A, it is observed that the *acpXL* mutants of *R. leguminosarum* and *S. meliloti* are able to substitute the VLCFA with a C16:0 or C18:0; which is not the case for *lpxXL* mutants (Ferguson et al., 2005; Bourassa et al., 2017). This suggests that in the absence of AcpXL, LpxXL could transfer shorter chain to the lipid A.

The OM of *Bradyrhizobium* strains has several peculiarities. First, unlike other rhizobia, hopanoid molecules are present in the membranes of all the *Bradyrhizobium* strains analyzed (Kannenberg et al., 1996). This family of compounds displays structural and functional similarities with eukaryotic sterols, such as cholesterol, and form an important class of membrane lipids that are widely distributed in diverse bacteria that reinforce the rigidity and stability of the OM (Ourisson et al., 1987; Kannenberg et al., 1996; Welander et al., 2009; Saenz et al., 2012). Second, structural analysis of the lipid A in various *Bradyrhizobium* strains revealed the occurrence of up to four VLCFAs that differ in their length and decoration (Choma and Komaniecka, 2011). Third, it has been reported that a hopanoid molecule can be covalently linked to the VLCFA(s) of the lipid A (**Figure 1**); this unusual lipid A structure was described for the first time in the photosynthetic *Bradyrhizobium* BTAi1 strain, named HoLA for Hopanoid-Lipid-A (Komaniecka et al., 2014; Silipo et al., 2014). Two recent studies reported that hopanoids play an important role in *Bradyrhizobium* strains by helping them to cope with various stresses in their two life styles (Silipo et al., 2014; Kulkarni et al., 2015). A hopanoid deficient mutant of the photosynthetic *Bradyrhizobium* BTAi1 strain, lacking a squalene hopene cyclase (Δ*shc*), displays increased sensitivity to stressful conditions and is unable to maintain chronic intracellular infection in *Aeschynomene* species (Silipo et al., 2014). Similarly, *hpnP* and *hpnH* mutants of *B. diazoefficiens* USDA110 affected in the synthesis of respectively methylated or extended (C35) hopanoids, displayed several disorders in both free-living and symbiotic states (Kulkarni et al., 2015). However, no study has been conducted on *Bradyrhizobium* strains to understand how the different VLCFAs linked to the lipid A are synthetized and to describe their respective roles.

Interestingly, only one VLCFA gene cluster has been identified in the bradyrhizobial genomes (**Figure 2**). In this study, we investigated whether this cluster is responsible for the synthesis of the different VLCFAs linked to the lipid A using the photosynthetic *Bradyrhizobium* ORS278 strain as model. This strain has the unusual property of inducing the formation of nitrogen-fixing nodules on some tropical legumes of the *Aeschynomene* genus in the absence of the synthesis of Nod factor

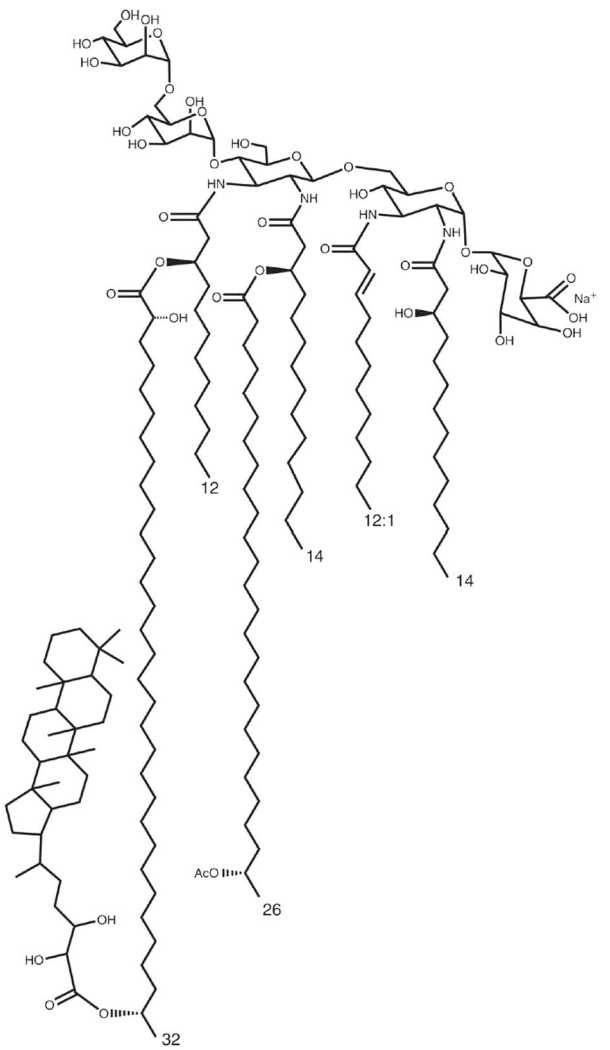

FIGURE 1 | *Bradyrhizobium* BTAi1 lipid A structure (Silipo et al., 2014).

(Giraud et al., 2007). In addition, inside the host cell, bacteria undergo a drastic morphological change, suggesting important modifications of the bacterial cell wall (Bonaldi et al., 2011). This study focused on the effects of the mutations of the VLCFA gene cluster on the structure of the lipid A and on the free and symbiotic state of the bacteria.

MATERIALS AND METHODS

Bacterial Strains and Growth Conditions

The bacteria used in this study are indicated in Supplementary Table S1. The *Bradyrhizobium* strain ORS278 and its derivatives mutants were grown in yeast extract mannitol (YM) medium at 34°C or in minimal medium buffered nodulation medium (BNM) (Podlešáková et al., 2013). *Escherichia coli* strains were grown in Luria-Bertani medium (LB) at 37°C. When required, the media were supplemented with kanamycin (100 μg ml^{-1}) or spectinomycin (20 μg ml^{-1}) or a mixture of the two (100 and 20 μg ml^{-1}).

Construction of ORS278 VLCFA Mutants

Standard molecular biology techniques were used for all cloning work. All the primers and plasmids used for cloning of DNA fragments are listed respectively in Supplementary Tables S1, S2. For the construction of *Bradyrhizobium* strain ORS278 insertional mutants, 300–400 base pair (bp) internal fragments were amplified by PCR and cloned into the plasmid pVO155-npt2-GFP (Okazaki et al., 2016). The constructions were first transferred into the *E. coli* S17-1 strain and then into ORS278 by mating as previously described (Giraud et al., 2010). For the construction of mutants by deletion mutagenesis, flanking regions of the genes were first amplified by PCR and then merged by overlap extension PCR. The overlap PCR fragment obtained was then digested by restriction enzymes corresponding to the restrictions sites of the primers (Supplementary Table S1) and was subsequently cloned in the *sacB* suicide pNPTS129 plasmid by ligation (Tsai and Alley, 2000). The spectinomycin resistance gene cassette from the pHRP315 vector (Parales and Harwood, 1993) was liberated by *Bam*HI digestion and was introduced between the upstream and downstream regions previously cloned in the pNPTS129 plasmid. The resulting plasmid was then transferred into ORS278 by biparental conjugation, as previously described (Giraud et al., 2010). Antibiotic selection was used to select single recombinant which were verified by PCR. Double recombinant clones were then obtained by growth on sucrose in the presence of spectinomycin but without the addition of kanamycin. Candidate clones were checked for the loss of kanamycin resistance from the pNPTS129 plasmid, and the deletion of the gene was verified by PCR.

Lipid A Structure Analysis – MALDI MS and MS/MS

Lipopolysaccharide was isolated and purified from the ORS278 WT strain and the *lpxXl,* BRADO4680 and BRADO0045 mutants, as previously described, and the lipid A isolated through a mild acid hydrolysis (Silipo et al., 2014). Like for MS data, the lipid A was analyzed using a 4800 MALDI MS/MS (ABSciex) mass spectrometer equipped with a Nd:YAG laser at a wavelength (λ) of 355 nm with a 500-ps pulse and a 200 Hz firing rate. External calibrations were performed using an ABSciex calibration mixture, allowing mass accuracies close to 55 ppm. An aliquot of bacterial pellets was also subjected to a micro-extraction procedure to obtain the lipid A moiety, as described by El Hamidi et al. (2005), and analyzed in an ABSCIEX TOF/TOF^{TM} 5800 Applied Biosystems mass spectrometer equipped with an Nd:YLF laser with a λ of 345 nm, a <500-ps pulse length and a repetition rate of up to 1000 Hz. All mass spectra were acquired either in negative (not shown) and positive polarity. In the MS experiments, each spectrum resulted from the accumulation of 1,500 laser shots, whereas 5,000–7,000 shots were summed for the MS/MS data acquisitions (Spina et al., 2000; Sturiale et al., 2011). Samples were dissolved in $CHCl_3/CH_3OH$ (50:50, v/v) at a concentration of 1 mg ml^{-1}. Matrix solution was

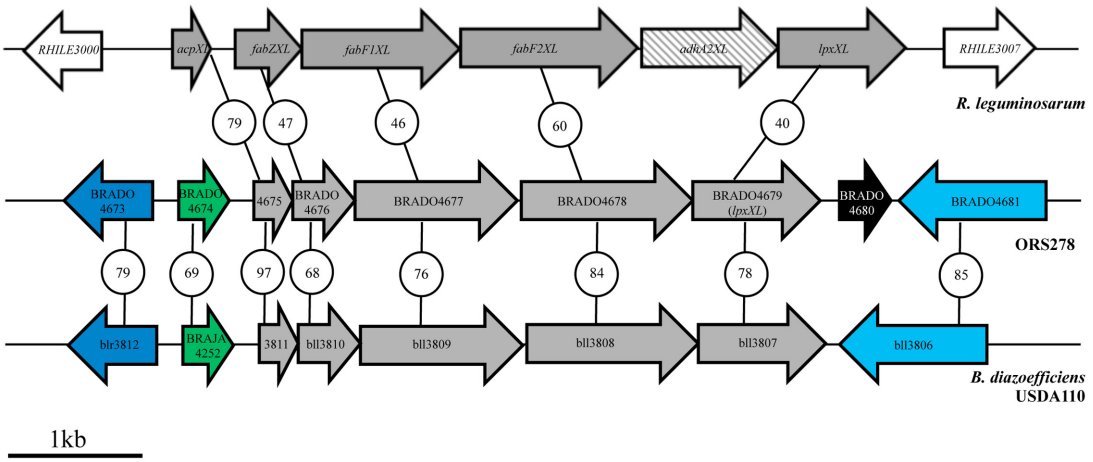

FIGURE 2 | Identification of a gene cluster putatively involved in VLCFA biosynthesis in *Bradyrhizobium* strains by comparative genomic analysis with *R. leguminosarum*. The values in the circles represent the percentage of identity between the corresponding proteins. Genes in gray have been shown to be involved in VLCFA biosynthesis and their transfer to the lipid A in *R. leguminosarum*. The CDS in black is specific to photosynthetic *Bradyrhizobium* strains. Homologous genes are indicated by the same color. The genes are named according to their annotation in the published genomes (*R. leguminosarum* bv. *viciae* 3841, NC_008380; *Bradyrhizobium* sp. ORS 278, NC_009445.1; and *B. diazoefficiens* USDA110, NC_004463).

prepared by dissolving 2,4,6 trihydroxyacetophenone (THAP) in CH_3OH/0.1% trifluoroacetic acid/CH_3CN (7:2:1, by volume) at a concentration of 75 mg ml^{-1}. One microliter of the sample/matrix solution (1:1, v/v) was deposited on the well plate and allowed to dry at room temperature (Leone et al., 2007).

Growth Curves at Different Temperatures

To monitor growth in rich (YM) and minimal (BNM) media, cultures were inoculated at 10^{-2} dilution using YM-grown log-phase (OD_{600} = 0.5–0.7) WT or mutant strains. Growth was measured at OD_{600} using a Cary 50 Scan (Varian). Different incubation temperatures were tested (28, 34, and 37°C). Growth curves were performed in duplicate.

Disk Diffusion Assays and NaCl Resistance Assay

The sensitivity to various abiotic stresses (SDS, H_2O_2, HCl, and NaCl) was assayed as previously described (Silipo et al., 2014). The experiments were conducted in triplicate for the *lpxXL* and BRADO4680 mutants and only once for the two BRADO0045 mutants.

Resistance to Antibiotics

The minimum inhibitory concentration (MIC) of polymyxin B was determined as previously described (Kulkarni et al., 2015) by the Etest method using the disk diffusion assay (Biomérieux, Marcy-l'Etoile, France). The experiment was performed in triplicate.

Plant Cultivation and Symbiotic Analysis

Aeschynomene indica and *A. evenia* seeds were surface sterilized, cultivated, and inoculated as previously described (Gully et al., 2016). For the nodulation and nitrogen fixation assay, 10 plants per condition were taken at 14 days post infection (dpi) to count the number of nodules on the roots and to analyze nitrogenase activity using an acetylene reduction assay (ARA) as previously described (Bonaldi et al., 2010).

Cytological Analyses and Microscopy

Cytological analyses were conducted on 5–10 nodules originating from three different plants for each condition using the protocol described by Bonaldi et al. (2011). Confocal microscopy observations were carried out using a confocal laser-scanning microscope (Carl Zeiss LSM 700; Jena, Germany). Sections of ORS278 WT and BRADO4680 nodules were incubated for 20 min in live/dead staining solution [5 μM SYTO 9 and 30 μM propidium iodide (PI) in 50 mM Tris pH 7.0 buffer; Live/Dead BacLight, Invitrogen]. All the nodule sections were incubated for 15 min in 10 mM phosphate saline buffer (PBS) containing calcofluor white M2R (Sigma, Munich) at a final concentration of 0.01% (w/v) to stain the plant cell wall (Nagata and Takebe, 1970). Calcofluor was excited at 405 nm and emission signals were collected from 405 to 470 nm. For SYTO 9 or GFP and PI, an excitation wavelength of 488 and 555 nm was used with emission signal collected at 490–522 nm and 555–700 nm, respectively. Images were obtained using the ZEN 2008 software (Zeiss).

Statistical Analysis

Statistical analysis was performed using XLSTAT version 2016.6 software. Differences between groups of samples were evaluated with the Tukey's range test. Differences were considered statistically significant at a P-value < 0.01. The box plots were made in R 3.2.2 software. Results are shown as box plots. Each graph contains median, quartiles, and whiskers which show the last sample in [1st quartile −1.5*IQR, 3rd quartile + 1.5* IQR] range. The free points on the graph represent the outliers samples.

Accession Numbers

The GenBank accession numbers of BRADO4675 to BRADO4680 are respectively CAL78405 to CAL78410 and the one of BRADO0045 is CAL74017.

RESULTS

Bradyrhizobium Strains Displayed Only One VLCFA Gene Cluster

A BLAST search of the ORS278 genome led to the identification of a single gene cluster containing several homologs of genes shown to be involved in VLCFA biosynthesis in the *R. leguminosarum* bv. *viciae* 3841 strain (**Figure 2**) (Bourassa et al., 2017). This gene cluster is composed of the CDS BRADO4675 to BRADO4679, which are homologs of *acpXL*, *fabZXL*, *fabF1XL*, *fabF2XL,* and *lpxXL* genes, respectively (**Figure 2**). Besides sharing a high level of identity (>40%) with the corresponding *R. leguminosarum* proteins, except for the absence of the a*dhA2XL* gene in ORS278, the organization of the genes is perfectly conserved between the two strains (**Figure 2**).

We also analyzed the distribution and the organization of the VLCFA genes in other photosynthetic (ORS285, BTAi1, *B. oligotrophicum* S58) and non-photosynthetic (*B. diazoefficiens* USDA110, *B. japonicum* USDA124, and *B. elkanii* USDA76) *Bradyrhizobium* strains. In all cases, only one homolog region was identified in which the genes displayed similar organization to that in ORS278 notably with the absence of the a*dhA2XL* homolog. However, the photosynthetic *Bradyrhizobium* strains differed from the non-photosynthetic ones by the presence, downstream of *lpxXL,* of a gene (BRADO4680) that codes for a protein of unknown function (**Figure 2**).

The identification of only one VLCFA gene cluster among the *Bradyrhizobium* genomes suggests that the genes present in this region might be sufficient for the synthesis and the attachment of the various VLCFAs that are linked to the lipid A in these bacteria.

Lipid A of the *lpxXL* Mutant Lost the C_{26}:25OH VLCFA, but Still Contains the C_{30}:29OH VLCFA

To confirm that the identified region in the ORS278 strain is involved in the synthesis of VLCFAs and in their transfer to the lipid A, we tried to mutate the different genes present in this region, including BRADO4680. Different mutagenesis strategies were tested, deletion by double crossing over in *acpXL* and BRADO4680 and disruption of *fabZXL*, *fabF1XL*, *fabF2XL,* or *lpxXL* by insertion of the non-replicative plasmid pVO155-npt2-GFP in the corresponding coding region. Despite several attempts, only two mutants were obtained, one in the *lpxXL* homolog (BRADO4679) and the second in BRADO4680. The repeated failure to select mutants in *acpXL, fabZXL*, *fabF1XL*, or *fabF2XL* suggests that these four genes are essential because they are required for the synthesis of VLCFAs without which the bacteria cannot survive or grow under the conditions used to select the mutants. Conversely, the selection of mutants in BRADO4680 and *lpxXL* could result in functional redundancy, the absence of role, or in a specific role in the synthesis or the attachment of only one type of VLCFA to the lipid A.

To investigate the impact of the BRADO4679 and BRADO4680 mutations on the synthesis of the VLCFAs, MALDI MS analyses were performed on the lipid A of the ORS278 WT and mutants strains. The mass spectrometry analysis of the WT lipid A showed a mixture of ion species which essentially varied by the acylation pattern, i.e., penta- and hexa-acylated species. All the lipid A species were stoichiometrically built up of a pentasaccharide backbone formed by a β-(1-6)-linked 2,3-diamino-2,3-di-deoxy-D-glucopyranose (DAG) carrying a GalpA residue on the vicinal DAG and an α-(1-6)-Manp disaccharide on the distal DAG residue. Indeed, the mass differences among neighboring ion species were due to acyl number and length of ester linked fatty acids (**Figure 3A**). The ion peak at m/z 2128.52 was established to be a penta-acylated sodiated lipid A carrying two 14:0 (3-OH), one 12:0 (3-OH), one 12:1 and one acetylated VLCFA, 26:0 (25-OAc). The most abundant sodiated hexa-acylated lipid A species (m/z 2594.81) further carried a secondary VLCFA, the 30:0 (2,29-2OH), in turn esterified, in the hepta-acylated species centered around *m/z* 3107.22, by the hopanoid moiety (**Figures 3A,D**). The ORS278 lipid A structure was therefore very similar to the one previously described for the BTAi1 strain with the presence of two VLCFAs, the longest of which harbored a hopanoid molecule (Silipo et al., 2014). The lipid A of the BRADO4680 mutant had a similar structure to that of the WT-strain (**Figures 3B,D**), showing that BRADO4680 is not involved in the modification of the lipid A.

In contrast, the lipid A of the *lpxXl* mutant showed differences in the acylation pattern. In fact, it was composed of a mixture of tetra-, penta-, and hexa-acylated species in which the 26:0 (25-OAc) VLCFA was absent (**Figures 3C,E** and Supplementary Figure S2), indicating that LpxXL is exclusively involved in the transfer of the C_{26}:25OH VLCFA to the lipid A of ORS278.

The C_{26}:25OH VLCFA Lipid A Is Essential for the ORS278 Strain to Deal with Stresses in Free-Living Conditions

Very long-chain fatty acids have been shown to contribute to stress tolerance in free-living and symbiotic states, in diverse rhizobia like *R. leguminosarum* or *S. meliloti* (Becker et al., 2005; Gibson et al., 2008; Bourassa et al., 2017). To test the hypothesis that the removal of the C_{26}:25OH of ORS278 lipid A reduces the ability of the strain to resist stressful conditions, we challenged *lpxXl* and BRADO4680 mutants with a variety of stressors that occur during the initiation and progression of symbiosis. In addition, the growth kinetics of the *lpxXl* and BRADO4680 mutants at various temperatures and their resistance to membrane destabilizer were quantified to determine if these mutations have an effect on the stability of the membrane.

As shown in **Figures 4A,D**, the *lpxXl* mutant displayed similar growth to that of the WT strain at 28°C in both rich and minimal media. In contrast, at higher temperatures (34 and 37°C), the growth kinetics of the mutant were reduced compared with those of the WT strain (**Figures 4B,C,E,F**). These observations

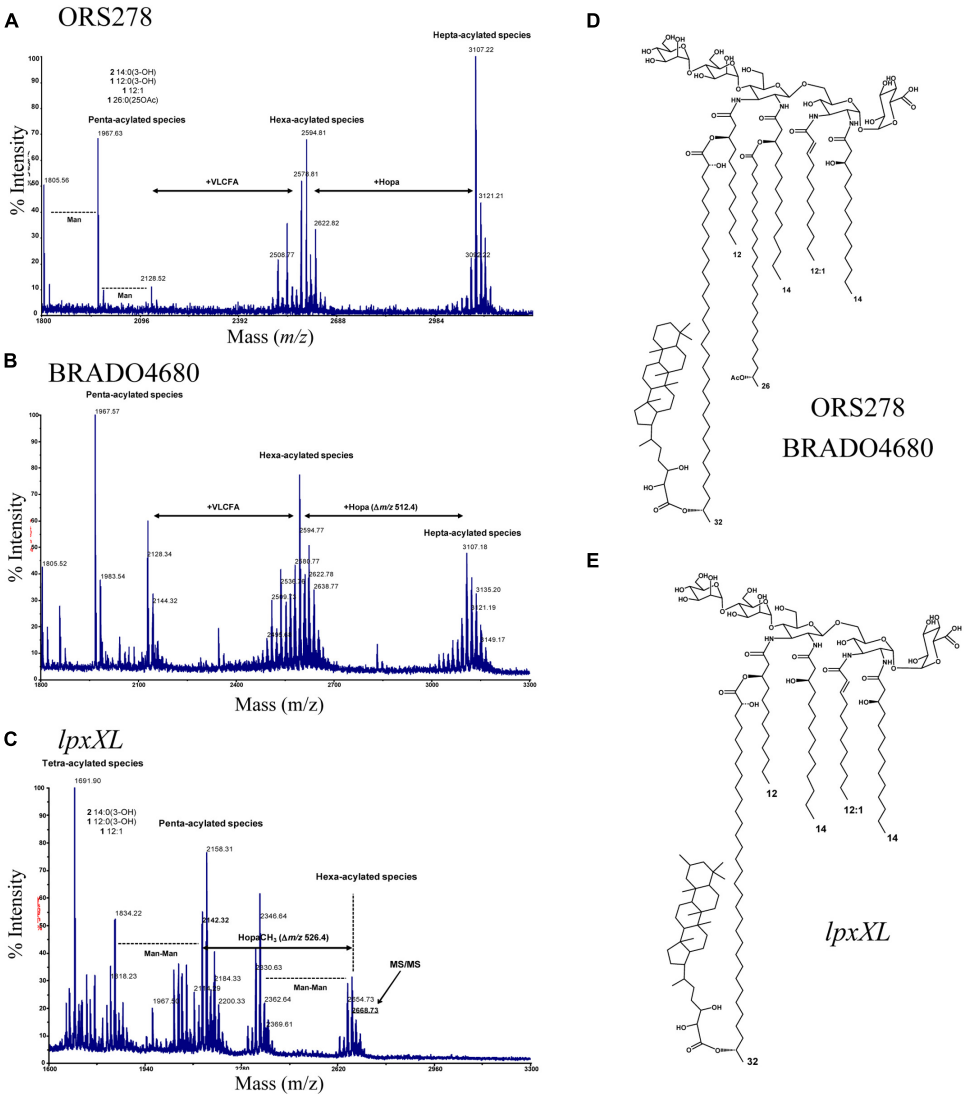

FIGURE 3 | BRADO4679 (*lpxXL*) is involved in the transfer of the C_{26}:25OH VLCFA to the lipid A of ORS278. **(A)** MALDI mass spectrum of lipid A from *Bradyrhizobium* ORS278; **(B)** MALDI MS analysis of lipid A from *Bradyrhizobium* ORS278Δ4680. The spectrum showed a series of intense sodiated molecular ions in the region between *m/z* 2400 and 2700, due to the hexa-acylated species carrying a VLCFA, and a further series of ions in the region between *m/z* 2900 and 3200 corresponding to hepta-acylated lipid A carrying a hopanoid unit (Δ*m/z* 512.4). The highest heterogeneity of lipid A from BRADO4680 is mainly due to variation of the chain length but not affecting the skeleton of the molecule. **(C)** MALDI mass spectrum of lipid A from *Bradyrhizobium lpxXL* mutant. The sodiated hexa-acylated lipid A, in the mass range between *m/z* 2500 and 3000, also comprised species carrying hopanoid moieties with an additional methyl-group (Δ*m/z* 526.4), as confirmed by the MS/MS analysis of the precursor ion at *m/z* 2668.73 (see Supplementary Figure S2). It is likely that methylation took place at C-2 of hopanoid residue, which frequently occurs under stress conditions and might play a key role in the permeability of the membrane. Proposed lipid A structures of ORS278 and BRADO4680 mutant **(D)** and *lpxXL* mutant **(E)**. The C_{26}:25OH VLCFA was not observed in the *lpxXL* mutant of ORS278.

suggest a reduction in the stability of the membrane. In addition, disk diffusion assays showed that the *lpxXl* mutant was more sensitive to H_2O_2 and SDS than the WT strain (**Figure 4H**). The mutant was also more sensitive to osmotic stress than the WT strain, as evidenced by a reduction in its growth at a concentration of 100 mM of NaCl (**Figure 4G**). Because ORS278 is exposed to NCR-like peptides in *Aeschynomene* plants, we also tested the sensitivity of the mutants to polymyxin B which is a cationic peptide displaying similar effects than some NCRs on the alteration of the bacterial OM permeability (Mikulás et al., 2016). Contrary to the *lpxXL* mutant of *R. leguminosarum* which is not affected in polymyxin B resistance (Bourassa et al., 2017), we observed that the *lpxXl* mutant of ORS278 displayed an eightfold lower MIC (8 μg/ml) for polymyxin B than the WT strain (64 μg/ml) (**Figure 4I**). The BRADO4680 mutant withstood all the stressors, as did the WT (**Figures 4A–I**). Together, these data suggest that the C_{26}:25OH VLCFA linked to the lipid A of ORS278 plays an important role in the ability of this strain to cope with various stressful conditions by increasing the stability of the OM.

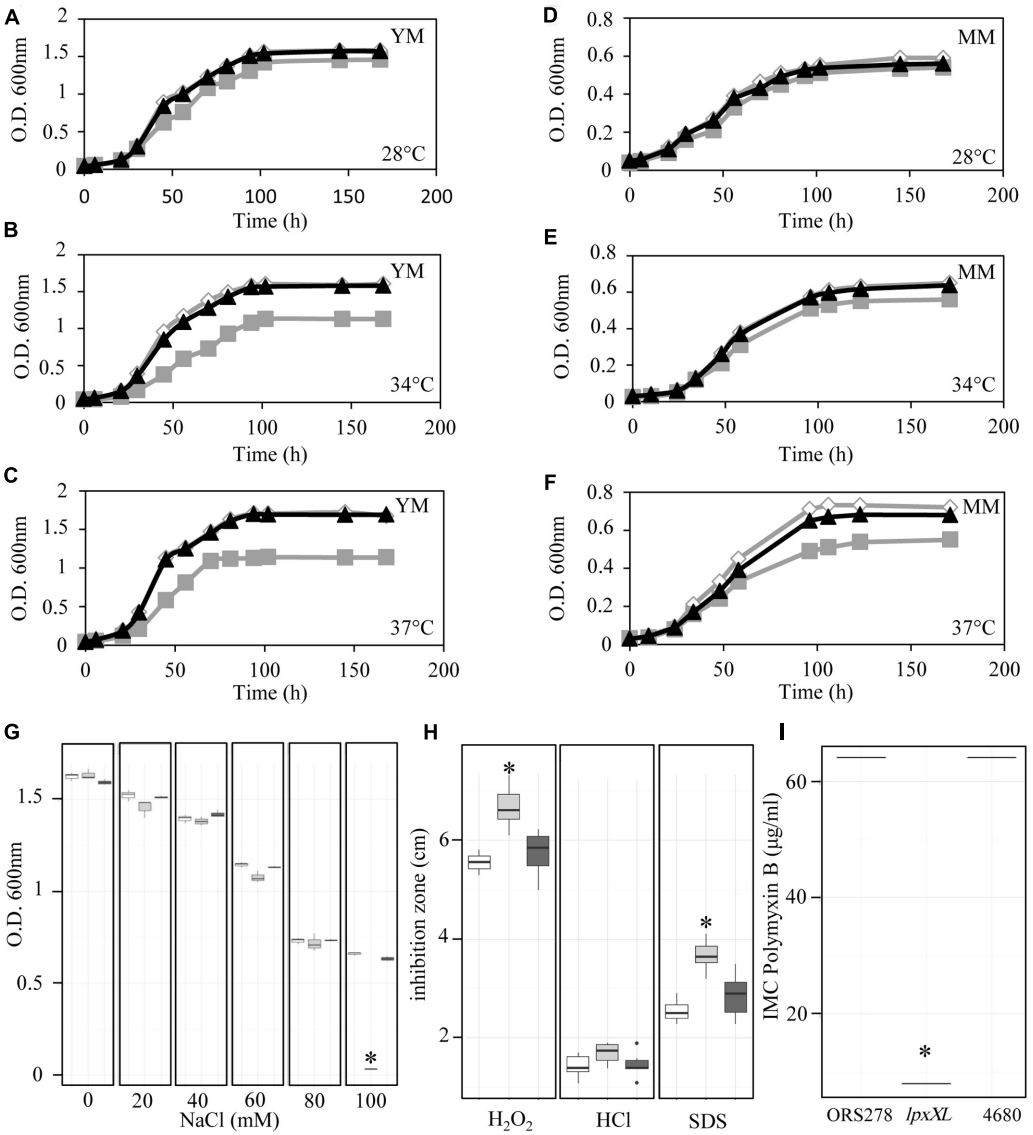

FIGURE 4 | The lack of C_{26}:25OH VLCFA affects the physiology of ORS278 in free-living state. **(A–F)** Growth kinetics of ORS278 (white), *lpxXL* (gray), and BRADO4680 (black) mutants in **(A–C)** YM medium and **(D–F)** Minimal medium at 28°C **(A–D)**, 34°C **(B–E)** and 37°C **(C–F)**, The experiment was carried out in duplicate. **(G)** Box plots representation of the NaCl resistance of ORS278 (white), *lpxXL* (gray) and BRADO4680 (dark gray) strains cultivated in rich medium (YM), at 34°C ($n = 3$). **(H)** Box plots representation of the hydrogen peroxide (H_2O_2), hydrogen chloride (HCl) and sodium dodecyl sulfate (SDS) resistance of ORS278 (white), *lpxXL* (gray) and BRADO4680 (dark gray) mutants, as determined by disk diffusion assays using 5 µl of 5.5 M H_2O_2, 2N HCl or 10% of SDS ($n = 9$). **(I)** Box plots representation of the polymyxin B resistance of ORS278 and the *lpxXL* and BRADO4680 mutants, determined by Etest (Etest® bioMérieux) on YM medium ($n = 3$). **(G–I)** $^*P < 0.01$, by Tukey's honestly significant difference test.

The C_{26}:25OH VLCFA Lipid A Is Essential for an Effective Symbiosis between the Photosynthetic *Bradyrhizobium* ORS278 Strain and *Aeschynomene* Plants

To investigate if the *lpxXl* and BRADO4680 mutations have an effect on the symbiotic properties of ORS278, we inoculated the WT and the two mutants strains on two *Aeschynomene* plants, *A. evenia* and *A. indica,* that can be nodulated in a Nod-independent manner by this strain.

No effect of the BRADO4680 mutation was detected on either *Aeschynomene* species (Supplementary Figure S1). In contrast, a clear effect of the *lpxXl* mutation was observed in both *Aeschynomene* species. Plants inoculated with this mutant, particularly *A. evenia*, displayed typical symptoms of nitrogen starvation, including leaf chlorosis and reduced plant growth at 14-dpi (**Figures 5A,B**). These observations were correlated with reduced nitrogenase activity, as estimated by the ARA compared to the WT strain, despite the fact that the *lpxXL* mutant led to a higher number of nodules per plant (**Figures 5C,D**). In

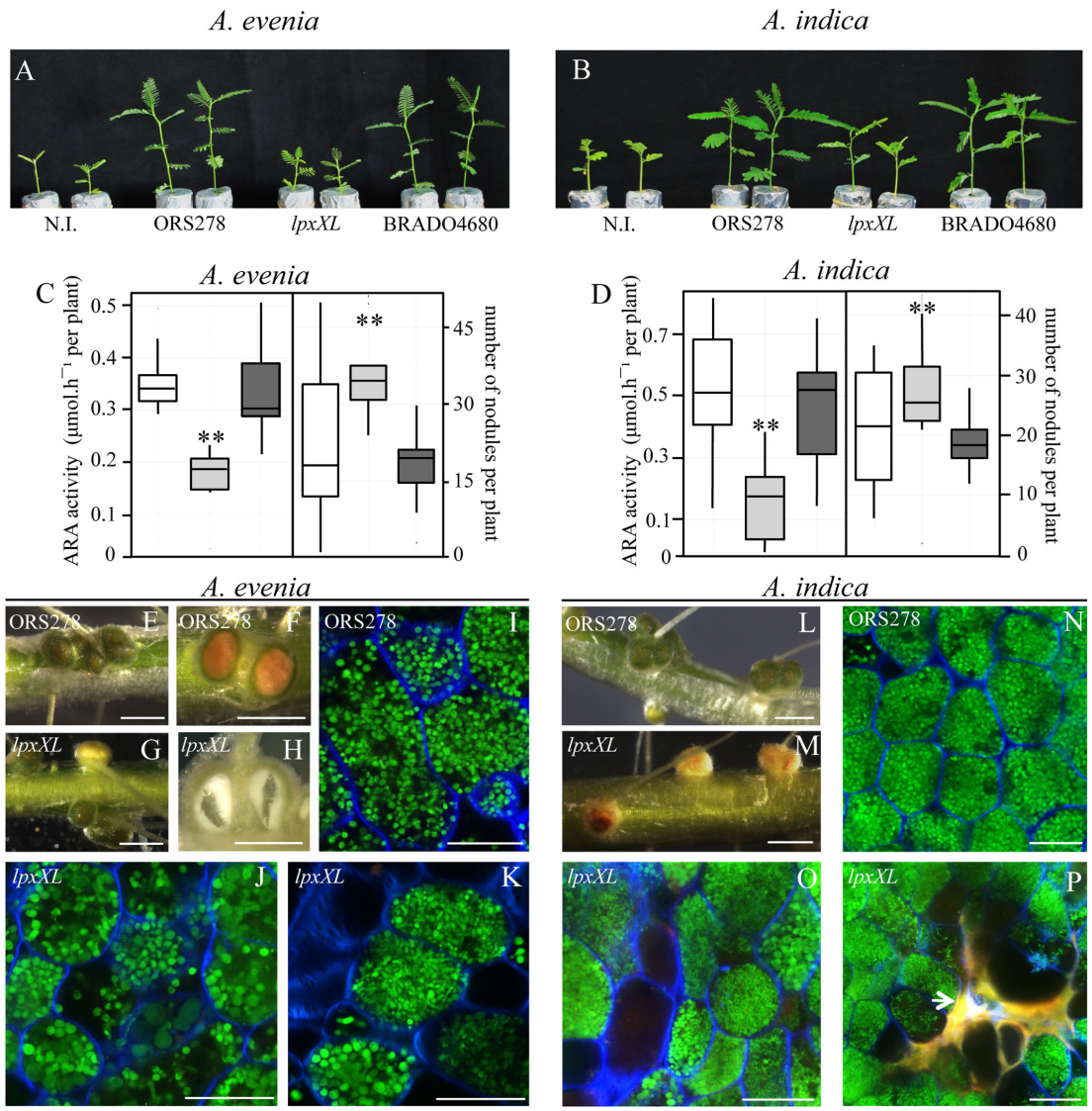

FIGURE 5 | The *lpxXL* mutant of ORS278 is drastically impaired in symbiosis with *Aeschynomene* plants. Comparison of the growth of *A. evenia* **(A)** and *A. indica* **(B)** (aerial part), non-inoculated (N.I.) or inoculated with ORS278, *lpxXL* or BRADO4680 mutants. **(C,D)** Box plots representation of the quantification of acetylene reduction activity (ARA) and number of nodules per plant inoculated with ORS278 (white), *lpxXL* (gray) or BRADO4680 (dark gray) mutants in *A. evenia* **(C)** and *A. indica* **(D)**. The experiment was carried out in duplicate with 10 plants per condition; Tukey's honestly significant difference test indicates a significant effect (*$P < 0.1$; **$P < 0.01$). **(E–H,L,M)** Whole roots of *A. evenia* **(E–H)** and *A. indica* **(L,M)** inoculated with ORS278 **(E,F,L)** or the *lpxXL* mutant **(G,H,M)**; **(F,H)** cut nodules; scale bars: 2 mm. **(I–K,N–P)** Confocal microscopy observations of nodules from *A. evenia* **(I–K)** and *A. indica* **(N–P)** elicited by ORS278 **(I,N)**, or the *lpxXL* mutant **(J,K,O,P)**; scale bars: 20 µm. **(P)** The white arrow indicates a plant defense reaction.

addition, some nodules induced by the *lpxXL* mutant in both *A. evenia* and *A. indica* plants were yellowish instead of green, as observed for the WT nodules (**Figures 5E–G,L,M**). The absence of chloroplasts in the epidermal tissue of the *Aeschynomene* nodules is typically observed in mutants with altered nitrogen fixation, such as *nif* or hopanoid-minus mutants (Bonaldi et al., 2010; Silipo et al., 2014). Furthermore, some *A. evenia* nodules elicited by the *lpxXl* mutant were hollow suggesting a degradation of the tissue of the infection zone (**Figure 5H**), which is a sign of early senescence, as already reported in inefficient nitrogen-fixing mutants (Delmotte et al., 2014; Silipo et al., 2014). In *A. indica,* no hollow nodules were found, but brownish compounds that autofluorescent in the red spectrum (excitation, 488 nm; emission, 600–660 nm) were observed in some *lpxXl* nodules (**Figure 5P**). This is indicative of the accumulation of polyphenol compounds generally associated with plant defense reactions, as previously described in other legumes (Bourcy et al., 2013). Finally, cytological analysis performed by confocal microscopy showed that the process of bacteroid differentiation was altered in the *lpxXL* mutant, in both *A. evenia* and *A. indica* plants. In fact, in the *lpxXL* mutant, both undifferentiated bacteria and bacteroids were observed, which were not perfectly spherical

and were of abnormal size, in contrast to the WT bacteroids (**Figures 5I–K,N–P**). As a WT reference, we used a tagged strain containing the pVO155-npt2-GFP plasmid inserted in the BRADO5083 gene which encodes a protein of unknown function. Previous studies did not reveal any particular symbiotic defect due to the plasmid insertion.

Taken together, these data indicate that the *lpxXL* mutation drastically alters the ability of the ORS278 strain to form an efficient symbiosis with *Aeschynomene* plants.

Search for Another Acyltransferase Transferring the C_{30}:29OH VLCFA to the Lipid A of ORS278

The fact that the lipid A of the *lpxXL* mutant still contains the C_{30}:29OH VLCFA suggests that another acyltransferase exists that allows the specific transfer of this VLCFA to the lipid A. Sequence genome analysis of ORS278 did not enable identification of another homolog of *lpxXL*, suggesting that this acyltransferase should be strongly different from BRADO4679. Conversely, a search for genes annotated as containing an acyl transferase domain retrieved more than 40 candidates. This number was too high to envisage the systematic mutagenesis of all of them. On the other hand, a Tn5 mutant in one of them (BRADO0045) was previously described for its nitrogen fixing deficiency in *A. indica* (Bonaldi et al., 2010) suggesting that this gene plays an important role during symbiosis. This CDS has 42% identity with the ActA protein of *S. meliloti,* which has been shown to play an essential role in the acid tolerance of the bacteria (Tiwari et al., 1996), and 30% identity with the Apo-lipoprotein acyltransferase Lnt characterized in *E. coli*, which is involved in the maturation of lipoprotein (Gupta et al., 1993). Together, these different elements prompted us to examine in more detail the role of BRADO0045 in both the physiology and symbiotic properties of ORS278 and to explore the possibility of its direct involvement in the transfer of the C_{30}:29OH VLCFA to the lipid A.

To be sure that the phenotype reported for the Tn5 mutant corresponds to the inactivation of BRADO0045, we constructed a new insertional mutant in this CDS using the non-replicative plasmid pVO155-npt2-GFP. The ability of the two BRADO0045 mutants (Tn5 and pVO155) of ORS278, called **Ω*0045*T** and **Ω*0045*P**, respectively, to cope with various stresses was then analyzed as previously. Analysis of growth kinetics at 28 and 34°C showed that the two BRADO0045 mutants underwent alteration of their growth at the higher temperature, pointing to destabilization of the membrane, as observed in the *lpxXL* mutant (**Figures 6A,B**). In addition, the two mutants were found to be more sensitive to salt, oxidative and detergent stresses and to the polymyxin B (**Figures 6C–E**) than the WT strain. These results show that the mutation in BRADO0045 reduces the ability of ORS278 to cope with abiotic stresses in the same way as the *lpxXL* mutation.

To test if the mutations in BRADO0045 have an impact on the symbiotic properties of ORS278, *A. indica* plants were inoculated with the WT strain and the two mutants. At 14-dpi, we observed that the plants inoculated with the two mutants were smaller than the plants inoculated by the WT-strain (**Figure 6F**), which is correlated with lower nitrogenase activity (**Figure 6G**). As previously observed in the *lpxXL* mutant, some nodules elicited by the two BRADO0045 mutants were yellow and hollow (**Figures 6H,L**) and some displayed massive plant defense reactions (**Figures 6I–K**). In addition, cytological analysis showed that the intracellular bacteria were not differentiated or not perfectly spherical, and were of abnormal size, the same as observed in the *lpxXL* mutant (**Figures 6M,N**). The BRADO0045 protein thus appears to be essential for the establishment of an efficient symbiosis between ORS278 and *A. indica*.

To determine if this phenotype was due to alteration of the lipid A structure of ORS278, MALDI MS analyses were performed on the lipid A from ORS278 WT and from **Ω*0045*P** mutant. As can be seen in Supplementary Figure S3, the two spectra were very similar, showing that the effects of the BRADO0045 mutation on the phenotypic and symbiotic properties of ORS278 were not due to modification of the lipid A.

DISCUSSION

The fact that a VLCFA is attached to the lipid A of rhizobia was first described in *R. leguminosarum* bv. *trifolii* more than two decades ago (Hollingsworth and Carlson, 1989). Since this discovery, several studies have (i) highlighted the ubiquitous presence of a VLCFA in all the rhizobium lipid A studied, (ii) revealed the importance of this VLCFA in both the free and symbiotic life forms of several rhizobium species and (iii) characterized the genes involved in its biosynthesis (Bhat et al., 1991; Ferguson et al., 2005; Raetz et al., 2007; Haag et al., 2009; Ardissone et al., 2011; Bourassa et al., 2017). More recently, it was shown that the lipid A of several *Bradyrhizobium* strains differs in the presence of at least two VLCFAs, one of which can be linked to a hopanoid molecule (Choma and Komaniecka, 2011; Komaniecka et al., 2014; Silipo et al., 2014). However, nothing is known on the synthesis and the respective role of these VLCFAs.

In this study, we have shown that *Bradyrhizobium* genomes contain a gene cluster homologous to the one described in *R. leguminosarum* that enables the synthesis and the attachment of the VLCFA to the lipid A. In the *Bradyrhizobium* ORS278 strain, we succeeded in obtaining a mutant in only one gene of this cluster, the BRADO4679 gene homologous to *lpxXL* and showed that this mutation led to the suppression of only the C_{26}:25OH VLCFA. This indicates that this gene encodes an acyltransferase which catalyzes the transfer of such a VLCFA to the lipid A but not the one of the C_{30}:29OH VLCFA. Despite the fact that the mutant maintains this second VLCFA linked to the lipid A, it displays several phenotypes similar to those reported in *lpxXl* mutants in other rhizobia species, such as a higher sensitivity to various stresses (NaCl, H_20_2, HCl) and alteration of the efficiency of the symbiosis (Ferguson et al., 2005; Haag et al., 2009; Ardissone et al., 2011). In particular, we observed that the *Aeschynomene* nodules elicited by the *lpxXL* mutant of ORS278 displayed several disorders: some nodules were yellowish and the bacteroids were malformed. Furthermore, some *A. indica* nodules accumulated autofluorescent brown compounds suggesting the induction of plant defense reactions

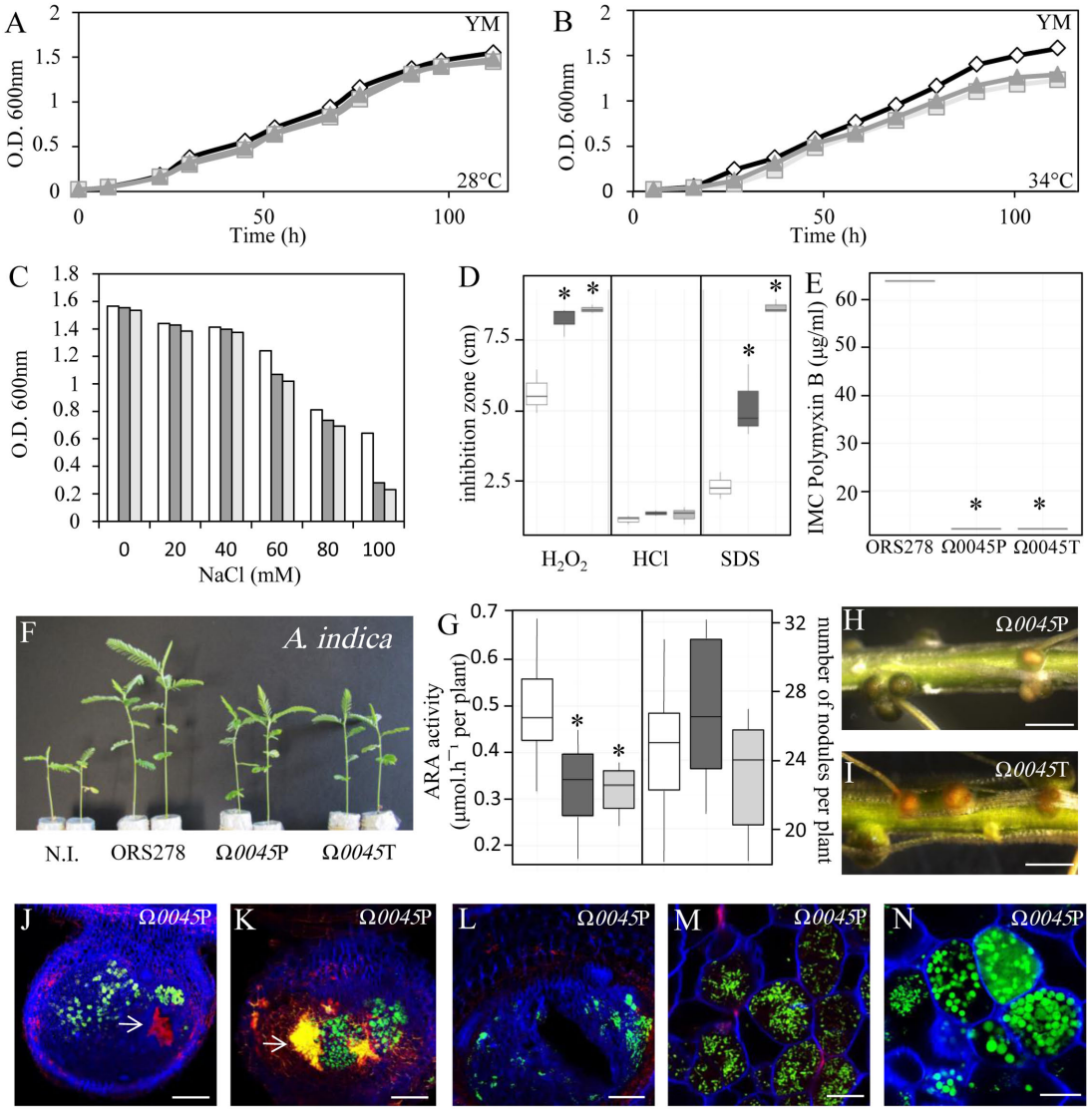

FIGURE 6 | The BRADO0045 mutation affect both free-living and symbiotic states of ORS278. **(A–F)** Growth of ORS278 (white), Ω*0045*P (dark gray) and Ω*0045*T (gray) mutants in YM medium at 28°C **(A)** and 34°C **(B)** ($n = 1$). **(C)** NaCl resistance of ORS278 (white), Ω*0045*P (dark gray) and Ω*0045*T (gray) strains cultivated in rich medium (YM), at 34°C, $n = 1$. **(D)** Box plots representation of the Hydrogen peroxide (H_2O_2), hydrogen chloride (HCl) and sodium dodecyl sulfate (SDS) resistance of ORS278 (white), Ω*0045*P (dark gray) and Ω*0045*T (gray) mutants, as determined by disk diffusion assays using 5 µl of 5.5 M H_2O_2, 2N HCl or 10% of SDS ($n = 9$). **(E)** Box plots representation of the Polymyxin B resistance of ORS278 and the two Ω*0045*P and Ω*0045*T mutants, as determined by Etest (Etest®bioMérieux) on YM medium ($n = 3$); **(F)** Comparison of the growth of *A. indica* (aerial part), non-inoculated (N.I.) or inoculated with ORS278, Ω*0045*P or Ω*0045*T mutants. The experiment was carried out in duplicate with 10 plants per condition. **(G)** Box plots representation of the quantification of ARA and number of nodules per plant inoculated with ORS278 (white), Ω*0045*P (dark gray) or Ω*0045*T (gray) mutants in *A. indica*. Whole roots of *A. indica* inoculed with the Ω*0045*P mutant **(H)** or the Ω*0045*T mutant of ORS278 **(I)**; scale bars: 2 mm. **(J–N)** Nodule thin sections of *A. indica* elicited by the Ω*0045*P mutant and viewed by confocal microscopy; scale bars: 300 µm **(J–L)** and 20 µm **(M,N)**. **(J,K)** Whites arrows indicate plant defense reactions. **(D,E,G)** $^*P < 0.01$, by Tukey's honestly significant difference test.

while the central tissue of some *A. evenia* nodules was digested. This degradation of the symbiotic tissue is typically observed in senescing nodules such as described in *Medicago* or other legume species (Puppo et al., 2004). It would be interesting to confirm that the *LpxxL* mutant can induce plant defense reactions and early nodule degeneracy, respectively, on *A. indica* and *A. evenia*, by checking the expression of some senescence and pathogenesis-related genes. Nevertheless, *Aeschynomene* is just emerging as a new model legume and marker genes of these two cellular programs have to be first characterized for these two species. These severe phenotypes are probably related to the inability of the mutant to cope with the stresses found in the host cell (oxidative stresses, NCR peptides, acid stress) but also to perturbations of the LPS and/or the OM structure that could compromise the recognition of the bacteria by the plant which then reacts by the induction of a defense response or by

triggering senescence. In agreement with this latter possibility, it has been recently identified in *Arabidopsis* a lectin S-domain receptor kinase that detects the lipid A moiety and modulates immune response to bacterial infection (Ranf et al., 2015). It is also important to note that other mutants which displayed some modifications in the structure of their cell wall, such as the DD-CPase1 mutant of ORS278 strain, which is altered in the level of reticulation of the peptidoglycan, or a hopanoid *minus* mutant of the BTAi1 strain, exhibited very similar phenotypes to the *lpxXL* mutant (Silipo et al., 2014; Gully et al., 2016). This suggests that the structural integrity of the bacterial cell envelope of which the attachment of the C_{26}:25OH VLCFA to the lipid A is an important determinant, is essential to maintain chronic intracellular infection during symbiosis.

In this study, we did not succeed in mutating the *acpXL*, *fabZXL*, *fabF1XL*, or *fabF2XL* genes of the ORS278 strain. Taking into account the fact that an *lpxXL* mutant was obtained with the previously described features, it can be assumed that these four genes are involved in the synthesis of the two VLCFAs and that in the absence of their synthesis, the ORS278 strain cannot survive. In support of this last hypothesis, a Tn-seq-based study of *Rhodopseudomonas palustris* CGA009, a strain phylogenetically close to *Bradyrhizobium*, indicates that these genes are also essential in this bacteria (Pechter et al., 2015). In addition to this common pool of genes, we predict that at least three additional enzymes are necessary to achieve the complete synthesis of the lipid A in its most complex form: (i) an enzyme permitting elongation of the C_{26}:25OH VLCFA to the C_{30}:29OH VLCFA genes, (ii) an acyltransferase specific to the C_{30}:29OH VLCFA allowing its transfer to the lipid A, and finally, (iii) an enzyme catalyzing the attachment of the C_{35}-hopanoid to this VLCFA. The fact that a *shc* mutant of BTAi1 displayed a lipid A with the two VLCFAs but lacking the hopanoid moiety leads us to think that, first, the C_{30}:29OH VLCFA is attached to the lipid A and, second, the hopanoid is attached to the C_{30}:29OH VLCFA. Some genes of the lipid A biosynthesis pathway in *Bradyrhizobium* strains therefore remain to be identified. Their discovery will be a real challenge considering that their mutation could be lethal and that no other homolog of *lpxXL* has been identified in the *Bradyrhizobium* genomes.

In this context, we examined whether the BRADO0045, that encodes a putative acyltransferase and for which a Tn5 mutant has been reported to be affected in nitrogen fixation, can catalyze the transfer of the C_{30}:29OH VLCFA to the lipid A. MALDI MS analyses of the lipid A clearly showed that BRADO0045 does not play this role since no structural difference was observed with the WT lipid A. On the other hand, the phenotypic properties of the BRADO0045 mutants are very similar to those of the *lpxXL* mutant indicating that the mutation of BRADO0045 would affect the structure of the cell envelope. The protein BRADO0045 has a low level of identity with the apo-lipoprotein *N*-acyltransferase Lnt of *E. coli*. This enzyme plays a role in the maturation of lipoproteins by catalyzing the attachment of a third acyl chain that enables their transfer to the OM by the Lol system in Gram-negative bacteria (Fukuda et al., 2002). It has been shown in *E. coli* that the mutation of *lnt* affects the properties of both the inner and OM by reducing the level of incorporation of lipoproteins in the OM and, consequently increasing it in the inner membrane, which is lethal in this bacterium (Robichon et al., 2005; Narita and Tokuda, 2011). It would therefore be interesting to compare the lipoprotein composition of the different membrane compartments in the BRADO0045 mutant and in the WT strain to check whether BRADO0045 corresponds to an apo-lipoprotein *N*-acyltransferase. It is also to note that the three downstream genes of BRADO0045 (BRADO0046 to BRADO0048) are in the same direction than BRADO0045 (see Supplementary Figure S4), we cannot therefore exclude the possibility that the phenotype observed for the BRADO0045 insertional mutants was due to polar effects.

Numerous studies have revealed an essential role for VLCFA-modified lipid A in bacteria with an intracellular lifestyle, whether they are pathogens or symbionts like rhizobia (Bhat et al., 1991; Zähringer et al., 1995; Becker et al., 2005). One may wonder why, unlike other rhizobia, *Bradyrhizobium* strains, which have similar lifestyles, have at least two VLCFAs linked to their lipid A instead of one and why a hopanoid molecule is covalently linked to this second VLCFA. It was previously shown by analysis of reconstituted liposomes using electron spin resonance (ESR) spectroscopy, that, thanks to their VLCFAs, HoLA molecules can span the whole OM by placing the hopanoid moiety in the inner leaflet, which results in a higher stabilization of the inner and the outer leaflets of the OM (Silipo et al., 2014). This rigidification of the OM might be a functional advantage by strengthening its barrier role, which could facilitate the survival of the bacteria under stress conditions. This could contribute to the ecological success of the *Bradyrhizobium* genus which nodulates the widest range of legume species and which is distributed worldwide but predominately in tropical areas and acid soils (Parker, 2015; Sprent et al., 2017).

AUTHOR CONTRIBUTIONS

NB, EG, AM, and AS conceived the experiments, NB, FDL, AP, LS, FG, JF, DG, and CC conducted the experiments; NB, EG, AM, and AS analyzed the results and wrote the paper.

FUNDING

This work was supported by the French National Research Agency (ANR-Bugsinacell-13-BSV7-0013).

SUPPLEMENTARY MATERIAL

The Supplementary Material for this article can be found online at: http://journal.frontiersin.org/article/10.3389/fmicb.2017.01821/full#supplementary-material

REFERENCES

Ardissone, S., Kobayashi, H., Kambara, K., Rummel, C., Noel, K. D., Walker, G. C., et al. (2011). Role of BacA in lipopolysaccharide synthesis, peptide transport, and nodulation by *Rhizobium* sp. strain NGR234. *J. Bacteriol.* 193, 2218–2228. doi: 10.1128/JB.0126010

Becker, A., Fraysse, N., and Sharypova, L. (2005). Recent advances in studies on structure and symbiosis-related function of rhizobial K-antigens and lipopolysaccharides. *Mol. Plant Microbe Interact.* 18, 899–905. doi: 10.1094/MPMI-180899

Bhat, U. R., Forsberg, L. S., and Carlson, R. W. (1994). Structure of lipid A component of *Rhizobium leguminosarum* bv. *phaseoli* lipopolysaccharide. Unique nonphosphorylated lipid A containing 2-amino-2-deoxygluconate, galacturonate, and glucosamine. *J. Biol. Chem.* 269, 14402–14410.

Bhat, U. R., Mayer, H., Yokota, A., Hollingsworth, R. I., and Carlson, R. W. (1991). Occurrence of lipid A variants with 27-hydroxyoctacosanoic acid in lipopolysaccharides from members of the family Rhizobiaceae. *J. Bacteriol.* 173, 2155–2159. doi: 10.1128/jb.173.7.2155-2159.1991

Bonaldi, K., Gargani, D., Prin, Y., Fardoux, J., Gully, D., Nouwen, N., et al. (2011). Nodulation of *Aeschynomene afraspera* and *A. indica* by photosynthetic *Bradyrhizobium* Sp. strain ORS285: the nod-dependent versus the nod-independent symbiotic interaction. *Mol. Plant Microbe Interact.* 24, 1359–1371. doi: 10.1094/MPMI-04-110093

Bonaldi, K., Gourion, B., Fardoux, J., Hannibal, L., Cartieaux, F., Boursot, M., et al. (2010). Large-scale transposon mutagenesis of photosynthetic *Bradyrhizobium* sp. strain ORS278 reveals new genetic loci putatively important for nod-independent symbiosis with *Aeschynomene indica*. *Mol. Plant Microbe Interact.* 23, 760–770. doi: 10.1094/MPMI-23-60760

Bourassa, D. V., Kannenberg, E. L., Sherrier, D. J., Buhr, R. J., and Carlson, R. W. (2017). The lipopolysaccharide Lipid A long-chain fatty acid is important for *Rhizobium leguminosarum* growth and stress adaptation in free-living and nodule environments. *Mol. Plant Microbe Interact.* 30, 161–175. doi: 10.1094/MPMI-11-16-0230-R

Bourcy, M., Brocard, L., Pislariu, C. I., Cosson, V., Mergaert, P., Tadege, M., et al. (2013). *Medicago truncatula* DNF2 is a PI-PLC-XD-containing protein required for bacteroid persistence and prevention of nodule early senescence and defense-like reactions. *New Phytol.* 197, 1250–1261. doi: 10.1111/nph.12091

Brown, D. B., Huang, Y. C., Kannenberg, E. L., Sherrier, D. J., and Carlson, R. W. (2011). An *acpXL* mutant of *Rhizobium leguminosarum* bv. *phaseoli* lacks 27-hydroxyoctacosanoic acid in its lipid A and is developmentally delayed during symbiotic infection of the determinate nodulating host plant *Phaseolus vulgaris*. *J. Bacteriol.* 193, 4766–4778. doi: 10.1128/JB.0039211

Choma, A., and Komaniecka, I. (2011). Straight and branched (omega-1)-hydroxylated very long chain fatty acids are components of *Bradyrhizobium* lipid A. *Acta Biochim. Pol.* 58, 51–58.

Czernic, P., Gully, D., Cartieaux, F., Moulin, L., Guefrachi, I., Patrel, D., et al. (2015). Convergent evolution of endosymbiont differentiation in dalbergioid and inverted repeat-lacking clade legumes mediated by nodule-specific cysteine-rich peptides. *Plant Physiol.* 169, 1254–1265. doi: 10.1104/pp.15.00584

Delmotte, N., Mondy, S., Alunni, B., Fardoux, J., Chaintreuil, C., Vorholt, J. A., et al. (2014). A proteomic approach of *Bradyrhizobium*/*Aeschynomene* root and stem symbioses reveals the importance of the *fixA* locus for symbiosis. *Int. J. Mol. Sci.* 15, 3660–3670. doi: 10.3390/ijms15033660

El Hamidi, A., Tirsoaga, A., Novikov, A., Hussein, A., and Caroff, M. (2005). Microextraction of bacterial lipid A: easy and rapid method for mass spectrometric characterization. *J. Lipid Res.* 46, 1773–1778. doi: 10.1194/jlr.D500014-JLR200

Ferguson, G. P., Datta, A., Carlson, R. W., and Walker, G. C. (2005). Importance of unusually modified lipid A in *Sinorhizobium* stress resistance and legume symbiosis. *Mol. Microbiol.* 56, 68–80. doi: 10.1111/j.1365-2958.2005.04536.x

Fukuda, A., Matsuyama, S., Hara, T., Nakayama, J., Nagasawa, H., and Tokuda, H. (2002). Aminoacylation of the N-terminal cysteine is essential for Lol-dependent release of lipoproteins from membranes but does not depend on lipoprotein sorting signals. *J. Biol. Chem.* 277, 43512–43518. doi: 10.1074/jbc.M206816200

Gibson, K. E., Kobayashi, H., and Walker, G. C. (2008). Molecular determinants of a symbiotic chronic infection. *Annu. Rev. Genet.* 42, 413–441. doi: 10.1146/annurev.genet.42.110807.091427

Giraud, E., Lavergne, J., and Vermeglio, A. (2010). Characterization of bacteriophytochromes from photosynthetic bacteria: histidine kinase signaling triggered by light and redox sensing. *Methods Enzymol.* 471, 135–159. doi: 10.1016/S0076-6879(10)710090

Giraud, E., Moulin, L., Vallenet, D., Barbe, V., Cytryn, E., Avarre, J. C., et al. (2007). Legumes symbioses: absence of Nod genes in photosynthetic bradyrhizobia. *Science* 316, 1307–1312. doi: 10.1126/science.1139548

Gourion, B., Berrabah, F., Ratet, P., and Stacey, G. (2015). *Rhizobium*-legume symbioses: the crucial role of plant immunity. *Trends Plant Sci.* 20, 186–194. doi: 10.1016/j.tplants.2014.11.008

Grohmann, E., Muth, G., and Espinosa, M. (2003). Conjugative plasmid transfer in gram-positive bacteria. *Mol. Biol. Rev.* 67, 277–301. doi: 10.1128/MMBR.67.2.277-301.2003

Gully, D., Gargani, D., Bonaldi, K., Grangeteau, C., Chaintreuil, C., Fardoux, J., et al. (2016). A peptidoglycan-remodeling enzyme is critical for bacteroid differentiation in *Bradyrhizobium* spp. during legume symbiosis. *Mol. Plant Microbe Interact.* 29, 447–457. doi: 10.1094/MPMI-03-16-0052-R

Gupta, S. D., Gan, K., Schmid, M. B., and Wu, H. C. (1993). Characterization of a temperature-sensitive mutant of *Salmonella typhimurium* defective in apolipoprotein N-acyltransferase. *J. Biol. Chem.* 268, 16551–16556.

Haag, A. F., Arnold, M. F., Myka, K. K., Kerscher, B., Dall'Angelo, S., Zanda, M., et al. (2013). Molecular insights into bacteroid development during *Rhizobium*-legume symbiosis. *FEMS Microbiol. Rev.* 37, 364–383. doi: 10.1111/1574-6976.12003

Haag, A. F., Wehmeier, S., Beck, S., Marlow, V. L., Fletcher, V., James, E. K., et al. (2009). The *Sinorhizobium meliloti* LpxXL and AcpXL proteins play important roles in bacteroid development within alfalfa. *J. Bacteriol.* 191, 4681–4686. doi: 10.1128/JB.00318-09

Hollingsworth, R. I., and Carlson, R. W. (1989). 27-Hydroxyoctacosanoic acid is a major structural fatty acyl component of the lipopolysaccharide of *Rhizobium trifolii* Anu-843. *J. Biol. Chem.* 264, 9300–9303.

Kannenberg, E. L., and Carlson, R. W. (2001). Lipid A and O-chain modifications cause *Rhizobium* lipopolysaccharides to become hydrophobic during bacteroid development. *Mol. Microbiol.* 39, 379–391. doi: 10.1046/j.1365-2958.2001.02225.x

Kannenberg, E. L., Perzl, M., Muller, P., Hartner, T., and Poralla, K. (1996). Hopanoid lipids in *Bradyrhizobium* and other plant-associated bacteria and cloning of the *Bradyrhizobium japonicum* squalene-hopene cyclase gene. *Plant Soil* 186, 107–112. doi: 10.1007/BF00035063

Komaniecka, I., Choma, A., Mazur, A., Duda, K. A., Lindner, B., Schwudke, D., et al. (2014). Occurrence of an unusual hopanoid-containing lipid A among lipopolysaccharides from *Bradyrhizobium* species. *J. Biol. Chem.* 289, 35644–35655. doi: 10.1074/jbc.M114.614529

Kulkarni, G., Busset, N., Molinaro, A., Gargani, D., Chaintreuil, C., Silipo, A., et al. (2015). Specific hopanoid classes differentially affect free-living and symbiotic states of *Bradyrhizobium diazoefficiens*. *mBio* 6:e01251-15. doi: 10.1128/mBio.0125115

Leone, S., Sturiale, L., Pessione, E., Mazzoli, R., Giunta, C., Lanzetta, R., et al. (2007). Detailed characterization of the lipid A fraction from the nonpathogen *Acinetobacter radioresistens* strain S13. *J. Lipid Res.* 48, 1045–1051. doi: 10.1194/jlr.M600323-JLR200

Lerouge, I., and Vanderleyden, J. (2002). O-antigen structural variation: mechanisms and possible roles in animal/plant-microbe interactions. *FEMS Microbiol. Rev.* 26, 17–47. doi: 10.1111/j.1574-6976.2002.tb00597.x

Mikuláss, K. R., Nagy, K., Bogos, B., Szegletes, Z., Kovács, E., Farkas, A., et al. (2016). Antimicrobial nodule specific cysteine rich peptides disturb the integrity of bacterial outer and inner membranes and cause loss of membrane potential. *Ann. Clin. Microbiol. Antimicrob.* 15, 43. doi: 10.1186/s12941-016-01598

Montiel, J., Downie, J. A., Farkas, A., Bihari, P., Herczeg, R., Bálint, B., et al. (2017). Morphotype of bacteroids in different legumes correlates with the number and type of symbiotic NCR peptides. *Proc. Natl. Acad. Sci. U.S.A.* 114, 5041–5046. doi: 10.1073/pnas.1704217114

Nagata, T., and Takebe, I. (1970). Cell wall regeneration and cell division in isolated tobacco mesophyll protoplasts. *Planta* 92, 301–308. doi: 10.1007/BF00385097

Narita, S., and Tokuda, H. (2011). Overexpression of LolCDE allows deletion of the *Escherichia coli* gene encoding apolipoprotein N-acyltransferase. *J. Bacteriol.* 193, 4832–4840. doi: 10.1128/JB.0501311

Okazaki, S., Tittabutr, P., Teulet, A., Thouin, J., Fardoux, J., Chaintreuil, C., et al. (2016). *Rhizobium*-legume symbiosis in the absence of Nod factors: two possible scenarios with or without the T3SS. *ISME J.* 10, 64–74. doi: 10.1038/ismej.2015.103

Ourisson, G., Rohmer, M., and Poralla, K. (1987). Prokaryotic hopanoids and other polyterpenoid sterol surrogates. *Annu. Rev. Microbiol.* 41, 301–333. doi: 10.1146/annurev.mi.41.100187.001505

Parales, R. E., and Harwood, C. S. (1993). Construction and use of a new broad-host-range lacZ transcriptional fusion vector, pHRP309, for gram- bacteria. *Gene* 133, 23–30. doi: 10.1016/0378-1119(93)90220-W

Parker, M. A. (2015). The spread of *Bradyrhizobium* lineages across host legume clades: from *Abarema* to *Zygia*. *Microb. Ecol.* 69, 630–640. doi: 10.1007/s00248-014-05035

Pechter, K. B., Gallagher, L., Pyles, H., Manoil, C. S., and Harwood, C. S. (2015). The essential genome of the metabolically versatile alphaproteobacterium *Rhodopseudomonas palustris*. *J. Bacteriol.* 28, 867–876. doi: 10.1128/JB.0077115

Podlešáková, K., Fardoux, J., Patrel, D., Bonaldi, K., Novák, O., Strnad, M., et al. (2013). Rhizobial synthesized cytokinins contribute to but are not essential for the symbiotic interactions between photosynthetic *Bradyrhizobia* and *Aeschynomene* legumes. *Mol. Plant Microbe Interact.* 26, 1232–1238. doi: 10.1094/MPMI-03-13-0076-R

Puppo, A., Groten, K., Bastian, F., Carzaniga, R., Soussi, M., Lucas, M. M., et al. (2004). Legume nodule senescence: roles for redox and hormone signalling in the orchestration of the natural aging process. *New Phytol.* 165, 683–701. doi: 10.1111/j.1469-8137.2004.01285.x

Raetz, C. R., Reynolds, C. M., Trent, M. S., and Bishop, R. E. (2007). Lipid A modification systems in gram-negative bacteria. *Annu. Rev. Biochem.* 76, 295–329. doi: 10.1146/annurev.biochem.76.010307.145803

Raetz, C. R., and Whitfield, C. (2002). Lipopolysaccharide endotoxins. *Annu. Rev. Biochem.* 71, 635–700. doi: 10.1146/annurev.biochem.71.110601.135414

Ranf, S., Gisch, N., Schäffer, M., Illig, T., Westphal, L., Knirel, Y. A., et al. (2015). A lectin S-domain receptor kinase mediates lipopolysaccharide sensing in *Arabidopsis thaliana*. *Nat. Immunol.* 16, 426–433. doi: 10.1038/ni.3124

Robichon, C., Vidal-Ingigliardi, D., and Pugsley, A. P. (2005). Depletion of apolipoprotein N-acyltransferase causes mislocalization of outer membrane lipoproteins in *Escherichia coli*. *J. Biol. Chem.* 280, 974–983. doi: 10.1074/jbc.M411059200

Saenz, J. P., Sezgin, E., Schwille, P., and Simons, K. (2012). Functional convergence of hopanoids and sterols in membrane ordering. *Proc. Natl. Acad. Sci. U.S.A.* 109, 14236–14240. doi: 10.1073/pnas.1212141109

Silipo, A., Vitiello, G., Gully, D., Sturiale, L., Chaintreuil, C., Fardoux, J., et al. (2014). Covalently linked hopanoid-lipid A improves outer-membrane resistance of a *Bradyrhizobium* symbiont of legumes. *Nat. Commun.* 5:5106. doi: 10.1038/ncomms6106

Spina, E., Sturiale, L., Romeo, D., Impallomeni, G., Garozzo, D., Waidelich, D., et al. (2000). New fragmentation mechanisms in matrix-assisted laser desorption/ionization time-of-flight/time-of-flight tandem mass spectrometry of carbohydrates. *Rapid Commun. Mass Spectrom.* 18, 392–398. doi: 10.1002/rcm.1350

Sprent, J. I., Ardley, J., and James, E. K. (2017). Biogeography of nodulated legumes and their nitrogen-fixing symbionts. *New Phytol.* 215, 40–56. doi: 10.1111/nph.14474

Sturiale, L., Palmigiano, A., Silipo, A., Knirel, Y. A., Anisimov, A. P., Lanzetta, R., et al. (2011). Reflectron MALDI TOF and MALDI TOF/TOF mass spectrometry reveal novel structural details of native lipooligosaccharides. *J. Mass Spectrom.* 46, 1135–1142. doi: 10.1002/jms.2000

Tiwari, R. P., Reeve, W. G., Dilworth, M. J., and Glenn, A. R. (1996). An essential role for actA in acid tolerance of *Rhizobium meliloti*. *Microbiology* 142, 601–610. doi: 10.1099/13500872-142-3-601

Tsai, J. W., and Alley, M. R. (2000). Proteolysis of the McpA chemoreceptor does not require the *Caulobacter* major chemotaxis operon. *J. Bacteriol.* 182, 504–507. doi: 10.1128/JB.182.2.504-507.2000

Van de Velde, W., Zehirov, G., Szatmari, A., Debreczeny, M., Ishihara, H., Kevei, Z., et al. (2010). Plant peptides govern terminal differentiation of bacteria in symbiosis. *Science* 327, 1122–1126. doi: 10.1126/science.1184057

Wang, Q., Yang, S., Liu, J., Terecskei, K., Ábrahám, E., Gombár, A., et al. (2017). Host-secreted antimicrobial peptide enforces symbiotic selectivity in *Medicago truncatula*. *Proc. Natl. Acad. Sci. U.S.A.* 114, 6854–6859. doi: 10.1073/pnas.1700715114

Welander, P. V., Hunter, R. C., Zhang, L., Sessions, A. L., Summons, R. E., and Newman, D. K. (2009). Hopanoids play a role in membrane integrity and pH homeostasis in *Rhodopseudomonas palustris* TIE-1. *J. Bacteriol.* 191, 6145–6156. doi: 10.1128/JB.00460-09

Zähringer, U., Knirel, Y. A., Lindner, B., Helbig, J. H., Sonesson, A., Marre, R., et al. (1995). The lipopolysaccharide of *Legionella pneumophila* serogroup 1 (strain Philadelphia 1): chemical structure and biological significance. *Prog. Clin. Biol. Res.* 392, 113–139.

Conflict of Interest Statement: The authors declare that the research was conducted in the absence of any commercial or financial relationships that could be construed as a potential conflict of interest.

frontiers in Microbiology

ORIGINAL RESEARCH
published: 20 September 2017
doi: 10.3389/fmicb.2017.01810

Type 3 Secretion System (T3SS) of *Bradyrhizobium* sp. DOA9 and Its Roles in Legume Symbiosis and Rice Endophytic Association

Pongpan Songwattana[1], Rujirek Noisangiam[2], Kamonluck Teamtisong[3], Janpen Prakamhang[4], Albin Teulet[5], Panlada Tittabutr[1], Pongdet Piromyou[1], Nantakorn Boonkerd[1], Eric Giraud[5]† and Neung Teaumroong[1]*†*

[1] School of Biotechnology, Institute of Agricultural Technology, Suranaree University of Technology, Nakhon Ratchasima, Thailand, [2] National Bureau of Agricultural Commodity and Food Standards, Ministry of Agriculture and Cooperatives, Bangkok, Thailand, [3] The Center for Scientific and Technological Equipment, Suranaree University of Technology, Nakhon Ratchasima, Thailand, [4] Department of Applied Biology, Faculty of Sciences and Liberal Arts, Rajamangala University of Technology Isan, Nakhon Ratchasima, Thailand, [5] Institut de Recherche pour le Développement, LSTM, UMR IRD/SupAgro/INRA/Univ. Montpellier/CIRAD, Montpellier, France

OPEN ACCESS

Edited by:
Pascal Ratet,
Centre National de la Recherche Scientifique (CNRS), France

Reviewed by:
Francisco Javier López-Baena,
University of Seville, Spain
Brian H. Kvitko,
University of Georgia, United States

***Correspondence:**
Neung Teaumroong
neung@sut.ac.th
Eric Giraud
eric.giraud@ird.fr

† These authors have contributed equally to this work.

Specialty section:
This article was submitted to Plant Microbe Interactions, a section of the journal Frontiers in Microbiology

Received: 15 June 2017
Accepted: 05 September 2017
Published: 20 September 2017

Citation:
Songwattana P, Noisangiam R, Teamtisong K, Prakamhang J, Teulet A, Tittabutr P, Piromyou P, Boonkerd N, Giraud E and Teaumroong N (2017) Type 3 Secretion System (T3SS) of Bradyrhizobium sp. DOA9 and Its Roles in Legume Symbiosis and Rice Endophytic Association. Front. Microbiol. 8:1810. doi: 10.3389/fmicb.2017.01810

The *Bradyrhizobium* sp. DOA9 strain isolated from a paddy field has the ability to nodulate a wide spectrum of legumes. Unlike other bradyrhizobia, this strain has a symbiotic plasmid harboring *nod*, *nif*, and type 3 secretion system (T3SS) genes. This T3SS cluster contains all the genes necessary for the formation of the secretory apparatus and the transcriptional activator (TtsI), which is preceded by a *nod*-box motif. An *in silico* search predicted 14 effectors putatively translocated by this T3SS machinery. In this study, we explored the role of the T3SS in the symbiotic performance of DOA9 by evaluating the ability of a T3SS mutant (Ω*rhcN*) to nodulate legumes belonging to Dalbergioid, Millettioid, and Genistoid tribes. Among the nine species tested, four (*Arachis hypogea*, *Vigna radiata*, *Crotalaria juncea*, and *Macroptilium atropurpureum*) responded positively to the *rhcN* mutation (ranging from suppression of plant defense reactions, an increase in the number of nodules and a dramatic improvement in nodule development and infection), one (*Stylosanthes hamata*) responded negatively (fewer nodules and less nitrogen fixation) and four species (*Aeschynomene americana*, *Aeschynomene afraspera*, *Indigofera tinctoria*, and *Desmodium tortuosum*) displayed no phenotype. We also tested the role of the T3SS in the ability of the DOA9 strain to endophytically colonize rice roots, but detected no effect of the T3SS mutation, in contrast to what was previously reported in the *Bradyrhizobium* SUTN9-2 strain. Taken together, these data indicate that DOA9 contains a functional T3SS that interferes with the ability of the strain to interact symbiotically with legumes but not with rice.

Keywords: type 3 secretion system, effector proteins, *Bradyrhizobium*, legume, symbiosis

INTRODUCTION

The establishment of the legume–rhizobium symbiosis relies on the exchange of diffusible signal molecules between the two partners. The first important bacterial signals are lipochitooligosaccharides (LCOs) called Nod factors (NFs) that are synthetized and secreted after activation of bacterial nodulation (*nod*) genes by the transcriptional regulator protein NodD in specific response to host flavonoids. In return, perception of the NFs signal by the plant triggers nodule organogenesis and bacterial infection processes (Oldroyd et al., 2011). Besides NFs, other bacterial components are important for the successful establishment of the symbiosis, including exopolysaccharides (EPS), lipopolysaccharides (LPS), capsular polysaccharides (KPS), and cyclic β-glucans (Gibson et al., 2008; Janczarek et al., 2015). These bacterial compounds can also act as a symbiotic signal or permit to avoid plant immune responses (Gourion et al., 2015; Kawaharada et al., 2015).

In addition, some rhizobia use a type 3 secretion system (T3SS), which shares homology with the T3SS apparatus of plant and animal pathogenic bacteria, to translocate some putative effectors into the host cell, named nodulation outer proteins (Nops). Those putative effector proteins may have contrasting effects on nodulation depending on the host plant (Staehelin and Krishnan, 2015). Some secreted effector proteins can play a positive role in the establishment and maintenance of symbiosis by suppressing plant defense reactions thereby facilitating the bacterial infection (Bartsev et al., 2004; Jiménez-Guerrero et al., 2015). Conversely, secreted Nop proteins can be recognized by plant receptor proteins [resistant (R) proteins] leading to effector-triggered immunity, which blocks infection and nodulation (Yang et al., 2010; Yasuda et al., 2016).

It is important to indicate that the term Nop has been initially introduced by Marie et al. (2001) to mirror the nomenclature of *Yersinia* outer proteins (Yops) and that the first identified Nops was done by characterizing the proteins secreted in *Sinorhizobium* NGR234 culture supernatants in a NodD1- and a flavonoid-dependent manner (Marie et al., 2003). As consequence, this term has been used to name some components of the extracellular appendages or pili of the T3SS, i.e., NopA, NopB, and NopX but also effector proteins secreted through the T3SS that are translocated to the interior of the host cell, i.e., NopL, NopE, and NopC. In this paper, we will consider the term Nop to speak about the effector proteins translocated into the host cell.

The involvment of the T3SS in the establishement of the symbiosis is supported by two facts: (i) the genes that code for T3SS machinery and some Nops are found in the same region as the *nod* and *nif* genes (on a symbiotic island or a symbiotic plasmid) and (ii) expression of the T3SS genes is also controlled via a regulatory cascade involving NodD. In the latter case, NodD regulates, in a flavonoid-dependent manner, the expression of the transcriptional activator (TtsI), which, in return, activates the expression of T3SS genes by binding to their promoter region at the level of a specific motif, called *tts*-box (Krause et al., 2002; Tampakaki, 2014).

The importance of T3SS in the modulation of the host spectrum has been extensively demonstrated in several rhizobial strains (*Sinorhizobium* sp. NGR234, *S. fredii* USDA257, *S. fredii* HH103, *Mesorhizobium loti* MAFF303099, *Bradyrhizobium diazoefficiens* USDA110, *B. elkanii* USDA61) (Viprey et al., 1998; Krause et al., 2002; Krishnan et al., 2003; de Lyra Mdo et al., 2006; López-Baena et al., 2009; Okazaki et al., 2009, 2010). More recently, some non-photosynthetic *Bradyrhizobium* strains have been shown to be able to nodulate some legume plants (*Glycine max* cv. Enrei and several *Aeschynomene* species) in the absence of NF synthesis but in these cases, nodulation requires a functional T3SS. This points to the existence of an alternative Nod-independent symbiotic pathway in which some Nop effectors can directly activate the nodulation signaling pathway (Okazaki et al., 2013, 2016). Moreover, in *Bradyrhizobium* sp. SUTN9-2, T3SS has been reported to be an important determinant of rice-endophyte colonization (Piromyou et al., 2015b). Taken together, these data show that the role played by the T3SS in rhizobia during the interaction with their host plants is more important and broader than previously believed.

The non-photosynthetic *Bradyrhizobium* sp. strain DOA9 was originally isolated from a paddy field in Thailand using *Aeschynomene americana* as trap plant (Noisangiam et al., 2012). In addition to its ability to endophytically colonize rice roots, this strain has been shown to be able to induce the formation of nodules in a large spectrum of legume hosts (Teamtisong et al., 2014). Unlike other bradyrhizobia, the DOA9 is the only strain yet identified to possess a symbiotic plasmid that harbors nitrogen fixation (*nif*), nodulation (*nod*), and T3SS genes (Okazaki et al., 2015). In this study, we examined the role of T3SS in the DOA9 strain by testing the symbiotic performance of a T3SS mutant (Ω*rhcN*) on various legume species as well as on rice.

MATERIALS AND METHODS

Bacterial Strains and Culture Conditions

The bacterial strains used in this study are listed in **Table 1**. *Bradyrhizobium* sp. strain DOA9 and its Ω*rhcN* derivative were grown in YM medium (Vincent, 1970) at 28°C. *Escherichia coli* strains were cultured at 37°C in LB medium (Sambrook et al., 2001). The media were supplemented with antibiotics at the following concentrations when appropriate: 200 μg/mL streptomycin (Sm), 20 μg/mL nalidixic acid (Nal), and 50 μg/mL kanamycin (Km).

Construction of the Reporter and Mutant Strains

The single cross-homologous recombination technique was used to construct the insertion mutant in the structural type III secretion system gene (*rhcN*) of strain DOA9. For this purpose, an internal fragment (263-bp) of *rhcN* was amplified by polymerase chain reaction (PCR) using the following primers: RhcN.D9p.int.f (5′-CATCTCGTCGACTCGCAGCA AAGGATGTCGATAC-3′) and RhcN.D9p.int.r (5′-GAGCAG TCTAGACCCGACTGACACTTCCTGCATG-3′). The PCR

TABLE 1 | Bacterial strains, plasmids used, and plants tested in this study.

	Relevant characteristics	Source or reference
Strains		
Bradyrhizobium sp. DOA9	Isolated from paddy field using *A. americana* as trap legume	Noisangiam et al., 2012
Ω*rhcN*	*rhcN* mutant of DOA9 strain obtained by integration of pVO155-Sm-npt2-gfp; Sm^r Sp^r Km^r	This study
Escherichia coli S17-1	hsdR pro thi (RP4-2 km::Tn7 tc::Mu)	
Plasmid		
pVO155-Sm-npt2-gfp	pUC119-derived suicide vector with *gusA* gene, GFP, and Sm^r cassette, Km^R Sm^r Sp^r	Wongdee et al., 2016
pMG103-npt2-Sm-npt2-gfp	Cloning vector harboring *gfp* gene under the control of the constitutive *npt2* promoter; Sm^r Sp^r Km^r	Bonaldi et al., 2010

product was then digested by *Xba*I and *Sal*I and cloned onto the corresponding sites of the plasmid pVO155-Sm-npt2-gfp (Wongdee et al., 2016). This plasmid, which is non-replicative in *Bradyrhizobium* strains, is a derivative of the plasmid pVO155 (Oke and Long, 1999) and carries the promoterless *gusA* gene, a constitutively expressed gfp, and a Km- and a Sm/spectinomycin-resistance genes (Wongdee et al., 2016). The resulting plasmid was introduced into *E. coli* S17-1 by electroporation (15 kv/cm, 100 Ω, and 25 μF) and was transferred into the *Bradyrhizobium* sp. strain DOA9 by biparental mating, using the protocol described by Giraud et al. (2010). The transconjugants were spread on YM medium supplemented with an antibiotic mixture of Sm, Km, and Nal, and the successful insertion of the plasmid in *rhcN* was checked by PCR.

The GFP-labeled DOA9 strain was constructed by introducing the replicative plasmid pMG103-npt2-Sm-npt2-gfp harboring a constitutive *gfp* gene by electroporation (15 kv/cm, 100 Ω, and 25 μF). Plasmid-containing strains were selected on YM plates supplemented with Sm.

Plant Nodulation and Symbiosis Analysis

DOA9 and its derivatives were grown for 5 days as previously described and used as inoculum. Sterilization and germination of the seeds of all plants tested (Supplementary Table S1) were performed as described by Teamtisong et al. (2014). Plants were sown in Leonard's jar filled with sterilized vermiculite (Somasegaran and Hoben, 1994). All the plants were watered with BNM medium (Ehrhardt et al., 1992) and grown under the following controlled environmental conditions: 28 ± 2°C with a 16 h light/8 h dark cycle at light intensities of 300 $\mu E/m^2S$ and with 50% humidity. Five days after planting, each seedling was inoculated with 1 mL of a 5 day old inoculum (log-phase) after washing and adjusting the optical density to 600 nm to 1 (approximately 10^9 cells). The experiment was conducted with five replicates with the following treatments: control (no inoculation), GPF-labeled DOA9, and Ω*rhcN*. To check nodulation and nitrogen fixation abilities, five plants were taken at 21 day post-inoculation (dpi) and the number of nodules and nitrogenase activity were assessed using the acetylene reduction assay (ARA). Briefly, all the nodules on each plant were collected and placed in headspace bottles with 10% acetylene, and incubated at 28°C for 1 h. Gas chromatography was used to measure the peak height of ethylene and acetylene with 1 mL gas samples from the bottles by using a PE-alumina packed column with injector at 150°C, an oven temperature of 200°C, and ionization detector (FID) at a temperature of 50°C (Somasegaran and Hoben, 1994).

Rice Experiment

Rice (*Oryza sativa* L. ssp. *indica* cv. Pathum Thani) seeds were surface sterilized by soaking in 70% (v/v) ethanol for 30 s, then washed twice with 10% (v/v) hydrogen peroxide for 10 min, washed again in 3% (v/v) sodium hypochlorite for 1 h. Finally, the seeds were washed in sterilized water five times and germinated overnight on YM medium containing 0.8% (v/v) agar. The germinated seeds with 1 cm of root were soaked in DOA9 cell suspension ($OD_{600} = 1$) overnight. The rice seedlings were transferred to metal net in 80 mL tubes containing 15 mL Hoagland's plant growth medium (Hoagland and Arnon, 1950) in presence of 0.1 mM NH_4NO_3. The experiment was conducted with three technical replicates with the following treatments: control (no inoculation), GFP-labeled DOA9, and Ω*rhcN*. Plants were grown under the following controlled environmental conditions: 28 ± 2°C with a 16 h light/8 h dark cycle at light intensities of 300 $\mu E/m^2S$ and with 50% humidity.

Enumeration of Epiphytic and Endophytic Bacteria in Rice Roots

Two and 3 weeks after inoculation with the DOA9 tagged strains and Ω*rhcN* containing *gfp* and Sm^r, the rice roots were washed in normal saline solution (0.85% of NaCl) to remove debris and any bacteria not firmly attached to the root surface. Next, the bacterial cells remaining on the surface of the roots were harvested by vortex with normal saline containing 0.3% (v/v) tween-80 for 30 s. The washing solution containing the epiphytic bacteria was then spread on YM plates containing Sm. For the enumeration of endophytic bacterial, root tissues were surface sterilized with 70% (v/v) ethanol for 5 min followed by 3% (v/v) sodium hypochlorite for 5 min and rinsed with sterilized water five times. The surface sterilized roots were macerated with a sterilized mortar and pestle and diluted in saline solution prior to being spread on medium as described above (Piromyou et al., 2015a). The epiphyte and endophyte population counted on agar plates are expressed as colony-forming unit per gram of root fresh weight.

Preparation of Root Exudates and Bacterial Induction

The sterilized legume seeds were germinated and transferred into tubes containing BNM medium (50 mg seeds/mL). Plants were

maintained in controlled environmental conditions as described above for 5 days. The root exudates were obtained from plant medium after filtration using a 0.2 μm filter syringe. Root exudates were stored at −20°C until use.

The mid-log phase culture of DOA9 was washed and the OD_{600} was adjusted to approximately 0.4 with YM supplemented with 1/3 (v/v) of the root exudates or purified flavonoids (20 μM of naringenin or genistein dissolved in DMSO). The sterilized BNM medium and DMSO were used as negative controls. The bacterial cells were cultured at 28°C for 24 h and then collected by centrifugation (4,000 × *g* for 10 min, 4°C) and immediately frozen in liquid nitrogen and stored at −80°C for further total RNA isolation.

RNA Isolation and qRT-PCR

Total bacterial RNA was extracted from induced cells using the RNeasy® Mini Kit (QIAGEN, United States) according to the manufacturer's protocol. Total RNA was treated with RNase-free DNase I (NEB) for 30 min at 37°C. cDNA was synthesized from 500 ng total RNA using High Capacity cDNA Reverse Transcription Kits (Applied Biosystems™) according to the manufacturers' protocols. Thirty nanograms of cDNA was subjected to PCR amplification using specific primers of *rhcN* (rhcN.RT.D9.f: 5′-CATTGGCGATATGGTAGGCT-3′; rhcN.RT.D9.r: 5′-GGACAAGTGTGAACCGTCCT-3′) and *nopX* (nopX.RT.D9.f: 5′-CATCAACCCGAACAACACAG-3′; nopX.RT.D9.r: 5′-GGCTCGATAGACAAGGTCCACAA-3′) genes. PCR amplification was performed using QuantStudio 3 Real-Time PCR System Mix (Applied Biosystems™) and the following program: an initial denaturation step at 95°C for 2 min; 35 cycles at 95°C for 30 s, 55°C for 30 s, and at 72°C for 1.5 min; and a final extension step at 72°C for 10 min. The relative gene expression was analyzed using the comparative Ct method (−ΔΔCT) normalized to the endogenous housekeeping gene (16S rRNA) using PBA338F (5′-ACTCCTACGGGAGGCAGCAG-3′) and PRUN518R (5′-ATTACCGCGGCTGCTGG-3′). Three biological replicates were pooled and analyzed. At least three replicate PCR amplifications were performed for each sample.

Microscopy

An Olympus Fluoview FV1000 confocal laser scanning microscope was used to investigate nodule development, bacteroid differentiation, and rice colonization. For this purpose, 40–50 μm thick sections of fresh nodules and rice roots were prepared using a VT1000S vibratome (Leica Nanterre, France). Nodule sections were stained for 20 min with 0.01% calcofluor (to stain the plant cell wall) and with 30 μM propidium iodide (PI) in 50 mM Tris–HCl pH 7.0 buffer to identify dead cells (Haag et al., 2011). Calcofluor was excited at 405 nm and detected with a 460–500 nm emission filter. The GFP-labeled DOA9 and Ω*rhcN* strains were detected after excitation with the 488 nm laser line and emission signal collection at 490–522 nm, while the PI used to identify dead cells was excited with the 535 nm laser line and emission signals were collected at 617–636 nm. Confocal images were reconstructed with NIS elements software (Nikon), and images were colored and prepared for publication with Adobe Photoshop software. To detect β-glucuronidase (GUS) activity in the nodules elicited by the *rhcN* mutant the same protocol than Bonaldi et al. (2010) was used.

Search for Genes Encoding Putative T3 Effectors on the DOA9 Genome

Two complementary approaches were used to identify putative effector genes: (i) a TBlastN search of the genome for known Nops identified in rhizobia (Kimbrel et al., 2013; Staehelin and Krishnan, 2015), the identified homologs were considered as possible candidates when they matched the following parameters (% of identity ≥40% over 80% of the length of the sequence) and (ii) a search for *tts*-boxes on the chromosome and plasmid of DOA9 genome (GenBank accession numbers DF820425 and DF820426, respectively) using a hidden Markov model initially trained with the sequences of 26 confirmed *tts*-boxes from *Sinorhizobium* (*Ensifer*) sp. strain NGR234, *B. diazoefficiens* USDA110, and *B. elkanii* USDA61 (Eddy, 1998; Marie et al., 2004; Zehner et al., 2008; Okazaki et al., 2009). To be considered as a candidate, the gene had to contain a *tts*-box with a score ≥9 located on the same strand in its upstream region (up to 1 kb).

Statistical Analysis

The experiment data were subjected to analysis of variance (ANOVA). When confirming a statistically significant value in the *F*-test ($p \leq 0.05$), a *post hoc* test (Duncan's multiple-range test at $p \leq 0.05$) was used as a multiple comparison procedure (Duncan, 1955) using SPSS1 software for WINDOWS™, Version 14.0.

RESULTS

Gene Organization and Comparison of the T3SS Genes of *Bradyrhizobium* sp. DOA9 and Other Rhizobial Strains

Sequence genome analysis revealed the presence of a T3SS gene cluster organized in several operons on the pDOA9 plasmid (**Figures 1A,B**). The main putative operon preceded by a *tts*-box contained most of the genes coding for components of the secretion machinery in the order *nopB*, *rhcJ*, *nolU*, *rhcL*, *rhcN*, *rhcU*, *rhcQ*, *rhcR*, *rhcS*, *rhcT*, and *rhcU*. This genetic organization is similar to that found in other *Bradyrhizobium* or *Sinorhizobium* strains and a very high level of AA identity was observed with the corresponding homologous proteins. However, unlike these strains, a large intergenic region of 650 bp was observed between *rhcS* and *rhcT* also containing a *tts*-box (**Figure 1A**), raising the possibility that the *rhcT* and *rhcU* genes are transcribed independently.

As described in other rhizobia, we could assume that this main cluster is under the dual control of TtsI and NodD since a *ttsI* homolog was found at the vicinity of the main operon preceded by a *nod*-box (**Figure 1A**). However, it is to highlight the presence of a gene encoding a putative transposase between this *nod*-box and *ttsI*. To confirm that the presence of this putative

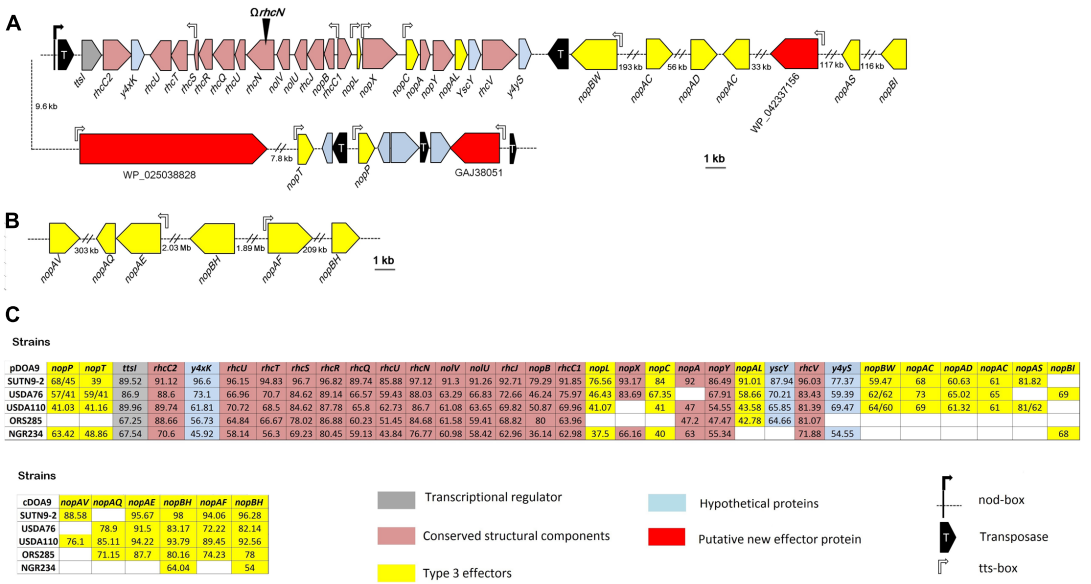

pDOA9	nopP	nopT	ttsI	rhcC2	y4xK	rhcU	rhcT	rhcS	rhcR	rhcQ	rhcU	rhcN	nolV	nolU	rhcJ	nopB	rhcC1	nopL	nopX	nopC	nopA	nopY	nopAL	yscY	rhcV	y4yS	nopBW	nopAC	nopAD	nopAC	nopAS	nopBI
SUTN9-2	68/45	39	89.52	91.12	96.6	96.15	94.83	96.7	96.82	89.74	85.88	97.12	91.3	91.26	92.71	79.29	91.85	76.56	93.17	84	92	86.49	91.01	87.94	96.03	77.37	59.47	68	60.63	61	81.82	
USDA76	57/41	59/41	86.9	88.6	73.1	66.96	70.7	84.62	89.14	66.57	59.43	88.03	63.29	66.83	72.66	46.24	75.97	46.43	83.69	67.35		67.91	58.66	70.21	83.43	59.39	62/62	73	65.02	65		69
USDA110	41.03	41.16	89.96	89.74	61.81	70.72	68.5	84.62	87.78	65.8	62.73	86.7	61.08	63.65	69.82	50.87	69.96	41.07		41	47	54.55	43.58	65.85	81.39	69.47	64/60	69	61.32	61	81/62	
ORS285			67.25	88.66	56.73	64.84	66.67	78.02	86.88	60.23	51.45	84.68	61.58	59.41	68.82	80	63.96				47.2	47.47	42.78	64.66	81.07							
NGR234	63.42	48.86	67.54	70.6	45.92	58.14	56.3	69.23	80.45	59.13	43.84	76.77	60.98	58.42	62.96	36.14	62.98	37.5	66.16	40	63	55.34			71.88	54.55						68

cDOA9	nopAV	nopAQ	nopAE	nopBH	nopAF	nopBH
SUTN9-2	88.58		95.67	98	94.06	96.28
USDA76		78.9	91.5	83.17	72.22	82.14
USDA110	76.1	85.11	94.22	93.79	89.45	92.56
ORS285		71.15	87.7	80.16	74.23	78
NGR234				64.04		54

FIGURE 1 | Genetic organization of the type 3 secretion gene (T3SS) cluster and putative effectors in *Bradyrhizobium* sp. DOA9 strain **(A)** on the plasmid pDOA9 and **(B)** on the chromosome. The orientations and sizes of the ORFs are indicated by arrows. Location and orientation of *tts*-box motifs are shown by rectangular open arrows, while the *nod*-box motif is shown by a black rectangular arrow. The site of insertional mutation for Ω*rhcN* is indicated by a black arrowhead. **(C)** % of similarity of the T3SS apparatus and effector proteins between DOA9 strain and other rhizobial strains, including *Bradyrhizobium* sp. SUTN9-2, *B. elkanii* USDA76, *B. diazoefficiens* USDA110, *Bradyrhizobium* sp. ORS285, and *Sinorhizobium fredii* NGR234.

transposase does not interfere with the formation of the T3SS secretion apparatus, we analyzed the expression of two structural T3SS genes (*rhcN* and *nopX*) in the presence of two flavonoids (genistein or naringenin) previously reported to induce T3SS genes in rhizobial strains (Krause et al., 2002; Okazaki et al., 2010). As shown in Supplementary Figure S1, both flavonoids strongly induced *nopX* and *rhcN* expression, showing that despite this transposase, the T3SS genes in DOA9 strain are classically regulated by flavonoids, most probably via the control of NodD and TtsI.

To identify putative effectors that are possibly translocated by this T3SS machinery, we combined two *in silico* searches: (i) a TBlastN search of the genome for Nops previously identified in other rhizobia and (ii) a search of the *tts*-box motif using a hidden Markov model. After eliminating the Nops proteins predicted to correspond to components of the secretory apparatus (NopA, NopX, and NopB) (Staehelin and Krishnan, 2015), this analysis retrieved 20 putative translocated effectors. Of these, six were located on the chromosome (**Figure 1C**). However, all six candidates remain doubtful because homologous proteins for all of them can be identified in photosynthetic *Bradyrhizobium* strains that lack a T3SS gene cluster (Supplementary Table S2). Interestingly, among the other putative effectors found on the plasmid, three correspond to new effectors not previously identified in other rhizobia. They were preceded by a *tts*-box and all contained the small ubiquitin-like modifier (SUMO) protease domain of the C48 peptidase [ubiquitin-like protease 1 (Ulp1)] family. Several effectors containing this functional domain have already been characterized in pathogenic and symbiotic bacteria (Hotson et al., 2003; Hubber et al., 2004; Rodrigues et al., 2007; Tsurumaru et al., 2015), reinforcing the hypothesis that these three effector candidates are *bona fide* new effectors.

Symbiotic Role of the T3SS

To analyze the role of the T3SS in DOA9 strain during symbiosis, we constructed a T3SS mutant by inserting the non-replicative plasmid pVO155-Sm-npt2-gfp into the 5′-region of *rhcN*. The *rhcN* gene was selected as target because it encodes an ATPase that is indispensable for the functioning of the T3SS injectisome. Furthermore, the pVO155 plasmid used for inactivation of the gene contains a constitutive expressed GFP that enables monitoring of the bacteria inside the nodules. The symbiotic performance of the WT and Ω*rhcN* mutant was compared on several legume species belonging to Genistoid (*Crotalaria juncea*), Dalbergioid (*Aeschynomene americana*, *A. afraspera*, *Arachis hypogaea*, and *Stylosanthes hamata*), and Millettioid tribes (*Macroptillium atropurpureum*, *Vigna radiata*, *Indigofera tinctoria*, and *Desmodium tortuosum*) by analyzing several symbiotic parameters (number of nodules per plant, nitrogen fixation estimated using the ARA, plant dry weight, and cytological aspect of the nodules).

Depending on the plant species, the Ω*rhcN* mutant displayed contrasted responses compared to the WT strain. The responses were classified in three categories. In category 1, non-responsive phenotype (called T3SS-no effect group), the plants inoculated with the mutant displayed the same number of nodules and the same nitrogen fixing capacity as the plants inoculated with the WT strain. Furthermore, no cytological differences were observed between the mutant and WT nodules. These plants

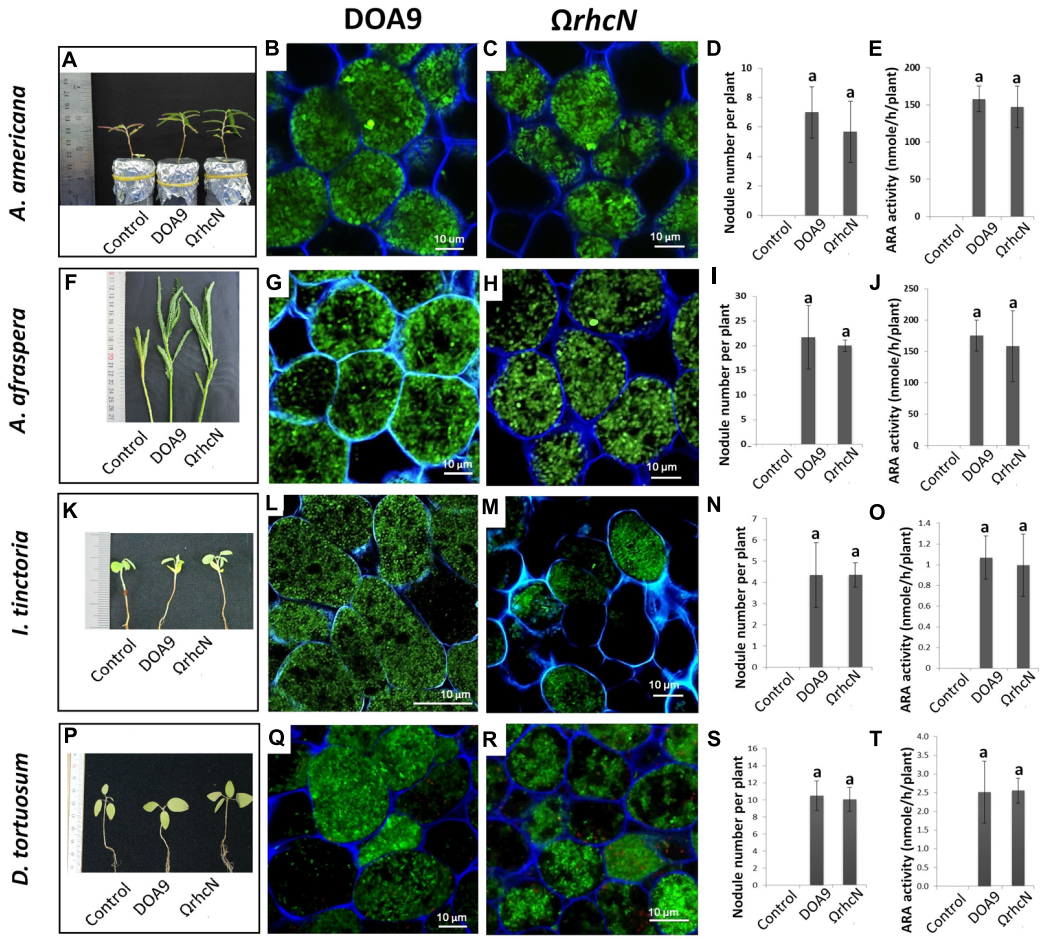

FIGURE 2 | Symbiotic analysis of legume species displaying no phenotype with the T3SS mutant of the DOA9 strain. Plant growth, cytological aspect of the nodules, number of nodules per plant, and the ARA activity of *A. americana* **(A–E)**, *A. afraspera* **(F–J)**, *I. tinctoria* **(K–O)**, and *D. tortuosum* **(P–T)** after inoculation with the WT strain and the Ω*rhcN* mutant. Values represent mean ± SD ($n = 5$). Within treatment, means labeled with different letters are statistically different at $p < 0.05$.

were *A. americana*, *A. afraspera*, *I. tinctoria*, and *D. tortuosum* (**Figure 2**).

In category 2, the *rhcN* mutation had a positive effect on one of the symbiotic parameters analyzed (**Figure 3**). This group comprised *A. hypogaea*, *V. radiata*, *C. juncea*, and *M. atropurpureum*. Inoculation with the Ω*rhcN* mutant led to an almost 65% increase in the number of nodules on *A. hypogea* compared with WT (**Figure 3F**). This result suggests that in DOA9, T3SS compromises either the infection or nodule organogenesis process in this species. **Figure 3** shows that the higher number of nodules is not correlated with an increase in N_2 fixation. We assume that the plant compensates for the small number of nodules elicited by the WT strain by stimulating their expansion, as can be seen in **Figures 3B,C**. The same mechanism has been reported in *Medicago* and is related to plant N demand (Laguerre et al., 2012). The deleterious effect of the T3SS on the establishment of the symbiosis was more marked in the cases of *C. juncea* and *V. radiata*. Indeed, whereas the WT strain only elicited bumps or small completely necrotic nodules in *C. juncea* and *V. radiata*, respectively, the Ω*rhcN* mutant formed perfectly developed nodules on these two plants (**Figures 3H–U**). This suggests that some effectors translocated by the T3SS could activate plant defense reactions in these two species, thereby preventing infection and the development of nodules. Similar stimulation of plant immunity probably also occurred in *M. atropurpureum* but to a lesser extent, since the nodules induced by the WT strain were well formed, but displayed brown necrotic areas. The bacteroids in these areas were dead as revealed by the red PI staining, whereas the Ω*rhcN* nodules were perfectly normal and the host cells were filled with viable bacteroids, as revealed by the green of GFP tagging cells (**Figures 3V–AB**). Nevertheless, while the T3SS mutation made it possible to restore nodule formation capacity in *V. radiata* and *C. juncea*, only very weak nitrogenase activity was detected, and no real benefit for plant growth was observed (**Figures 3N,U** and Supplementary Table S3). This shows that other restrictions exist between DOA9 and these two plant species resulting in inefficient symbiosis.

Only one species, *S. hamata*, was attributed to category 3, corresponding to a negative effect of the *rhcN* mutation.

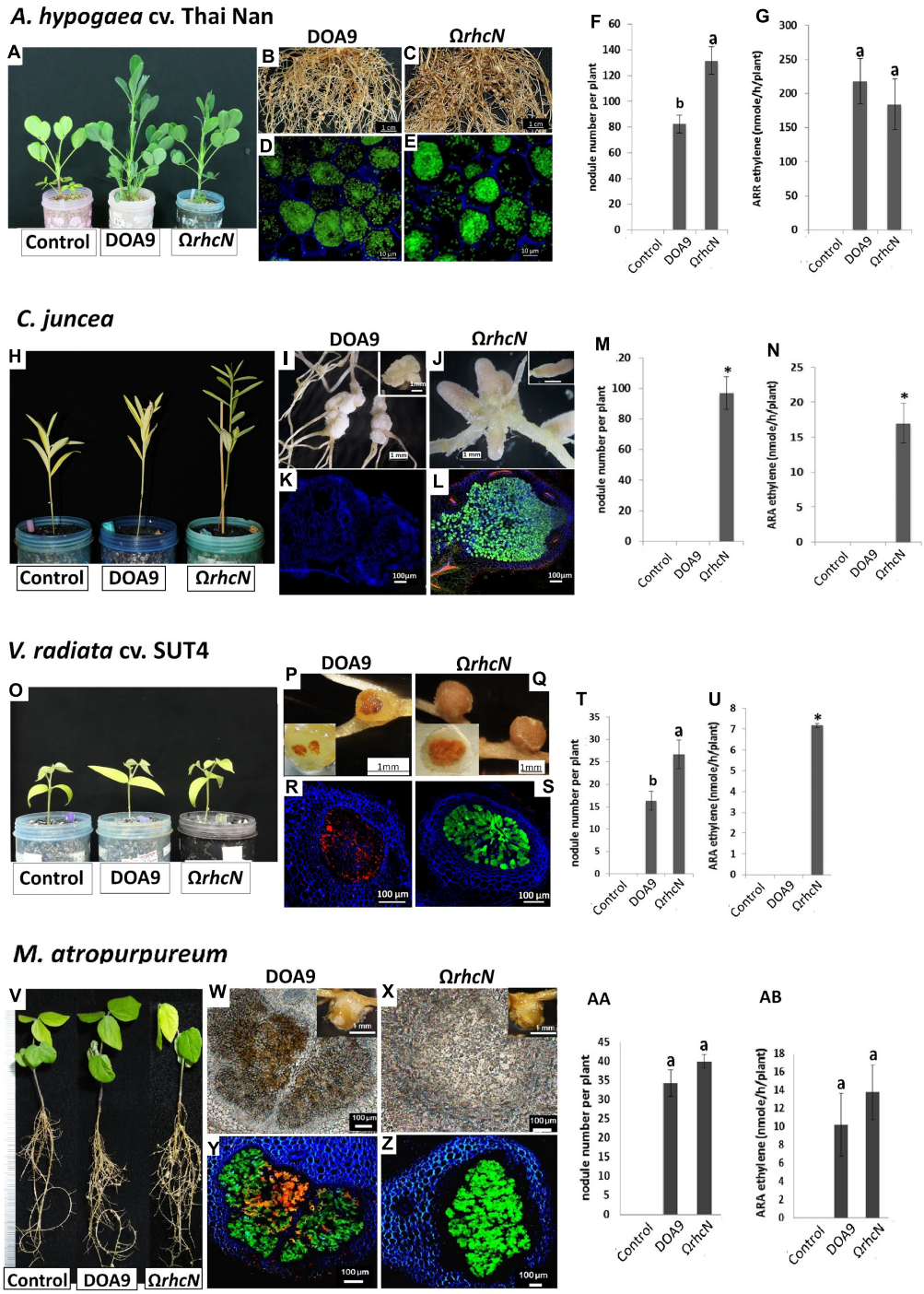

FIGURE 3 | Symbiotic analysis of legume species displaying a positive phenotype with the T3SS mutant of DOA9 strain. Plant growth, cytological aspect of the nodules, number of nodules per plant, and the ARA activity of *A. hypogaea* cv. Thai Nan **(A–G)**, *C. juncea* **(H–N)**, *V. radiata* cv. SUT4 **(O–U)**, and *M. atropurpureum* (siratro) **(V–AB)** after inoculation with the WT strain and the Ω*rhcN* mutant. In **(D**,**E**,**L**,**R**,**S**,**Y**,**Z)**, dead cells are stained red with propidium iodide (PI). The green cells are viable cells labeled with GFP. Values represent mean ± SD ($n = 5$). Within treatment, means labeled with different letters are statistically different at $p < 0.05$.

The number of nodules and nitrogenase activity of nodules induced by the Ω*rhcN* strain were reduced by approximately 30% compared with the wild-type strain (**Figures 4A–G**). These data suggest that the T3SS of strain DOA9 also plays a positive role in the establishment of the symbiosis, most probably by translocating effectors that weaken the plant immune system.

We also examined the effect of root exudates on the expression of *rhcN* and *nopX* genes to determine whether the absence of

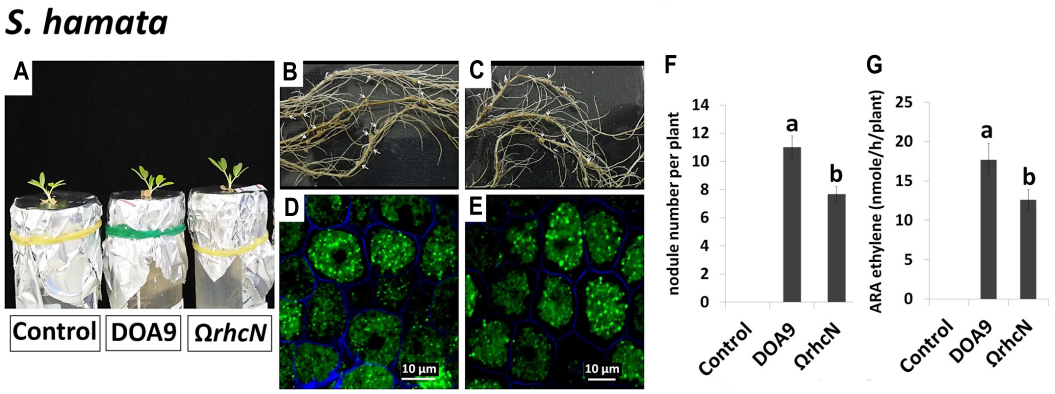

FIGURE 4 | Symbiotic analysis of legume species displaying a negative phenotype with the T3SS mutant of DOA9 strain. Plant growth, cytological aspect of the nodules, the number of nodules per plant, and ARA activity of *S. hamata* **(A–G)** after inoculation with the WT strain and the Ω*rhcN* mutant. Values represent mean ± SD ($n = 5$). Within treatment, means labeled with different letters are statistically different at $p < 0.05$.

phenotype observed for the *rhcN* mutant in some legume species could be linked with the absence of formation of the T3SS apparatus. As expected, a significant level of expression of the two T3SS genes was detected in the five species displaying a positive or negative phenotype with the Ω*rhcN* strain (Supplementary Figure S1). In contrast, of the four species that displayed no phenotype with the *rhcN* mutant, the root exudates of two of them (*I. tinctoria* and *D. tortuosum*) displayed a similar level of expression to the control without inducers raising the possibility that the T3SS machinery is not formed during the early steps of the interaction between the DOA9 strain and these two legumes species. We also took advantage of the promoterless *gusA* reporter gene present in the insertional pVO155 plasmid used to construct the *rhcN* mutant to determine whether the T3SS is expressed in mature nodules as already reported in *B. diazoefficiens* USDA110 nodulating soybean (Zehner et al., 2008). As shown in Supplementary Figure S2, for the three tested species (*A. americana*, *M. atropurpureum*, and *I. tinctoria*), a GUS activity was detected in the infected nodule cells, in contrast to the WT nodules, in which no activity was observed (Supplementary Figure S2). Altogether, these data suggest that T3SS genes of DOA9 strain are active during the early and/or late stages of symbiosis on the different species tested.

Role of the T3SS in Rice Colonization and Infection

We also investigated the effect of the T3SS mutation on the ability of DOA9 to colonize the surface of rice roots and to infect deep root tissue. These observations were made on a Thai rice (cultivar Pathum Thani 1) at the second and third week post-inoculation (wpi) (**Figure 5F**). The total population density of WT and Ω*rhcN* strains on the surface of the rice roots was almost the same (around 8 $\log_{10}$ CFU/g of root fresh weight), and this level of population remained constant at 2 and 3 wpi. When the roots were surface sterilized to conserve only the endophytic bacteria cells, the estimated population of both WT and mutant strains was also very close (around 4 $\log_{10}$ CFU/g root fresh weight). We also took advantage of the GFP tag added on the WT and Ω*rhcN* strains to monitor invasion of the roots. As can be seen in **Figures 5A–C,E**, both WT and Ω*rhcN* cells were attached to the root hairs and to the surface of the root epidermis. Analysis of root sections revealed endophytic bacterial cells in the intercellular space of the root cortex and endodermis. Taken together, these data suggest that the T3SS mutation did not affect the ability of the DOA9 strain to colonize and infect the rice root tissue intercellularly. This absence of effect of the T3SS mutation was not related to the absence of T3SS genes expression considering that a GUS activity could be detected at the surface of the rice roots inoculated with the *rhcN* mutant (**Figure 5D**).

DISCUSSION

The *Bradyrhizobium* sp. DOA9 strain isolated from a paddy field has been shown to have the ability to induce the development of symbiotic nodules in various legume species (Teamtisong et al., 2014). Unlike other bradyrhizobia, this strain contains a symbiotic megaplasmid (pDOA9) that harbors the *nod* and *nif* genes as well as a T3SS gene cluster (Okazaki et al., 2015). This T3SS cluster contains all the genes necessary for the formation of the secretory apparatus and the transcriptional activator (TtsI), which is preceded by a *nod*-box promoter motif. This genetic organization is similar to that described in other bradyrhizobial strains. Why DOA9 harbors a symbiotic plasmid while all the other *Bradyrhizobium* strains sequenced contain a symbiotic island remains an open question. In both cases, the lower GC content and the codon usage of the genes present in the symbiotic region suggest an acquisition by lateral transfer. This indicates that, in addition to the possibility of a difference in the origin of the symbiotic region, the mechanisms of its transfer and its maintenance inside the bacterial genome could also differ from one *Bradyrhizobium* strain to another.

Despite high conservation of T3SS genes encoding the injectisome, the T3SS effector contents of DOA9 strain differ from those in other bradyrhizobia, notably in their number,

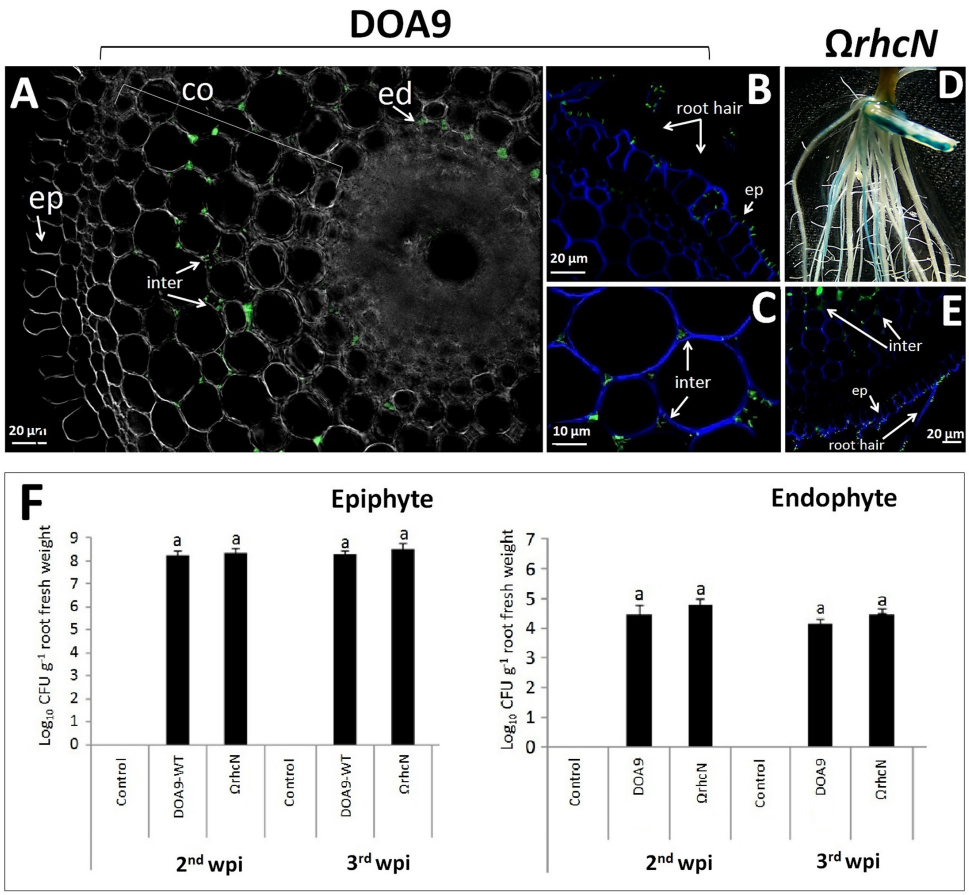

FIGURE 5 | Ability of DOA9 strain and its derivative T3SS mutant to colonize rice roots. Endophytic colonization of the rice roots by *Bradyrhizobium* sp. DOA9-WT **(A–C)** and T3SS mutant (Ω*rhcN*) **(D,E)** 24 h after inoculation. **(D)** Expression of the *gusA* reporter gene inserted in *rhcN* revealed on rice roots [2 week post-inoculation (wpi)] stained with X-Gluc after 3 h of incubation. The intercellular spaces (inter) of the cortex (co) and endodermis (ed) are occupied by endophytic cells. **(F)** Bacteria colonizing the root surface (epiphyte) and root tissue (endophyte) at 2 and 3 wpi with *Bradyrhizobium* sp. DOA9 and T3SS mutant (Ω*rhcN*) strains. Values represent mean ± SD ($n = 3$). Within treatment, means labeled with different letters are statistically different at $p < 0.05$.

which is comparatively lower. Indeed, in the DOA9 strain, only 14 candidate effector proteins have been predicted versus between 30 and 35 putative effectors in other bradyrhizobia (Zehner et al., 2008; Kimbrel et al., 2013). In particular, the effectors NopM and NopE, classically found in *Bradyrhizobium* strains, often as multicopies, are clearly absent in the DOA9 genome. Conversely, three putative effectors that were not previously identified in rhizobia are predicted in the DOA9 strain. These three new putative effectors proteins (WP_042337156, WP_025038828, and GAJ3805) most probably correspond to SUMO peptidases that contain the catalytic domain of members of the family of C48 cysteine proteases involved in the de-ubiquitinization of eukaryotic proteins (Hotson et al., 2003). Interestingly, a SUMO peptidase protein named NopD in *S. fredii* HH103 was identified to be secreted through the T3SS in the culture supernatant indicating that this family protein could constitute *bona fide* effectors translocated into the host cell (Rodrigues et al., 2007). Furthermore, more recently, other SUMO protease putative effectors were reported to be responsible for the incompatibility of some *Bradyrhizobium* strains (*B. japonicum* Is-1 and *B. elkanii* USDA61), which prevents them from interacting symbiotically with Rj4 genotype soybeans (Faruque et al., 2015; Tsurumaru et al., 2015). Taken together, this reinforces the hypothesis that the three new Nop candidats identified in DOA9 strain are effectors that could also affect the ability to interact with some plants.

It has previously been shown that T3SS in bradyrhizobia can have a positive or negative effect on nodule formation by stimulating or repressing the plant immune system depending on the host plant. For example, the deletion of T3SS in *B. diazoefficiens* delayed nodulation on soybean and reduced the number of nodules on *M. atropurpureum* (Krause et al., 2002), while the absence of T3SS in *B. elkanii* USDA61 induced the formation of nodules on *V. radiata* L. cv. KPS1 and on the soybean cultivar Hill, which contains the Rj4 allele (Okazaki et al., 2009). In the present study, we observed that the T3SS mutation affected the ability of DOA9 strain to interact with five out of the nine species tested. In particular, the T3SS mutation dramatically improved nodule formation and development in *C. juncea* and *V. radiata* and had a more moderate but also positive impact

on nodulation in *A. hypogaea* and *M. atropurpureum*. This suggests that among the cocktail of effectors that are translocated into the host cell, some are recognized as virulence factors by R-proteins and block infection and nodule organogenesis to a greater or lesser extent. As previously mentioned above, some SUMO protease effectors and also NopT have been observed to act as negative effectors in some hosts (Dai et al., 2008), which raises the possibility that the effector(s) responsible for this incompatibility could be one or some of the new effectors identified in the DOA9 strain or even NopT, which is also present in DOA9.

Conversely, the T3SS mutation had a negative impact on the number of nodules elicited on *S. hamata*, suggesting, in this case, that some effectors act positively on the symbiosis most probably, either by helping the bacteria to overcome plant defense reactions that limit the interaction or by directly inducing the nodulation signaling pathway as recently described for some non-photosynthetic bradyrhizobia shown to nodulate some legume species in the absence of NFs synthesis but thanks to the T3SS (Okazaki et al., 2013, 2016).

Identifying the effectors responsible for these contrasted symbiotic effects depending on the host plant, and understanding their role are real challenges. To date, a specific role in the symbiosis has been described for only a few effectors (Staehelin and Krishnan, 2015). One limitation is that the different effectors translocated into the host cell mostly act synergistically by interfering in different plant defense pathways. The DOA9 strain may be an ideal model to study the specific role of effectors individually or in combination. Indeed, all the symbiotic determinants are found on the pDOA9 plasmid and it has been possible to create a plasmid-free DOA9 strain (Tittabutr, personal communication). We can imagine designing plasmids encompassing a minimum set of canonical *nod*, *nif*, and T3SS injectisome genes supplemented by different combinations of effectors and to study the symbiotic properties of a DOA9 strain lacking pDOA9 in which these synthetic plasmids are re-introduced. This kind of approach may seem too ambitious and time consuming, but with the development of synthetic biology and a reduction in the cost of synthetizing DNA, it could be feasible in the near future.

Among the four species in which the T3SS mutation had no effect on the symbiosis, we observed that the root exudate of two of them (*I. tinctoria* and *D. tortuosum*) did not induce the expression of *nopX* and *rhcN* genes, suggesting that the T3SS apparatus is not formed during the early stages of the symbiosis between the DOA9 strain and these two species. These results were surprising considering that these two species were found to be nodulated by the DOA9 strain, indicating that the *nod* genes are expressed. It would be interesting to explore more deeply the regulation of the T3SS and *nod* genes in presence of flavonoids and root exudates to determine if decoupling between their expression is possible. In the same vein, we observed that some putative T3SS effector genes are not preceded by a *tts*-box, which raises the question of whether these genes are expressed when the T3SS is formed or if their regulation involves another activator than TtsI. The observation that T3SS genes were found expressed in mature nodules while they were not found activated by root exudates is also puzzling. This could be related to the fact that we used different technics to analyze genes expression or that the technic of extraction of root exudate was not adapted for *I. tinctoria* considering that this very small plant do not grow well in liquid medium. We cannot also exclude the possibility that the regulation of the T3SS genes could be more complex involving other input signals than flavonoids and additional regulators than NodD and TtsI leading to different gene expression controls during the early and late stages of symbiosis.

Finally, given that a previous study focusing on the SUTN9-2 strain showed that the T3SS is an important determinant in rice infection (Piromyou et al., 2015b), we also investigated if the T3SS plays a similar role during the interaction between the DOA9 strain and rice. However, despite the use of the same cultivar (Pathum Thani 1), our observations indicate that the T3SS mutation does not affect the ability of DOA9 strain to colonize the root surface and to infect the root tissue intercellularly. This result was surprising given that the two strains were isolated from similar ecological niches (Thai paddy fields using *A. americana* as trap legumes) and considering that we observed that the T3SS genes are active during the interaction of DOA9 strain with rice. These two strains differ in the origin of the symbiotic region, which harbors a different cortege of *nod* and *nop* genes. We can suppose that during evolution, each strain adapted this symbiotic toolbox differently as a function of the variety of plant partners it encountered during its life history. This might explain why, via a different cocktail of effectors, the same T3SS machinery can lead to different responses from one strain to another and from one host to another.

AUTHOR CONTRIBUTIONS

PS, PT, NB, EG, and NT conceived the experiment(s). PS, RN, KT, JP, AT, PT, and PP conducted the experiment(s). PS, PT, EG, and NT analyzed the result(s) and wrote the paper. All authors reviewed the manuscript.

FUNDING

This work was financially supported by Suranaree University of Technology (OROG), the Franco-Thai Cooperation Program in Higher Education and Research (PHC SIAM 2017 – No. 38280WF) and by the ANR, grant "SymEffectors" number ANR-16-CE20-0013.

ACKNOWLEDGMENT

The authors would like to thank Dr. Issra Pramoolsook for advice and comments on the language of the manuscript.

SUPPLEMENTARY MATERIAL

The Supplementary Material for this article can be found online at: http://journal.frontiersin.org/article/10.3389/fmicb.2017.01810/full#supplementary-material

REFERENCES

Bartsev, A. V., Deakin, W. J., Boukli, N. M., McAlvin, C. B., Stacey, G., Malnoe, P., et al. (2004). NopL, an effector protein of *Rhizobium* sp. NGR234, thwarts activation of plant defense reactions. *Plant Physiol.* 134, 871–879. doi: 10.1104/pp.103.031740

Bonaldi, K., Gherbi, H., Franche, C., Bastien, G., Fardoux, J., Barker, D., et al. (2010). The Nod factor-independent symbiotic signaling pathway development of Agrobacterium rhizogenes-mediated transformation for the legume *Aeschynomene indica*. *Mol. Plant Microbe Interact.* 23, 1537–1544. doi: 10.1094/MPMI-06-10-0137

Dai, W. J., Zeng, Y., Xie, Z. P., and Staehelin, C. (2008). Symbiosis-promoting and deleterious effects of NopT, a novel type 3 effector of *Rhizobium* sp. strain NGR234. *J. Bacteriol.* 190, 5101–5110. doi: 10.1128/JB.00306-08

de Lyra Mdo, C., Lopez-Baena, F. J., Madinabeitia, N., Vinardell, J. M., Espuny Mdel, R., Cubo, M. T., et al. (2006). Inactivation of the *Sinorhizobium fredii* HH103 *rhcJ* gene abolishes nodulation outer proteins (Nops) secretion and decreases the symbiotic capacity with soybean. *Int. Microbiol.* 9, 125–133.

Duncan, D. B. (1955). Multiple range and multiple F tests. *Biometrics* 11, 1–42. doi: 10.2307/3001478

Eddy, S. R. (1998). Profile hidden Markov models. *Bioinformatics* 14, 755–763. doi: 10.1093/bioinformatics/14.9.755

Ehrhardt, D. W., Atkinson, E. M., and Long, S. R. (1992). Depolarization of alfalfa root hair membrane potential by *Rhizobium meliloti* Nod factors. *Sci. (New York, NY)* 256, 998–1000. doi: 10.1126/science.10744524

Faruque, O. M., Miwa, H., Yasuda, M., Fujii, Y., Kaneko, T., Sato, S., et al. (2015). Identification of *Bradyrhizobium elkanii* genes involved in incompatibility with soybean plants carrying the Rj4 allele. *Appl. Environ. Microbiol.* 81, 6710–6717. doi: 10.1128/AEM.01942-15

Gibson, K. E., Kobayashi, H., and Walker, G. C. (2008). Molecular determinants of a symbiotic chronic infection. *Annu. Rev. Genet.* 42, 413–441. doi: 10.1146/annurev.genet.42.110807.091427

Giraud, E., Lavergne, J., and Vermeglio, A. (2010). Characterization of bacteriophytochromes from photosynthetic bacteria: Histidine kinase signaling triggered by light and redox sensing. *Methods Enzymol.* 471, 135–159. doi: 10.1016/S0076-6879(10)71009-0

Gourion, B., Berrabah, F., Ratet, P., and Stacey, G. (2015). Rhizobium-legume symbioses: the crucial role of plant immunity. *Trends Plant Sci.* 20, 186–194. doi: 10.1016/j.tplants.2014.11.008

Haag, A. F., Baloban, M., Sani, M., Kerscher, B., Pierre, O., Farkas, A., et al. (2011). Protection of Sinorhizobium against host cysteine-rich antimicrobial peptides is critical for symbiosis. *PLOS Biol.* 9:e1001169. doi: 10.1371/journal.pbio.1001169

Hoagland, D. R., and Arnon, D. I. (1950). *The Water-Culture Method for Growing Plants Without Soil*. Oakland, CA: University of California.

Hotson, A., Chosed, R., Shu, H., Orth, K., and Mudgett, M. B. (2003). *Xanthomonas* type III effector XopD targets SUMO-conjugated proteins in planta. *Mol. Microbiol.* 50, 377–389. doi: 10.1046/j.1365-2958.2003.03730.x

Hubber, A., Vergunst, A. C., Sullivan, J. T., Hooykaas, P. J. J., and Ronson, C. W. (2004). Symbiotic phenotypes and translocated effector proteins of the *Mesorhizobium loti* strain R7A VirB/D4 type IV secretion system. *Mol. Microbiol.* 54, 561–574. doi: 10.1111/j.1365-2958.2004.04292.x

Janczarek, M., Rachwał, K., Marzec, A., Grządziel, J., and Palusinska-Szysz, M. (2015). Signal molecules and cell-surface components involved in early stages of the legume-rhizobium interactions. *Appl. Soil Ecol.* 85, 94–113. doi: 10.1016/j.apsoil.2014.08.010

Jiménez-Guerrero, I., Pérez-Montaño, F., Monreal, J. A., Preston, G. M., Fones, H., Vioque, B., et al. (2015). The *Sinorhizobium (Ensifer) fredii* HH103 Type 3 secretion system suppresses early defense responses to effectively nodulate soybean. *Mol. Plant Microbe Interact.* 28, 790–799. doi: 10.1094/MPMI-01-15-0020-R

Kawaharada, Y., Kelly, S., Nielsen, M. W., Hjuler, C. T., Gysel, K., Muszyński, R. W., et al. (2015). Receptor-mediated exopolysaccharide perception controls bacterial infection. *Nature* 523, 308–312. doi: 10.1038/nature14611

Kimbrel, J. A., Thomas, W. J., Jiang, Y., Creason, A. L., Thireault, C. A., Sachs, J. L., et al. (2013). Mutualistic co-evolution of type III effector genes in *Sinorhizobium fredii* and *Bradyrhizobium japonicum*. *PLOS Pathog.* 9:e1003204. doi: 10.1371/journal.ppat.1003204

Krause, A., Doerfel, A., and Gottfert, M. (2002). Mutational and transcriptional analysis of the type III secretion system of *Bradyrhizobium japonicum*. *Mol. Plant Microbe Interact.* 15, 1228–1235. doi: 10.1094/MPMI.2002.15.12.1228

Krishnan, H. B., Lorio, J., Kim, W. S., Jiang, G., Kim, K. Y., DeBoer, M., et al. (2003). Extracellular proteins involved in soybean cultivar-specific nodulation are associated with pilus-like surface appendages and exported by a type III protein secretion system in *Sinorhizobium fredii* USDA257. *Mol. Plant Microbe Interact.* 16, 617–625. doi: 10.1094/MPMI.2003.16.7.617

Laguerre, G., Heulin-Gotty, K., Brunel, B., Klonowska, A., Le Quéré, A., Tillard, P., et al. (2012). Local and systemic N signaling are involved in *Medicago truncatula* preference for the most efficient Sinorhizobium symbiotic partners. *New Phytol.* 195, 437–449. doi: 10.1111/j.1469-8137.2012.04159.x

López-Baena, F. J., Monreal, J. A., Pérez-Montaño, F., Guasch-Vidal, B., Bellogín, R. A., Vinardell, J. M., et al. (2009). The absence of Nops secretion in *Sinorhizobium fredii* HH103 increases GmPR1 expression in Williams soybean. *Mol. Plant Microbe Interact.* 22, 1445–1454. doi: 10.1094/MPMI-22-11-1445

Marie, C., Broughton, W. J., and Deakin, W. J. (2001). *Rhizobium* type III secretion systems: legume charmers or alarmers? *Curr. Opin. Plant Biol.* 4, 336–342. doi: 10.1016/S1369-5266(00)00182-5

Marie, C., Deakin, W. J., Ojanen-Reuhs, T., Diallo, E., Reuhs, B., Broughton, W. J., et al. (2004). TtsI, a key regulator of *Rhizobium* species NGR234 is required for type III-dependent protein secretion and synthesis of rhamnose-rich polysaccharides. *Mol. Plant Microbe Interact.* 9, 958–966. doi: 10.1094/MPMI.2004.17.9.958

Marie, C., Deakin, W. J., Viprey, V., Kopciñska, J., Golinowski, W., Krishnan, H. B., et al. (2003). Characterization of Nops, nodulation outer proteins, secreted via the type III secretion system of NGR234. *Mol. Plant Microbe Interact.* 16, 743–751. doi: 10.1094/MPMI.2003.16.9.743

Noisangiam, R., Teamtisong, K., Tittabutr, P., Boonkerd, N., Toshiki, U., Minamisawa, K., et al. (2012). Genetic diversity, symbiotic evolution, and proposed infection process of *Bradyrhizobium* strains isolated from root nodules of *Aeschynomene americana* L. in Thailand. *Appl. Environ. Microbiol.* 78, 6236–6250. doi: 10.1128/AEM.00897-12

Okazaki, S., Kaneko, T., Sato, S., and Saeki, K. (2013). Hijacking of leguminous nodulation signaling by the rhizobial type III secretion system. *Proc. Natl. Acad. Sci. U.S.A.* 110, 17131–17136. doi: 10.1073/pnas.1302360110

Okazaki, S., Noisangiam, R., Okubo, T., Kaneko, T., Oshima, K., Hattori, M., et al. (2015). Genome analysis of a novel *Bradyrhizobium* sp. DOA9 carrying a symbiotic plasmid. *PLOS ONE* 10:e0117392. doi: 10.1371/journal.pone.0117392

Okazaki, S., Okabe, S., Higashi, M., Shimoda, Y., Sato, S., Tabata, S., et al. (2010). Identification and functional analysis of type III effector proteins in *Mesorhizobium loti*. *Mol. Plant Microbe Interact.* 23, 223–234. doi: 10.1094/MPMI-23-2-0223

Okazaki, S., Tittabutr, P., Teulet, A., Thouin, J., Fardoux, J., Chaintreuil, C., et al. (2016). *Rhizobium*-legume symbiosis in the absence of Nod factors: two possible scenarios with or without the T3SS. *ISME J.* 1, 64–74. doi: 10.1038/ismej.2015.103

Okazaki, S., Zehner, S., Hempel, J., Lang, K., and Gottfert, M. (2009). Genetic organization and functional analysis of the type III secretion system of *Bradyrhizobium elkanii*. *FEMS Microbiol. Lett.* 295, 88–95. doi: 10.1111/j.1574-6968.2009.01593.x

Oke, V., and Long, S. R. (1999). Bacterial genes induced within the nodule during the Rhizobium-legume symbiosis. *Mol. Microbiol.* 32, 837–849. doi: 10.1046/j.1365-2958.1999.01402.x

Oldroyd, G. E., Murray, J. D., Poole, P. S., and Downie, J. A. (2011). The rules of engagement in the legume-rhizobial symbiosis. *Annu. Rev. Genet.* 45, 119–144. doi: 10.1146/annurev-genet-110410-132549

Piromyou, P., Greetatorn, T., Teamtisong, K., Okubo, T., Shinoda, R., Nuntakij, A., et al. (2015a). Preference of endophytic bradyrhizobia in different rice cultivars and the implication of rice endophyte evolution. *Appl. Environ. Microbiol.* 81, 3049–3061. doi: 10.1128/AEM.04253-14

Piromyou, P., Songwattana, P., Greetatorn, T., Okubo, T., Kakizaki, K. C., Prakamhang, J., et al. (2015b). The type III secretion system (T3SS) is a determinant for rice-endophyte colonization by non-photosynthetic *Bradyrhizobium*. *Microbes Environ.* 30, 291–300. doi: 10.1264/jsme2.ME15080

Rodrigues, J. A., López-Baena, F. J., Ollero, F. J., Vinardell, J. M., Espuny, M., del, R., et al. (2007). NopM and NopD are rhizobial nodulation outer proteins:

identification using LC-MALDI and LC-ESI with a monolithic capillary column. *J. Proteome Res.* 6, 1029–1037. doi: 10.1021/pr060519f

Sambrook, J., Fritsch, E. F., and Maniatis, T. (2001). *Molecular Cloning: A Laboratory Manual*. Cold Spring Harbor, NY: Cold Spring Harbor Laboratory Press.

Somasegaran, P., and Hoben, H. J. (1994). *Handbook for Rhizobia: Methods in Legume-Rhizobium Technology*. Berlin: Springer-Verlag.

Staehelin, C., and Krishnan, H. B. (2015). Nodulation outer proteins: double-edged swords of symbiotic rhizobia. *Biochem. J.* 470, 263–274. doi: 10.1042/BJ20150518

Tampakaki, A. P. (2014). Commonalities and differences of T3SSs in rhizobia and plant pathogenic bacteria. *Front. Plant Sci.* 5:114. doi: 10.3389/fpls.2014.00114

Teamtisong, K., Songwattana, P., Noisangiam, R., Piromyou, P., Boonkerd, N., Tittabutr, P., et al. (2014). Divergent nod-containing *Bradyrhizobium* sp. DOA9 with a megaplasmid and its host range. *Microbes Environ.* 29, 370–376. doi: 10.1264/jsme2.ME14065

Tsurumaru, H., Hashimoto, S., Okizaki, K., Kanesaki, Y., Yoshikawa, H., and Yamakawa, T. (2015). A putative type III secretion system effector encoded by the MA20_12780 gene in *Bradyrhizobium japonicum* Is-34 causes incompatibility with Rj4 genotype soybeans. *Appl. Environ. Microbiol.* 81, 5812–5819. doi: 10.1128/AEM.00823-15

Vincent, J. (1970). *A Manual for the Practical Study of Root-Nodule Bacteria*. Oxford: Blackwell Scientific Publications.

Viprey, V., Del-Greco, A., Golinowski, W., Broughton, W., and Perret, X. (1998). Symbiotic implications of type III protein secretion machinery in *Rhizobium*. *Mol. Microbiol.* 28, 1381–1389. doi: 10.1046/j.1365-2958.1998.00920.x

Wongdee, J., Songwattana, P., Nouwen, N., Noisangiam, R., Fardoux, J., Chaintreuil, C., et al. (2016). nifDK clusters located on the chromosome and megaplasmid of *Bradyrhizobium* sp. strain DOA9 contribute differently to nitrogenase activity during symbiosis and free-living growth. *Mol. Plant Microbe Interact.* 29, 767–773. doi: 10.1094/MPMI-07-16-0140-R

Yang, S., Tang, F., Gao, M., Krishnan, H. B., and Zhu, H. (2010). *R* gene-controlled host specificity in the legume-rhizobia symbiosis. *Proc. Natl. Acad. Sci. U.S.A.* 107, 18735–18740. doi: 10.1073/pnas.1011957107

Yasuda, M., Miwa, H., Masuda, S., Takebayashi, Y., Sakakibara, H., and Okazaki, S. (2016). Effector-triggered immunity determines host genotype-specific incompatibility in legume-Rhizobium symbiosis. *Plant Cell Physiol.* 57, 1791–1800. doi: 10.1093/pcp/pcw104

Zehner, S., Schober, G., Wenzel, M., Lang, K., and Göttfert, M. (2008). Expression of the *Bradyrhizobium japonicum* type III secretion system in legume nodules and analysis of the associated tts-box promoter. *Mol. Plant Microbe Interact.* 21, 1087–1093. doi: 10.1094/MPMI-21-8-1087

Conflict of Interest Statement: The authors declare that the research was conducted in the absence of any commercial or financial relationships that could be construed as a potential conflict of interest.

frontiers in Plant Science

ORIGINAL RESEARCH
published: 20 August 2018
doi: 10.3389/fpls.2018.01218

Distinct *Lotus japonicus* Transcriptomic Responses to a Spectrum of Bacteria Ranging From Symbiotic to Pathogenic

Simon Kelly[1], *Terry Mun*[1], *Jens Stougaard*[1], *Cécile Ben*[2] *and Stig U. Andersen*[1]*

[1] Department of Molecular Biology and Genetics, Aarhus University, Aarhus, Denmark, [2] ECOLAB, Université de Toulouse, CNRS, INP, UPS, Toulouse, France

Lotus japonicus is a well-studied nodulating legume and a model organism for the investigation of plant-microbe interactions. The majority of legume transcriptome studies have focused on interactions with compatible symbionts, whereas responses to non-adapted rhizobia and pathogenic bacteria have not been well-characterized. In this study, we first characterized the transcriptomic response of *L. japonicus* to its compatible symbiont, *Mesorhizobium loti* R7A, through RNA-seq analysis of various plant tissues. Early symbiotic signaling was largely Nod factor-dependent and enhanced within root hairs, and we observed large-scale transcriptional reprogramming in nodule primordia and mature nitrogen-fixing nodules. We then characterized root transcriptional responses to a spectrum of *L. japonicus* interacting bacteria ranging from semi-compatible symbionts to pathogens. *M. loti* R7A and the semi-compatible strain *Sinorhizobium fredii* HH103 showed remarkably similar responses, allowing us to identify a small number of genes potentially involved in differentiating between fully and semi-compatible symbionts. The incompatible symbiont *Bradyrhizobium elkanii* USDA61 induced a more attenuated response, but the weakest response was observed for the foliar pathogen *Pseudomonas syringae* pv. *tomato* DC3000, where the affected genes also responded to other tested bacteria, pointing to a small set of common bacterial response genes. In contrast, the root pathogen *Ralstonia solanacearum* JS763 induced a pronounced and distinct transcriptomic pathogen response, which we compared to the results of the other treatments. This comparative analysis did not support the concept that an early defense-like response is generally evoked by compatible rhizobia during establishment of symbiosis.

Keywords: symbiosis, nodulation, RNA-seq, pathogen, legume, nitrogen fixation, plant-microbe interaction, rhizobia

OPEN ACCESS

Edited by:
Benjamin Gourion, UMR 2594, Laboratoire des Interactions Plantes-Microorganismes (LIPM), France

Reviewed by:
Ulrike Mathesius, Australian National University, Australia
Yangrong Cao, Huazhong Agricultural University, China
Jeremy Dale Murray, Shanghai Institutes for Biological Sciences (CAS), China

***Correspondence:**
Stig U. Andersen
sua@mbg.au.dk

Specialty section:
This article was submitted to Plant Microbe Interactions, a section of the journal Frontiers in Plant Science

Received: *22 March 2018*
Accepted: *30 July 2018*
Published: *20 August 2018*

Citation:
Kelly S, Mun T, Stougaard J, Ben C and Andersen SU (2018) Distinct Lotus japonicus Transcriptomic Responses to a Spectrum of Bacteria Ranging From Symbiotic to Pathogenic. Front. Plant Sci. 9:1218. doi: 10.3389/fpls.2018.01218

INTRODUCTION

Lotus japonicus develops determinate root nodules in association with its compatible rhizobia *Mesorhizobium loti*. Establishment of an effective nitrogen-fixing symbiosis requires molecular communication to ensure compatibility and coordinate the developmental processes of rhizobial infection and nodule organogenesis with legume LysM-receptor kinases playing an integral role in

these processes (Madsen et al., 2010; Oldroyd et al., 2011; Kelly et al., 2017a). Nod factor (NF) is the key signal molecule produced by rhizobia (Long, 1996) and is perceived by a NF receptor complex, which in *Lotus* consists of NFR1, NFR5 and SYMRK (Madsen et al., 2003; Radutoiu et al., 2003; Broghammer et al., 2012; Antolin-Llovera et al., 2014). Perception of compatible NF results in rapid physiological and transcriptional responses in the host (Desbrosses and Stougaard, 2011; Oldroyd, 2013). An additional level of compatibility scrutiny in *Lotus* occurs through the perception of rhizobial exopolysaccharides (EPSs) by the EPR3 receptor (Kelly et al., 2013; Kawaharada et al., 2015, 2017b).

Significant resources have been established to assist with investigations of *L. japonicus*. The genome sequence is available (Sato et al., 2008) as is an extensive *LORE1* retrotransposon mutant resource consisting of 150,000 lines that provides potential mutants for an estimated 90% of active protein coding genes (Malolepszy et al., 2016). A *Lotus japonicus* gene expression atlas (LjGEA) was established that incorporated and extended on available *Lotus* transcriptome data in response to rhizobia and abiotic stresses (Verdier et al., 2013). All of these genomic resources can now be accessed through *Lotus* Base (Mun et al., 2016). Comparable transcriptomic resources are available for the indeterminate nodulating model legume *Medicago truncatula* (Benedito et al., 2008) and additional significant transcriptome data for this host was provided by the specific analysis of root hairs, which revealed a role for auxin signaling in infection thread (IT) formation (Breakspear et al., 2014).

Transcriptome responses of *L. japonicus* to compatible rhizobia and arbuscular mycorrhiza form the bulk of host transcriptional data available, while responses to incompatible rhizobia and pathogens have been less well-defined. Microarray analysis has been performed on two *L. japonicus* ecotypes that show differing leaf phenotypes when challenged with *Pseudomonas syringae* pv. *tomato* DC3000 and the response to pathogenic fungal exudates has also been investigated, identifying potential defense related genes (Bordenave et al., 2013; Giovannetti et al., 2015).

The interplay between symbiotic and pathogenic responses in legumes has largely been investigated through co-inoculation experiments, which revealed a negative impact of pathogens and defense eliciting compounds on symbiotic efficiency (Lopez-Gomez et al., 2012; Chen et al., 2017). Analysis of a cDNA array of expressed sequence tags from *L. japonicus* at various time points after inoculation with *M. loti* TONO indicated that an initial defense-like transcriptional response in *L. japonicus* is subsequently dampened through symbiotic signaling. The identified defense-like genes encode hyper-sensitive related proteins, pathogenesis-related (PR) proteins, and proteins associated with phytoalexin biosynthesis and cell wall modification (Kouchi et al., 2004).

In this study, a comprehensive symbiotic transcriptomic response of *L. japonicus* to its compatible symbiont *M. loti* R7A and a spectrum of interacting bacteria was obtained through RNA-seq analysis, revealing distinct transcriptional responses and challenging the concept that an early defense-like response is evoked by compatible rhizobia in *L. japonicus* during the establishment of symbiosis.

MATERIALS AND METHODS

Plant Material and Growth Conditions

Lotus japonicus ecotype Gifu (Handberg and Stougaard, 1992) was used as the wild-type plant. Seed sterilization and plant-growth setups were as previously described (Kawaharada et al., 2015). For tissue-specific analysis of transcriptome responses to *M. loti* R7A, plants were grown at 21°C with a 16 h day and 8 h night cycle. For the analysis of transcriptome responses to a spectrum of interacting bacteria, plants were grown at 25°C with a 16 h day and 8 h night cycle. Plant growth plates, each containing 10 seedlings, were inoculated with 750 μL of OD_{600} = 0.02–0.05 bacterial suspensions along the length of the root. Purified *M. loti* R7A NF was obtained as previously described (Rodpothong et al., 2009) and used at 10^{-8} M for plant inoculation.

Bacterial Strains

Bacterial strains used in this study are listed in **Supplementary Table 1**. All strains were cultured at 28°C. *M. loti* R7A, *Bradyrhizobium elkanii* USDA61 and *Sinorhizobium fredii* HH103 were cultured in yeast mannitol broth (YMB) (Vincent, 1970), *Pseudomonas syringae* pv. *tomato* DC3000 in NYG medium (Daniels et al., 1984) and *Ralstonia solanacearum* JS763 in BGT medium (BG medium plus 0.005% tetrazolium chloride) (Saile et al., 1997). Antibiotics were added to media as required at the following concentrations: polymyxin, 50 μg mL^{-1}; rifampicin, 50 μg mL^{-1}; kanamycin, 50 μg mL^{-1}.

Plant Phenotyping

Phenotypic responses of *L. japonicus* to the spectrum of interacting bacteria was determined though observation of plants at weekly intervals following inoculation. Symbiotic phenotypes at 21 dpi were observed using a Zeiss Discovery V8 stereomicroscope. Disease responses, root-browning and wilting symptoms, of *L. japonicus* to *R. solanacearum* JS763 were analyzed at 5 and 29 dpi.

Plant Tissue Harvesting

Whole root samples were harvested by removing the root tip (∼3 mm), to minimize hormone and meristematic activity specific to the root tip, and then collecting roots in tubes immersed in liquid nitrogen. Each whole root sample consisted of 10 roots. Root hairs were harvested using a previously described method (Sauviac et al., 2005). Roots were separated from shoots and root tips were removed. Ten roots were transferred to 50 mL Falcon tubes immersed in liquid nitrogen and after 1 min were twice vortexed for 15 s, tubes were returned to liquid nitrogen between vortexing. Falcon tubes were gently tapped to collect root hairs in the bottom and tweezers were used to remove roots stripped of root hairs. The process was then repeated with another 10 roots and a total of 100 roots was processed for each sample. Nodule primordia were collected at 7 dpi using a

scalpel to slice through the root above and below the developing primordia. Excised primordia were collected in tubes immersed in liquid nitrogen and each sample represents the total primordia collected from 30 roots. Nodules collected at 21 dpi were gently separated from the root using tweezers and collected in tubes immersed in liquid nitrogen. Each sample represents the total nodules collected from 30 roots.

RNA Isolation, Library Preparation, and Sequencing

Total RNA was isolated from whole root, nodule primordia, and nodule tissue samples using a NucleoSpin® RNA Plant kit (Macherey-Nagel) according to the manufacturer's instructions. mRNA was directly isolated from root hair samples using a Dynabeads mRNA DIRECT kit (Thermo Fisher Scientific) according to the manufacturer's instructions. RNA quality was assessed on an Agilent 2100 Bioanalyser and samples were sent to GATC-Biotech[1] for library preparation and sequencing. Sequencing data is deposited at the Short Read Archive with the BioProject ID SRP127678. Sequencing data for roots and shoots 3 dpi with R7A was obtained previously (Munch et al., 2018) and is deposited at the Short Read Archive with the BioProject ID PRJNA384655.

Bioinformatics and Statistical Analysis

Reads were mapped to the *L. japonicus* v. 3.0 genome and differential gene expression was analyzed using CLC Genomics Workbench 9.5.3 (Qiagen). For each sample a minimum of 30 million reads were obtained with >90% of reads mapped to the reference genome. A criterion of fourfold change with a FDR p-value ≤ 0.05 was applied to determine differential gene expression. Results of the analysis are available on *Lotus* Base[2] (Mun et al., 2016). Multidimensional scaling (MDS) analysis was performed in R (R Core Team, 2017) from total read count data using the script outlined in **Supplementary Data 1**. Heatmaps were generated in R using Heatmap and Heatmap3 functions (Zhao et al., 2014), an example script is provided in **Supplementary Data 1**. Venn diagrams were constructed using BioVenn (Hulsen et al., 2008). Detection of differentially expressed genes was also performed using the R package DEGseq (Wang et al., 2010) with a criterion of fourfold change with a FDR p-value ≤ 0.05 to examine the effects of combining replicates from different time points.

RESULTS

Tissue-Specific Responses of *Lotus japonicus* to Its Compatible Symbiont *Mesorhizobium loti* R7A

A comprehensive transcriptome response of *L. japonicus* ecotype Gifu to its compatible symbiotic partner *M. loti* R7A was obtained through RNA-seq analysis of specific tissues at various stages of symbiosis. Initial interactions between rhizobia and the legume were investigated through the isolation of root hairs following R7A inoculation at 1 and 3 dpi. The NF-deficient strain R7A*nodC* was included to reveal the role of NF in these early responses, which was further examined through the isolation of purified NF-treated root hairs 2 days post-treatment. Root hair deformations of *L. japonicus* are evident as early as 24 h following inoculation with *M. loti* or treatment with purified NF (Radutoiu et al., 2003; Maekawa-Yoshikawa and Murooka, 2009). Transcriptome responses during nodule colonization were examined through the harvesting of 7 dpi nodule primordia that are in the early stages of colonization by R7A and mature nitrogen-fixing nodules that are fully colonized by R7A. RNA-seq of whole roots (minus root tips) and shoots collected at 3 dpi to provide a basis for tissue-specific responses was previously performed (Munch et al., 2018). For each condition examined, biological triplicate samples were harvested and total RNA was isolated. The reads were mapped to the *L. japonicus* v3.0 genome and all data is available from the *Lotus* Base resource website (Mun et al., 2016)[2].

Multidimensional scaling analysis clearly separated the samples based on their tissue origin (**Figure 1A**). A closer examination of whole root samples revealed a clear shift following R7A inoculation (**Figure 1B**). Most root hair samples separated into distinct groups depending on their treatment (**Figure 1C**). H_2O and R7A*nodC* samples clustered together, indicating that the majority of early root hair transcriptome responses to R7A are dependent on NF production. R7A treated root hairs formed a cluster with separation between the 1 and 3 dpi samples, while NF-treated root hairs formed a distinct cluster removed from the R7A inoculated samples.

The expression of a set of known symbiotic genes was examined in the different tissues in response to inoculation with R7A or NF treatment compared to H_2O-treated controls (**Figure 1D**). No difference in gene expression was observed in shoots 3 dpi with R7A or root hairs 1 dpi with the R7A*nodC* mutant compared to their respective controls, 3 dpi H_2O-treated shoots and 3 dpi H_2O-treated root hairs. Similar expression patterns were observed for R7A and NF treated root hair and root samples compared to control 3 dpi H_2O-treated root hairs. Symbiotic transcription factors, *Nin* (Schauser et al., 1999), *NfyaA1* (Soyano et al., 2013), and *Ern1* (Cerri et al., 2017; Kawaharada et al., 2017a; Yano et al., 2017) were strongly induced while *Nsp1* and *Nsp2* (Heckmann et al., 2006; Kawaharada et al., 2017a) showed only slight induction. The EPS receptor *Epr3* (Kawaharada et al., 2015, 2017b), pectate lyase *Npl* (Xie et al., 2012) and *Lotus* homologs of *Vapyrin* (Murray et al., 2011) and *Rpg* (Arrighi et al., 2008) that were identified as required for IT formation in *Medicago* were all strongly induced. Notably, *Rpg* was not induced until 3 dpi with R7A. The receptors involved in NF perception, *Nfr1*, *Nfr5,* and *Symrk* (Stracke et al., 2002; Radutoiu et al., 2003) showed little change in expression other than a slight downregulation in root hairs 3 dpi.

Nodule primordia, compared to control 3 dpi H_2O-treated roots, shared a similar expression pattern to root hair and root samples with the exception that the NF receptors *Nfr1* and *Nfr5* were downregulated. This downregulation of the NF receptors

[1] https://gatc-biotech.com

[2] https://lotus.au.dk

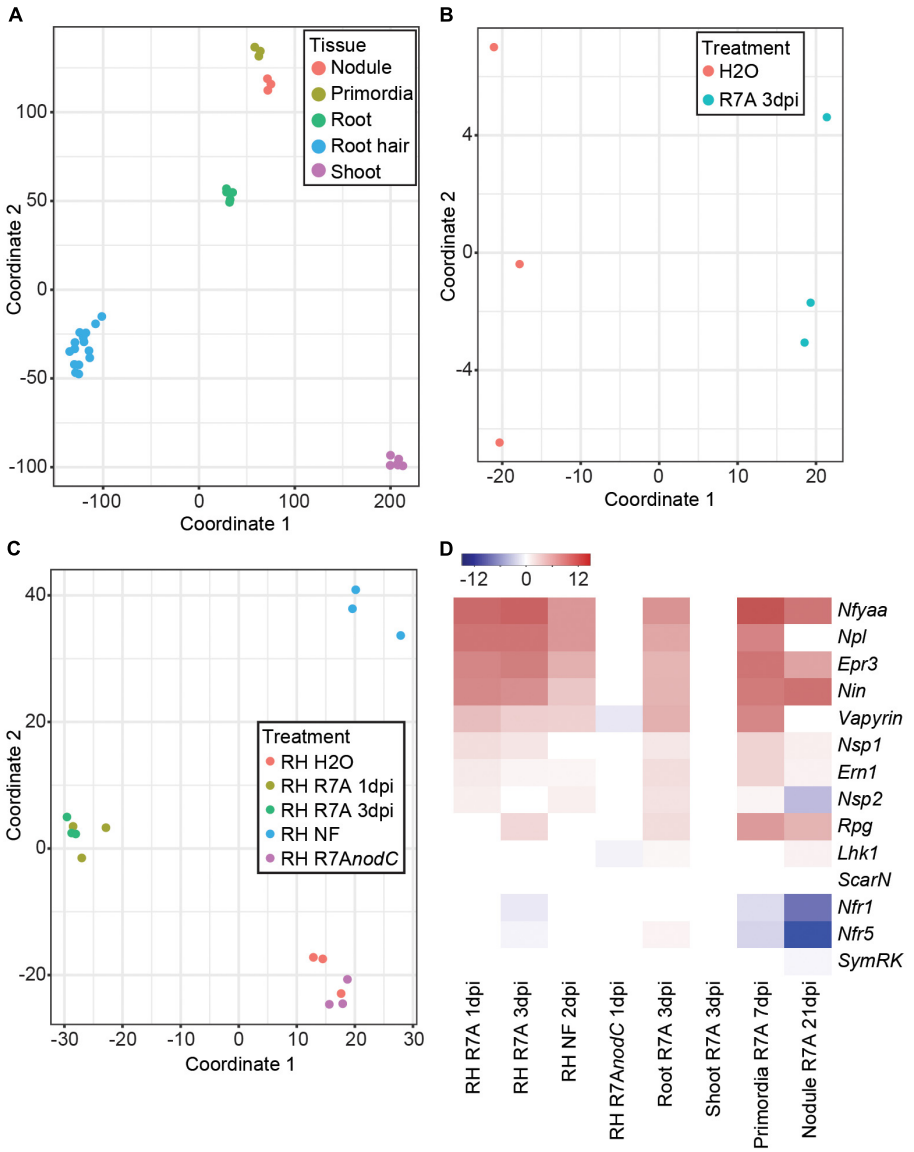

FIGURE 1 | *Lotus japonicus* tissue-specific responses to the compatible symbiont *Mesorhizobium loti* R7A. **(A)** MDS plot of *L. japonicus* tissue samples. **(B)** MDS plot of whole root samples following treatment with H_2O or R7A 3dpi. **(C)** MDS plot of all root hair samples following the indicated treatments. **(D)** Heatmap representation of $\log_2$ fold changes of various known symbiotic genes in tissues following treatment compared to H_2O controls. NF, Nod factor; RH, root hairs.

was stronger in the 21 dpi mature nodule samples compared to control 3 dpi H_2O-treated roots. The *Nsp2* transcription factor also showed downregulation in mature nodules and expression of *Epr3*, *Npl,* and *Vapyrin* was reduced compared to primordia, root hairs, and roots.

Early Symbiotic Responses Are Enhanced in Root Hairs and Largely Depend on Nod Factor Signaling

Predictably, significant overlap was observed in differentially expressed genes between root hairs harvested at 1 and 3 dpi compared to control 3 dpi H_2O-treated root hairs and whole roots at 3 dpi compared to control 3 dpi H_2O-treated whole roots (**Figure 2A**). Although expected symbiotic gene induction was observed in both tissues, the root hair samples showed enhanced transcriptional responses compared to whole roots (**Figure 1D** and **Supplementary Figure 1**). Among the most highly induced of the 93 genes identified as specifically differentially expressed within root hairs at 1 and 3 dpi compared to whole roots, we identified an aspartic protease and a calmodulin-binding protein as well as several blue copper proteins, expansins and pectinesterase/pectinesterase inhibitors (**Supplementary Table 2**). The root hair transcriptional changes observed in response to R7A are largely NF-dependent with root hairs inoculated with the NF-deficient R7A*nodC* strain sharing minimal overlap with R7A or NF treated samples

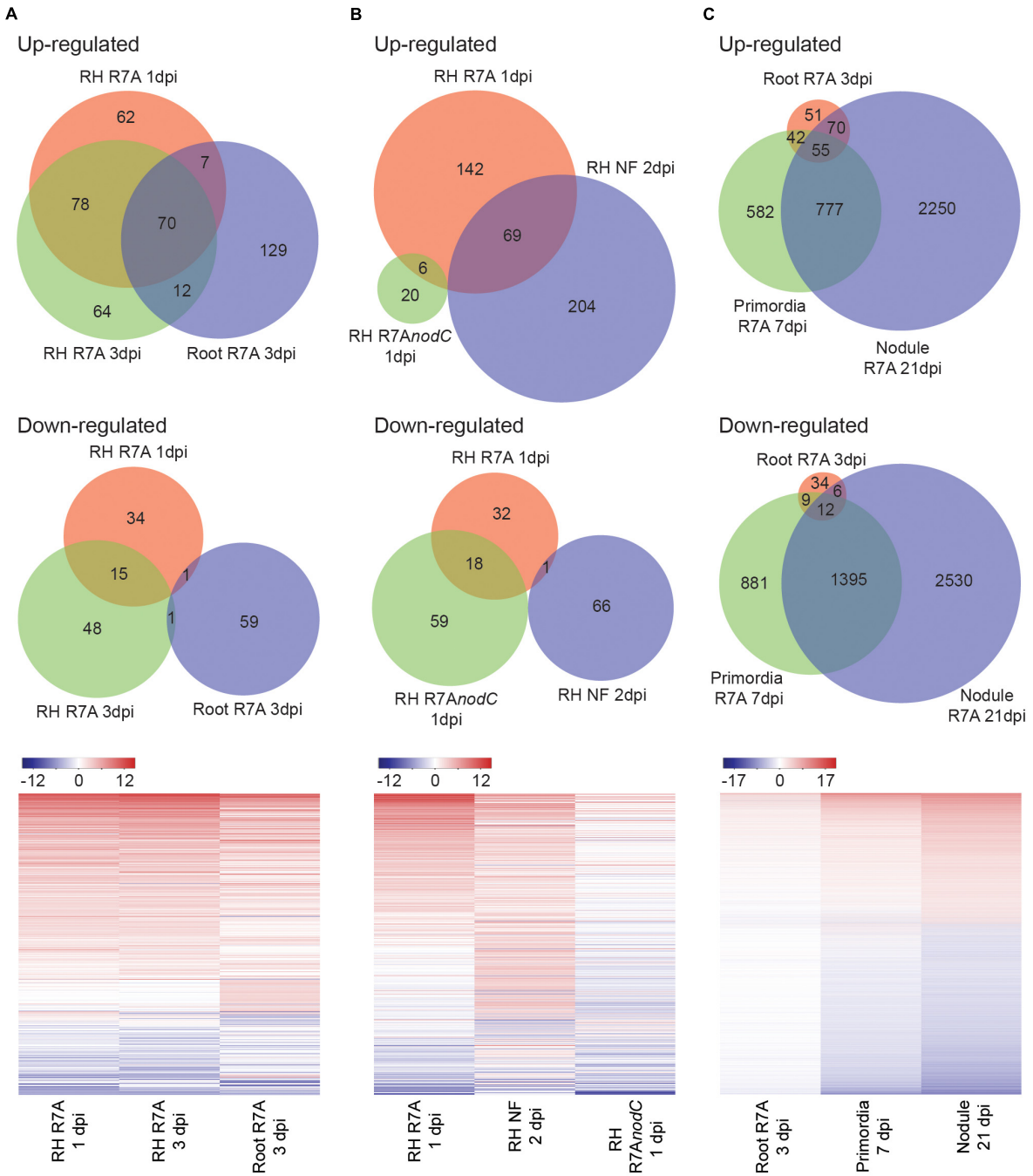

FIGURE 2 | *Lotus japonicus* tissue-specific responses to compatible *M. loti* R7A and Nod factor. Venn diagram and heatmap representation of differential gene expression in the indicated conditions compared to H_2O controls. Significant gene expression differences were designated based on a fourfold change in expression with a FDR *p*-value ≤ 0.05. **(A)** R7A induced gene expression in whole roots and root hairs. **(B)** NF-dependency of early root hair differential gene expression. **(C)** R7A induced gene expression in nodule primordia and mature nodules compared to whole roots. For heatmaps, Log_2 fold change values were used. NF, Nod factor; RH, root hairs.

(**Figure 2B**). Nodule primordia and mature nodules show a large transcriptional response compared to 3 dpi root samples with downregulation of genes more prominent than in other tissues investigated (**Figure 2C**).

Altogether, the tissue transcriptome data of *L. japonicus* responses to R7A provided here represents an important resource for future research into this determinate nodulating model system.

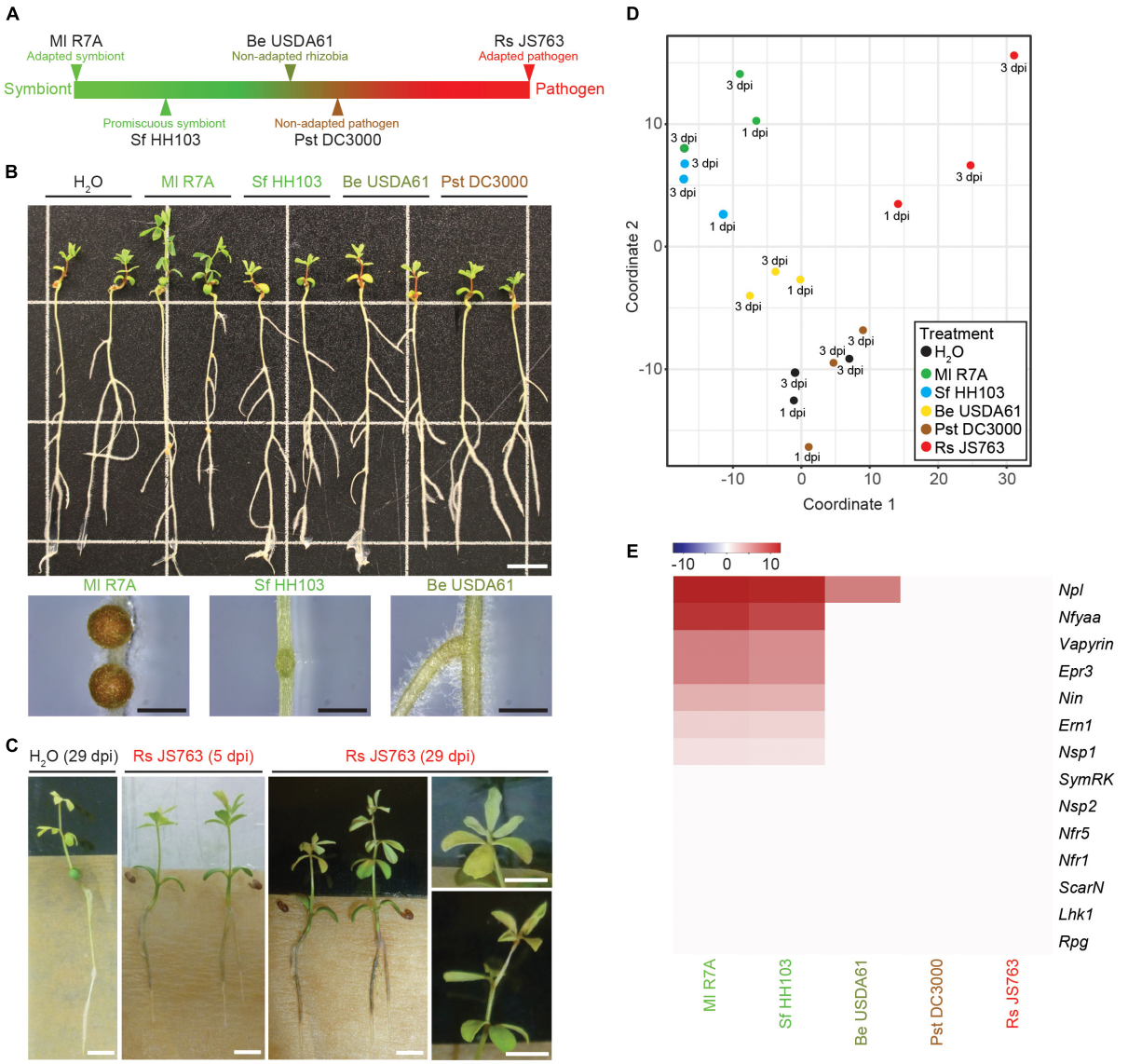

FIGURE 3 | *Lotus japonicus* responses to a spectrum of interacting bacteria ranging from compatible symbiont to pathogen. **(A)** Schematic representation of the positioning of investigated bacteria on a spectrum from compatible symbiont to pathogen. **(B)** Phenotypes of *L. japonicus* 21 dpi with the indicated strains. Close up images show the differences in nodule development induced by Ml R7A, Sf HH103, and Be USDA61. Scale bars are 1 cm in the whole plant image and 1 mm in nodule images. **(C)** Representative images of root-browning and shoot wilting pathogenic phenotypes caused by Rs JS763 inoculation of *L. japonicus* at 5 and 29 dpi. Scale bars are 5 mm. **(D)** MDS plot of whole root samples following treatment with the indicated strains. **(E)** Heatmap representation of $\log_2$ fold changes of various known symbiotic genes following inoculation with the indicated strains compared to H_2O controls.

Lotus japonicus Transcriptome Responses to a Spectrum of Interacting Bacteria

Transcriptional responses of *L. japonicus* to interacting bacteria representing a spectrum from compatible symbiont to pathogen were investigated to determine similarities or differences in the host transcriptome response to these diverse bacteria (**Figure 3A**). *M. loti* R7A (Ml R7A) represents an adapted symbiont that forms nitrogen-fixing nodules on *L. japonicus*. *Sinorhizobium fredii* HH103 (Sf HH103) is a broad host-range rhizobium that forms nitrogen-fixing nodules of some species of *Lotus* but induces uninfected primordia on *L. japonicus* (Acosta-Jurado et al., 2016) and (**Figure 3B**). *Bradyrhizobium elkanii* USDA61 (Be USDA61) is a symbiont of soybean that induces minimal responses on *L. japonicus* roots, with only an occasional root swelling near lateral root junctions observed (**Figure 3B**). *Pseudomonas syringae* pv. *tomato* DC3000 (Pst DC3000) is a well-known foliar phytopathogen (Xin and He, 2013). We observed no responses to root inoculation with Pst DC3000 indicating that the strain is non-pathogenic to *L. japonicus*

Gifu, as has been previously reported (Bordenave et al., 2013). *Ralstonia solanacearum* causes bacterial wilt in over 200 plant species and represents one of the most damaging bacterial pathogens in plants (Hayward, 1991). We observed that Rs JS763 causes brown discoloration of the roots from 3 dpi followed by discoloration at the base of the hypocotyl as well as chlorosis and wilting symptoms on leaves in *L. japonicus* Gifu (**Figure 3C**). These are typical plant disease symptoms due to *R. solanacearum* infection, confirming it to be a genuine root pathogen of *L. japonicus*, as previously described (Nagata et al., 2008).

Whole roots (minus root tips) treated with the spectrum of diverse bacterial strains or water were harvested at 1 and 3 dpi in biological duplicates. RNA isolation, Illumina sequencing and read mapping were performed as described above for the tissue samples. All data are available from the *Lotus* Base resource website (Mun et al., 2016)[2]. We detected outlier replicates for each inoculum and these were removed before proceeding with downstream analysis. The remaining three datasets, consisting of two 3 dpi and one 1 dpi samples, were combined to allow robust detection of differentially expressed genes. The effects of combining replicates from two 3 dpi and one 1 dpi samples were investigated using the R package DEGseq (Wang et al., 2010), which allows for differential gene expression analysis to be performed with fewer than three replicates. Differentially expressed genes were identified using the combined three replicates as well as using just the two 3 dpi replicates. A strong overlap in the genes identified between the three and two replicate analysis was observed. Almost all genes identified using the combined three replicates in our CLC genomics workbench analysis were also identified as differentially expressed in both the two and three replicate analyses using DEGseq, indicating that they likely represent genuine differentially regulated genes (**Supplementary Data 2**). However, genes oppositely regulated at 1 and 3 dpi or differentially expressed at only one time point may not have been detected due to the combined analysis of 1 and 3 dpi time points. We used the conservative lists of differentially expressed genes obtained from CLC genomics workbench in the downstream analyses. MDS analysis clustered Ml R7A and Sf HH103 together, Pst DC3000 clustered with H_2O while Be USDA61 was slightly removed from them and Rs JS763 samples formed a less defined group removed from the other samples (**Figure 3D**).

To assess the symbiotic response induced by the diverse strains, expression of the same set of known symbiotic genes analyzed in the various tissue samples following inoculation with R7A or NF was examined through comparing bacteria inoculated root samples to control H_2O-treated roots (**Figure 3E**). Ml R7A and Sf HH103 induced similar responses that are comparable to those obtained in analysis of the various tissues examined following R7A or NF treatment (**Figure 1D**) with the exception of *Rpg* expression, which was not induced in the Ml R7A and Sf HH103 samples. Only the *Npl* gene showed any expression change following inoculation with Be USDA61 and no response for any of the genes was observed following Pst DC3000 or Rs JS763 inoculation.

L. japonicus Responses to a Non-adapted Pathogen and Incompatible Rhizobia

Pst DC3000 induced no discernible phenotypic responses on *L. japonicus*. Only a small set of genes (44) showed significant expression changes following Pst DC3000 treatment, 8 of which showed similar regulation following Ml R7A inoculation (**Figure 4A** and **Supplementary Table 3**). Similar expression of the identified Pst DC3000 differentially regulated genes was observed following inoculation with the spectrum of strains investigated, indicating that these genes may represent a common response to bacteria by *L. japonicus* (**Figure 4A** and **Supplementary Table 3**). Of interest in the identified genes are two leucine-rich repeat (LRR) receptor like proteins (Lj0g3v0095839 and Lj0g3v0331049), an unknown-conserved GYF-domain containing protein (Lj5g3v0101610) and an exportin-7 like protein (Lj1g3v2392240) that show upregulated expression in response to all of the diverse strains. LRR receptors represent the largest receptor family in plants and are involved in diverse developmental, defense and symbiotic processes (Torii, 2004). Exportin-7 proteins are reportedly involved in nuclear export processes (Mingot et al., 2004).

Be USDA61 and Sf HH103 represent two rhizobial species that are incompatible for the establishment of nitrogen-fixing symbiosis with *L. japonicus* (**Figure 3B**). Significant gene expression changes were limited following Be USDA61 inoculation, whilst Sf HH103 inoculation induced a greater response and shared a large overlap with Ml R7A inoculation (**Figure 4B**).

Genes showing significant differential expression following Ml R7A inoculation but not Sf HH103 or Be USDA61 represent candidates involved in specifically promoting interaction with the compatible symbiont. The 34 genes identified that fit these criteria are listed in **Supplementary Table 4**. Of particular interest in this list are Lj5g3v2288900 that encodes a legume specific chalcone isomerase that has recently been shown to be involved in the biosynthesis of an Ml R7A NodD1 activating inducer, specifically within ITs (Kelly et al., 2017b) and Lj4g3v2365210 that encodes for the Nfy-B1 subunit, which forms part of the Nuclear Factor Y transcriptional factor known to be involved in nodulation (Soyano et al., 2013). Lj4g3v1983610 encodes an ENOD-like protein with a predicted cupredoxin domain. The protein shares 46% amino acid identity to ENOD16 of *M. truncatula*, which has been shown to be induced during symbiosis. No clear roles for ENOD16 have been demonstrated but it has been proposed that they may be involved in cell wall reorganization (Greene et al., 1998), which is required for IT development.

Interplay Between Symbiotic and Defense Responses in *L. japonicus*

Rs JS763 was shown to be a root pathogen of *L. japonicus* (**Figure 3B**). Rs JS763 inoculation resulted in a distinct transcription response, with 347 (277 upregulated and 70 downregulated) differentially expressed genes identified

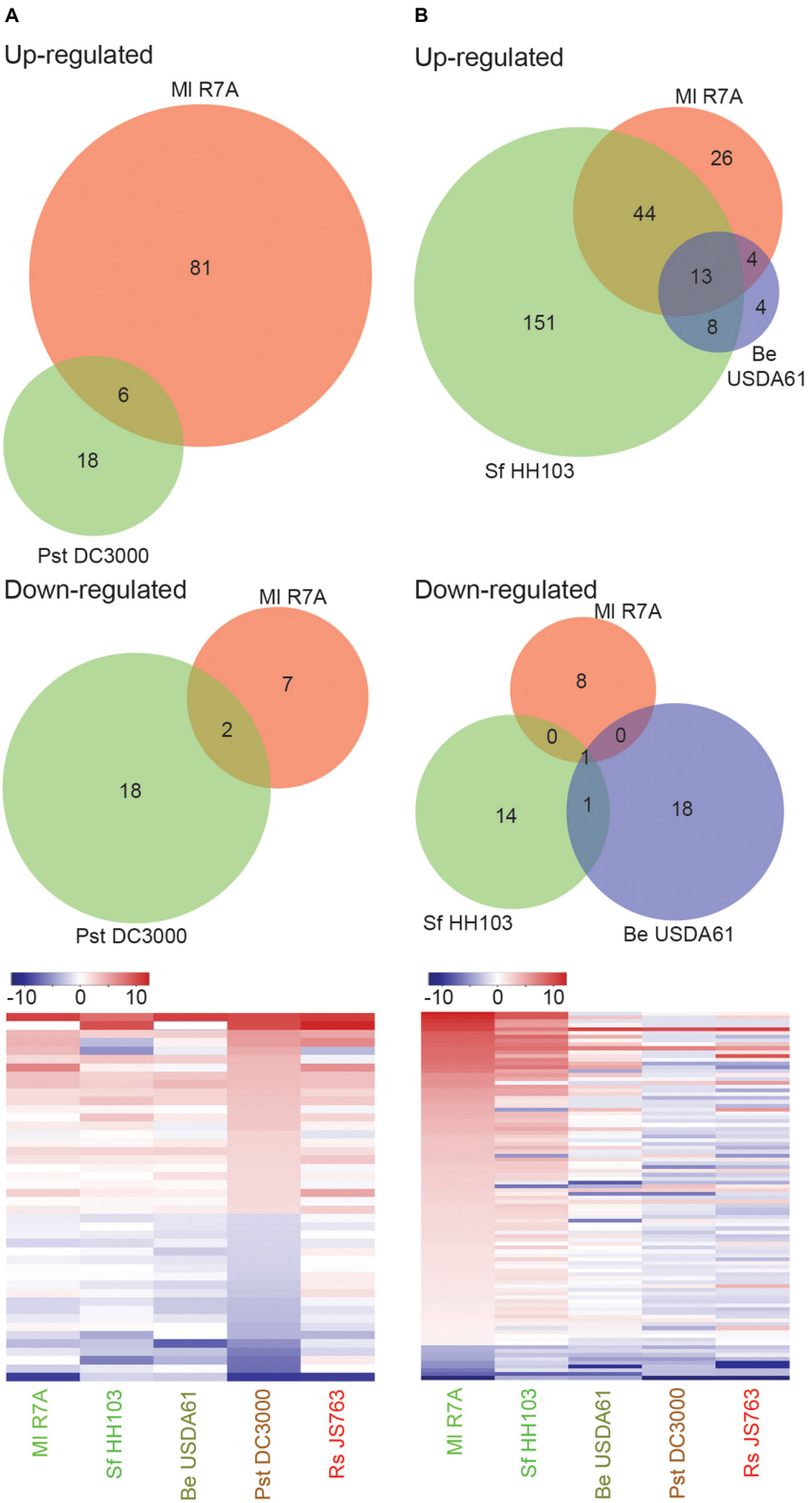

FIGURE 4 | *Lotus japonicus* root responses to non-adapted pathogenic bacteria and incompatible rhizobia. Venn diagram and heatmap representations of differential gene expression in the indicated conditions compared to H_2O controls. Significant gene expression differences were designated based on a fourfold change in expression with a FDR *p*-value ≤ 0.05. **(A)** Non-adapted pathogen Pst DC3000 induced differential gene expression. **(B)** Compatible symbiont MI R7A compared to incompatible rhizobia Sf HH103 and Be USDA61 differential gene expression. For heatmaps, Log_2 fold change values were used.

(**Supplementary Data 3**). Among the genes upregulated by Rs JS763 are five genes annotated as WRKY transcription factors (Lj0g3v0074419, Lj0g3v0244439, Lj1g3v1815540, Lj1g3v1787630, and Lj1g3v1220240). WRKY transcription factors belong to a large family of regulatory proteins involved in various plant processes but most notably in plant immunity against pathogen attack, including *R. solanacearum* infection (Mukhtar et al., 2008; Wang et al., 2013, 2014; Dang et al., 2014; Cai et al., 2015; Liu et al., 2017). Two 1-aminocyclopropane-1-carboxylate oxidase (ACO) 1-like genes (Lj2g3v0911860 and Lj6g3v0086450) were also induced. ACO proteins are involved in biosynthesis of ethylene, a plant hormone that is involved in many developmental and physiological responses including defense (Broekgaarden et al., 2015) and symbiosis (Reid et al., 2018). Ethylene signaling plays a critical role in bacterial wilt disease development in *A. thaliana* (Hirsch et al., 2002), *M. truncatula* (Moreau et al., 2014) and in tomato resistance to *R. solanacearum* (Zhang et al., 2004). In addition to inducing ethylene production by the host plant, *R. solanacearum* is also capable of producing ethylene itself (Weingart et al., 1999). Other defense related genes induced by Rs JS763 included pathogenesis-related proteins [such as PR1a: Lj6g3v2170740, beta-1,3-glucanase (PR-2): Lj0g3v0278459; PR10: Lj0g3v0286359; peroxidase 1-like: Lj0g3v0336889; two chitinases: Lj5g3v1961260 and Lj6g3v1078650] and several protease inhibitor proteins potentially involved in plant immunity (Lj0g3v0174139, Lj0g3v0174109, Lj2g3v0604160, Lj0g3v0265049, Lj5g3v1174410). Homologs of some of these genes were also reported as differentially expressed in response to *R. solanacearum* in *M. truncatula* according to proteomic and transcriptomic analyses (Yamchi et al., 2018). Interestingly, a gene annotated as a WAT1 (Walls Are Thin1)-related gene (Lj1g3v0913340) was downregulated in response to Rs JS763. In *A. thaliana*, inactivation of WAT1 gene, which is required for secondary cell-wall deposition, conferred broad-spectrum resistance to vascular pathogens, including *R. solanacearum* (Denance et al., 2013).

A transient defense response in *L. japonicus* roots during the early stages of symbiosis with compatible rhizobia had previously been reported (Kouchi et al., 2004). We investigated expression of the defense related genes identified by Kouchi et al. (2004) but did not observe comparable expression in response to symbiotic or pathogenic strains in our dataset (**Figure 5A** and **Supplementary Data 4**). Since symbiosis genes were consistently induced across all our experiments, we take this as an indication that the set of genes with defense-related annotations identified by Kouchi et al. (2004), are not generally associated with symbiotic or pathogenic interactions and our data does not support the notion that an early defense-like response is evoked by compatible rhizobia in the establishment of symbiosis with *L. japonicus*.

It remains possible, however, that overlaps in gene expression responses could exist between infection-competent symbiotic and pathogenic bacteria. To further examine such potential similarities, a list of commonly differentially expressed genes in early symbiotic samples was compiled from Ml R7A inoculated roots and root hairs. Expression of the 71 genes was analyzed in the spectrum of interacting bacteria, including Rs JS763 (**Figure 5B**). In a complementary analysis, expression of the 347 differentially expressed genes following Rs JS763 inoculation was compared in response to the diverse strains (**Figure 5C**). Rs JS763 inoculated roots did not show similar gene expression patterns with the symbiotic samples in either of these analyses. However, some overlapping expression changes were observed between Rs JS763 responsive genes and a compiled list of early symbiotic genes that were responsive to either Ml R7A or NF in whole roots or root hairs (**Figure 5D** and **Supplementary Table 5**).

This overlap included the cytokinin oxidase *Ckx3* (Lj5g3v0692300) that is involved in cytokinin breakdown during nodulation (Reid et al., 2016) and the sulfate transporter *Sst1* (Lj2g3v0776860.1) that is required for nitrogen-fixation within nodules. In addition, putative defense-related genes identified were a PR10-like gene (Lj0g3v0286359), the WAT1-related gene (Lj1g3v0913340) and a gene encoding a salicylate *O*-methyltransferase-like protein (Lj6g3v0509430) that is involved in the biosynthesis of methyl salicylate which was found to participate in root responses against fungal pathogens (Ament et al., 2010; Boba et al., 2016). Further studies will be required to determine the roles of the symbiosis-related genes in the *Lotus–Ralstonia* interaction and of the putative defense genes in *Lotus*–rhizobium interactions. However, the identification of genes responding to both *Ralstonia* and rhizobium treatments does not necessarily indicate that symbiotic rhizobia are initially perceived as pathogenic by *Lotus*. In contrast, our data indicate that the pathogenic and symbiotic responses are well-separated as early as 1 dpi (**Figure 3D**).

DISCUSSION

Lotus japonicus has been extensively utilized for the study of symbiotic interactions with rhizobial bacteria and mycorrhizal fungi. Analysis of the host transcriptional response during these interactions has been beneficial in developing our understanding of the molecular processes behind the symbiotic interactions and identifying potential genes important for these.

Transcriptome data collected from numerous microarray based studies of *L. japonicus* tissues at various stages of development or in association with biotic and abiotic treatments has been collated together in the LjGEA and is now accessible through *Lotus* Base[2] (Sanchez et al., 2008, 2011; Guether et al., 2009; Hogslund et al., 2009; Diaz et al., 2010; Verdier et al., 2013; Mun et al., 2016). We have expanded on this through the generation of a comprehensive RNA-seq based transcriptome analysis of the response of *L. japonicus* to its compatible symbiont *M. loti* R7A. Previous studies in *M. truncatula* have highlighted the benefits of isolating root hairs to amplify early symbiotic transcriptome responses (Breakspear et al., 2014). In our analysis, early symbiotic signaling was similarly amplified in root hair samples compared to whole roots. *Npl* (Xie et al., 2012), *Vapyrin* (Murray et al., 2011), and *Rpg* (Arrighi et al., 2008) represent genes known to be required for IT development that were highly induced in our root hair samples. Additional genes identified as showing enhanced expression within root hairs represent potential candidates that may be involved in

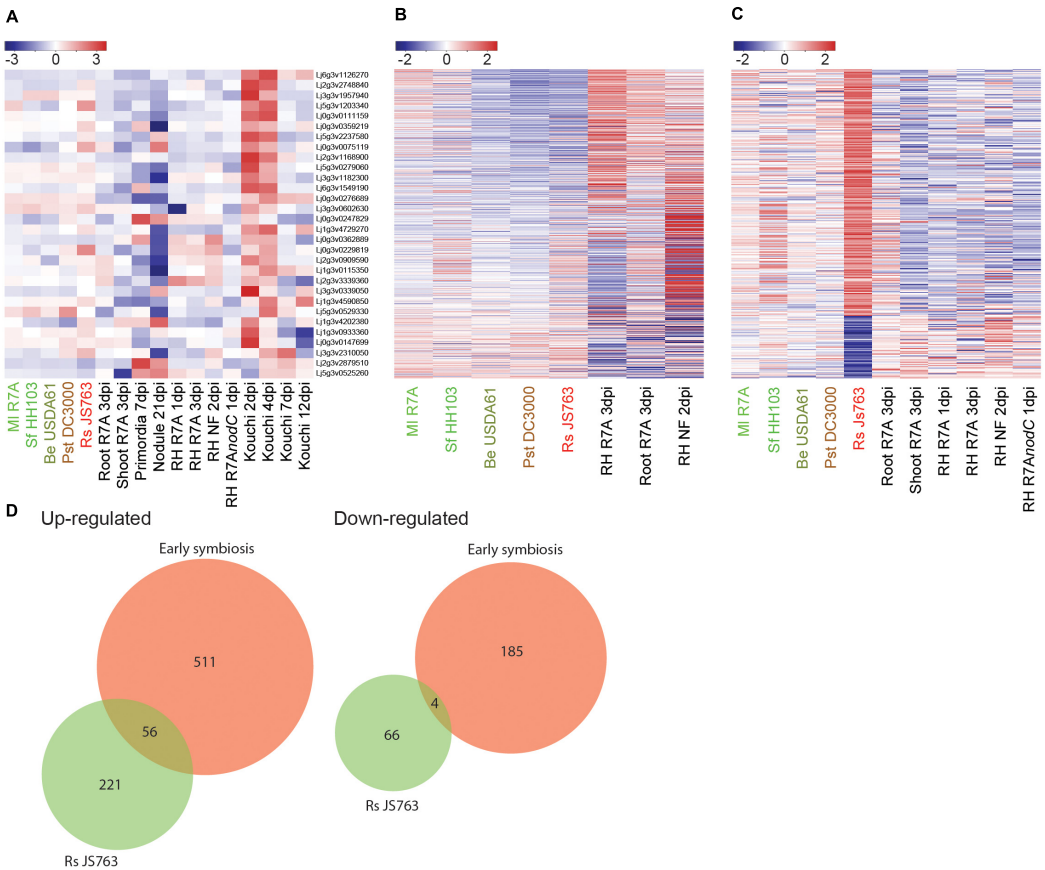

FIGURE 5 | Interplay between symbiotic and defense transcriptional responses. **(A)** Log_2 fold changes of potential defense associated genes identified as induced in the early stages of symbiosis by Kouchi et al. (2004) were examined across our datasets. **(B)** Expression patterns of 71 commonly differentially expressed genes in early symbiotic samples compiled from MI R7A inoculated roots and root hairs was analyzed in the spectrum of interacting bacteria. **(C)** Rs JS763 differentially regulated genes were examined for expression changes in early symbiotic and diverse strain datasets. **(D)** Venn diagrams showing the overlap in gene expression between early symbiosis, corresponding to a compiled list of genes that were responsive to either MI R7A or NF in whole roots or root hairs, and response to pathogenic Rs JS763. Differentially expressed genes were filtered by a minimum fourfold change and a FDR *p*-value ≤ 0.05.

IT development. An interesting candidate from this analysis is the aspartic peptidase APN1 (Lj3g3v0950730.1) that was recently discerned to be expressed in nodules and demonstrated to play a crucial role in nodule functioning. *apn1* mutant nodules fail to fix nitrogen and undergo early senescence in a *M. loti* strain-depended manner (Yamaya-Ito et al., 2017). Our identification of root hair enhanced expression of *Apn1* compared to whole roots suggests that IT phenotypes of *apn1* inoculated with R7A would be of interest to examine. As expected, early symbiotic signaling was largely NF-dependent and although considerable overlap was observed for differentially expressed genes following R7A or NF treatment, including most of the known symbiotic genes, there remains clear differences in the responses. A comparable difference in differentially expressed genes following NF treatment or *S. meliloti* inoculation was observed in *M. truncatula* (Breakspear et al., 2014). The observed differences in responses to purified NF compared to rhizobial inoculation may be due to the effects of other rhizobial factors, for example surface glycans, or differences in the concentration of NF roots are exposed to following rhizobial inoculation compared to purified NF treatment. Rhizobia produce an array of NF species and it is also possible that this induces differences in transcriptional responses compared to application of one particular purified NF species. Interestingly, *Rpg* induction was not observed in 2 dpi NF-treated or at 1 dpi with R7A, suggesting that *Rpg* induction is delayed compared to the other symbiotic genes investigated. This delay was not observed in *M. truncatula,* where *Rpg* induction was detected in roots at 1 dpi with *S. meliloti* or NF-treated root hairs (Arrighi et al., 2008; Breakspear et al., 2014). Nodule primordia and mature nodules exhibited large transcriptional reprogramming as has previously been observed for *Lotus* nodules (Takanashi et al., 2012). Highly upregulated genes include various transporters, auxin and cytokinin responsive genes as well as genes known to be required for nodule functioning such as the sulfate transporter *Sst1* (Krusell et al., 2005) and homocitrate synthase *Fen1* (Hakoyama et al., 2009).

Model legume resources, developed largely through the study of symbiotic interactions, have not been exploited to such an extent in interactions with diverse microbes. In this

study, we identified distinct transcriptome responses to a spectrum of interacting bacteria ranging from symbiotic to pathogenic. The broad host-range rhizobium Sf HH103 forms small nodule primordia that remain uninfected on *L. japonicus* (Sandal et al., 2012; Acosta-Jurado et al., 2016). A remarkably similar early transcriptome response of *L. japonicus* to Ml R7A and Sf HH103 was observed, indicating that NF-induced signaling is comparable between the two strains. Both strains produce a variety of NFs with one notable difference being the substitution on the reducing terminal residue, which is generally an acetylfucosyl for Ml R7A NF and a methylfucosyl for Sf HH103 NF (Gil-Serrano et al., 1997; Rodpothong et al., 2009). Genes identified as potentially limiting the symbiotic capacity of Sf HH103 based on differential expression compared to Ml R7A include a legume specific chalcone isomerase, Nfy-B1 and an ENOD16 encoding gene. Be USDA61 induced only occasional root swellings on *L. japonicus* and a limited transcriptome response was observed, suggesting that the NF species produced by this rhizobial strain are not well-perceived by *L. japonicus*. We also detected minimal transcriptome responses to Pst DC3000 inoculation, which appeared to be non-pathogenic to *L. japonicus* roots. Differentially expressed genes identified from these non-symbioitic/non-pathogenic strains may represent a common response to bacteria as similar transcription responses were overserved across the spectrum of interacting bacteria.

Rs JS763 was characterized as a genuine pathogen of *L. japonicus* with typical disease symptoms observed following root inoculation and a clear and distinct root transcriptome response was detected, allowing us to investigate the interplay between pathogenic and symbiotic signaling. Transcriptome-based studies have previously suggested that an initial defense-like response to rhizobia is subsequently dampened through symbiotic signaling in soybean/*B. japonicum*, *M. truncatula*/*S. meliloti,* and *L. japonicus*/*M. loti* symbioses (Kouchi et al., 2004; Lohar et al., 2006; Libault et al., 2010). Kouchi et al. (2004) identified a set of potential defense-related genes that were induced at early time points before being suppressed at later stages of *L. japonicus*/*M. loti* interactions. We did not observe similar induction of the identified genes in our RNA-seq transcriptome analysis following *M. loti* R7A inoculation, indicating that the gene set is not reproducibly associated with symbiotic infection. Furthermore, only two of these genes (Lj0g3v0229819 and Lj5g3v1203340) encoding carboxylesterase 6-like and basic 7S globulin-like proteins respectively, showed a significant response following Rs JS763 inoculation in our analysis, suggesting that although the genes identified by Kouchi et al. (2004) have potential defense associated annotations they may not represent genes that are generally pathogen responsive in *L. japonicus*. It is possible that differences in host and *M. loti* genotypes as well as growth setups used in our analysis and by Kouchi et al. (2004) may be responsible for the differences in transcriptional responses observed.

We did however identify a small overlap between early time point Ml R7A responsive genes and Rs JS763 differentially expressed genes. The only known symbiotic genes identified as commonly transcriptionally regulated are the cytokinin oxidase *Ckx3* and the sulfate transporter *Sst1*. Cytokinin is a key plant hormone and is tightly regulated in root development and symbiotic processes (Reid et al., 2017). Transcriptional changes in the expression of cytokinin related genes have previously been reported following *R. solanacearum* inoculation of *M. truncatula* (Moreau et al., 2014). SST1 functions during the later stages of symbiosis to transport sulfate from the plant to rhizobia where it is essential for protein synthesis, including nitrogenase biosynthesis (Krusell et al., 2005). It is unclear if a similar role is performed by SST1 in earlier stages of interactions with rhizobia or other bacteria. The only obvious potentially defense-related genes identified in the list of commonly induced genes were a PR10-like gene (Lj0g3v0286359), WAT1-related gene (Lj1g3v0913340) and a gene encoding a salicylate *O*-methyltransferase-like protein (Lj6g3v0509430). Lj6g3v0509430 is one of several salicylate *O*-methyltransferase-like proteins with high similarity encoded by *L. japonicus* and additional studies are required to determine if it is involved in salicylic acid responses.

Altogether, our analysis of transcriptome responses to a spectrum of interacting bacteria indicates that distinct transcriptome responses are observed in response to symbiotic and pathogenic bacteria and does not support the concept that an early defense-like response is generally evoked by compatible rhizobia in *L. japonicus* during the establishment of symbiosis.

AUTHOR CONTRIBUTIONS

SK and TM performed the plant experiments, isolated RNA, and analyzed the sequencing data. SUA conceived and supervised the study. CB and JS devised the experiments and contributed resources. SK, CB, and SUA wrote the manuscript with input from all authors.

FUNDING

The work was supported by the Danish National Research Foundation grant DNRF79 (JS) and a fellowship from the Institut Français du Danemark in the frame of the Blåtand Program (CB).

ACKNOWLEDGMENTS

We thank J. Luisetti for providing strain JS763 of *R. solanacearum* used in this work, Finn Pedersen for greenhouse assistance and Clive Ronson, John Sullivan, and Nicolai Maolanon for purified Nod factor.

SUPPLEMENTARY MATERIAL

The Supplementary Material for this article can be found online at: https://www.frontiersin.org/articles/10.3389/fpls.2018.01218/full#supplementary-material

REFERENCES

Acosta-Jurado, S., Rodriguez-Navarro, D. N., Kawaharada, Y., Perea, J. F., Gil-Serrano, A., Jin, H., et al. (2016). *Sinorhizobium fredii* HH103 invades Lotus burttii by crack entry in a Nod factor-and surface polysaccharide-dependent manner. *Mol. Plant Microbe Interact.* 29, 925–937. doi: 10.1094/MPMI-09-16-0195-R

Ament, K., Krasikov, V., Allmann, S., Rep, M., Takken, F. L., and Schuurink, R. C. (2010). Methyl salicylate production in tomato affects biotic interactions. *Plant J.* 62, 124–134. doi: 10.1111/j.1365-313X.2010.04132.x

Antolin-Llovera, M., Ried, M. K., and Parniske, M. (2014). Cleavage of the SYMBIOSIS RECEPTOR-LIKE KINASE ectodomain promotes complex formation with Nod factor receptor 5. *Curr. Biol.* 24, 422–427. doi: 10.1016/j.cub.2013.12.053

Arrighi, J. F., Godfroy, O., De Billy, F., Saurat, O., Jauneau, A., and Gough, C. (2008). The RPG gene of *Medicago truncatula* controls *Rhizobium*-directed polar growth during infection. *Proc. Natl. Acad. Sci. U.S.A.* 105, 9817–9822. doi: 10.1073/pnas.0710273105

Benedito, V. A., Torres-Jerez, I., Murray, J. D., Andriankaja, A., Allen, S., Kakar, K., et al. (2008). A gene expression atlas of the model legume *Medicago truncatula*. *Plant J.* 55, 504–513. doi: 10.1111/j.1365-313X.2008.03519.x

Boba, A., Kostyn, K., Kostyn, A., Wojtasik, W., Dziadas, M., Preisner, M., et al. (2016). Methyl salicylate level increase in lax after *Fusarium oxysporum* infection is associated with phenylpropanoid pathway activation. *Front. Plant Sci.* 7:1951.

Bordenave, C. D., Escaray, F. J., Menendez, A. B., Serna, E., Carrasco, P., Ruiz, O. A., et al. (2013). Defense responses in two ecotypes of *Lotus japonicus* against non-pathogenic *Pseudomonas syringae*. *PLoS One* 8:e83199. doi: 10.1371/journal.pone.0083199

Breakspear, A., Liu, C., Roy, S., Stacey, N., Rogers, C., Trick, M., et al. (2014). The root hair "infectome" of *Medicago truncatula* uncovers changes in cell cycle genes and reveals a requirement for *Auxin signaling* in rhizobial infection. *Plant Cell* 26, 4680–4701. doi: 10.1105/tpc.114.133496

Broekgaarden, C., Caarls, L., Vos, I. A., Pieterse, C. M., and Van Wees, S. C. (2015). Ethylene: traffic controller on hormonal crossroads to defense. *Plant Physiol.* 169, 2371–2379. doi: 10.1104/pp.15.01020

Broghammer, A., Krusell, L., Blaise, M., Sauer, J., Sullivan, J. T., Maolanon, N., et al. (2012). Legume receptors perceive the rhizobial lipochitin oligosaccharide signal molecules by direct binding. *Proc. Natl. Acad. Sci. U.S.A.* 109, 13859–13864. doi: 10.1073/pnas.1205171109

Cai, H., Yang, S., Yan, Y., Xiao, Z., Cheng, J., Wu, J., et al. (2015). CaWRKY6 transcriptionally activates CaWRKY40, regulates *Ralstonia solanacearum* resistance, and confers high-temperature and high-humidity tolerance in pepper. *J. Exp. Bot.* 66, 3163–3174. doi: 10.1093/jxb/erv125

Cerri, M. R., Wang, Q., Stolz, P., Folgmann, J., Frances, L., Katzer, K., et al. (2017). The ERN1 transcription factor gene is a target of the CCaMK/CYCLOPS complex and controls rhizobial infection in *Lotus japonicus*. *New Phytol.* 215, 323–337. doi: 10.1111/nph.14547

Chen, T., Duan, L., Zhou, B., Yu, H., Zhu, H., Cao, Y., et al. (2017). Interplay of pathogen-induced defense responses and symbiotic establishment in *Medicago truncatula*. *Front. Microbiol.* 8:973. doi: 10.3389/fmicb.2017.00973

Dang, F., Wang, Y., She, J., Lei, Y., Liu, Z., Eulgem, T., et al. (2014). Overexpression of CaWRKY27, a subgroup IIe WRKY transcription factor of *Capsicum annuum*, positively regulates tobacco resistance to *Ralstonia solanacearum* infection. *Physiol. Plant.* 150, 397–411. doi: 10.1111/ppl.12093

Daniels, M. J., Barber, C. E., Turner, P. C., Cleary, W. G., and Sawczyc, M. K. (1984). Isolation of mutants of *Xanthomonas campestris* pv. campestris showing altered pathogenicity. *J. Gen. Microbiol.* 130, 2447–2455. doi: 10.1099/00221287-130-9-2447

Denance, N., Ranocha, P., Oria, N., Barlet, X., Riviere, M. P., Yadeta, K. A., et al. (2013). *Arabidopsis* wat1 (walls are thin1)-mediated resistance to the bacterial vascular pathogen, *Ralstonia solanacearum*, is accompanied by cross-regulation of salicylic acid and tryptophan metabolism. *Plant J.* 73, 225–239. doi: 10.1111/tpj.12027

Desbrosses, G. J., and Stougaard, J. (2011). Root nodulation: a paradigm for how plant-microbe symbiosis influences host developmental pathways. *Cell Host Microbe* 10, 348–358. doi: 10.1016/j.chom.2011.09.005

Diaz, P., Betti, M., Sanchez, D. H., Udvardi, M. K., Monza, J., and Marquez, A. J. (2010). Deficiency in plastidic glutamine synthetase alters proline metabolism and transcriptomic response in *Lotus japonicus* under drought stress. *New Phytol.* 188, 1001–1013. doi: 10.1111/j.1469-8137.2010.03440.x

Gil-Serrano, A. M., Franco-Rodriguez, G., Tejero-Mateo, P., Thomas-Oates, J., Spaink, H. P., Ruiz-Sainz, J. E., et al. (1997). Structural determination of the lipo-chitin oligosaccharide nodulation signals produced by *Rhizobium fredii* HH103. *Carbohydr. Res.* 303, 435–443. doi: 10.1016/S0008-6215(97)00189-4

Giovannetti, M., Mari, A., Novero, M., and Bonfante, P. (2015). Early *Lotus japonicus* root transcriptomic responses to symbiotic and pathogenic fungal exudates. *Front. Plant Sci.* 6:480. doi: 10.3389/fpls.2015.00480

Greene, E. A., Erard, M., Dedieu, A., and Barker, D. G. (1998). MtENOD16 and 20 are members of a family of phytocyanin-related early nodulins. *Plant Mol. Biol.* 36, 775–783. doi: 10.1023/A:1005916821224

Guether, M., Balestrini, R., Hannah, M., He, J., Udvardi, M. K., and Bonfante, P. (2009). Genome-wide reprogramming of regulatory networks, transport, cell wall and membrane biogenesis during arbuscular mycorrhizal symbiosis in Lotus japonicus. *New Phytol.* 182, 200–212. doi: 10.1111/j.1469-8137.2008.02725.x

Hakoyama, T., Niimi, K., Watanabe, H., Tabata, R., Matsubara, J., Sato, S., et al. (2009). Host plant genome overcomes the lack of a bacterial gene for symbiotic nitrogen fixation. *Nature* 462, 514–517. doi: 10.1038/nature08594

Handberg, K., and Stougaard, J. (1992). *Lotus japonicus*, an autogamous, diploid legume species for classical and molecular genetics. *Plant J.* 2, 487–496. doi: 10.1111/j.1365-313X.1992.00487.x

Hayward, A. C. (1991). Biology and epidemiology of bacterial wilt caused by *Pseudomonas solanacearum*. *Annu. Rev. Phytopathol.* 29, 65–87. doi: 10.1146/annurev.py.29.090191.000433

Heckmann, A. B., Lombardo, F., Miwa, H., Perry, J. A., Bunnewell, S., Parniske, M., et al. (2006). *Lotus japonicus* nodulation requires two GRAS domain regulators, one of which is functionally conserved in a non-legume. *Plant Physiol.* 142, 1739–1750. doi: 10.1104/pp.106.089508

Hirsch, J., Deslandes, L., Feng, D. X., Balague, C., and Marco, Y. (2002). Delayed symptom development in ein2-1, an Arabidopsis ethylene-insensitive mutant, in response to bacterial wilt caused by *Ralstonia solanacearum*. *Phytopathology* 92, 1142–1148. doi: 10.1094/PHYTO.2002.92.10.1142

Hogslund, N., Radutoiu, S., Krusell, L., Voroshilova, V., Hannah, M. A., Goffard, N., et al. (2009). Dissection of symbiosis and organ development by integrated transcriptome analysis of *Lotus japonicus* mutant and wild-type plants. *PLoS One* 4:e6556. doi: 10.1371/journal.pone.0006556

Hulsen, T., De Vlieg, J., and Alkema, W. (2008). BioVenn - a web application for the comparison and visualization of biological lists using area-proportional Venn diagrams. *BMC Genomics* 9:488. doi: 10.1186/1471-2164-9-488

Kawaharada, Y., James, E. K., Kelly, S., Sandal, N., and Stougaard, J. (2017a). The ethylene responsive factor required for nodulation 1 (ERN1) transcription factor is required for infection-thread formation in *Lotus japonicus*. *Mol. Plant Microbe Interact.* 30, 194–204. doi: 10.1094/MPMI-11-16-0237-R

Kawaharada, Y., Nielsen, M. W., Kelly, S., James, E. K., Andersen, K. R., Rasmussen, S. R., et al. (2017b). Differential regulation of the Epr3 receptor coordinates membrane-restricted rhizobial colonization of root nodule primordia. *Nat Commun.* 8:14534. doi: 10.1038/ncomms14534

Kawaharada, Y., Kelly, S., Nielsen, M. W., Hjuler, C. T., Gysel, K., Muszynski, A., et al. (2015). Receptor-mediated exopolysaccharide perception controls bacterial infection. *Nature* 523, 308–312. doi: 10.1038/nature14611

Kelly, S., Radutoiu, S., and Stougaard, J. (2017a). Legume LysM receptors mediate symbiotic and pathogenic signalling. *Curr. Opin. Plant Biol.* 39, 152–158. doi: 10.1016/j.pbi.2017.06.013

Kelly, S., Sullivan, J., Kawaharada, Y., Radutoiu, S., Ronson, C., and Stougaard, J. (2017b). Regulation of Nod factor biosynthesis by alternative NodD proteins at distinct stages of symbiosis provides additional compatibility scrutiny. *Environ. Microbiol.* 20, 97–110. doi: 10.1111/1462-2920.14006

Kelly, S. J., Muszynski, A., Kawaharada, Y., Hubber, A. M., Sullivan, J. T., Sandal, N., et al. (2013). Conditional requirement for exopolysaccharide in the *Mesorhizobium*-Lotus symbiosis. *Mol. Plant Microbe Interact.* 26, 319–329. doi: 10.1094/MPMI-09-12-0227-R

Kouchi, H., Shimomura, K., Hata, S., Hirota, A., Wu, G. J., Kumagai, H., et al. (2004). Large-scale analysis of gene expression profiles during early stages

of root nodule formation in a model legume, *Lotus japonicus*. *DNA Res.* 11, 263–274. doi: 10.1093/dnares/11.4.263

Krusell, L., Krause, K., Ott, T., Desbrosses, G., Kramer, U., Sato, S., et al. (2005). The sulfate transporter SST1 is crucial for symbiotic nitrogen fixation in *Lotus japonicus* root nodules. *Plant Cell* 17, 1625–1636. doi: 10.1105/tpc.104.030106

Libault, M., Farmer, A., Brechenmacher, L., Drnevich, J., Langley, R. J., Bilgin, D. D., et al. (2010). Complete transcriptome of the soybean root hair cell, a single-cell model, and its alteration in response to *Bradyrhizobium japonicum* infection. *Plant Physiol.* 152, 541–552. doi: 10.1104/pp.109.148379

Liu, Q., Liu, Y., Tang, Y., Chen, J., and Ding, W. (2017). Overexpression of NtWRKY50 increases resistance to *Ralstonia solanacearum* and alters salicylic acid and jasmonic acid production in Tobacco. *Front. Plant Sci.* 8:1710. doi: 10.3389/fpls.2017.01710

Lohar, D. P., Sharopova, N., Endre, G., Penuela, S., Samac, D., Town, C., et al. (2006). Transcript analysis of early nodulation events in *Medicago truncatula*. *Plant Physiol.* 140, 221–234. doi: 10.1104/pp.105.070326

Long, S. R. (1996). Rhizobium symbiosis: nod factors in perspective. *Plant Cell* 8, 1885–1898. doi: 10.1105/tpc.8.10.1885

Lopez-Gomez, M., Sandal, N., Stougaard, J., and Boller, T. (2012). Interplay of flg22-induced defence responses and nodulation in *Lotus japonicus*. *J. Exp. Bot.* 63, 393–401. doi: 10.1093/jxb/err291

Madsen, E. B., Madsen, L. H., Radutoiu, S., Olbryt, M., Rakwalska, M., Szczyglowski, K., et al. (2003). A receptor kinase gene of the LysM type is involved in legume perception of rhizobial signals. *Nature* 425, 637–640. doi: 10.1038/nature02045

Madsen, L. H., Tirichine, L., Jurkiewicz, A., Sullivan, J. T., Heckmann, A. B., Bek, A. S., et al. (2010). The molecular network governing nodule organogenesis and infection in the model legume *Lotus japonicus*. *Nat. Commun.* 1:10. doi: 10.1038/ncomms1009

Maekawa-Yoshikawa, M., and Murooka, Y. (2009). Root hair deformation of symbiosis-deficient mutants of *Lotus japonicus* by application of Nod factor from *Mesorhizobium loti*. *Microbes Environ.* 24, 128–134. doi: 10.1264/jsme2.ME09103

Malolepszy, A., Mun, T., Sandal, N., Gupta, V., Dubin, M., Urbanski, D., et al. (2016). The LORE1 insertion mutant resource. *Plant J.* 88, 306–317. doi: 10.1111/tpj.13243

Mingot, J. M., Bohnsack, M. T., Jakle, U., and Gorlich, D. (2004). Exportin 7 defines a novel general nuclear export pathway. *EMBO J.* 23, 3227–3236. doi: 10.1038/sj.emboj.7600338

Moreau, S., Fromentin, J., Vailleau, F., Vernie, T., Huguet, S., Balzergue, S., et al. (2014). The symbiotic transcription factor MtEFD and cytokinins are positively acting in the *Medicago truncatula* and *Ralstonia solanacearum* pathogenic interaction. *New Phytol.* 201, 1343–1357. doi: 10.1111/nph.12636

Mukhtar, M. S., Deslandes, L., Auriac, M. C., Marco, Y., and Somssich, I. E. (2008). The *Arabidopsis* transcription factor WRKY27 influences wilt disease symptom development caused by *Ralstonia solanacearum*. *Plant J.* 56, 935–947. doi: 10.1111/j.1365-313X.2008.03651.x

Mun, T., Bachmann, A., Gupta, V., Stougaard, J., and Andersen, S. U. (2016). Lotus Base: An integrated information portal for the model legume *Lotus japonicus*. *Sci. Rep.* 6:39447. doi: 10.1038/srep39447

Munch, D., Gupta, V., Bachmann, A., Busch, W., Kelly, S., Mun, T., et al. (2018). The brassicaceae family displays divergent, shoot-skewed NLR resistance gene expression. *Plant Physiol.* 176, 1598–1609. doi: 10.1104/pp.17.01606

Murray, J. D., Muni, R. R., Torres-Jerez, I., Tang, Y., Allen, S., Andriankaja, M., et al. (2011). Vapyrin, a gene essential for intracellular progression of arbuscular mycorrhizal symbiosis, is also essential for infection by rhizobia in the nodule symbiosis of *Medicago truncatula*. *Plant J.* 65, 244–252. doi: 10.1111/j.1365-313X.2010.04415.x

Nagata, M., Murakami, E., Shimoda, Y., Shimoda-Sasakura, F., Kucho, K., Suzuki, A., et al. (2008). Expression of a class 1 hemoglobin gene and production of nitric oxide in response to symbiotic and pathogenic bacteria in *Lotus japonicus*. *Mol. Plant Microbe Interact.* 21, 1175–1183. doi: 10.1094/MPMI-21-9-1175

Oldroyd, G. E. (2013). Speak, friend, and enter: signalling systems that promote beneficial symbiotic associations in plants. *Nat. Rev. Microbiol.* 11, 252–263. doi: 10.1038/nrmicro2990

Oldroyd, G. E. D., Murray, J. D., Poole, P. S., and Downie, J. A. (2011). The rules of engagement in the legume-rhizobial symbiosis. *Annu. Rev. Genet.* 45, 119–144. doi: 10.1146/annurev-genet-110410-132549

R Core Team. (2017). *R: A Language and Environment for Statistical Computing*. Vienna: R Foundation for Statistical Computing.

Radutoiu, S., Madsen, L. H., Madsen, E. B., Felle, H. H., Umehara, Y., Gronlund, M., et al. (2003). Plant recognition of symbiotic bacteria requires two LysM receptor-like kinases. *Nature* 425, 585–592. doi: 10.1038/nature02039

Reid, D., Liu, H., Kelly, S., Kawaharada, Y., Mun, T., Andersen, S. U., et al. (2018). Dynamics of ethylene production in response to compatible Nod factor. *Plant Physiol.* 176, 1764–1772. doi: 10.1104/pp.17.01371

Reid, D., Nadzieja, M., Novak, O., Heckmann, A. B., Sandal, N., and Stougaard, J. (2017). Cytokinin biosynthesis promotes cortical cell responses during nodule development. *Plant Physiol.* 175, 361–375. doi: 10.1104/pp.17.00832

Reid, D. E., Heckmann, A. B., Novak, O., Kelly, S., and Stougaard, J. (2016). CYTOKININ OXIDASE/DEHYDROGENASE3 maintains cytokinin homeostasis during root and nodule development in *Lotus japonicus*. *Plant Physiol.* 170, 1060–1074. doi: 10.1104/pp.15.00650

Rodpothong, P., Sullivan, J. T., Songsrirote, K., Sumpton, D., Cheung, K. W., Thomas-Oates, J., et al. (2009). Nodulation gene mutants of Mesorhizobium loti R7A-nodZ and nolL mutants have host-specific phenotypes on Lotus spp. *Mol. Plant Microbe Interact.* 22, 1546–1554. doi: 10.1094/MPMI-22-12-1546

Saile, E., Mcgarvey, J. A., Schell, M. A., and Denny, T. P. (1997). Role of extracellular polysaccharide and endoglucanase in root invasion and colonization of tomato plants by *Ralstonia solanacearum*. *Phytopathology* 87, 1264–1271. doi: 10.1094/PHYTO.1997.87.12.1264

Sanchez, D. H., Lippold, F., Redestig, H., Hannah, M. A., Erban, A., Kramer, U., et al. (2008). Integrative functional genomics of salt acclimatization in the model legume *Lotus japonicus*. *Plant J.* 53, 973–987. doi: 10.1111/j.1365-313X.2007.03381.x

Sanchez, D. H., Pieckenstain, F. L., Szymanski, J., Erban, A., Bromke, M., Hannah, M. A., et al. (2011). Comparative functional genomics of salt stress in related model and cultivated plants identifies and overcomes limitations to translational genomics. *PLoS One* 6:e17094. doi: 10.1371/journal.pone.0017094

Sandal, N., Jin, H., Rodriguez-Navarro, D. N., Temprano, F., Cvitanich, C., Brachmann, A., et al. (2012). A set of Lotus japonicus Gifu x *Lotus burttii* recombinant inbred lines facilitates map-based cloning and QTL mapping. *DNA Res.* 19, 317–323. doi: 10.1093/dnares/dss014

Sato, S., Nakamura, Y., Kaneko, T., Asamizu, E., Kato, T., Nakao, M., et al. (2008). Genome structure of the legume, *Lotus japonicus*. *DNA Res.* 15, 227–239. doi: 10.1093/dnares/dsn008

Sauviac, L., Niebel, A., Boisson-Dernier, A., Barker, D. G., and De Carvalho-Niebel, F. (2005). Transcript enrichment of Nod factor-elicited early nodulin genes in purified root hair fractions of the model legume *Medicago truncatula*. *J. Exp. Bot.* 56, 2507–2513. doi: 10.1093/jxb/eri244

Schauser, L., Roussis, A., Stiller, J., and Stougaard, J. (1999). A plant regulator controlling development of symbiotic root nodules. *Nature* 402, 191–195. doi: 10.1038/46058

Soyano, T., Kouchi, H., Hirota, A., and Hayashi, M. (2013). Nodule inception directly targets NF-Y subunit genes to regulate essential processes of root nodule development in *Lotus japonicus*. *PLoS Genet.* 9:e1003352. doi: 10.1371/journal.pgen.1003352

Stracke, S., Kistner, C., Yoshida, S., Mulder, L., Sato, S., Kaneko, T., et al. (2002). A plant receptor-like kinase required for both bacterial and fungal symbiosis. *Nature* 417, 959–962. doi: 10.1038/nature00841

Takanashi, K., Takahashi, H., Sakurai, N., Sugiyama, A., Suzuki, H., Shibata, D., et al. (2012). Tissue-specific transcriptome analysis in nodules of *Lotus japonicus*. *Mol. Plant Microbe Interact.* 25, 869–876. doi: 10.1094/MPMI-01-12-0011-R

Torii, K. U. (2004). Leucine-rich repeat receptor kinases in plants: structure, function, and signal transduction pathways. *Int. Rev. Cytol.* 234, 1–46. doi: 10.1016/S0074-7696(04)34001-5

Verdier, J., Torres-Jerez, I., Wang, M., Andriankaja, A., Allen, S. N., He, J., et al. (2013). Establishment of the *Lotus japonicus* gene expression atlas (LjGEA) and its use to explore legume seed maturation. *Plant J.* 74, 351–362. doi: 10.1111/tpj.12119

Vincent, J. M. (1970). *A Manual for the Practical Study of Root-Nodule Bacteria*. Oxford: Blackwell Scientific Publications.

Wang, L., Feng, Z., Wang, X., Wang, X., and Zhang, X. (2010). DEGseq: an R package for identifying differentially expressed genes from RNA-seq data. *Bioinformatics* 26, 136–138. doi: 10.1093/bioinformatics/btp612

Wang, X., Yan, Y., Li, Y., Chu, X., Wu, C., and Guo, X. (2014). GhWRKY40, a multiple stress-responsive cotton WRKY gene, plays an important role in the wounding response and enhances susceptibility to *Ralstonia solanacearum* infection in transgenic *Nicotiana benthamiana*. *PLoS One* 9:e93577. doi: 10.1371/journal.pone.0093577

Wang, Y., Dang, F., Liu, Z., Wang, X., Eulgem, T., Lai, Y., et al. (2013). CaWRKY58, encoding a group I WRKY transcription factor of *Capsicum annuum*, negatively regulates resistance to *Ralstonia solanacearum* infection. *Mol. Plant Pathol.* 14, 131–144. doi: 10.1111/j.1364-3703.2012.00836.x

Weingart, H., Volksch, B., and Ullrich, M. S. (1999). Comparison of ethylene production by *Pseudomonas* syringae and *Ralstonia solanacearum*. *Phytopathology* 89, 360–365. doi: 10.1094/PHYTO.1999.89.5.360

Xie, F., Murray, J. D., Kim, J., Heckmann, A. B., Edwards, A., Oldroyd, G. E., et al. (2012). Legume pectate lyase required for root infection by rhizobia. *Proc. Natl. Acad. Sci. U.S.A.* 109, 633–638. doi: 10.1073/pnas.1113992109

Xin, X. F., and He, S. Y. (2013). *Pseudomonas* syringae pv. *tomato DC*3000: a model pathogen for probing disease susceptibility and hormone signaling in plants. *Annu. Rev. Phytopathol.* 51, 473–498. doi: 10.1146/annurev-phyto-082712-102321

Yamaya-Ito, H., Shimoda, Y., Hakoyama, T., Sato, S., Kaneko, T., Hossain, M. S., et al. (2017). Loss-of-function of ASPARTIC PEPTIDASE NODULE-INDUCED 1 (APN1) in *Lotus japonicus* restricts efficient nitrogen-fixing symbiosis with specific *Mesorhizobium loti* strains. *Plant J.* 93, 5–16. doi: 10.1111/tpj.13759

Yamchi, A., Ben, C., Rossignol, M., Zareie, S. R., Mirlohi, A., Sayed-Tabatabaei, B. E., et al. (2018). Proteomics analysis of *Medicago truncatula* response to infection by the phytopathogenic bacterium *Ralstonia solanacearum* points to jasmonate and salicylate defence pathways. *Cell Microbiol.* 20:e12796. doi: 10.1111/cmi.12796

Yano, K., Aoki, S., Liu, M., Umehara, Y., Suganuma, N., Iwasaki, W., et al. (2017). Function and evolution of a Lotus japonicus AP2/ERF family transcription factor that is required for development of infection threads. *DNA Res.* 24, 193–203. doi: 10.1093/dnares/dsw052

Zhang, H., Zhang, D., Chen, J., Yang, Y., Huang, Z., Huang, D., et al. (2004). Tomato stress-responsive factor TSRF1 interacts with ethylene responsive element GCC box and regulates pathogen resistance to *Ralstonia solanacearum*. *Plant Mol. Biol.* 55, 825–834. doi: 10.1007/s11103-005-2140-3

Zhao, S., Guo, Y., Sheng, Q., and Shyr, Y. (2014). Advanced heat map and clustering analysis using heatmap3. *Biomed. Res. Int.* 2014:986048. doi: 10.1155/2014/986048

Conflict of Interest Statement: The authors declare that the research was conducted in the absence of any commercial or financial relationships that could be construed as a potential conflict of interest.

frontiers in Plant Science

MINI REVIEW
published: 03 September 2018
doi: 10.3389/fpls.2018.01247

Mini-Review: Nod Factor Regulation of Phytohormone Signaling and Homeostasis During Rhizobia-Legume Symbiosis

*William P. Buhian and Sandra Bensmihen**

LIPM, Université de Toulouse, INRA, CNRS, Toulouse, France

The rhizobia-legume symbiosis is a mutualistic association in which bacteria provide plants with nitrogen compounds and the plant provides bacteria with carbon sources. A successful symbiotic interaction relies on a molecular dialog between the plant and the bacteria, and generally involves rhizobial lipo-chitooligosaccharide signals called Nod factors (NFs). In most cases, specific NF perception is required for rhizobia to enter root cells through newly formed intracellular structures called infection threads (ITs). Concomitantly to IT formation in root hairs, root cortical cells start to divide to create a new root organ called the nodule, which will provide the bacteria with a specific micro-environment required for symbiotic nitrogen fixation. During all these steps of plant–bacteria interaction, new plant cellular compartments and developmental programs are activated. This interaction is costly for the plant that tightly controls symbiosis establishment and functioning. Phytohormones are key regulators of cellular and developmental plasticity in plants, and they are influential endogenous signals that rapidly control plant responses. Although early symbiotic responses were known for decades to be linked to phytohormone-related responses, new data reveal the molecular mechanisms involved and links between phytohormones and the control of early symbiotic events. Reciprocally, NF signaling also targets phytohormone signaling pathways. In this review, we will focus on the emerging notion of NF and phytohormone signaling crosstalk, and how it could contribute to the tight control of symbiosis establishment in legume host plants.

Keywords: auxin, cytokinins, gibberellin, ethylene, strigolactone, infection, nodule organogenesis, LCOs

OPEN ACCESS

Edited by:
Pascal Ratet,
Centre National de la Recherche Scientifique (CNRS), France

Reviewed by:
Jeanne Marie Harris,
University of Vermont, United States
Brendan Keith Riely,
University of California, Davis, United States

***Correspondence:**
Sandra Bensmihen
sandra.bensmihen@inra.fr

Specialty section:
This article was submitted to Plant Microbe Interactions, a section of the journal Frontiers in Plant Science

Received: *06 April 2018*
Accepted: *06 August 2018*
Published: *03 September 2018*

Citation:
Buhian WP and Bensmihen S (2018) Mini-Review: Nod Factor Regulation of Phytohormone Signaling and Homeostasis During Rhizobia-Legume Symbiosis. Front. Plant Sci. 9:1247. doi: 10.3389/fpls.2018.01247

INTRODUCTION

Legume plants can interact with soil bacteria, named rhizobia, to establish the rhizobium legume (RL) symbiosis. Legumes host Rhizobia in specific root organs called nodules, where they fix atmospheric nitrogen. This symbiosis provides the plant with nitrogen compounds (ammonium) and the plant provides the bacteria with carbon sources. The efficiency of this interaction relies for a great part on the massive intracellular infection of plant cells by rhizobia and the protective structure of the nodule. The plant host must invest a great deal of energy to both house and support nitrogen fixing bacteria, and as such, must tightly regulate this process.

Nod factors (NFs) are lipo-chitooligosaccharide (LCO) molecules produced by rhizobia in response to flavonoids present in root exudates. NFs are generally essential for the onset and the

maintenance of the RL symbiosis (Dénarié, 1996). Intriguingly, NFs can also stimulate lateral root formation via the symbiotic signaling pathway implying that similar host mechanisms are involved in both nodule and lateral root development (Olah et al., 2005). Genetic pathways governing NF perception and signaling are now quite well understood (Gough and Cullimore, 2011). NFs are perceived by the plant at the root epidermis and are likely produced by rhizobia all along the infection process (Sharma and Signer, 1990).

Rhizobia first attach to root hairs (RHs) in a susceptible zone of host roots (Bhuvaneswari et al., 1981) and then enter RHs through a membrane invagination called an infection thread (IT). Even before the IT is formed, pericycle cells are activated and divide to start organogenesis of the nodule (Timmers et al., 1999). NFs are usually essential for the infection process and, in *Medicago sativa*, purified NFs can trigger pericycle activation and initiate nodule organogenesis (Truchet et al., 1991; Timmers et al., 1999). Defects in the infection process often result in defective nodule organogenesis. Infection and organogenesis events of the RL symbiosis are thus tightly coordinated. This tight coordination and signaling across root layers, and the events of cellular reactivation and cell division associated with symbiotic establishment strongly imply the involvement of hormonal pathways.

Recent transcriptomic data suggest that NF signaling regulates the host hormone biosynthesis and signal transduction pathways. Hormones function in the pico to nano-molar range (Gaspar et al., 2003). Their activity depends on a tight balance of activation (biosynthesis) and inactivation (conjugation, degradation) pathways, as well as transport and signaling. In this mini-review, we will focus on data showing positive and negative feedback regulatory mechanisms between NF signaling and hormonal pathways. We present data from legumes producing both indeterminate (*Medicago truncatula*, pea) and determinate [*Lotus japonicus*, *Glycine max* (soybean)] nodules. These two types of nodule differ in the site of initial cortical divisions, persistency of the nodule meristem and auxin sensitivity (Bensmihen, 2015; Ng and Mathesius, 2018). Effects of NF signaling on both hormone homeostasis and hormone signaling will be discussed.

NF SIGNALING AND REGULATION OF HORMONE HOMEOSTASIS

Phytohormones are key regulators of plant growth and responses to biotic and abiotic stresses. Several transcriptomic studies show that hormone biosynthesis, activation or degradation genes are differentially expressed upon NF treatment (see **Table 1** and **Figure 1**).

Cytokinins

Biosynthesis and Activation

Numerous studies document the role of CKs as key regulators of nodule organogenesis (Gonzalez-Rizzo et al., 2006; Murray et al., 2007; Tirichine et al., 2007) and IT formation/progression (Held et al., 2014; Jardinaud et al., 2016). Recent transcriptomic data show that expression of CK biosynthesis genes such as *isopentenyl transferases (IPT)* and *CYP735A* that contribute to the biosynthesis of the bioactive CK form trans-zeatin, as well as CK activation genes such as *LONELY GUYs* (LOGs), can be induced by a 3 h NF treatment (van Zeijl et al., 2015b). Moreover, *MtIPT1*and *MtCYP735A1* regulation is independent of the CK receptor *MtCRE1*, suggesting a direct (and possibly local) production of CK as an early event following NF signaling. Similarly, *LjIPT2* and *LjLOG4* are regulated by NF application independently of the CK receptor *LjLHK1* in *L. japonicus* (Reid et al., 2017). Accumulation of bioactive CKs is also detected in the root susceptible zone following a 3 h NF treatment, and this is dependent on the NF signaling gene *MtDMI3* (van Zeijl et al., 2015b). Several genes from the trans-zeatin metabolic network are regulated in RHs after a 24 h NF treatment, suggesting accumulation of the bioactive CK trans-zeatin upon NF treatment. However, bioactive CK levels have not been measured in NF treated RHs (Jardinaud et al., 2016).

Inactivation and Degradation

Interestingly, CK inactivation enzymes adenyl phosphoribosides transferases (APT) and cytokinin oxidases (CKX) are also induced by a 3 h NF treatment but in an *MtCRE1* dependent manner, suggesting downstream negative regulatory feedback loops on CK accumulation (see **Figure 1**). Indeed, expression of the *AtCKX3* gene in *M. truncatula* plants under an epidermis specific promoter enhanced the number of ITs and nodules formed upon rhizobium inoculation. In contrast, expression of *AtCKX3* under a cortical specific promoter reduced nodulation (Jardinaud et al., 2016). In *L. japonicus*, NFs also induce expression of the *LjCKX3* gene but its promoter activity is specific to inner root tissues. Inactivation of *LjCKX3* leads to enhanced production of bioactive CK forms and reduces nodule organogenesis and IT formation (Reid et al., 2016). Altogether, this suggests that reducing the levels of active CKs may increase the efficiency of the infection process. This fits with the model suggested by Held et al. (2014) that argues for an inhibitory feedback loop driven by CK accumulation in the epidermis at late stages of nodulation. This is also consistent with antagonistic effects of CK application on the induction of the NF responsive gene *MtENOD11*. Indeed, a 3 h CK pretreatment of *M. truncatula* roots significantly reduces the induction of *MtENOD11* by NF. Conversely, epidermal expression of the *AtCKX3* gene enhanced the NF induction of *MtENOD11* (Jardinaud et al., 2016). In summary, growing evidence suggests that NFs induce CK production, which first controls nodule organogenesis, then rapidly activates negative feedbacks on NF signaling and infection processes, notably in the epidermis.

Gibberellins

Increasing evidence also suggests a role for gibberellins (GAs) in controlling early events of symbiosis. A 24 h NF treatment induces both GA metabolic and biosynthetic genes in *M. truncatula* RHs, suggesting accumulation of the bio-active GA precursor GA12 in the root epidermis upon NF treatment (Breakspear et al., 2014; Jardinaud et al., 2016). An important NF-dependent and transient activation of GA biosynthesis

TABLE 1 | Summary of major hormone homeostasis and signaling genes differentially regulated by Nod factors or rhizobia during symbiosis.

		Role	Regulation	Representative functional studies, if present
Auxin	*TAR*	Auxin biosynthesis	UP (10 h NF+ NAA[9])	
	YUCCA, ASA	Auxin biosynthesis	UP (>0.5 h[6])	
	ARF16a	Auxin signaling	UP (24 h)[2]	Controls infection at earliest stages. *ARF16a* mutants show a decreased number of infection events[2].
	GH3.1	Auxin conjugation	UP (4 h[1], 24 h[2])	Found to be enriched in nodules, and has distinct expression patterns, activated first in epidermis than in cortex upon *S. meliloti* infection[5]. GmGH3-14, 15 control nodule number and size[3].
	PIN2, PIN4, PIN10	Polar auxin transport	Indirect control through MtCRE1[4,5]	Differential expression dependent on CRE1[4]. Application of auxin transport inhibitors rescues *Mtcre1* phenotype[5].
	LBD18, LBD16	Auxin signaling	UP (6 hpi)[a,6]	
	PLT	Auxin signaling	UP (6 hpi[a,6], 4 h[1])	Required for the maintenance of the nodule meristem (NM). Downregulation of all MtPLT produced nodules deficient in NM and infection zone[8].
CK	*IPT*	Cytokinin biosynthesis	UP (3 h[7], 4 h[1], 10 h[9], 24 h[1])	Early response is not LHK1 dependent. Overexpression of the entire biosynthetic pathway is necessary for visible phenotypes[12].
	CYP735A, APT4	Cytokinin biosynthesis	UP (3 h[7], 4 h, 24 h[1])	
	LOG1, LOG2	Cytokinin biosynthesis	UP (3 h)[7]	Expression in RL symbiosis dependent on *MtCRE1*[7]. *MtLOG1* positively regulates nodule organogenesis, and in autoregulation of nodulation[13].
	MtCRE1/LjLHK1	Cytokinin signaling	UP (4 h[1])	*Ljhit1/lhk1* mutants are hyperinfected, infection threads (ITs) fail to penetrate cortex [10]. *MtCRE1* controls IT progression and nodule organogenesis[11].
	RR4, RR5, RR8, RR9, RR11	Cytokinin signaling	UP (3 h[16], 4 h[1]) UP (48 hpi)[a,15]	Spatiotemporal expression as function of Nod factor response of (RR9, RR11) largely overlap. Controls lateral root and nodule number[16].
	CKX	Cytokinin catabolism	UP (3 h[7])	Expressed in nodulation. Mutants show decreased infection and nodulation efficiency[14]. Synergistic NF+auxin regulation[9].
Ethylene	*ACS, ACS3*	Ethylene biosynthesis	UP (3 h)[6,7]	
	ACO	Ethylene biosynthesis	UP (1 h[19], 10 h NF + NAA[9], 0.5–3 h[6])	
	EIN2/MtSKL	Ethylene signaling	Down (10 h NF + NAA[9])	EIN2 regulates IT growth and cortical cell division; also regulates number and distribution of infection events[17,18].
GA	*Ga20ox*	GA biosynthesis	UP (3 h[7], 24 h[1])	
	Ga2ox	GA catabolism	UP (24 h[2])	
SL	*D27*	SL biosynthesis	UP (3 h[20], 24 h[1,2])	Nod factor-induced expression dependent on NSP1 and NSP2[20]
	CCD8	SL biosynthesis	UP (5 dpi[a,2])	
JA	*AOS*	JA biosynthesis	DOWN (24 h[2])	
	JAZ, COI	JA signaling	DOWN (24 h[2])	
BR	*HYD1*	BR synthesis	DOWN (48 hpi)[a,15]	
	DWARF1	BR synthesis	DOWN (5 dpi)[a,2]	

Data from Breakspear et al. (2014) and Jardinaud et al. (2016) were obtained from epidermal samples. All other transcriptomic data were obtained from whole root samples of Medicago truncatula (Larrainzar et al., 2015; van Zeijl et al., 2015b; Herrbach et al., 2017), Glycine max (Hayashi et al., 2012), and Lotus japonicus (Miyata et al., 2013). Unless otherwise indicated, samples were treated with Nod factors. [a]Root samples inoculated with rhizobia. CK, cytokinins; GA, Gibberellins; SL, strigolactones; JA, jasmonic acid; BR, brassinosteroids; NF, Nod factors. [1]Jardinaud et al., 2016. [2]Breakspear et al., 2014. [3]Damodaran et al., 2017. [4]Plet et al., 2011. [5]Ng et al., 2015. [6]Larrainzar et al., 2015. [7]van Zeijl et al., 2015b. [8]Franssen et al., 2015. [9]Herrbach et al., 2017. [10]Murray et al., 2007. [11]Gonzalez-Rizzo et al., 2006. [12]Reid et al., 2017. [13]Mortier et al., 2015. [14]Reid et al., 2016. [15]Hayashi et al., 2012. [16]Op den Camp et al., 2011. [17]Penmetsa and Cook, 1997. [18]Penmetsa et al., 2003. [19]Miyata et al., 2013. [20]van Zeijl et al., 2015a.

genes was observed in soybean roots 12 hpi with rhizobia (Hayashi et al., 2012). Interestingly, 10^{-7} M GA3 treatment was previously shown to suppress NF-induced expression of the transcription factors *NSP2* and *NIN* in *L. japonicus* and 10^{-6} M GA3 suppressed NF induced RH deformation (Maekawa et al., 2009). Likewise, pretreatment of *M. truncatula* roots with 10^{-6} M GA3 suppressed NF dependent *ENOD11* induction. NF treatment also induced expression of the GA catabolic and biosynthetic enzymes GA2 and GA20ox, respectively (Fonouni-Farde et al., 2016). Moreover, this GA2ox catabolic gene was positively regulated by a 10 h NF treatment (Herrbach et al., 2017) and down-regulated in RHs after a 24 h NF treatment

(Zaat et al., 1989; Breakspear et al., 2014). These data suggest that NFs can rapidly induce the biosynthesis of bioactive GA in RHs, which consequently triggers a negative feedback leading both to the downregulation of NF signaling and the activation of GA catabolic enzymes (see **Figure 1**). Increasing evidence also shows that bioactive GAs negatively regulate nodulation and infection in both determinate and indeterminate nodules (Maekawa et al., 2009; Fonouni-Farde et al., 2016). Thus, NF induced GAs could help fine-tune NF signaling and rhizobium infection during symbiosis.

Ethylene

Previous genetic, physiologic, and pharmacologic studies highlight the key regulatory role ethylene plays in early symbiotic processes (Zaat et al., 1989; Heidstra et al., 1997; Oldroyd et al., 2001; Penmetsa et al., 2008). NFs can induce the expression of several ethylene biosynthetic genes, including two 1-aminocyclopropane-1-carboxylate (ACC) synthase genes (*MtACS1* and *MtACS2*; van Zeijl et al., 2015b). Moreover, three *ACS* genes are upregulated by NF signaling at 6 hpi with rhizobium (Larrainzar et al., 2015). Similarly, NF dependent ethylene production is detected in *L. japonicus* roots as early as 6 hpi (Reid et al., 2018). *MtACS3* is also synergistically regulated by a 10 h treatment with a combination of NFs and auxin (Herrbach et al., 2017). Promoter:GUS fusions showed RH expression of three *ACS* genes in *M. truncatula* (Larrainzar et al., 2015). This is consistent with previous data obtained in *L. japonicus* where a 1 h treatment with 10^{-8} M NF increased the expression of the ACC oxidase *LjACO2*, which was synergistically regulated by the combined application of NFs and ACC (Miyata et al., 2013). In contrast, NF-dependent downregulation of ethylene biosynthesis was observed at 48 hpi in the susceptible zone of soybean roots (Hayashi et al., 2012). Altogether, these data suggest that NF signaling rapidly and transiently induces the production of a negative regulator of infection, ethylene.

Auxin

Auxin Metabolism

Nod factor-dependent induction of genes encoding auxin biosynthetic enzymes such as *YUCCA* and *ANTHRANILATE SYNTHASE* (*ASA*) was observed early after *Sinorhizobium meliloti* inoculation in whole roots (Larrainzar et al., 2015). Several auxin signaling genes are activated in RHs after a 24 h NF treatment (Breakspear et al., 2014), which argues for an effect of NFs on auxin production and signaling (see section "Auxin Signaling"). Similarly, we recently described a synergistic effect of NFs and auxin on the transcription of a large number of hormone biosynthesis genes, including an auxin biosynthesis *TRYPTOPHAN AMINOTRANSFERASE*-related (*TAR2*) homolog (Herrbach et al., 2017). Interestingly, a *GH3.1* gene, predicted to encode an auxin conjugation and inactivation enzyme (Yang et al., 2015) is expressed both in NF treated RHs as well as developing nodules (Breakspear et al., 2014; Ng et al., 2015; Jardinaud et al., 2016). We found this same *GH3* gene to be synergistically upregulated by NFs and auxin (Herrbach et al., 2017). This suggests fine tuning of bioactive pools of auxin, in RHs and probably inner cortical tissues for indeterminate nodules, upon NF perception and rhizobium infection.

Auxin Transport

Several studies link NF signaling to auxin transport. Spot inoculation of compatible rhizobia (but not a non-host strain) or micro-targeting of specific LCOs can modify auxin gradients, as measured by the GH3:GUS reporter gene in white clover (Mathesius et al., 1998). Likewise, flavonoid application also inhibits auxin transport. NF application or *S. meliloti* infection inhibits auxin transport from shoot to root at 24 h, as well as regulating expression of some *MtPIN* auxin efflux transporter genes, in an *MtCRE1* dependent manner (van Noorden et al., 2006; Plet et al., 2011; Ng et al., 2015). Moreover, MtCRE1 dependent pathways also control the accumulation of flavonoids in *M. truncatula* roots upon infection and flavonoid application can rescue the *Mtcre1* nodulation phenotype. These data suggest that NF induced, CK signaling triggers flavonoid induction and the subsequent inhibition of polar auxin transport. The resulting accumulation of auxin initiates cortical cell division and nodule organogenesis (**Figure 1**).

Strigolactones

Strigolactones (SGLs) show a dose-dependent effect on nodulation in *M. truncatula* (Gomez-Roldan et al., 2008; De Cuyper et al., 2015). Interestingly, several studies (Larrainzar et al., 2015; van Zeijl et al., 2015a; Herrbach et al., 2017) showed a direct NF regulation of the expression of the SGL biosynthesis gene *DWARF27* (D27). The promoter of the *D27* gene is active in the root epidermis after a 3 h NF treatment and upon early steps of nodule organogenesis (van Zeijl et al., 2015a). Moreover, we observed that a combined auxin+NF treatment reduced the NF induction of *D27* expression, suggesting that auxin can antagonize NF effects (Herrbach et al., 2017).

Jasmonic Acid (JA) and Brassinosteroids (BR)

Jasmonic acid (JA) and BR regulate plant stress responses and plant growth, but their role in RL symbiosis is not well understood. Conflicting reports indicate that host responses to these hormones vary depending on the legume species, hormone dose, or type of treatment studied (see Ferguson and Mathesius, 2014 for review and Conclusion and Perspectives section below). Some evidence suggests NF regulation of JA biosynthetic enzymes. Larrainzar et al. (2015) observed NF-dependent induction of two JA biosynthesis genes at 3–6 hpi and Breakspear et al. (2014) observed downregulation of a few JA biosynthetic genes in RHs after a 24 h NF treatment. In contrast, NF-dependent upregulation of several JA biosynthesis genes was observed in soybean at 48 hpi, while there seemed to be a reduction in expression of BR biosynthetic genes (Hayashi et al., 2012).

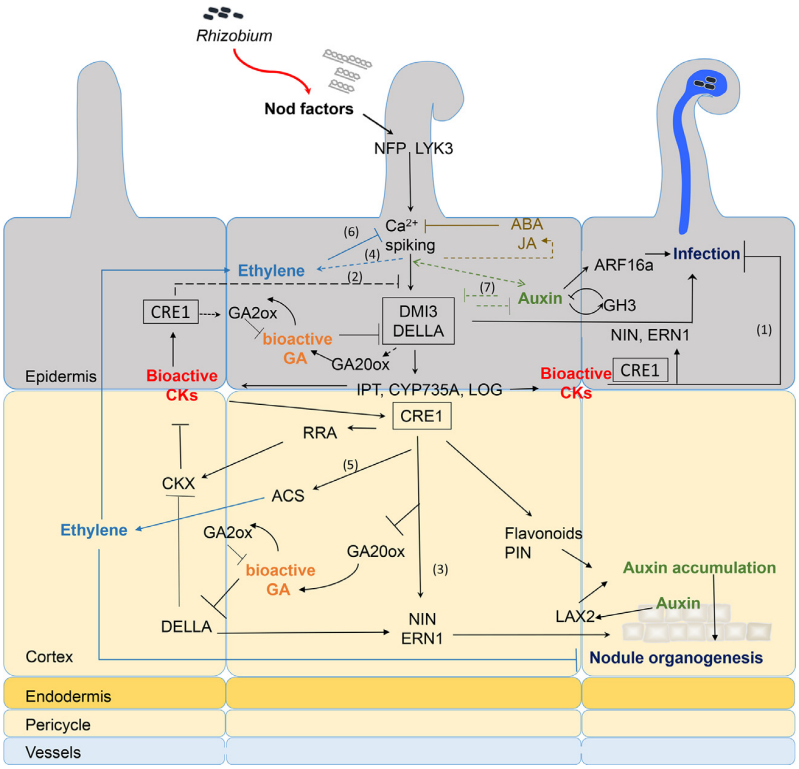

FIGURE 1 | Recapitulative spatio-temporal scheme of the interactions between NF signaling and downstream hormonal pathways. Rhizobia produce NFs that are perceived in root hairs (RHs) through LysM-RLK receptors such as NFP and LYK3. NF perception leads to calcium spiking and activation of DMI3 that acts upstream of the CK receptor MtCRE1. The signaling cascade involving DMI3 and CRE1 is likely involved in both epidermal and cortical signaling (black boxes). NF treatment triggers early CK biosynthesis gene (*IPT/CYP735A/LOG*) expression and CK accumulation in *M. truncatula* roots downstream of *DMI3* but independently of CRE1 signaling (van Zeijl et al., 2015b). Although tissue specificity of this CK production was not determined, evidence from *L. japonicus* and *M. truncatula* suggests that epidermal CK accumulation is a negative regulator of RH infection (1) and NF signaling (2) (Held et al., 2014; Jardinaud et al., 2016). In contrast, cortical CK is a positive regulator of nodule organogenesis (3) (Gonzalez-Rizzo et al., 2006; Murray et al., 2007; Reid et al., 2017). Bioactive CKs are perceived by CRE1 and induce expression of *NIN* and *ERN1* (Ariel et al., 2012), which are positive regulators of both infection and nodule organogenesis (Andriankaja et al., 2007; Marsh et al., 2007). This induction might be partly through regulation of DELLA activities. GA is a negative regulator of DELLA protein stability. Bioactive GA pools are likely present in both epidermis and cortex early after NF treatment (Fonouni-Farde et al., 2016; Jardinaud et al., 2016; Herrbach et al., 2017). DELLAs play a positive regulatory role on symbiotic gene expression such as *ERN1* and they negatively regulate CK degradation (Fonouni-Farde et al., 2016, 2017; Jin et al., 2016). In contrast, CK positively regulate GA inactivation enzymes and down-regulate expression of the GA20ox activation enzyme (Fonouni-Farde et al., 2018), suggesting a negative feedback of CK on GA active pools. NF signaling induces ethylene production, both independently of the LHK1/CRE1 CK pathway (4) (Reid et al., 2018) and downstream of CK perception (5) (van Zeijl et al., 2015b). Ethylene reduces CK production in *M. truncatula* roots, possibly through negative feedback on NF signaling (6) (van Zeijl et al., 2015b). Ethylene negatively regulates NF-induced calcium spiking, RH infection, and nodule organogenesis (Heidstra et al., 1997; Penmetsa et al., 2008). Regulation of auxin biosynthetic and conjugation enzyme (GH3) genes occurs in NF treated RHs and upon *S. meliloti* inoculation in an NF-dependent manner (Breakspear et al., 2014; Larrainzar et al., 2015; Jardinaud et al., 2016; Herrbach et al., 2017). Reciprocal positive and negative feedback regulatory loops between some auxin and NF regulated genes (7) was shown by comparing the combined effect of auxin and NFs to either treatment alone (Herrbach et al., 2017). Downstream of CK perception, control of auxin transport in the cortex seems regulated by differential expression of *PIN* genes (Plet et al., 2011) or accumulation of flavonoid compounds. Auxin accumulation is also mediated by *MtLAX2* that is induced upon *S. meliloti* infection in vasculature and early nodule primordia, and which is required for nodule organogenesis (Roy et al., 2017). In parallel, epidermal auxin signaling controls infection thread (IT) formation, at least partly through *ARF16a* (Breakspear et al., 2014). Exogenous application of high concentrations (μM range) of ABA or JA inhibits NF-induced calcium spiking (Sun et al., 2006; Ding et al., 2008) but this inhibition is so far not supported by any transcriptomic data. Plain bars represent negative and plain arrows positive regulations. Dashed lines are hypothetical relationships, and solid lines have evidence from the literature. Different hormones are highlighted by different colors. CK, cytokinins; GA, gibberellins; ABA, abscisic acid; JA, jasmonic acid; NF, Nod factors. Bacteria entrapped in curled root hair and IT are shown in blue.

Hence, these data suggest that NF-signaling regulates several hormonal biosynthesis and activation pathways, with subsequent negative feedback loops that are rapidly activated after a brief NF treatment or upon rhizobium inoculation. Further evidence for a temporal regulation of bioactive hormone pools by NF signaling comes from the downstream regulation of many hormonal signaling genes (**Table 1**).

NF REGULATION OF HORMONE SIGNALING GENES

CK Signaling

CK signaling utilizes a two-component signaling system comprised of a histidine-kinase (HK) receptor, phospho-transfer

proteins (AHPs), and response regulators (RRs). Two types of RRs operate in CK signal transduction: A-type RRs are transcriptionally regulated upon CK perception but do not contain a DNA binding domain, and are generally considered as negative regulators of the CK response. In contrast, B-type RRs contain a Myb DNA binding domain, function as transcription factors and are generally considered as positive regulators (Kieber and Schaller, 2014). In *M. truncatula* and *L. japonicus*, the HK genes *MtCRE1* and *LjLHK1* have positive roles in cortical cell divisions and nodule organogenesis (Gonzalez-Rizzo et al., 2006; Murray et al., 2007; Tirichine et al., 2007). Recent transcriptomic and promoter fusion analyses demonstrate the induction of these CK receptor genes upon rhizobium infection or NF application; in Lotus, this epidermal expression inhibits infection (Held et al., 2014; Jardinaud et al., 2016).

Independent data suggest NF induced, RR gene expression occurs downstream of CK receptor activation. For instance, the A-type *MtRR4*, *MtRR8*, *MtRR9*, *MtRR11*, and the B-type *MtRR1* are expressed in *M. truncatula* roots following inoculation with either NF or wild-type *S. meliloti*, but not with nod$^-$ *S. meliloti* mutants (Gonzalez-Rizzo et al., 2006; Op den Camp et al., 2011; van Zeijl et al., 2015b; Jardinaud et al., 2016). Likewise, an HK and an RR (*GmRR5*) gene are also induced in soybean in an NF-dependent manner (Hayashi et al., 2012). Finally, the CK signaling reporter construct, TCSn:GUS, can be induced in *M. truncatula* RHs upon a 4 h NF treatment (Jardinaud et al., 2016).

Altogether, an early activation of CK signaling probably occurs both in RHs and cortical cells, directly downstream of the NF signaling pathway (**Figure 1**).

Auxin Signaling

Accumulating evidence suggests that NFs regulate the expression of auxin signaling genes. NF application induces the auxin related transcription factors genes *MtARF16a* and *MtPLETHORA3* in RHs, while several *ARF* genes are downregulated in RHs after a 24 h NF treatment (Breakspear et al., 2014; Jardinaud et al., 2016). These genes are also induced by auxin in *M. truncatula* roots (Herrbach et al., 2017). This suggests that NF perception could lead to auxin accumulation that would in turn activate some specific auxin signaling genes (**Figure 1**). Such genes could control cell divisions or IT formation (Breakspear et al., 2014).

GA Signaling

DELLAs are well-known negative regulators of GA signaling (Sun, 2011). Recent data showed a positive effect of DELLAs on nodulation, and more specifically on IT formation (Fonouni-Farde et al., 2016; Jin et al., 2016). DELLAs reside in the NSP1/NSP2/IPD3 transcription factor complex that mediates NF signaling (Fonouni-Farde et al., 2016; Jin et al., 2016). External application of GAs can repress NF induction of several genes, such as *ERN1*, *ENOD11*, *NSP2*, and *NIN* (Maekawa et al., 2009; Fonouni-Farde et al., 2016). However, NFs do not induce DELLA gene expression (Fonouni-Farde et al., 2016).

Ethylene and JA Signaling

Larrainzar et al. (2015) observed a biphasic regulation of expression of 47 AP2/ERF transcription factor genes in *M. truncatula* upon *S. meliloti* infection. The first wave of AP2/ERF expression takes place 1 hpi independent of NF perception, whereas the second wave of NF dependent, ethylene-regulated transcription occurs 6 hpi (Larrainzar et al., 2015). Although little is known about JA signaling during symbiosis, a 24 h NF treatment downregulates the expression of the putative JA receptor *COI1* in *M. truncatula* RHs implying that NF perception may attenuate this signaling pathway (Breakspear et al., 2014).

CONCLUSION AND PERSPECTIVES

Growing evidence shows that early events of NF signaling lead to the production and/or activation of hormones such as CK and GAs and the activation of their downstream signaling pathways. These hormones, in turn, interfere with other hormonal pathways, such as ethylene, ABA, and auxin, which can impinge upon NF signaling itself. For example, external application of CK or GA inhibits NF induction of *MtENOD11* (Fonouni-Farde et al., 2016; Jardinaud et al., 2016). Similarly, JA, ABA, and ethylene are well-known negative regulators of NF signaling (Oldroyd et al., 2001; Sun et al., 2006; Ding et al., 2008). We observed that auxin both positively and negatively regulated different NF responsive genes in a combined auxin + NF treatment (Herrbach et al., 2017) providing further evidence for the regulation of symbiosis signaling pathways by hormones. These negative effects may underpin the mechanism by which the host controls nodulation following the initial NF/rhizobium recognition.

It should, however, be noted that the concentrations of hormones applied in these studies are often in the micro-molar range. In the absence of quantitative data reporting endogenous hormone levels during symbiotic responses, it is difficult to assess if these studies reflect biologically relevant responses to plant hormones and this field requires such analyses.

Furthermore, recent evidence suggests that hormones function in a tissue-specific manner during symbiotic responses (see Gamas et al., 2017) but the specificity of these hormonal pathways is only partly resolved. Future work should address the respective contribution of different root tissues in producing, sensing, and responding to NF induced hormones, using tissue specific tools or quantitative hormone biosensors (Jones et al., 2014; Liao et al., 2015).

Finally, the NF signaling pathway overlaps with other symbiotic and developmental pathways suggesting that hormones may also impinge upon these processes. Similar to Rhizobia, arbuscular mycorrhizal fungi produce LCOs and utilize the same core signaling pathway to initiate symbiosis (Maillet et al., 2011). Future work should address whether LCO/hormone crosstalk regulates mycorrhization, where evidence

already implicates a role for auxin, SGLs, GA, and LCO pathways (Lauressergues et al., 2012; Floss et al., 2013; Etemadi et al., 2014). Likewise, LCOs stimulate LR development and some NF induced genes are also involved in LR development (Herrbach et al., 2017). How LCO/hormone crosstalk could be involved in LCO stimulation of lateral root formation and how this could compare to its role in nodulation still requires further investigation.

AUTHOR CONTRIBUTIONS

SB and WB drafted the review and produced **Figure 1**. SB wrote the review with help of WB. WB produced **Table 1**.

FUNDING

Research conducted by WB and SB at the LIPM was partly supported by the "Laboratoire d'Excellence" (LABEX) entitled TULIP (ANR-10-LABX-41). WB's Ph.D. is funded by a joint French Embassy and Commission on Higher Education from the Philippines Government (CHED-Phil France) program.

ACKNOWLEDGMENTS

We thank Clare Gough and Frédéric Debellé for critical reading of the manuscript. We apologize for colleagues whose work was not cited due to space limitation or our focus on crosstalk between NF and hormone signaling aspects only.

REFERENCES

Andriankaja, A., Boisson-Dernier, A., Frances, L., Sauviac, L., Jauneau, A., Barker, D. G., et al. (2007). AP2-ERF transcription factors mediate Nod factor dependent Mt ENOD11 activation in root hairs via a novel cis-regulatory motif. *Plant Cell* 19, 2866–2885. doi: 10.1105/tpc.107.052944

Ariel, F., Brault-Hernandez, M., Laffont, C., Huault, E., Brault, M., Plet, J., et al. (2012). Two direct targets of cytokinin signaling regulate symbiotic nodulation in Medicago truncatula. *Plant Cell* 24, 3838–3852. doi: 10.1105/tpc.112.103267

Bensmihen, S. (2015). Hormonal control of lateral root and nodule development in legumes. *Plants (Basel)* 4, 523–547. doi: 10.3390/plants4030523

Bhuvaneswari, T. V., Bhagwat, A. A., and Bauer, W. D. (1981). Transient susceptibility of root cells in four common legumes to nodulation by rhizobia. *Plant Physiol.* 68, 1144–1149. doi: 10.1104/pp.68.5.1144

Breakspear, A., Liu, C., Roy, S., Stacey, N., Rogers, C., Trick, M., et al. (2014). The root hair "infectome" of *Medicago truncatula* uncovers changes in cell cycle genes and reveals a requirement for Auxin signaling in rhizobial infection. *Plant Cell* 26, 4680–4701. doi: 10.1105/tpc.114.133496

Damodaran, S., Westfall, C. S., Kisely, B. A., Jez, J. M., and Subramanian, S. (2017). Nodule-enriched GRETCHEN HAGEN 3 enzymes have distinct substrate specificities and are important for proper soybean nodule development. *Int. J. Mol. Sci.* 18:2547. doi: 10.3390/ijms18122547

De Cuyper, C., Fromentin, J., Yocgo, R. E., De Keyser, A., Guillotin, B., Kunert, K., et al. (2015). From lateral root density to nodule number, the strigolactone analogue GR24 shapes the root architecture of *Medicago truncatula*. *J. Exp. Bot.* 66, 137–146. doi: 10.1093/jxb/eru404

Dénarié, J., Debellé, F., and Promé, J. C. (1996). Rhizobium lipo-chitooligosaccharide nodulation factors: signaling molecules mediating recognition and morphogenesis. *Annu. Rev. Biochem.* 65, 503–535. doi: 10.1146/annurev.bi.65.070196.002443

Ding, Y., Kalo, P., Yendrek, C., Sun, J., Liang, Y., Marsh, J. F., et al. (2008). Abscisic acid coordinates Nod factor and cytokinin signaling during the regulation of nodulation in *Medicago truncatula*. *Plant Cell* 20, 2681–2695. doi: 10.1105/tpc.108.061739

Etemadi, M., Gutjahr, C., Couzigou, J. M., Zouine, M., Lauressergues, D., Timmers, A., et al. (2014). Auxin perception is required for arbuscule development in arbuscular mycorrhizal symbiosis. *Plant Physiol.* 166, 281–292. doi: 10.1104/pp.114.246595

Ferguson, B. J., and Mathesius, U. (2014). Phytohormone regulation of legume-rhizobia interactions. *J. Chem. Ecol.* 40, 770–790. doi: 10.1007/s10886-014-0472-7

Floss, D. S., Levy, J. G., Lévesque-Tremblay, V., Pumplin, N., and Harrison, M. J. (2013). DELLA proteins regulate arbuscule formation in arbuscular mycorrhizal symbiosis. *Proc. Natl. Acad. Sci. U.S.A.* 110, E5025–E5034. doi: 10.1073/pnas.1308973110

Fonouni-Farde, C., Kisiala, A., Brault, M., Emery, R. J. N., Diet, A., and Frugier, F. (2017). DELLA1-Mediated gibberellin signaling regulates cytokinin-dependent symbiotic nodulation. *Plant Physiol.* 175, 1795–1806. doi: 10.1104/pp.17.00919

Fonouni-Farde, C., McAdam, E., Nichols, D., Diet, A., Foo, E., and Frugier, F. (2018). Cytokinins and the CRE1 receptor influence endogenous gibberellin levels in *Medicago truncatula*. *Plant Signal. Behav.* 13:e1428513. doi: 10.1080/15592324.2018.1428513

Fonouni-Farde, C., Tan, S., Baudin, M., Brault, M., Wen, J., Mysore, K. S., et al. (2016). DELLA-mediated gibberellin signalling regulates Nod factor signalling and rhizobial infection. *Nat Commun* 7:12636. doi: 10.1038/ncomms12636

Franssen, H. J., Xiao, T. T., Kulikova, O., Wan, X., Bisseling, T., Scheres, B., et al. (2015). Root developmental programs shape the Medicago truncatula nodule meristem. *Development* 142, 2941–2950. doi: 10.1242/dev.120774

Gamas, P., Brault, M., Jardinaud, M. F., and Frugier, F. (2017). Cytokinins in symbiotic nodulation: when, where, what for? *Trends Plant Sci.* 22, 792–802. doi: 10.1016/j.tplants.2017.06.012

Gaspar, T., Kevers, C., Faivre-rampant, O., Crèvecoeur, M., Penel, C., Greppin, H., et al. (2003). Changing concepts in plant hormone action. *Soc. In Vitro Biol._Plant* 39, 85–106. doi: 10.1079/IVP2002393

Gomez-Roldan, V., Fermas, S., Brewer, P. B., Puech-Pages, V., Dun, E. A., Pillot, J. P., et al. (2008). Strigolactone inhibition of shoot branching. *Nature* 455, 189–194. doi: 10.1038/nature07271

Gonzalez-Rizzo, S., Crespi, M., and Frugier, F. (2006). The *Medicago truncatula* CRE1 cytokinin receptor regulates lateral root development and early symbiotic interaction with *Sinorhizobium meliloti*. *Plant Cell* 18, 2680–2693. doi: 10.1105/tpc.106.043778

Gough, C., and Cullimore, J. (2011). Lipo-chitooligosaccharide signaling in endosymbiotic plant-microbe interactions. *Mol. Plant Microbe Interact.* 24, 867–878. doi: 10.1094/MPMI-01-11-0019

Hayashi, S., Reid, D. E., Lorenc, M. T., Stiller, J., Edwards, D., Gresshoff, P. M., et al. (2012). Transient Nod factor-dependent gene expression in the nodulation-competent zone of soybean (*Glycine max* [L.] Merr.) roots. *Plant Biotechnol. J.* 10, 995–1010. doi: 10.1111/j.1467-7652.2012.00729.x

Heidstra, R., Yang, W. C., Yalcin, Y., Peck, S., Emons, A. M., van Kammen, A., et al. (1997). Ethylene provides positional information on cortical cell division but is not involved in Nod factor-induced root hair tip growth in Rhizobium-legume interaction. *Development* 124, 1781–1787.

Held, M., Hou, H., Miri, M., Huynh, C., Ross, L., Hossain, M. S., et al. (2014). Lotus japonicus cytokinin receptors work partially redundantly to mediate nodule formation. *Plant Cell* 26, 678–694. doi: 10.1105/tpc.113.119362

Herrbach, V., Chirinos, X., Rengel, D., Agbevenou, K., Vincent, R., Pateyron, S., et al. (2017). Nod factors potentiate auxin signaling for transcriptional regulation and lateral root formation in *Medicago truncatula*. *J. Exp. Bot.* 68, 568–582. doi: 10.1093/jxb/erw474

Jardinaud, M. F., Boivin, S., Rodde, N., Catrice, O., Kisiala, A., Lepage, A., et al. (2016). A laser dissection-RNAseq analysis highlights the activation of cytokinin pathways by Nod factors in the *Medicago truncatula* root epidermis. *Plant Physiol.* 171, 2256–2276. doi: 10.1104/pp.16.00711

Jin, Y., Liu, H., Luo, D., Yu, N., Dong, W., Wang, C., et al. (2016). DELLA proteins are common components of symbiotic rhizobial and mycorrhizal signalling pathways. *Nat. Commun.* 7:12433. doi: 10.1038/ncomms12433

Jones, A. M., Danielson, J. A., Manojkumar, S. N., Lanquar, V., Grossmann, G., and Frommer, W. B. (2014). Abscisic acid dynamics in roots detected with genetically encoded FRET sensors. *eLife* 3:e01741. doi: 10.7554/eLife.01741

Kieber, J. J., and Schaller, G. E. (2014). Cytokinins. *Arabidopsis Book* 12, e0168. doi: 10.1199/tab.0168

Larrainzar, E., Riely, B. K., Kim, S. C., Carrasquilla-Garcia, N., Yu, H. J., Hwang, H. J., et al. (2015). Deep Sequencing of the *Medicago truncatula* root transcriptome reveals a massive and early interaction between nodulation factor and ethylene signals. *Plant Physiol.* 169, 233–265. doi: 10.1104/pp.15.00350

Lauressergues, D., Delaux, P. M., Formey, D., Lelandais-Brière, C., Fort, S., Cottaz, S., et al. (2012). The microRNA miR171h modulates arbuscular mycorrhizal colonization of *Medicago truncatula* by targeting NSP2. *Plant J.* 72, 512–522. doi: 10.1111/j.1365-313X.2012.05099.x

Liao, C. Y., Smet, W., Brunoud, G., Yoshida, S., Vernoux, T., and Weijers, D. (2015). Reporters for sensitive and quantitative measurement of auxin response. *Nat. Methods* 12, 207–210, 2 p following 210. doi: 10.1038/nmeth.3279

Maekawa, T., Maekawa-Yoshikawa, M., Takeda, N., Imaizumi-Anraku, H., Murooka, Y., and Hayashi, M. (2009). Gibberellin controls the nodulation signaling pathway in *Lotus japonicus*. *Plant J.* 58, 183–194. doi: 10.1111/j.1365-313X.2008.03774.x

Maillet, F., Poinsot, V., André, O., Puech-Pages, V., Haouy, A., Gueunier, M., et al. (2011). Fungal lipochitooligosaccharide symbiotic signals in arbuscular mycorrhiza. *Nature* 469, 58–63. doi: 10.1038/nature09622

Marsh, J. F., Rakocevic, A., Mitra, R. M., Brocard, L., Sun, J., Eschstruth, A., et al. (2007). *Medicago truncatula* NIN is essential for rhizobial-independent nodule organogenesis induced by autoactive calcium/calmodulin-dependent protein kinase. *Plant Physiol.* 144, 324–335. doi: 10.1104/pp.106.093021

Mathesius, U., Schlaman, H. R., Spaink, H. P., Of Sautter, C., Rolfe, B. G., and Djordjevic, M. A. (1998). Auxin transport inhibition precedes root nodule formation in white clover roots and is regulated by flavonoids and derivatives of chitin oligosaccharides. *Plant J.* 14, 23–34. doi: 10.1046/j.1365-313X.1998.00090.x

Miyata, K., Kawaguchi, M., and Nakagawa, T. (2013). Two distinct EIN2 genes cooperatively regulate ethylene signaling in *Lotus japonicus*. *Plant Cell Physiol.* 54, 1469–1477. doi: 10.1093/pcp/pct095

Mortier, V., Wasson, A., Jaworek, P., De Keyser, A., Decroos, M., Holsters, M., et al. (2014). Role of LONELY GUY genes in indeterminate nodulation on Medicago truncatula. *New Phytol.* 202, 582–593. doi: 10.1111/nph.12681

Murray, J. D., Karas, B. J., Sato, S., Tabata, S., Amyot, L., and Szczyglowski, K. (2007). A cytokinin perception mutant colonized by Rhizobium in the absence of nodule organogenesis. *Science* 315, 101–104. doi: 10.1126/science.1132514

Ng, J. L., Hassan, S., Truong, T. T., Hocart, C. H., Laffont, C., Frugier, F., et al. (2015). Flavonoids and auxin transport inhibitors rescue symbiotic nodulation in the *Medicago truncatula* cytokinin perception mutant cre1. *Plant Cell* 27, 2210–2226. doi: 10.1105/tpc.15.00231

Ng, J. L. P., and Mathesius, U. (2018). Acropetal auxin transport inhibition is involved in indeterminate but not determinate nodule formation. *Front. Plant Sci.* 9:169. doi: 10.3389/fpls.2018.00169

Olah, B., Briere, C., Bécard, G., Dénarié, J., and Gough, C. (2005). Nod factors and a diffusible factor from arbuscular mycorrhizal fungi stimulate lateral root formation in *Medicago truncatula* via the DMI1/DMI2 signalling pathway. *Plant J.* 44, 195–207. doi: 10.1111/j.1365-313X.2005.02522.x

Oldroyd, G. E., Engstrom, E. M., and Long, S. R. (2001). Ethylene inhibits the Nod factor signal transduction pathway of *Medicago truncatula*. *Plant Cell* 13, 1835–1849. doi: 10.1105/tpc.13.8.1835

Op den Camp, R. H., De Mita, S., Lillo, A., Cao, Q., Limpens, E., Bisseling, T., et al. (2011). A phylogenetic strategy based on a legume-specific whole genome duplication yields symbiotic cytokinin type-a response regulators. *Plant Physiol.* 157, 2013–2022. doi: 10.1104/pp.111.187526

Penmetsa, R. V., and Cook, D. R., (1997). A legume ethylene-insensitive mutant hyperinfected by its rhizobial symbiont. *Science* 275, 527–530. doi: 10.1126/science.275.5299.527

Penmetsa, R. V., Frugoli, J. A., Smith, L. S., Long, S. R., and Cook, D. R. (2003). Dual genetic pathways controlling nodule number in *Medicago truncatula*. *Plant Physiol.* 131, 998–1008. doi: 10.1104/pp.015677

Penmetsa, R. V., Uribe, P., Anderson, J., Lichtenzveig, J., Gish, J. C., Nam, Y. W., et al. (2008). The *Medicago truncatula* ortholog of Arabidopsis EIN2, sickle, is a negative regulator of symbiotic and pathogenic microbial associations. *Plant J.* 55, 580–595. doi: 10.1111/j.1365-313X.2008.03531.x

Plet, J., Wasson, A., Ariel, F., Le Signor, C., Baker, D., Mathesius, U., et al. (2011). MtCRE1-dependent cytokinin signaling integrates bacterial and plant cues to coordinate symbiotic nodule organogenesis in *Medicago truncatula*. *Plant J.* 65, 622–633. doi: 10.1111/j.1365-313X.2010.04447.x

Reid, D., Liu, H., Kelly, S., Kawaharada, Y., Mun, T., Andersen, S. U., et al. (2018). Dynamics of ethylene production in response to compatible nod factor. *Plant Physiol.* 176, 1764–1772. doi: 10.1104/pp.17.01371

Reid, D., Nadzieja, M., Novák, O., Heckmann, A. B., Sandal, N., and Stougaard, J. (2017). Cytokinin biosynthesis promotes cortical cell responses during nodule development. *Plant Physiol.* 175, 361–375. doi: 10.1104/pp.17.00832

Reid, D. E., Heckmann, A. B., Novák, O., Kelly, S., and Stougaard, J. (2016). CYTOKININ OXIDASE/DEHYDROGENASE3 maintains cytokinin homeostasis during root and Nodule Development in *Lotus japonicus*. *Plant Physiol.* 170, 1060–1074. doi: 10.1104/pp.15.00650

Roy, S., Robson, F., Lilley, J., Liu, C. W., Cheng, X., Wen, J., et al. (2017). MtLAX2, a functional homologue of the Arabidopsis auxin influx transporter AUX1, is required for nodule organogenesis. *Plant Physiol.* 174, 326–338. doi: 10.1104/pp.16.01473

Sharma, S. B., and Signer, E. R. (1990). Temporal and spatial regulation of the symbiotic genes of *Rhizobium meliloti* in planta revealed by transposon Tn5-gusA. *Genes Dev.* 4, 344–356. doi: 10.1101/gad.4.3.344

Sun, J., Cardoza, V., Mitchell, D. M., Bright, L., Oldroyd, G., and Harris, J. M. (2006). Crosstalk between jasmonic acid, ethylene and Nod factor signaling allows integration of diverse inputs for regulation of nodulation. *Plant J.* 46, 961–970. doi: 10.1111/j.1365-313X.2006.02751.x

Sun, T. P. (2011). The molecular mechanism and evolution of the GA-GID1-DELLA signaling module in plants. *Curr. Biol.* 21, R338–R345. doi: 10.1016/j.cub.2011.02.036

Timmers, A. C., Auriac, M. C., and Truchet, G. (1999). Refined analysis of early symbiotic steps of the Rhizobium-Medicago interaction in relationship with microtubular cytoskeleton rearrangements. *Development* 126, 3617–3628.

Tirichine, L., Sandal, N., Madsen, L. H., Radutoiu, S., Albrektsen, A. S., Sato, S., et al. (2007). A gain-of-function mutation in a cytokinin receptor triggers spontaneous root nodule organogenesis. *Science* 315, 104–107. doi: 10.1126/science.1132397

Truchet, G., Roche, P., Lerouge, P., Vasse, J., Camut, S., de Billy, F., et al. (1991). Sulphated lipo-oligosaccharide signals of Rhizobium meliloti elicit root nodule organogenesis in alfalfa. *Nat. Rev. Genet.* 351, 670–673. doi: 10.1038/351670a0

van Noorden, G. E., Ross, J. J., Reid, J. B., Rolfe, B. G., and Mathesius, U. (2006). Defective long-distance auxin transport regulation in the *Medicago truncatula* super numeric nodules mutant. *Plant Physiol.* 140, 1494–1506. doi: 10.1104/pp.105.075879

van Zeijl, A., Liu, W., Xiao, T. T., Kohlen, W., Yang, W. C., Bisseling, T., et al. (2015a). The strigolactone biosynthesis gene DWARF27 is co-opted in rhizobium symbiosis. *BMC Plant Biol.* 15:260. doi: 10.1186/s12870-015-0651-x

van Zeijl, A., Op den Camp, R., Deinum, E., Charnikhova, T., Franssen, H., Op den Camp, H., et al. (2015b). Rhizobium lipo-chitooligosaccharide signaling triggers accumulation of cytokinins in *Medicago truncatula* roots. *Mol. Plant* 8, 1213–1226. doi: 10.1016/j.molp.2015.03.010

Yang, Y., Yue, R., Sun, T., Zhang, L., Chen, W., Zeng, H., et al. (2015). Genome-wide identification, expression analysis of GH3 family genes in *Medicago truncatula* under stress-related hormones and Sinorhizobium meliloti infection. *Appl. Microbiol. Biotechnol.* 99, 841–854. doi: 10.1007/s00253-014-6311-5

Zaat, S. A., Van Brussel, A. A., Tak, T., Lugtenberg, B. J., and Kijne, J. W. (1989). The ethylene-inhibitor aminoethoxyvinylglycine restores normal nodulation by *Rhizobium leguminosarum* biovar. viciae on Vicia sativa subsp. nigra by suppressing the 'Thick and short roots' phenotype. *Planta* 177, 141–150. doi: 10.1007/BF00392802

Conflict of Interest Statement: The authors declare that the research was conducted in the absence of any commercial or financial relationships that could be construed as a potential conflict of interest.

frontiers in Plant Science

ORIGINAL RESEARCH
published: 08 August 2018
doi: 10.3389/fpls.2018.01150

Local and Systemic Effect of Cytokinins on Soybean Nodulation and Regulation of Their *Isopentenyl Transferase* (*IPT*) Biosynthesis Genes Following Rhizobia Inoculation

Celine Mens[†‡], *Dongxue Li*[†], *Laura E. Haaima, Peter M. Gresshoff and Brett J. Ferguson*[*]

Centre for Integrative Legume Research, School of Agriculture and Food Sciences, The University of Queensland, Brisbane, QLD, Australia

Cytokinins are important regulators of cell proliferation and differentiation in plant development. Here, a role for this phytohormone group in soybean nodulation is shown through the exogenous application of cytokinins (6-benzylaminopurine, N^6-(Δ^2-isopentenyl)-adenine and *trans*-zeatin) via either root drenching or a petiole feeding technique. Overall, nodule numbers were reduced by treatment with high cytokinin concentrations, but increased with lower concentrations. This was especially evident when feeding the solutions directly into the vasculature via petiole feeding. These findings highlight the importance of cytokinin in nodule development. To further investigate the role of cytokinin in controlling nodule numbers, the *IPT* gene family involved in cytokinin biosynthesis was characterized in soybean. Bioinformatic analyses identified 17 *IPT* genes in the soybean genome and homeologous duplicate gene partners were subsequently identified including *GmIPT5* and *GmIPT6*, the orthologs of *LjIPT3*. Expression of *GmIPT5* was upregulated in the shoot in response to nodulation, but this was independent of a functional copy of the autoregulation of nodulation (AON) receptor, GmNARK, which suggests it is unlikely to have a role in the negative feedback system called AON. Legumes also control nodule numbers in the presence of soil nitrogen through nitrate-dependent regulation of nodulation, a locally acting pathway in soybean. Upon nitrate treatment to the root, the tandem duplicates *GmIPT3* and *GmIPT15* were upregulated in expression indicating a role for these genes in the plant's response to soil nitrogen, potentially including the nitrate-dependent regulation of legume nodulation pathway. Additional roles for cytokinin and their *IPT* biosynthetic genes in nodulation and the control of nodule numbers are discussed.

Keywords: autoregulation of nodulation, cytokinin, legumes, nodulation, plant signaling and development, symbiosis, IPT, isopentenyltransferase

OPEN ACCESS

Edited by:
Stig U. Andersen, Aarhus University, Denmark

Reviewed by:
Katharina Markmann, Universität Tübingen, Germany
Florian Frugier, Centre National de la Recherche Scientifique (CNRS), France

***Correspondence:**
Brett J. Ferguson
b.ferguson1@uq.edu.au

[†]*These authors have contributed equally to this work*

[‡]*orcid.org/0000-0001-6104-0442*

Specialty section:
This article was submitted to Plant Microbe Interactions, a section of the journal Frontiers in Plant Science

Received: *17 December 2017*
Accepted: *18 July 2018*
Published: *08 August 2018*

Citation:
Mens C, Li D, Haaima LE, Gresshoff PM and Ferguson BJ (2018) Local and Systemic Effect of Cytokinins on Soybean Nodulation and Regulation of Their Isopentenyl Transferase (IPT) Biosynthesis Genes Following Rhizobia Inoculation. Front. Plant Sci. 9:1150. doi: 10.3389/fpls.2018.01150

INTRODUCTION

Legumes are economically important food, feed and fuel crops (Gresshoff et al., 2015). The majority are able to engage in a symbiotic relationship with nitrogen-fixing soil bacteria referred to as rhizobia, allowing legumes to grow under low soil nitrogen conditions. While rhizobia fix atmospheric nitrogen (N_2) into ammonia that is readily assimilated by the plant, rhizobia in return receive photosynthetic carbohydrates in the protected nodule environment.

Reciprocal plant-microbe signaling is required to establish this relationship, which results in the formation of new root organs called nodules. Both nodulation and nitrogen fixation come at a high energy and resource cost to the plant. It is therefore important for the host to regulate its nodule numbers. This can be achieved via a nitrate-dependent regulation of nodulation mechanism in the presence of high soil nitrogen and through autoregulation of nodulation (AON) (Ferguson et al., 2010; Reid et al., 2011; Ferguson et al., 2018). The AON pathway is a negative feedback system involving extensive signaling between the root and shoot. Following rhizobia inoculation, plant-derived CLAVATA3/embryo-surrounding region (CLE) peptide signals are produced in the root (Reid et al., 2011; Hastwell et al., 2015a,b, 2018). These peptides are transported via the xylem to the shoot where they are perceived by a receptor complex that centers around a CLAVATA1 (CLV1)-like leucine-rich repeat receptor kinase [such as GmNARK in *Glycine max* (soybean), LjHAR1 in *Lotus japonicus* and MtSUNN in *Medicago truncatula*] (Okamoto et al., 2009, 2013; Mortier et al., 2010; Reid et al., 2011). Perception of the CLE peptides results in the differential regulation of a novel shoot-derived signal that travels back down to the roots to regulate nodule numbers (Ferguson et al., 2010; Ferguson et al., 2018). The shoot-derived signal and many other factors acting in the control of nodule numbers, are currently unknown or poorly understood.

Phytohormones are important signals involved in the formation and regulation of legume nodules (reviewed by Ferguson and Mathesius, 2014). Cytokinin hormones are a class of structurally similar N^6-substituted adenine derivatives with a central role in plant growth and development. Since their discovery in cell proliferation and differentiation, several other functions have been attributed to this class of phytohormones, including maintenance of the shoot apical meristem, branching, organogenesis, delay of senescence, long-distance communication of nutritional status and the plant's response to biotrophic pathogens (reviewed by Kamada-Nobusada and Sakakibara, 2009). Like auxins, they can act both locally and as long-distance messengers. Natural cytokinins are classified into aromatic and isoprenoid cytokinins, the latter are most prevalent in higher plants and include *trans*-zeatin (tZ), *cis*-zeatin (cZ), dihydrozeatin (DZ) and N^6-(Δ^2-isopentenyl)-adenine (2-iP). Cytokinins show further variation through the addition of side chains, which seem to confer receptor specificity. Kinetin and 6-benzylaminopurine (BAP) are synthetic cytokinins frequently used for research purposes.

In legumes, the exogenous application of cytokinins induces the formation of nodule-like structures through the induction of early nodulin genes and cortical cell divisions (Mathesius et al., 2000; Heckmann et al., 2011). Mutants defective in the cytokinin receptor histidine kinase, Cytokinin Response 1 (CRE1) in *M. truncatula* and its ortholog Lotus Histidine Kinase 1 (LHK1) in *L. japonicus*, lack the ability to effectively form nodule primordia, whereas gain-of-function mutants exhibit spontaneous nodule formation (Gonzalez-Rizzo et al., 2006; Murray et al., 2007; Tirichine et al., 2007; Plet et al., 2011). Moreover, *Lonely Guy* (*LOG*) genes encoding cytokinin riboside 5′-monophosphate phosphoribohydrolase, which are involved in the biological activation of cytokinins, were found to be expressed in the proliferating cells of the nodule primordium (Mortier et al., 2014). Upregulation of *LOG* genes resulted in less nodules and was independent of the leucine-rich repeat receptor kinase that acts in the shoot to perceive root-derived CLE peptide signals during AON (Mortier et al., 2014).

Isopentenyl transferases (IPTs) carry out the first and rate-limiting step in cytokinin biosynthesis, where an isopentenyl group is transferred to either AMP, ADP or ATP (Kakimoto, 2001). Recently, *IPT3* was shown to be required for nodule development in the model legume *L. japonicus* (Chen et al., 2014; Sasaki et al., 2014; Reid et al., 2017). It has also been proposed that LjIPT3 could have a role in the synthesis of cytokinin molecules that act as the shoot-derived inhibitory factor in AON (Sasaki et al., 2014). LjIPT2 is thought to be responsible for the initial cytokinin build-up required for nodulation initiation, alongside LjLOG4 and independent of the LHK1 receptor (Reid et al., 2017). Interestingly, IPT encoding genes are also differentially expressed following treatment with certain nitrogen sources (Miyawaki et al., 2004), with nitrogen promoting plant development, but also inhibiting nodule organogenesis. However, it is important to remember that in addition to synthesis, post-transcriptional processing and degradation are also important to maintaining homeostasis of biologically active cytokinins.

Here, we report that exogenous application of low concentrations of cytokinin promotes nodule numbers in soybean, while high concentrations reduce them. This was achieved by treating soybean with either BAP, 2-iP or tZ type cytokinins using root-drench or petiole-feeding methods. These findings support the notion that cytokinin promotes nodule organogenesis, but suggest that the hormone is unlikely the shoot-derived factor of AON and that the inhibition we observe by feeding high concentrations is more likely the result of toxicity to the plant. In addition, 17 *IPT* genes were identified in the soybean genome and genetically characterized. Of these genes, the tandem duplicates *GmIPT3* and *GmIPT15* were upregulated in the root upon nitrate treatment, indicating a role for these genes in nitrate response. Upon rhizobia inoculation, *GmIPT5* (a soybean ortholog of *LjIPT3*) was significantly upregulated in the shoot following rhizobia inoculation of the root, consistent with previous reports (Chen et al., 2014; Sasaki et al., 2014). Upregulation of *GmIPT5* occurred in both the root and shoot in wild-type and GmNARK mutant plants (*nts382*), indicating that it functions in the leaf and root in response to nodulation, but likely does not have a role in the AON pathway.

MATERIALS AND METHODS

General Plant and Bacterial Growth Conditions

Soybean lines used include wild-type Bragg and the GmNARK mutant lines *nts1116* (weak allele) and *nts382* (strong allele), a hypernodulating and supernodulating line, respectively (Carroll et al., 1985). Seeds were surface-sterilized overnight with chlorine gas or in 70% ethanol/3.5% H_2O_2 for 1 min followed by extensive rinsing with sterilized water.

Plants were grown in controlled glasshouse conditions with a 16 h/8 h photoperiod at 28 and 26°C, respectively and watered as required with a modified nutrient solution (Broughton and Dilworth, 1971; Herridge, 1982). For the nitrate treatments, the nutrient solution was supplemented with 10 mM of KNO_3 in the week before harvest and applied every second day for 6 days prior to sample collection.

Plants were inoculated with *Bradyrhizobium diazoefficiens* CB1809/USDA110 (formerly *Bradyrhizobium japonicum*) or the incompatible Nod-factor mutant *nodC*$^{-}$. The rhizobia were grown at 28°C in a yeast-mannitol broth for 3 days and inoculated at an optical density at 600 nm of 0.1. Nodule numbers were determined 9 days after inoculation and subsequently root dry weights were recorded.

Cytokinin Treatments

Six-week old plants were treated with water as a control or three different types of cytokinin (BAP, 2-iP and tZ) at concentrations of 0.1 or 100 μM. The hormones were dissolved in MilliQ water and the treatments were administered through either root drenching (Lorteau et al., 2001) or petiole feeding (Lin et al., 2010, 2011). For the root-drench assay, the hormone solutions (150 ml) were poured directly onto the vermiculite every second day. For the petiole-feeding assay, a feeding apparatus consisting of a syringe and silicon tubing was constructed that enables the cytokinin solution to be fed continuously into the shoot via a severed petiole. This method directly supplies the solutions into the plant, including the phloem, which mimics the source of the shoot-derived inhibitor. In both cases, plants were inoculated with *B. diazoefficiens* CB1809 1 day after the start of feeding. Plants were harvested after 10 days of treatment.

Bioinformatic Analysis

To identify the *IPT* gene family in soybean, common bean (*Phaseolus vulgaris*), *M. truncatula* and *L. japonicus*, multiple BLASTP searches were conducted against various online databases including Phytozome, NCBI, DOBLAST and Lotus Base using the LjIPT3 and the nine previously identified AtIPT amino acid sequences as a query (Takei et al., 2001; Miyawaki et al., 2004). Functional domains were predicted via the Pfam (EMBL-EBI) and PANTHER^{TM} v11.0 databases (Punta et al., 2012; Mi et al., 2017). Synteny between genomic environments was analyzed using Phytozome JBrowse. The obtained sequences were further characterized through a multiple sequence alignment via Clustal Omega hosted by EMBL-EBI (Goujon et al., 2010; Sievers et al., 2011; McWilliam et al., 2013; Corcilius et al., 2017). Phylogenetic trees were constructed using the PHYML plugin embedded in Geneious Pro v10.0.9 (Guindon and Gascuel, 2003) based on the protein sequence alignment adjusted by an algorithm in Geneious Pro v10.0.9 to retain only the homologous sequences and remove 75% of the gap regions. This plugin implements the maximum likelihood method to generate phylogenetic trees with 1,000 bootstraps supporting the branches.

Gene Expression Analysis

For gene expression analyses, the first trifoliate leaf and the entire root from rhizobia-inoculated plants or root from 23-day-old nitrate-treated plants, were harvested, snap-frozen and homogenized in liquid nitrogen. The tissue was harvested 10 days after rhizobia inoculation of 2-week old plants. Total RNA was extracted the automated Maxwell® LEV simplyRNA Tissue kit (Promega) according to the manufacturer's protocol. The quality and quantity of the RNA samples were assessed using the NanoDrop^{TM} One Spectrophotometer (Thermo Fisher Scientific). SuperScript® III Reverse Transcriptase (Invitrogen) was used to generate cDNA from 500 ng of DNase-treated RNA. An initial PCR on cDNA was done to identify *IPT* genes expressed in the different conditions. An RT-qPCR analysis was performed using the Roche LightCycler® 96 with SYBR green fluorescence detection in a 96-well plate. All reactions were conducted in duplicate for at least two biological replicates and a target amplicon size of approximately 100 bp (**Supplementary Table S1**). The *GmCons6* housekeeping gene was included to normalize gene expression levels (Libault et al., 2008).

Statistical Analysis

A statistical analysis was performed on all results using the GraphPad Prism 7 software. A Student's *t*-test was used to determine the statistical significance of differences in nodule numbers assuming normal distribution of the data, root dry weights and relative expression of the target genes.

RESULTS

Effect of Cytokinin Treatment on Soybean Nodulation

To determine the effect of cytokinin on soybean nodulation, 0.1 or 100 μM of BAP, tZ or 2-IP or a water control, were applied to the hypernodulating GmNARK mutant, *nts1116*. Concentrations lower than 0.1 μM were not applied as these are too low to induce a response in soybean. The hypernodulating mutant was used as a possible effect on nodule numbers caused by the cytokinin treatments would be easier to observe and quantify on a hypernodulating *nts1116* root system compared with the wild-type. The cytokinin treatments were administered using one of two methods; root-drenching or a petiole-feeding method to introduce the hormone to the shoot (Lin et al., 2010, 2011), after which the nodule number and root dry weight were determined.

Petiole feeding of 100 μM solutions with any of the three types of cytokinin significantly reduced nodule numbers compared with the water control ($P < 0.001$) (**Figure 1A**). In contrast, low 0.1 μM concentrations of both BAP and 2-IP significantly increase the number of nodules formed ($P = 0.0004$ and $P = 0.030$, respectively). A slight increase was also observed using 0.1 μM tZ, but this was not significant ($P = 0.096$). No significant differences in root dry weight were observed with any of the treatments used.

The root drenching results were similar, but generally less pronounced. Application of 100 μM BAP almost completely abolished nodulation ($P < 0.0001$), with 100 μM tZ also resulting

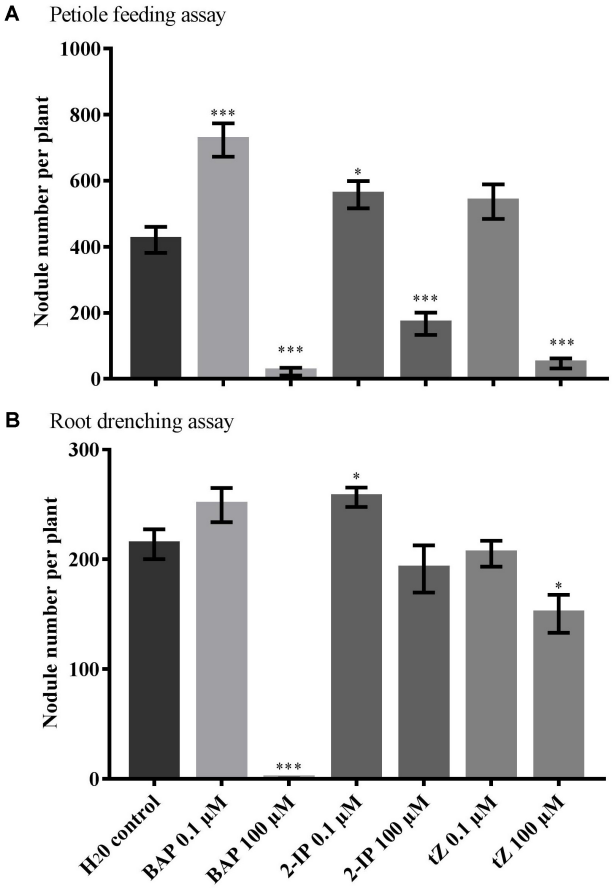

FIGURE 1 | Effect of cytokinin treatment on nodule number. Supernodulating soybean plants (*nts1116*) were fed water (control) or cytokinin through **(A)** petiole feeding or **(B)** root drenching. Plants were inoculated with *Bradyrhizobium diazoefficiens* (CB1809) 1 day after the start of treatment. Nodule numbers were counted after 10 days of treatment ($n = 8$). Data and error bars represent mean ± SEM. Asterisks indicate significant differences in nodule number compared with the water control (Student's *t*-test, $^{***}P \leq 0.001$, $^{**}P \leq 0.01$, $^{*}P \leq 0.05$).

in a significant reduction in nodule numbers ($P = 0.012$) (**Figure 1B**). Treatment with 100 µM 2-IP resulted in a slight, but not significant reduction ($P = 0.390$). Drenching with 0.1 µM of 2-IP significantly increased nodule numbers ($P = 0.019$), similar to what was observed using petiole feeding, whereas 0.1 µM of BAP or tZ led to a slight, but not significant, change in nodulation.

Identification and Sequence Characterization of the *IPT* Gene Family in Soybean

To determine the role of cytokinin biosynthesis during the development and control of soybean nodulation, *IPT* gene expression was investigated. First, the complete *IPT* gene family was identified in soybean via multiple BLAST searches using the LjIPT3 amino acid sequence as a query. LjIPT3 was previously reported to have a role in nodulation and/or AON (Chen et al., 2014; Sasaki et al., 2014; Reid et al., 2017). The BLAST results lead to the identification of 17 *IPT* gene members in soybean having high sequence identity to LjIPT3 (**Table 1** and **Supplementary Table S2**). All of the translated IPT gene products were predicted via the Pfam database to possess a tRNA delta(2)-isopentenyl pyrophosphate (IPP) transferase domain, which is critical for the enzyme's function in cytokinin biosynthesis, with the exception of GmIPT10, GmIPT15 and GmIPT17. However, additional searches using PANTHER^{TM} v11.0 confirmed the classification of GmIPT10, GmIPT15 and GmIPT17 within the IPP family of proteins. To further confirm their classification within the soybean *IPT* gene family and provide information on their potential function, synteny between their genomic environments was analyzed (see below, **Figure 3**).

The BLAST searches were broadened to include the databases for common bean, *L. japonicus*, *M. truncatula* and the non-legume *Arabidopsis thaliana*. This confirmed the presence of 23 putative IPT genes in *M. truncatula*, making it the largest gene family compared with the eight, six and nine members identified in common bean, *L. japonicus* and *A. thaliana*, respectively (Takei et al., 2001; Azarakhsh et al., 2018) (**Supplementary Tables S3–S6**).

To further characterize the sequences obtained here, a multiple sequence alignment and phylogenetic tree were produced using Clustal Omega and PHYML. The multiple sequence alignments revealed a high level of conservation of amino acid residues among the different members of both the legume and non-legume *IPT* gene families (**Supplementary Figures S1**, **S2**). This is most evident between the amino acid residues situated at the positions 102–213 in the alignment at the N-terminal end of the protein sequences where the functional IPP domain is located.

Seven homeologous (i.e., duplicate) gene pairs are present within the soybean genome grouping together in the phylogenetic tree (**Figure 2**). This is a common occurrence with soybean genes due to previous whole genome duplication events 59 and 13 million years ago (Schmutz et al., 2010).

The orthologs of LjIPT3 are the homeologous duplicates, GmIPT5 and GmIPT6, with 75.1 and 72.2% amino acid sequence identity, respectively, while sharing 83.1% identity. Other soybean IPT family members clustering closely to LjIPT3, are the homeologous duplicates GmIPT7 and GmIPT8 with 50.8 and 49.8% amino acid identity. These four soybean genes are present in duplicated regions in the genome showing their close relationship. Homologous versions of LjIPT3 in common bean, *M. truncatula* and *A. thaliana* have the identifiers Phvul.007G170100, Medtr1g072540 (MtIPT3) and AT3G63110 (AtIPT3) with a protein sequence identity of 76, 74 and 53%, respectively.

Six *IPT* genes group into two groups of three genes (*GmIPT3/GmIPT4/GmIPT15* and *GmIPT11/GmIPT12/GmIPT17*) (**Figure 2**). The first group clusters closely to *LjIPT2* that was recently shown to be responsible for the initial cytokinin burst required for nodulation initiation (Reid et al., 2017). The genomic regions of *GmIPT3* and *GmIPT4* display a high level of synteny with five identical genes surrounding the two *IPT* genes (**Figure 3A**). This indicates

that *GmIPT3* and *GmIPT4* are true homeologous duplicates. The third gene, *GmIPT15*, shares a protein sequence identity of 92.9% with *GmIPT3*. In addition, the two genes are present on the same chromosome (chromosome 17) and lack duplications of their genomic regions, indicating a recent tandem duplication of *GmIPT3* resulting in *GmIPT15*. Interestingly, the predicted GmIPT15 protein is truncated to only 75 amino acid residues and does not feature the highly conserved IPP amino acid sequence motif at the N-terminal end that is required for function. In addition to having a gap upstream of the predicted coding sequence that puts it out of frame, the currently available genome includes a 100 bp stretch of unconfirmed nucleic acid identity (denoted in the sequence as: -NNN-). Similar to GmIPT15, the GmIPT10 product is truncated with a stretch of nucleic acids of unconfirmed identity. This lack of identified nucleic acid residues in *GmIPT15* and *GmIPT10* may be due to the high level of sequence identity amongst the *IPT* genes and/or the presence of repetitive sequences within a gene, making the identity of some nucleic acid residues difficult to confirm with absolute certainty.

The second group (*GmIPT11/GmIPT12/GmIPT17*) is closely related to *LjIPT5* as well as *Phvul.011G091500* and *MtIPT5* in common bean and *M. truncatula*. The role of *LjIPT5* was previously investigated in nodule development and AON by Sasaki et al. (2014) and unlike *LjIPT3*, no differences in transcript levels were observed in the shoot after inoculation with compatible rhizobia. These orthologs are all characterized by the presence of a high number of introns (6–9 introns), except for *GmIPT17*, which has only one predicted intron (**Table 1**). A multiple sequence alignment of their genomic sequences using Clustal Omega indicated little conservation. *GmIPT11* and *GmIPT12* share 69.9% sequence identity and are located in a highly similar genomic region highlighted by the presence of six conserved genes (**Figure 3B**). The GmIPT12 protein is missing part of the N-terminal conserved region. Wrongly predicted intron locations might put the sequence out of frame leading to a truncated protein sequence. The genomic sequence of *GmIPT17* is much less conserved compared with *GmIPT11* and *GmIPT12* showing no conservation of the genomic region. *GmIPT17* likely does not have a homeologous duplicate. In addition, *GmIPT17* is predicted to be a truncated protein with only the central region translated. Like *GmIPT17*, *GmIPT16* is another gene that appears to completely lack a duplicate partner, indicating that it was lost or that *GmIPT16* arose after the most recent whole genome duplication event. A high level of genetic synteny is present for *GmIPT16* and orthologs in other legumes species including *MtIPT9* and *Phvul.005G067800* in contrast to *GmIPT17* (**Figure 3C**). Therefore, its homeologous duplicate was most likely lost over time.

IPT Gene Expression in the Shoot and Root Following Rhizobia Inoculation

Previously, cytokinin was suggested to be the unidentified shoot-derived inhibitor in AON as demonstrated by the upregulation of *LjIPT3* in wild-type shoots, but not in LjHAR1 defective mutants (Sasaki et al., 2014). To identify *IPT* genes in soybean that are differentially regulated following rhizobia inoculation of the root, the expression of all 17 *IPT* genes was examined in both the root and shoot (i.e., trifoliate leaves) (**Supplementary Figure S3**). The first trifoliate leaf was tested as the GmNARK receptor is highly expressed in mature trifoliate leaves (Nontachaiyapoom et al., 2007). Tissues were harvested from wild-type Bragg and its supernodulating GmNARK mutant (*nts382*) inoculated with either compatible *B. diazoefficiens* USDA110 or its incompatible *nodC*$^{-}$ mutant strain as a negative control. GmNARK function

TABLE 1 | Features of the *IPT* gene family in soybean.

Name	Phytozome identifier	Chromosome location	Orientation	IPP transferase domain	Predicted introns	Protein length
GmIPT1	Glyma.10G273500.1	Chr10:49594484..49595398	Reverse	Y	0	304
GmIPT2	Glyma.20G116500.1	Chr20:35894331..35895981	Forward	Y	1	231
GmIPT3	Glyma.17G017400.1	Chr17:1313758..1315795	Forward	Y	0	340
GmIPT4	Glyma.07G256700.1	Chr07:43274336..43276366	Reverse	Y	0	336
GmIPT5	Glyma.10G025300.1	Chr10:2189157..2190507	Reverse	Y	0	344
GmIPT6	Glyma.02G148600.1	Chr02:15319273..15320731	Forward	Y	0	327
GmIPT7	Glyma.19G154400.1	Chr19:41471430..41472362	Reverse	Y	0	310
GmIPT8	Glyma.03G151800.1	Chr03:36688884..36690099	Reverse	Y	0	309
GmIPT9	Glyma.15G103800.1	Chr15:8102824..8104803	Reverse	Y	0	342
GmIPT10	Glyma.13G209100.1	Chr13:32310692..32311377	Forward	N	0	154
GmIPT11	Glyma.11G188100.1	Chr11:25981523..25986063	Forward	Y	9	478
GmIPT12	Glyma.12G086300.1	Chr12:6987142..6990386	Reverse	Y	6	301
GmIPT13	Glyma.18G297300.1	Chr18:57479558..57480756	Forward	Y	0	333
GmIPT14	Glyma.08G364900.1	Chr08:47581368..47582279	Reverse	Y	1	293
GmIPT15	Glyma.17G045700.1	Chr17:3401249..3401828	Forward	N	0	75
GmIPT16	Glyma.13G271500.1	Chr13:37340399..37347149	Forward	Y	10	448
GmIPT17	Glyma.08G278400.1	Chr08:37592042..37592547	Reverse	N	1	69

tRNA delta(2)-isopentenyl pyrophosphate transferase domain (IPP) predicted via Pfam.

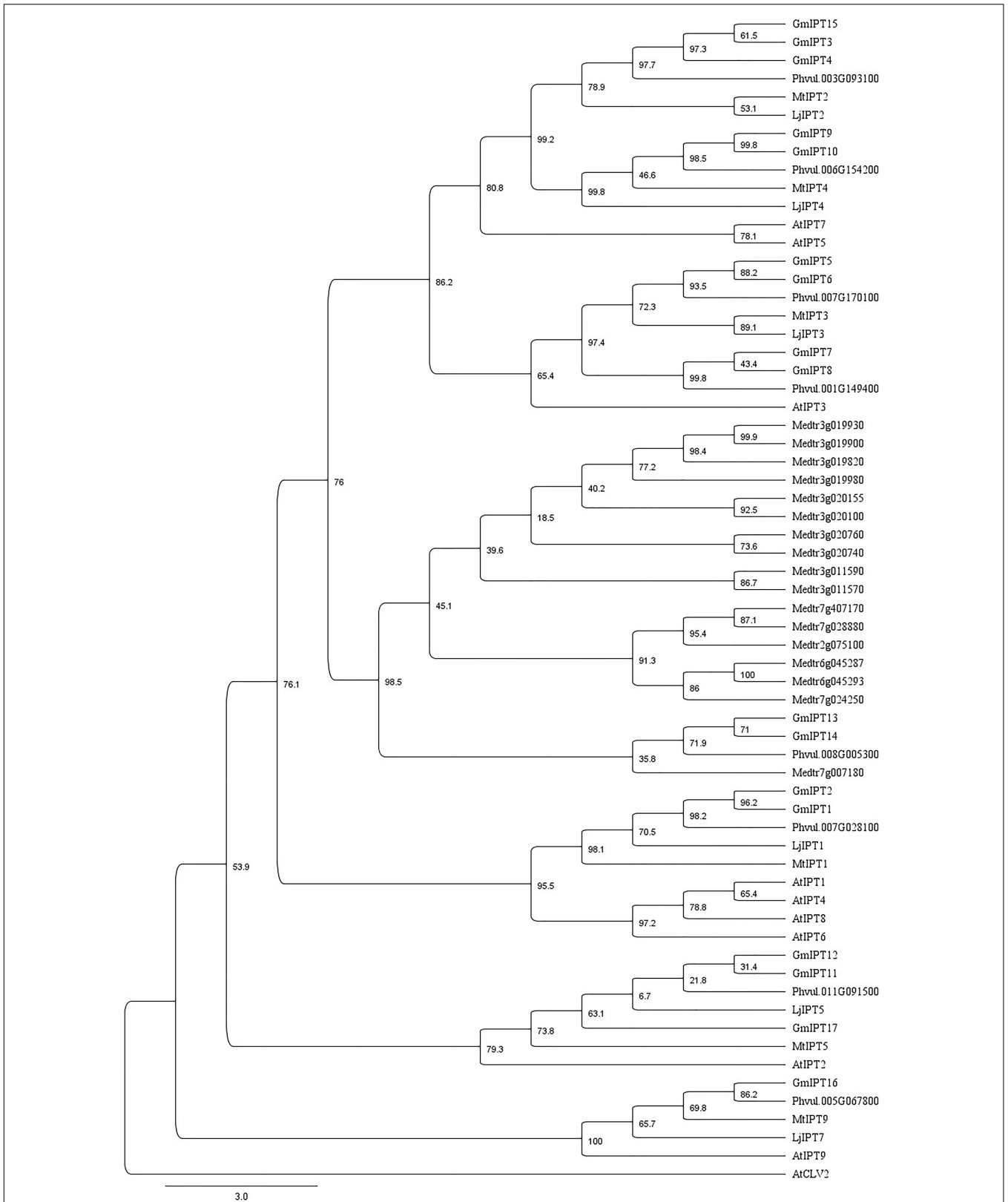

FIGURE 2 | Characterization of IPT orthologs. Phylogenetic tree generated using a multiple sequence alignment of homologous amino acid sequences with 75% of the gap regions removed showing similarity between IPT orthologs of soybean, *L. japonicus*, *M. truncatula*, common bean (*P. vulgaris*) and *A. thaliana* including AtCLV2 as an outgroup. The phylogenetic tree is shown with bootstrap confidence values as percentages from 1,000 bootstrap replications.

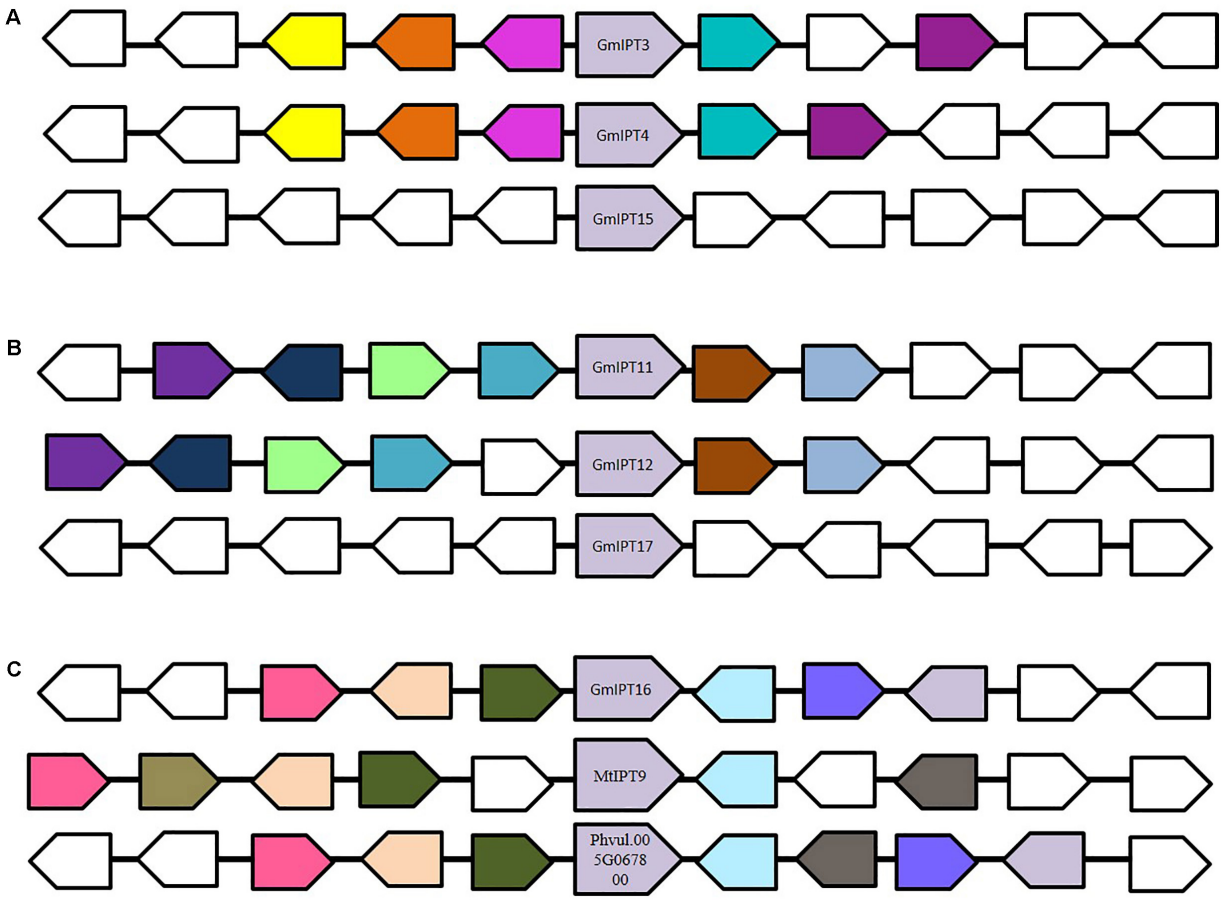

FIGURE 3 | Genomic environment of **(A)** *GmIPT3/GmIPT4/GmIPT5*, **(B)** *GmIPT11/GmIPT12/GmIPT17* and **(C)** *GmIPT16* in soybean. The genes of interest are centrally positioned and highlighted in purple. Surrounding genes with an identical putative function are shown in the same colors with genes with an unrelated function left uncolored. The direction of the arrow indicates the gene direction compared to the *IPT* genes. **(A)** *GmIPT3* and *GmIPT4* are true homologous with a highly conserved genomic region. *GmPT15* arose as a tandem duplication of *GmPT3*, in which only the *IPT* gene was duplicated and not its environment. **(B)** *GmIPT11* and *GmIPT12* are homeologous duplicates represented by the high level of gene synteny. *GmIPT17* does not share this conservation. **(C)** *GmIPT16* does not share synteny with any of the other 16 soybean *IPT* genes, but its surrounding genes are highly identical to those surrounding its orthologs *MtIPT9* and *Phvul.005G067800* in *M. truncatula* and common bean (*P. vulgaris*).

is completely blocked in the *nts382* background, enabling characterization of possible IPT candidates involved in the AON pathway.

The homeologous duplicates *GmIPT1* and *GmIPT2* respond to inoculation in the root, but not the shoot (**Figure 4**). This change in expression is significant for *GmIPT2* in both WT Bragg and GmNARK mutant (*nts382*) roots (P = 0.002 and P = 0.021, respectively); and is consistent with *LjIPT1* expression, the ortholog of *GmIPT1* and *GmIPT2*, which is upregulated in the root and not in the shoot (Chen et al., 2014; Sasaki et al., 2014).

Expression of the second homeologous pair, *GmIPT3* and *GmIPT4*, was root-specific and GmNARK-independent with transcript levels of *GmIPT4* increasing following inoculation (P = 0.161 in WT and P = 0.044 in *nts382*) (**Figure 4**). These genes cluster with *GmIPT15*, a duplicate of *GmIPT3* and possibly a pseudogene, which does not show a clear trend in expression in response to the presence of rhizobia. The ortholog of these genes is *LjIPT2*; it is expressed in roots in conjunction with *LjLOG4* and is reported to be required for the initial cytokinin burst in early nodulation (Reid et al., 2017).

One of the orthologs of *LjIPT3*, *GmIPT5*, was found to be significantly induced in the wild-type shoot upon inoculation with compatible rhizobia (P = 0.014) (**Figure 4**). This trend of elevated *GmIPT5* expression was observed in the root as well (P = 0.165) and similarly observed in the GmNARK mutant root and shoot; however, these increases in expression were not significant (P = 0.060 and 0.244, respectively). As a trend of upregulation was noticeable, a second set of GmNARK mutant shoot samples was analyzed to determine whether *GmIPT5* expression is GmNARK-dependent or not (**Figure 5**). This established a significant increase in *GmIPT5* transcript levels in a GmNARK-independent manner (P = 0.0003). Expression of *GmIPT6*, the homeologous duplicate of *GmIPT5*, exhibited a similar pattern in response to inoculation with compatible rhizobia, with the exception of GmNARK mutant shoots, but

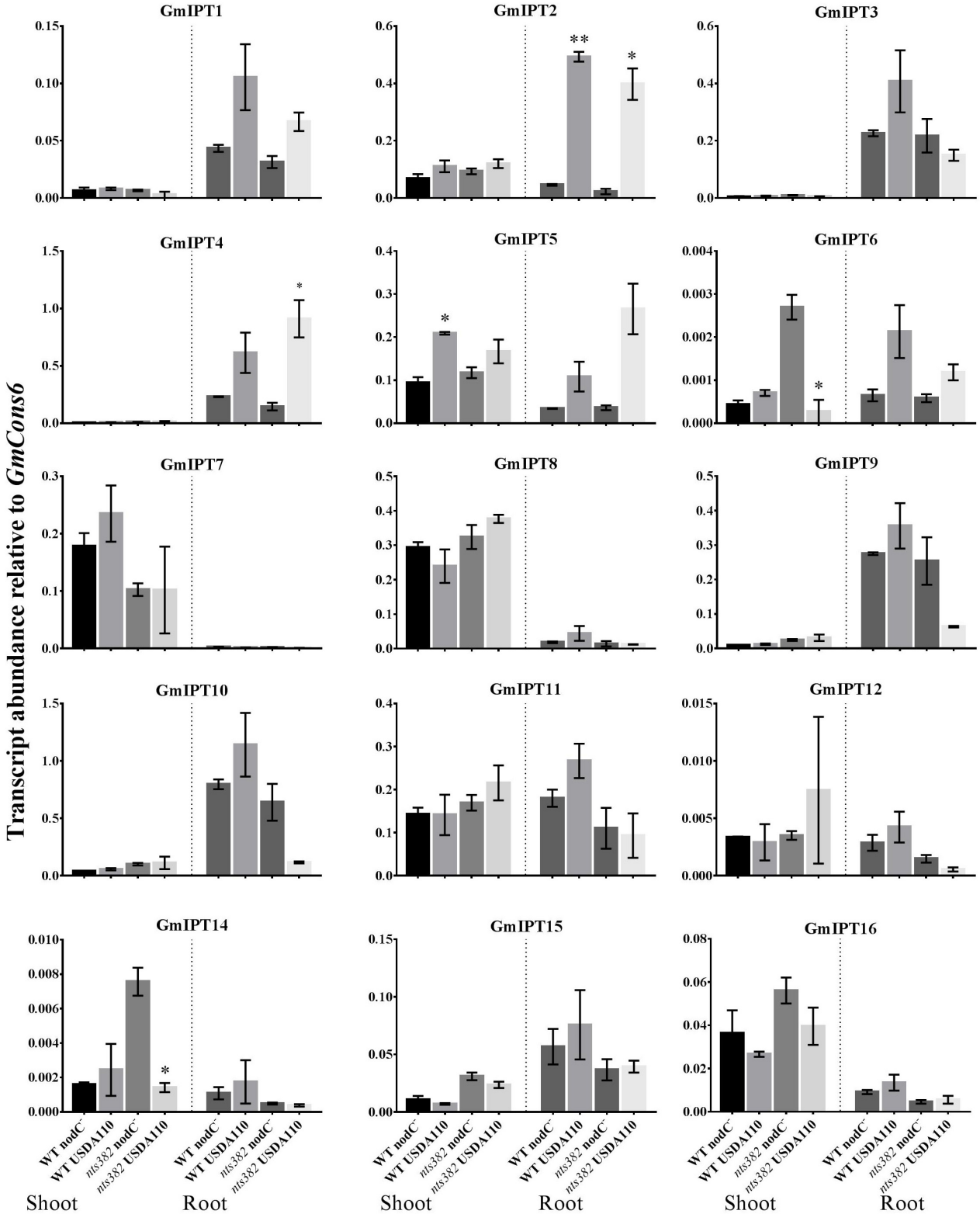

FIGURE 4 | Expression of soybean *IPT* genes in the shoot and roots following inoculation with *B. diazoefficiens*. Two-week old wild-type Bragg (WT) and GmNARK mutant (*nts382*) plants were inoculated with *B. diazoefficiens* USDA110 or its isogenic and incompatible *nodC*$^{-}$ mutant. The first trifoliate leaf and total root were harvested 10 days after inoculation. Expression levels are relative to the housekeeping gene *GmCons6*. Bars represent mean ± SEM of two biological replicates (n = 6 plants per replicate). Asterisks show significant differences in expression (Student's t-test, $^{**}P \leq 0.01$, $^{*}P \leq 0.05$).

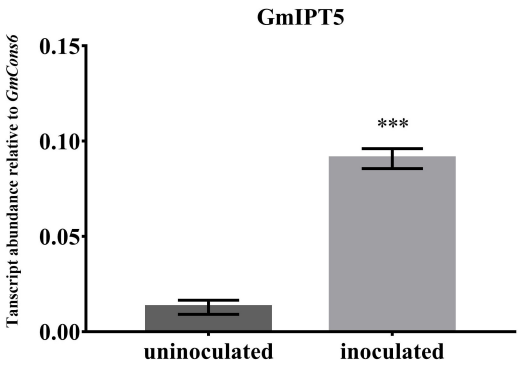

FIGURE 5 | Expression of *GmIPT5* in the GmNARK mutant shoot following inoculation with *B. diazoefficiens*. Three-week old trifoliate leaves were harvested after plants were either inoculated with *B. diazoefficiens* or uninoculated. Expression levels are relative to the housekeeping gene *GmCons6*. Bars represent mean ± SEM of two biological replicates (n = 5 plants per replicate). Asterisk shows significant differences in expression (Student's t-test, $^{***}P \leq 0.001$).

the transcripts levels of *GmIPT6* were much lower compared to *GmIPT5* ($P = 0.150$ and $P = 0.143$ in shoot and root, respectively) and hence caution should be taken when assessing its expression here (**Supplementary Figure S3**). This difference in expression levels is often observed for soybean homeologous with one of the duplicates often becoming reduced or even silenced over long periods of time (Lynch and Conery, 2000; Granger et al., 2002). Likewise, a decrease in *GmIPT14* mRNA levels in the GmNARK mutant shoot was observed, but again the transcript levels were very low for this gene and may not be biologically relevant (**Figure 4** and **Supplementary Figure S3**). The homeologous partner of *GmIPT14*, *GmIPT13*, was omitted as its expression could not be detected.

GmIPT7 and *GmIPT8* cluster closely to *GmIPT5*, *GmIPT6* and *LjIPT3* (**Figure 2**). They are shoot-specific in expression, but unlike *GmIPT5*, their expression remained constant after inoculation with compatible rhizobia in both wild-type and GmNARK mutant plants (**Figure 4**). *GmIPT9* and *GmIPT10* are root-specific in expression, but also were not differentially expressed by inoculation with the different rhizobia strains.

The remaining genes (*GmIPT11*, *GmIPT12* and *GmIPT16*) do not show a noticeable trend in shoot or root gene expression after inoculation with *B. diazoefficiens*. GmIPT17 was predicted to be truncated and its gene expression could not be detected. This gene is likely a pseudogene and is therefore not shown in **Figure 4**.

IPT Gene Expression in the Root Following Nitrate Treatment

Nitrate-dependent regulation of nodulation acts locally in soybean as demonstrated by overexpression experiments using *GmNIC1a* where nodulation was only suppressed in transgenic, but not in non-transgenic roots on the same plant (Reid et al., 2011). Therefore, the expression of all 17 *IPT* genes of soybean was assessed in the root following nitrate-treatment to identify members of the gene family involved in nitrogen response and possibly nitrate-dependent regulation of nodulation.

Nitrate treatment induced the upregulation of the duplicates *GmIPT3* ($P = 0.027$) and *GmIPT15* ($P = 0.021$) (**Figure 6**). The transcript level of the third copy clustering with these two genes, *GmIPT4*, also increased, but not significantly ($P = 0.095$). *GmIPT3* is expressed at levels twice that of both *GmIPT15* and *GmIPT4*, which showed a trend of upregulation in the rhizobia inoculated roots. Other rhizobia-responsive genes, e.g., *GmIPT2* and *GmIPT5*, as well as all remaining *IPT* genes, were not differentially regulated in the root in response to nitrate (**Supplementary Figure S4**).

DISCUSSION

Cytokinins are important regulators of plant growth and development, fine-tuning the balance between cell proliferation and differentiation. They are essential for rhizobia infection and nodule development through the initiation of cortical cell divisions and the induction of early nodulation transcription factors, such as NSP2 (Nodulation Signaling Pathway 2), NIN (Nodule Inception) and ERN1 (Ethylene-Responsive binding domain factor required for Nodulation 1), acting in an LHK1-dependent manner (Murray et al., 2007; Tirichine et al., 2007; Plet et al., 2011; van Zeijl et al., 2015). Indeed, a lack of cytokinin perception in the early stages of nodulation leads to infection thread formation without subsequent nodule organogenesis (Murray et al., 2007; Held et al., 2014). Here, we set out to further characterize the role of cytokinin and the *IPT* gene family in the AON and nitrate-regulation control pathways.

Exogenous application of cytokinin promoted nodule development at low concentrations, while high concentrations reduced nodulation. The former result supports a promoting effect of the hormone on nodulation, while the later finding is likely the result of toxicity induced by an excess level of the hormone (e.g., elevated ethylene production; Lorteau et al., 2001; Ferguson et al., 2005). This effect is particularly evident when BAP is directly applied to the root. BAP is a synthetic cytokinin that is very active and more stable in aqueous solution and once taken up by the plant than other cytokinin compounds (Deleuze et al., 1972). Despite the negative effect on plant growth and development, high doses of phytohormones are commonly used in current research and care should be taken in the selection of appropriate physiologically relevant concentrations in relation to the species and growing conditions used. The promoting effect was most evident when using petiole feeding to deliver the hormone directly and continuously into the plant mimicking the action of the shoot-derived inhibitor in AON, compared with root drenching, which is influenced by plant uptake, metabolism and the physical properties of the growing substrate. Exogenous cytokinin supply has previously been shown to induce nodulin genes, amyloplast depositions and the formation of nodule primordia (Bauer et al., 1996; Heckmann et al., 2011). Furthermore, overexpression of cytokinin biosynthesis genes and subsequent secretion by nodulation-defective rhizobia was reported to initiate organogenesis in alfalfa

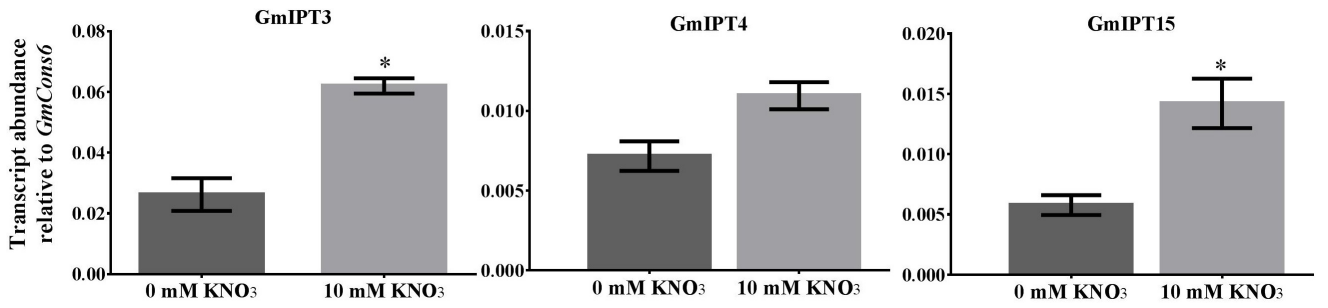

FIGURE 6 | Expression of *GmIPT3*, *GmIPT4* and *GmIPT15* in response to nitrate. Soybean plants were treated with either 0 or 10 mM KNO_3 and roots were harvested from 23-day-old plants. Expression levels are relative to the housekeeping gene *GmCons6*. Bars represent mean ± SEM of two biological replicates ($n = 4$ plants per replicate). Asterisk shows significant differences in expression (Student's *t*-test, $^*P \leq 0.05$).

(Cooper and Long, 1994). Sasaki et al. (2014) also report an inhibitory effect on nodulation following the application of cytokinin (BAP) to the roots of *L. japonicus* and did not report a promotion of nodulation when using lower concentrations of cytokinin. However, these findings might not be contradictory and may instead reflect differences in cytokinin type and effective concentration range between species. Differences in age at harvest, growing conditions or another experimental parameter may also influence responses.

Cytokinin biosynthesis is catalyzed by IPT enzymes and an initial cytokinin burst is required to trigger nodule organogenesis (reviewed in Ferguson and Mathesius, 2014). Reid et al. (2017) recently demonstrated that LjIPT2, together with LjLOG4, is responsible for the build-up of cytokinins, independent to and upstream of the LHK1 cytokinin receptor in *L. japonicus*. In addition, *LjIPT3* is induced in the root after inoculation with compatible rhizobia (Chen et al., 2014; Sasaki et al., 2014). Sasaki et al. (2014) reported *LjIPT3* expression was also induced in the shoot and speculated that cytokinin might be the elusive shoot-derived inhibiting signal, acting downstream of the leucine-rich repeat receptor kinase LjHAR1 in AON.

In this study, 17 *IPT* genes were identified in the soybean genome. All members were found to have a homeologous duplicate or to be a duplicate of one of the homeologous copies, with the exception of *GmIPT16* and *GmIPT17*, which have no discernible partner. The comprehensive phylogenetic analysis reported here provides insight into the potential functions of these genes. The 17 family members of soybean are considerably more than the 8 and 6 members identified in common bean and *L. japonicus*. Having approximately double the number of gene family members of common bean is typical for soybean due to a whole genome duplication event that occurred roughly 13 million years ago (Schmutz et al., 2010; Hastwell et al., 2015a, 2017).

The orthologs of the root-induced *LjIPT2* (Reid et al., 2017) were identified as *GmIPT3* and *GmIPT4*, with *GmIPT15* identified as a duplicate of *GmIPT3*. The orthologs of the root- and shoot-induced *LjIPT3* (Chen et al., 2014; Sasaki et al., 2014) were found to be *GmIPT5* and its duplicate *GmIPT6*.

IPT gene expression was analyzed in both soybean shoots and roots of rhizobia-inoculated plants to identify potential candidates acting in nodulation and AON (Ferguson et al., 2018). *GmIPT5* was significantly induced in wild-type trifoliate leaves following inoculation of the root with compatible rhizobia. This is consistent with findings of Sasaki et al. (2014). Despite not being significant, the trend of increased *GmIPT5* transcript levels is also noticeable in the GmNARK mutant (*nts382*) in both the root and shoot. GmNARK defective plants that were either inoculated or non-inoculated confirmed a significant difference in *GmIPT5* transcript abundance. This seems to suggest that the upregulation of gene expression is independent of the GmNARK receptor and is unlikely to have a role in the AON pathway in soybean as suggested for *L. japonicus* by Sasaki et al. (2014) who found that regulation of *LjIPT3* is LjHAR1-dependent in the shoot. This might be due to any number of reasons including species-specific differences, different plant development stages, differences in growing conditions, etc. Expression of the homeologue of *GmIPT5*, *GmIPT6*, was considerably lower, indicating that it might not be biologically relevant in this process with *GmIPT5* being the dominant copy.

Upregulation of *LjIPT3* in the root has been reported to occur as early as 3 h after rhizobial inoculation (Chen et al., 2014) and as late as 10 days after inoculation (Reid et al., 2017). The latter finding is long after the CLE peptides, *LjCLE-RS1* and *LjCLE-RS2*, are induced to initiate the AON process (Okamoto et al., 2009). Furthermore, the differential regulation of nodulation-suppressing CLE peptides in *L. japonicus* and *M. truncatula* is dependent on the cytokinin-induced action of NIN, a transcription factor required for infection thread and nodule primordia formation (Schauser et al., 1999; Mortier et al., 2012; Soyano et al., 2014). Cytokinins and their *IPT* biosynthesis genes therefore seem to play a major role in the nodule development process upstream of AON rather than being a key factor in AON itself. Increased *GmIPT5* expression in the shoot after rhizobial inoculation might be the plant's way to enhance shoot growth in preparation of an influx in nitrogen via nitrogen fixation, rather than cytokinins acting as the shoot-derived inhibitor in AON (Rahayu et al., 2005). In support of this is work by Chen et al. (2014) who show that RNA interference of LjIPT3 results in reduced shoot development and increased chlorophyll breakdown resulting in subsequent leaf senescence, even in the absence of rhizobia.

AtIPT3-synthesised cytokinins induce the expression of shoot-type nitrate transporters (AtNRT) to translocate and partition nitrate in the shoot in the non-legume *A. thaliana* when plenty of nitrogen is available in the soil (Kiba et al., 2011).

Another gene, *GmIPT2*, was found to respond to rhizobial inoculation in the root in a clear GmNARK-independent manner. Its homeologous duplicate, *GmIPT1*, is root-specific as well and shows the same induction albeit less strong. This is consistent with the increased expression in the root but not the shoot of the ortholog of these genes in *L. japonicus*, *LjIPT1*, following rhizobia inoculation. The precise function of this gene remains unclear, but expression of *LjIPT1* is highest in the flower and only moderate in the roots (Chen et al., 2014).

The fourth gene responding to compatible rhizobia inoculation is the root-specific *GmIPT4*, the homeologue of *GmIPT3* that shows no clear change in expression. These genes are closely related to *LjIPT2*, which is required for the initial cytokinin burst during early nodulation events that are induced by rhizobia inoculation (Reid et al., 2017). Interestingly, expression of *GmIPT3* and its tandem duplicate *GmIPT15* (which is predicted to be truncated), is promoted in the root following nitrate treatment, but *GmIPT4* expression is not induced as strongly. Furthermore, transcript levels of *GmIPT4* are much higher than those of *GmIPT3* following rhizobia inoculation, while the opposite was observed in response to high soil nitrogen status. This might indicate that these genes have undergone genetic divergence (i.e., neofunctionalization) in which they developed a different function, as is sometimes observed with duplicated genes of soybean (Mirzaei et al., 2017).

In addition to the negative feedback system of AON, nodulation is controlled by environmental factors including the soil nitrogen status. In soybean, nitrate-dependent regulation of nodulation inhibits the nodulation process via a local pathway in contrast to systemic signaling required for AON (Hinson, 1975; Reid et al., 2011; reviewed in Ferguson et al., 2018). Therefore, only roots were tested in this study to investigate the role of cytokinins as the root-derived inhibitor in nitrate-dependent regulation of nodulation. In addition, *AtIPT* accumulation is highest in the root tissue in response to nitrogen, while expression in the shoot is relatively low (Takei et al., 2004). Systemic components of the nitrate-regulation of nodulation (e.g., nitrogen fixation, nodule size and nodule number) have been shown in other model legumes such as *M. truncatula* and *L. japonicus* (Jeudy et al., 2010; Soyano et al., 2014; Nishida et al., 2018; reviewed in Ferguson et al., 2018). Therefore, analysis of *IPT* gene expression in the shoot in response to soil nitrogen status could be investigated in future. The plant's response to low nitrogen in the soil requires root phenotypic plasticity. This can occur through association with symbiotic soil rhizobia or through the proliferation of the lateral root system via a process called foraging. Similar to the establishment of nodule primordia, a precise cytokinin balance is essential for lateral root initiation and development. This process of foraging requires a reduction in cytokinin levels to increase lateral root proliferation. Overexpression of *IPT* genes in tobacco reduced root growth, while lateral root numbers are reduced in transgenic tobacco plants overexpressing a cytokinin oxidase (Hewelt et al., 1994; Werner et al., 2001). Here, the transcript levels of the cytokinin biosynthesis genes *GmIPT3* and *GmIPT15* are upregulated in the root in response to nitrogen. This is consistent with findings in *M. truncatula* showing the cytokinin receptor, MtCRE1, is required for both nodule and lateral root development, indicating mechanisms for nodule organogenesis have diverged from existing molecular mechanisms (Gonzalez-Rizzo et al., 2006). In addition, cytokinins are frequently found to act in an opposite manner during lateral root development and nodulation, requiring low or high cytokinin concentrations, respectively (Lohar et al., 2004). In *A. thaliana*, *AtIPT3* and *AtIPT5*, the homologous of *GmIPT3*, *GmIPT4* and *GmIPT15*, are upregulated in response to nitrate (Miyawaki et al., 2004; Takei et al., 2004). While *AtIPT3* is important in the short-term response to nitrate, *AtIPT5* is expressed after long-term exposure to different sources of nitrogen (Takei et al., 2004). Once plants encounter a high nitrogen patch, systemic nitrogen signaling is required to induce lateral root proliferation into the patch and inhibit lateral root development elsewhere. Several studies suggest a role in systemic nitrogen signaling for root-produced cytokinins (tZ) that move up the shoot where they regulate systemic nitrogen-pathways in response to a heterogeneous supply of soil nitrogen (Rahayu et al., 2005; Poitout et al., 2018). In addition, cytokinins in the root reduce nitrate uptake by inhibiting expression of high-affinity nitrate transporters (e.g., NRT2.1) when nitrogen availability is high, while shoot-type transporters are upregulated to translocate and redistribute nitrogen (Kiba et al., 2011). The results obtained here, together with the findings of Reid et al. (2017), suggest a general role for GmIPT3/GmIPT15 and their ortholog LjIPT2 in response to nitrogen status, possibly indicating that IPT-synthesized cytokinins act as regulators of root architecture and nitrate-dependent regulation of nodulation.

Collectively, our results established that low levels of cytokinins can promote nodulation whereas higher levels inhibit it. We also identified *IPT* genes that are regulated in either the root or shoot in response to inoculation with compatible rhizobia and additional *IPT* genes that are regulated in the root in response to nitrate. Our findings do not suggest that cytokinin is likely to be the shoot-derived inhibitor in AON. This is based on the upregulation of *GmIPT5*, an ortholog of *LjIPT3*, in a GmNARK-independent manner in the shoot combined with the nodulation promoting effect of low concentrations of cytokinin applied to the root and shoot. Indeed, using the petiole-feeding technique, the hormone was fed directly into the plant where SDI is produced and therefore would not be expected to promote nodule development. It should be noted that differences in species, treatment type, concentration range and cytokinin type might be important factors for differences in results reported here and in previous studies. While instead, *IPT* expression in the shoot possibly prepares the plant for new growth while awaiting a burst of nitrogen, which is often a limiting factor for plant growth. The comprehensive bioinformatic

and expression analysis reported here can be used as tools to support future research into the role of cytokinin in nodule development. This could include establishing the exact function of various *IPT* genes in nodulation, including the role of increased *GmIPT5* expression in both shoot and root, in conjunction with the *LOG* genes that are crucial for cytokinin activation.

AUTHOR CONTRIBUTIONS

BF and PG devised the project and supervised. DL, CM and LH conducted the experiments. DL and CM performed bioinformatic and gene expression analyses. DL and LH performed petiole feeding and root drenching assays. CM analyzed the data, prepared the figures and wrote the manuscript with input from all authors. All authors read and approved the manuscript.

FUNDING

This work was funded by The Hermon Slade Foundation and the Australian Research Council Discovery Project grants (DP130103084 and DP130102266).

ACKNOWLEDGMENTS

The authors would like to thank Huanan Su, Mengbai Zhang, April Hastwell, Xitong Chu and Candice Jones for their technical assistance during this study.

SUPPLEMENTARY MATERIAL

The Supplementary Material for this article can be found online at: https://www.frontiersin.org/articles/10.3389/fpls.2018.01150/full#supplementary-material

REFERENCES

Azarakhsh, M., Lebedeva, M. A., and Lutova, L. A. (2018). Identification and expression analysis of *Medicago truncatula* isopentenyl transferase genes (IPTs) involved in local and systemic control of nodulation. *Front. Plant Sci.* 9:304. doi: 10.3389/fpls.2018.00304

Bauer, P., Ratet, P., Crespi, M. D., Schultze, M., and Kondorosi, A. (1996). Nod factors and cytokinins induce similar cortical cell division, amyloplast deposition and *MsEnod12A* expression patterns in alflalfa roots. *Plant J.* 10, 91–105. doi: 10.1046/j.1365-313X.1996.10010091.x

Broughton, W. J., and Dilworth, M. J. (1971). Control of leghaemoglobin synthesis in snake beans. *Biochem. J.* 125, 1075–1080. doi: 10.1042/bj1251075

Carroll, B. J., McNeil, D. L., and Gresshoff, P. M. (1985). Isolation and properties of soybean [*Glycine max* (L.) *Merr.*] mutants that nodulate in the presence of high nitrate concentrations. *Proc. Natl. Acad. Sci. U.S.A.* 82, 4162–4166. doi: 10.1073/pnas.82.12.4162

Chen, Y., Chen, W., Li, X., Jiang, H., Wu, P., Xia, K., et al. (2014). Knockdown of *LjIPT3* influences nodule development in *Lotus japonicus*. *Plant Cell Physiol.* 55, 183–193. doi: 10.1093/pcp/pct171

Cooper, J. B., and Long, S. R. (1994). Morphogenetic rescue of *Rhizobium meliloti* nodulation mutants by trans-zeatin secretion. *Plant Cell* 6, 215–225. doi: 10.1105/tpc.6.2.215

Corcilius, L., Hastwell, A. H., Zhang, M., Williams, J., Mackay, J. P., Gresshoff, P. M., et al. (2017). Arabinosylation modulates the growth-regulating activity of the peptide hormone CLE40a from soybean. *Cell Chem. Biol.* 24, 1–9. doi: 10.1016/j.chembiol.2017.08.014

Deleuze, G. G., McChesney, J. D., and Fox, J. E. (1972). Identification of a stable cytokinin metabolite. *Biochem. Biophys. Res. Commun.* 48, 1426–1432. doi: 10.1016/0006-291X(72)90872-8

Ferguson, B. J., and Mathesius, U. (2014). Phytohormone regulation of legume-rhizobia interaction. *J. Chem. Ecol.* 40, 770–790. doi: 10.1007/s10886-014-0472-7

Ferguson, B. J., Indrasumunar, A., Hayashi, S., Lin, M. H., Lin, Y. H., Reid, D. E., et al. (2010). Molecular analysis of legume nodule development and autoregulation. *J. Integr. Plant Biol.* 52, 61–76. doi: 10.1111/j.1744-7909.2010.00899.x

Ferguson, B. J., Mens, C., Hastwell, A. H., Zhang, M. B., Su,H., Jones, C. H., et al. (2018). Legume nodulation: the host controls the party. *Plant Cell Environ.* doi: 10.1111/pce.13348 [Epub ahead of print]. doi: 10.1111/pce.13348

Ferguson, B. J., Wiebe, E. M., Emery, R. J. N., and Guinel, F. C. (2005). Cytokinin accumulation and an altered ethylene response mediate the pleiotropic phenotype of the pea nodulation mutant R50 (*sym16*). *Can. J. Bot.* 83, 989–1000. doi: 10.1139/b05-049

Gonzalez-Rizzo, S., Crespi, M., and Frugier, F. (2006). *Medicago truncatula* CRE1 cytokinin receptor regulates lateral root development and early symbiotic interaction with *Sinorhizobium meliloti*. *Plant Cell* 18, 2680–2693. doi: 10.1105/tpc.106.043778

Goujon, M., McWilliam, H., Li, W., Valentin, F., Squizzato, S., Paern, J., et al. (2010). A new bioinformatics analysis tools framework at EMBL-EBI. *Nucleic Acids Res.* 38, W695–W699. doi: 10.1093/nar/gkq313

Granger, C., Coryell, V., Khanna, A., Keim, P., Vodkin, L., and Shoemaker, R. C. (2002). Identification, structure and differential expression of members of a BURP domain containing protein family in soybean. *Genome* 45, 693–701. doi: 10.1139/g02-032

Gresshoff, P. M., Hayashi, S., Biswas, B., Mirzaei, S., Indrasumunar, A., Reid, D., et al. (2015). The value of biodiversity in legume symbiotic nitrogen fixation and nodulation for biofuel and food production. *J. Plant Physiol.* 172, 128–136. doi: 10.1016/j.jplph.2014.05.013

Guindon, S., and Gascuel, O. (2003). A simple, fast and accurate algorithm to estimate large phylogenies by maximum likelihood. *Syst. Biol.* 52, 696–704. doi: 10.1080/10635150390235520

Hastwell, A. H., Corcilius, L., Williams, J., Gresshoff, P. M., Payne, R. J., and Ferguson, B. J. (2018). Triarabinosylation is required for nodulation-suppressive CLE peptides to systemically inhibit nodulation in *Pisum sativum*. *Plant Cell Environ.* doi: 10.1111/pce.13325 [Epub ahead of print].

Hastwell, A. H., de Bang, T. C., Gresshoff, P. M., and Fergusion, B. J. (2017). CLE peptide-encoding gene families in *Medicago truncatula* and *Lotus japonicus*, compared with those of soybean, common bean and Arabidopsis. *Sci. Rep.* 7:9384. doi: 10.1038/s41598-017-09296-w

Hastwell, A. H., Gresshoff, P. M., and Ferguson, B. J. (2015a). Genome-wide annotation and characterization of CLAVATA/ESR (CLE) peptide hormones of soybean (*Glycine max*) and common bean (*Phaseolous vulgaris*) and their orthologues of *Arabidopsis thaliana*. *J. Exp. Bot.* 66, 5271–5287. doi: 10.1093/jxb/erv351

Hastwell, A. H., Gresshoff, P. M., and Ferguson, B. J. (2015b). The structure and activity of nodulation-suppressing CLE peptide hormones of legumes. *Funct. Plant Biol.* 42, 229–238. doi: 10.1071/FP14222

Heckmann, A. B., Sandal, N., Bek, A. S., Madsen, L. H., Jurkiewicz, A., Nielsen, M. W., et al. (2011). Cytokinin induction of root nodule primordia in *Lotus japonicus* is regulated by a mechanism operating in the root cortex. *Mol. Plant Microbe Interact.* 24, 1385–1395. doi: 10.1094/MPMI-05-11-0142

Held, M., Hou, H., Miri, M., Huynh, C., Ross, L., Hossain, S. Md., et al. (2014). *Lotus japonicus* cytokinin receptors work partially redundantly to mediate nodule formation. *Plant Cell* 26, 678–694. doi: 10.1105/tpc.113.119362

Herridge, D. F. (1982). Relative abundance of ureides and nitrate in plant tissues of soybean as a quantitative assay of nitrogen fixation. *Plant Physiol.* 70, 1–6. doi: 10.1104/pp.70.1.1

Hewelt, A., Prinsen, E., Schell, J., Onckelen, H., and Schmülling, T. (1994). Promoter tagging with a promoterless IPT gene leads to cytokinin-induced phenotypic variability in transgenic tobacco plants: implications of gene dosage effects. *Plant J.* 6, 879–891. doi: 10.1046/j.1365-313X.1994.6060879.x

Hinson, K. (1975). Nodulation responses from nitrogen applied to soybean half-root systems. *Agron. J.* 67, 799–804. doi: 10.2134/agronj1975.00021962006700060018x

Jeudy, C., Ruffel, S., Freixes, S., Tillard, P., Santoni, A. L., Morel, S., et al. (2010). Adaptation of *Medicago truncatula* to nitrogen limitation is modulated via local and systemic nodule developmental responses. *New Phytol.* 185, 817–828. doi: 10.1111/j.1469-8137.2009.03103.x

Kakimoto, T. (2001). Identification of plant cytokinin biosynthetic enzymes as dimethylallyl diphosphate: ATP/ADP isopentenyltransferases. *Plant Cell Physiol.* 42, 677–685. doi: 10.1093/pcp/pce112

Kamada-Nobusada, T., and Sakakibara, H. (2009). Molecular basis for cytokinin biosynthesis. *Phytochemistry* 70, 444–449. doi: 10.1016/j.phytochem.2009.02.007

Kiba, T., Kudo, T., Kojima, M., and Sakakibara, H. (2011). Hormonal control of nitrogen acquisition: roles of auxin, abscisic acid and cytokinin. *J. Exp. Bot.* 62, 1399–1409. doi: 10.1093/jxb/erq410

Libault, M., Thibivilliers, S., Bilgin, D., Radwan, O., Benitez, M., Clough, S., et al. (2008). Identification of four soybean reference genes for gene expression normalization. *Plant Genome* 1, 44–54. doi: 10.3835/plantgenome2008.02.0091

Lin, Y.-H., Ferguson, B. J., Kereszt, A., and Gresshoff, P. M. (2010). Suppression of hypernodulation in soybean by a leaf-extracted, NARK- and Nod factor-dependent, low molecular mass fraction. *New Phytol.* 185, 1074–1086. doi: 10.1111/j.1469-8137.2009.03163.x

Lin, Y.-H., Lin, M. -H., Gresshoff, P. M., and Ferguson, B. J. (2011). An efficient petiole-feeding bioassay for introducing aqueous solutions into dicotyledonous plants. *Nat. Protoc.* 6, 36–45. doi: 10.1038/nprot.2010.171

Lohar, D. P., Schaff, J. E., Laskey, J. G., Kieber, J. J., Bilyeu, K. D., and Bird, D. M. (2004). Cytokinins play opposite roles in lateral root formation and nematode and Rhizobial symbioses. *Plant J.* 38, 203–214. doi: 10.1111/j.1365-313X.2004.02038.x

Lorteau, M. A., Ferguson, B. J., and Guinel, F. C. (2001). Effects of cytokinin on ethylene production and nodulation in pea (*Pisum sativum*) cv. Sparkle. *Physiol. Plant.* 112, 421–428. doi: 10.1034/j.1399-3054.2001.1120316.x

Lynch, M., and Conery, J. S. (2000). The evolutionary fate and consequences of duplicate genes. *Science* 290, 1151–1155. doi: 10.1126/science.290.5494.1151

Mathesius, U., Charon, C., Rolfe, B., Kondorosi, A., and Crespi, M. (2000). Temporal and spatial order of events during the induction of cortical cell divisions in white clover by *Rhizobium leguminosarum* bv. trifolii inoculation or localized cytokinin addition. *Mol. Plant-Microbe Interact.* 13, 617–628. doi: 10.1094/MPMI.2000.13.6.617

McWilliam, H., Li, W., Uludag, M., Squizzato, S., Park, Y. M., Buso, N., et al. (2013). Analysis tool web services from the EMBL-EBI. *Nucleic Acids Res.* 41, W597–W600. doi: 10.1093/nar/gkt376

Mi, H., Huang, X., Muruganujan, A., Tang, H., Mills, C., Kang, D., et al. (2017). PANTHER version 11: expanded annotation data from gene ontology and reactome pathways and data analysis tool enhancements. *Nucleic Acids Res.* 45, D183–D189. doi: 10.1093/nar/gkw1138

Mirzaei, S., Batley, J., El-Mellouki, T., Liu, S., Meksem, K., Ferguson, B. J., et al. (2017). Neodiversification of homeologous *CLAVATA1*-like receptor kinase genes in soybean leads to distinct developmental outcomes. *Sci. Rep.* 7:8878. doi: 10.1038/s41598-017-08252-y

Miyawaki, K., Matsumoto-Kitano, M., and Kakimoto, T. (2004). Expression of cytokinin biosynthetic isopentenyltransferase genes in *Arabidopsis*: tissue specificity and regulation by auxin, cytokinin and nitrate. *Plant J.* 37, 128–138. doi: 10.1046/j.1365-313X.2003.01945.x

Mortier, V., De Wever, E., Vuylsteke, M., Holsters, M., and Goormachtig, S. (2012). Nodule numbers are governed by interaction between CLE peptides and cytokinin signaling. *Plant J.* 70, 367–376. doi: 10.1111/j.1365-313X.2011.04881.x

Mortier, V., Den Herder, G., Whitford, R., Van de Velde, W., Rombauts, S., D'haeseleer, K., et al. (2010). CLE peptides control *Medicago truncatula* nodulation locally and systemically. *Plant Physiol.* 153, 222–237. doi: 10.1104/pp.110.153718

Mortier, V., Wasson, A., Jaworek, P., De Keyser, A., Decroos, M., Holsters, M., et al. (2014). Role of *LONELY GUY* genes in indeterminate nodulation on *Medicago truncatula*. *New Phytol.* 202, 582–593. doi: 10.1111/nph.12681

Murray, J. D., Karas, B. J., Sato, S., Tabata, S., Amyot, L., and Szczyglowski, K. (2007). A cytokinin perception mutant colonized by *Rhizobium* in the absence of nodule organogenesis. *Science* 315, 101–104. doi: 10.1126/science.1132514

Nishida, H., Tanaka, S., Handa, Y., Ito, M., Sakamoto, Y., Matsunaga, S., et al. (2018). A NIN-LIKE PROTEIN mediate nitrate-induced control of root nodule symbiosis in *Lotus japonicus*. *Nat. Commun.* 9:499. doi: 10.1038/s41467-018-02831-x

Nontachaiyapoom, S., Scott, P. T., Men, A. E., Kinkema, M., Schenk, P. M., and Gresshoff, P. M. (2007). Promoters of orthologous *Glycine max* and *Lotus japonicus* nodulation autoregulation genes interchangeably drive phloem-specific expression in transgenic plants. *Molecular Plant-Microbe Interact. J.* 20, 769–780. doi: 10.1094/ MPMI-20-7-0769

Okamoto, S., Ohnishi, E., Sato, S., Takahashi, H., Nakazono, M., Tabata, S., et al. (2009). Nod factor/nitrate-induced CLE genes that drive HAR1-mediated systemic regulation of nodulation. *Plant Cell Physiol.* 50, 67–77. doi: 10.1093/pcp/pcn194

Okamoto, S., Shinohara, H., Mori, T., Matsubayashi, Y., and Kawaguchi, M. (2013). Root-derived CLE glycopeptides control nodulation by direct binding to HAR1 receptor kinase. *Nat. Commun.* 4:2191. doi: 10.1038/ncomms3191

Plet, J., Wasson, A., Ariel, F., Le Signor, C., Baker, D., Mathesius, U., et al. (2011). MtCRE1-dependent cytokinin signaling integrates bacterial and plant cues to coordinate symbiotic nodule organogenesis in *Medicago truncatula*. *Plant J.* 65, 622–633. doi: 10.1111/j.1365-313X.2010.04447.x

Poitout, A., Crabos, A., Petřík, I., Novák, O., Krouk, G., Lacombe, B., et al. (2018). Responses to systemic nitrogen signaling in *Arabidopsis* roots involve trans-zeatin in shoots. *Plant Cell* 30, 1243–1257. doi: 10.1105/tpc.18.00011

Punta, M., Coggill, P. C., Eberhardt, R. Y., Mistry, J., Tate, J., Boursnell, C., et al. (2012). The Pfam protein families database. *Nucleic Acids Res.* 40(Database issue), D290–D301. doi: 10.1093/nar/gkr1065

Rahayu, Y. S., Walch-Liu, P., Neumann, G., Römheld, V., Von Wirèn, N., and Bangerth, F. (2005). Root-derived cytokinins as long-distance signals for NO3– induced stimulation of leaf growth. *J. Exp. Bot.* 56, 1143–1152. doi: 10.1093/jxb/eri107

Reid, D. E., Ferguson, B. J., and Gresshoff, P. M. (2011). Inoculation- and nitrate-induced CLE peptides of soybean control NARK-dependent nodule formation. *Mol. Plant Microbe Interact.* 24, 606–618. doi: 10.1094/MPMI-09-10-0207

Reid, D. E., Nadzieja, M., Novák, O., Heckmann, A. B., Sandal, N., and Stougaard, J. (2017). Cytokinin biosynthesis promotes cortical cell responses during nodule development. *Plant Physiol.* 175, 361–375. doi: 10.1104/pp.17.00832

Sasaki, T., Suzaki, T., Soyano, T., Kojima, M., Sakakibara, H., and Kawaguchi, M. (2014). Shoot-derived cytokinins systemically regulate root nodulation. *Nat. Commun.* 5:4983. doi: 10.1038/ncomms5983

Schauser, L., Roussis, A., Stiller, J., and Stougaard, J. (1999). A plant regulator controlling development of symbiotic root nodules. *Nature* 402, 191–195. doi: 10.1038/46058

Schmutz, J., Cannon, S. B., Schlueter, J., Ma, J., Mitros, T., Nelson, W., et al. (2010). Genome sequence of the palaeopolyploid soybean. *Nature* 463, 178–183. doi: 10.1038/nature08670

Sievers, F., Wilm, A., Dineen, D., Gibson, T. J., Karplus, K., Li, W., et al. (2011). Fast, scalable generation of high-quality protein multiple sequence alignments using Clustal Omega. *Mol. Syst. Biol.* 7:539. doi: 10.1038/msb.2011.75

Soyano, T., Hirakawa, H., Sato, S., Hayashi, M., and Kawaguchi, M. (2014). NODULE INCEPTION creates a long-distance negative feedback loop involved in homeostatic regulation of organ production. *Proc. Natl. Acad. Sci. U.S.A.* 111, 14607–14612. doi: 10.1073/pnas.1412716111

Takei, K., Sakakibara, H., and Sugiyama, T. (2001). Identification of genes encoding adenylate isopentenyltransferases, a cytokinin biosynthesis enzyme, in *Arabidopsis thaliana*. *J. Biol. Chem.* 276, 26405–26410. doi: 10.1074/jbc.M102130200

Takei, K., Ueda, N., Aoki, K., Kuromori, T., Hirayama, T., Shinozaki, K., et al. (2004). *AtIPT3* is a key determinant of nitrate-dependent cytokinin biosynthesis in *Arabidopsis*. *Plant Cell Physiol.* 45, 1053–1062. doi: 10.1093/pcp/pch119

Tirichine, L., Sandal, N., Madsen, L. H., Radutoiu, S., Albrektsen, A. S., Sato, S., et al. (2007). A gain-of-function mutation in a cytokinin receptor triggers spontaneous root nodule organogenesis. *Science* 315, 104–107. doi: 10.1126/science.1132397

van Zeijl, A., Op den Camp, R. H. M., Deinum, E. E., Charnikhova, T., Franssen, H., Op den Camp, H. J. M., et al. (2015). Rhizobium lipo-chitooligosaccharide signaling triggers accumulation of cytokinins in *Medicago truncatula* roots. *Mol. Plant* 8, 1213–1226. doi: 10.1016/j.molp.2015.03.010

Werner, T., Motyka, V., Strnad, M., and Schmülling, T. (2001). Regulation of plant growth by cytokinin. *Proc. Natl. Acad. Sci. U.S.A.* 98, 10487–10492. doi: 10.1073/pnas.171304098

Conflict of Interest Statement: The authors declare that the research was conducted in the absence of any commercial or financial relationships that could be construed as a potential conflict of interest.

frontiers in Plant Science

ORIGINAL RESEARCH
published: 15 February 2018
doi: 10.3389/fpls.2018.00169

Acropetal Auxin Transport Inhibition Is Involved in Indeterminate But Not Determinate Nodule Formation

Jason L. P. Ng and Ulrike Mathesius*

Division of Plant Sciences, Research School of Biology, Australian National University, Canberra, ACT, Australia

Legumes enter into a symbiotic relationship with nitrogen-fixing rhizobia, leading to nodule development. Two main types of nodules have been widely studied, indeterminate and determinate, which differ in the location of the first cell division in the root cortex, and persistency of the nodule meristem. Here, we compared the control of auxin transport, content, and response during the early stages of indeterminate and determinate nodule development in the model legumes *Medicago truncatula* and *Lotus japonicus*, respectively, to investigate whether differences in auxin transport control could explain the differences in the location of cortical cell divisions. While auxin responses were activated in dividing cortical cells during nodulation of both nodule types, auxin (indole-3-acetic acid) content at the nodule initiation site was transiently increased in *M. truncatula*, but transiently reduced in *L. japonicus*. Root acropetal auxin transport was reduced in *M. truncatula* at the very start of nodule initiation, in contrast to a prolonged increase in acropetal auxin transport in *L. japonicus*. The auxin transport inhibitors 2,3,5-triiodobenzoic acid and 1-*N*-naphthylphthalamic acid (NPA) only induced pseudonodules in legume species forming indeterminate nodules, but failed to elicit such structures in a range of species forming determinate nodules. The development of these pseudonodules in *M. truncatula* exhibited increased auxin responses in a small primordium formed from the pericycle, endodermis, and inner cortex, similar to rhizobia-induced nodule primordia. In contrast, a diffuse cortical auxin response and no associated cortical cell divisions were found in *L. japonicus*. Collectively, we hypothesize that a step of acropetal auxin transport inhibition is unique to the process of indeterminate nodule development, leading to auxin responses in pericycle, endodermis, and inner cortex cells, while increased auxin responses in outer cortex cells likely require a different mechanism during the formation of determinate nodules.

Keywords: auxin, indeterminate, determinate, auxin transport inhibitor, acropetal, legume, nodule

OPEN ACCESS

Edited by:
Pascal Ratet, Centre national de la recherche scientifique (CNRS), France

Reviewed by:
Sen Subramanian, South Dakota State University, United States
Sandra Bensmihen, UMR2594 Laboratoire des Interactions Plantes-Microorganismes (LIPM), France

****Correspondence:***
Jason L. P. Ng
jason.ng@anu.edu.au

Specialty section:
This article was submitted to Plant Microbe Interactions, a section of the journal Frontiers in Plant Science

Received: *02 November 2017*
Accepted: *30 January 2018*
Published: *15 February 2018*

Citation:
Ng JLP and Mathesius U (2018) Acropetal Auxin Transport Inhibition Is Involved in Indeterminate But Not Determinate Nodule Formation. Front. Plant Sci. 9:169. doi: 10.3389/fpls.2018.00169

INTRODUCTION

Many legume species form a symbiosis with nitrogen-fixing rhizobia, resulting in the development of nodules in the host roots. There are variations in the organogenesis of nodules in different species of legumes. Two main nodule types have been reported in the literature, indeterminate and determinate nodules. The model legume *Medicago truncatula* forms indeterminate nodules, while another model legume, *Lotus japonicus*, forms determinate nodules. Whereas indeterminate

nodules involve re-initiation of cell divisions in the pericycle, endodermis, and inner cortex of the root, determinate nodules are characterized by cell divisions mainly in the middle and outer cortex, with some contributions from the pericycle and endodermis (Hirsch, 1992). Another difference between the two nodule types is that indeterminate nodules are typically elongate and maintain an apical nodule meristem; determinate nodules lose the meristematic activity of the nodule meristem and are typically round (Hirsch, 1992). So far it is not known what determines the difference between these two organogenesis programs.

Previous studies have shown that the plant hormone auxin is essential for the initiation of cell divisions in plants and that auxin gradients accompany the formation of new plant organs (Benková et al., 2003). This also seems to be the case for nodule initiation, where increased auxin responses have been localized to nodule primordia in various legume species forming both indeterminate or determinate nodules (van Noorden et al., 2007; Takanashi et al., 2011; Suzaki et al., 2012; Turner et al., 2013).

Auxin represents a group of structurally related phytohormones. The most frequently studied auxin is indole-3-acetic acid (IAA). Auxins can be divided into active and inactive/storage forms, with the latter being the more abundant form in plants (Korasick et al., 2013). Active auxins, such as IAA, activate auxin-response genes, whose gene products regulate cell division and organ growth. Other active auxins include indole-3-butyric acid (IBA), 4-chloro-indole-3-acetic acid (4-Cl-IAA), and phenylacetic acid (PAA). Each of these active auxins can be inactivated by forming conjugates with amino acids (Korasick et al., 2013). For example, IAA-Alanine and IAA-Leucine have been suggested to be IAA storage forms in *Arabidopsis thaliana* (Kowalczyk and Sandberg, 2001; Novák et al., 2012), while IAA-Asp might lead to auxin degradation and inactivation (Korasick et al., 2013). IAA-Tryptophan, interestingly, was postulated to be an auxin antagonist, inhibiting IAA action (Staswick, 2009). The interconversion between free and conjugated IAA provides one mechanism to fine tune plant development through the spatio-temporal control of active IAA concentrations.

Auxin is transported within plants via two mechanisms – a passive, long distance auxin transport system through the phloem and an active, local cell-to-cell auxin transport machinery. Active auxin transport control plays an important role during root development. It is controlled by a suite of auxin transport carriers and cellular regulators that control their intracellular abundance and localization (Overvoorde et al., 2010). In particular, members of the auxin exporter family *PIN* (*PINFORMED*) and auxin importer family *AUX1*/*LAX* (*AUXIN RESISTANT1*/*LIKE AUX1*) have been shown to contribute to the formation of auxin gradients in *Arabidopsis* (Overvoorde et al., 2010). In *M. truncatula*, expression of the *PIN* auxin efflux carriers is altered during symbiotic interactions with *Sinorhizobium meliloti*. The expression of *PIN2*, *4*, and *10* was upregulated within 24 h in response to *S. meliloti* inoculation or Nod factor treatment (Plet et al., 2011; Ng et al., 2015). Knockdown of *PIN2*, *3*, and *4* reduced nodule numbers on transgenic *M. truncatula* roots (Huo et al., 2006). *In situ* hybridization of *M. truncatula LAX1* (homolog of the *Arabidopsis* auxin influx carrier *AUX1*) mRNAs suggested that these auxin influx carriers are involved in early nodule primordia development and vasculature differentiation (de Billy et al., 2001). Such evidence strongly supports the role of auxin transport during nodule development.

Computer modeling suggested that during the early stages of *M. truncatula*–*S. meliloti* symbiosis, a temporary decrease in acropetal auxin efflux is the most plausible mechanism to explain the observed patterns of auxin accumulation in the dividing cells that comprise a nodule primordium, although auxin import is also likely to contribute (Deinum et al., 2012; Roy et al., 2017). When changes in acropetal auxin transport through the stele were combined with a hypothesized diffusible signal from the epidermis – mimicking a signal from infecting rhizobia – auxin accumulation occurred in cells where auxin responses have been localized in *M. truncatula*, i.e., pericycle, endodermis, and inner cortex (Deinum et al., 2016). Interestingly, a temporary decrease in auxin efflux has so far only been documented for indeterminate nodules, such as those forming on *M. truncatula*, white clover, and vetch (Mathesius et al., 1998; Boot et al., 1999; van Noorden et al., 2006). This auxin transport inhibition was absent in the nodulation defective *cre1 (cytokinin response 1)* mutant of *M. truncatula* that has a mutation in a cytokinin receptor (Ng et al., 2015). In this mutant, auxin transport inhibitors (ATIs) could restore both auxin transport inhibition as well as nodule initiation and auxin responses, suggesting that auxin transport inhibition in *M. truncatula* is required for correct auxin localization in the pericycle, endodermis, and inner cortex, which then leads to their divisions (Ng et al., 2015). Pacios-Bras et al. (2003) reported a temporary increase in auxin transport in response to Nod factor treatment in *L. japonicus*, although this was not statistically analyzed. Based on findings that lack of flavonoids in *M. truncatula* abolished auxin transport control and nodulation by rhizobia (Wasson et al., 2006), but lack of auxin-transport reducing isoflavonoids in soybean could be compensated for by addition of nod-gene inducers to infecting Bradyrhizobia (Subramanian et al., 2006), it was suggested that auxin transport control may be specific to indeterminate nodulation (Subramanian et al., 2007). However, no detailed auxin transport measurements have been published in other determinate nodule-forming species. It therefore remains unclear whether auxin transport inhibition is likely a mechanism leading to auxin accumulation in inner cortical cells in indeterminate nodule-forming species, but not in determinate nodule-forming species where auxin accumulation is localized in the middle/outer cortex.

Experiments using synthetic ATIs, such as *N*-1-naphthylphthalamic acid (NPA) and 2,3,5-triiodobenzoic acid (TIBA), have been used to uncover the roles of polar auxin transport in plant development, including lateral root organogenesis, inflorescence growth, and meristem maintenance (Casimiro et al., 2001; Scanlon, 2003; Wu and McSteen, 2007). Intriguingly, the application of ATIs on the roots of indeterminate nodule-forming legumes, such as *M. truncatula*, alfalfa, pea, and white sweet clover, can induce the formation of nodule-like structures, broadly termed pseudonodules (Hirsch et al., 1989; Scheres et al., 1992;

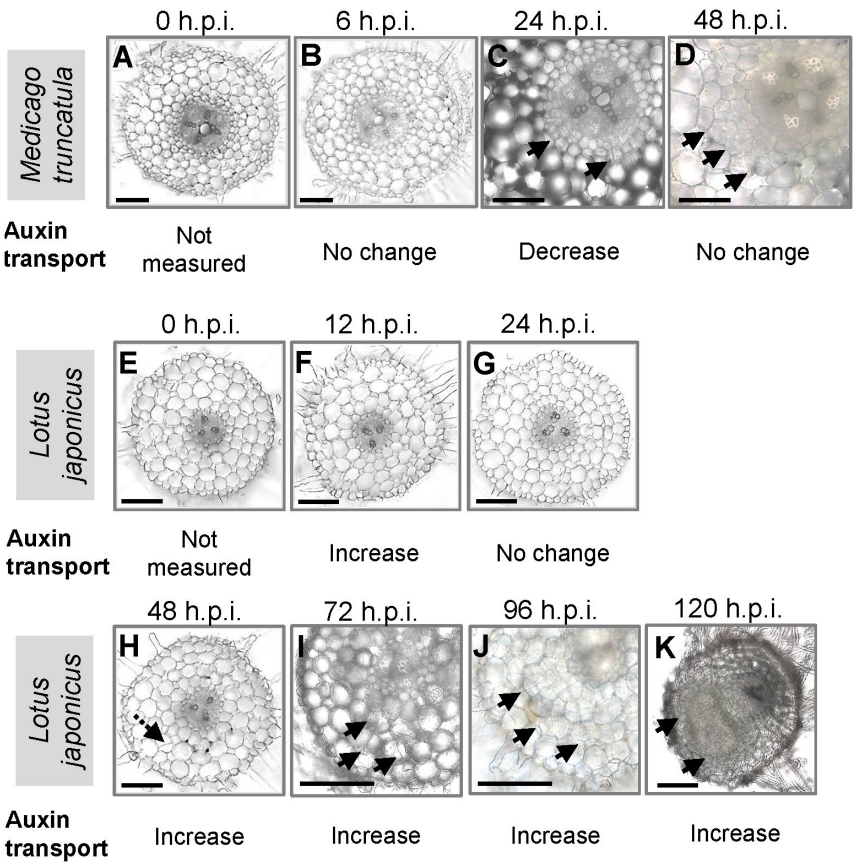

FIGURE 1 | Nodule development in *Medicago truncatula* and *Lotus japonicus*. Cross sections of roots showing the stages of nodulation at **(A)** 0, **(B)** 6, **(C)** 24, and **(D)** 48 h post-inoculation (h.p.i.) in *M. truncatula*; cross sections of roots showing the stages of nodulation at **(E)** 0, **(F)** 12, **(G)** 24, **(H)** 48, **(I)** 72, **(J)** 96, and **(K)** 120 h.p.i. in *L. japonicus*. Changes in acropetal auxin transport at each individual stage are summarized below each figure. At least 10 roots were examined at each stage. Black arrows indicate pericycle, endodermal, and cortical cell divisions. Dotted black arrow in **H** indicates a possible cortical cell division. Scale bars represent 200 μm.

Wu et al., 1996; Rightmyer and Long, 2011). Pseudonodules have a globular external structure resembling nodules, but contain undifferentiated cortical, endodermal, and pericycle cells. In addition, they fail to develop the characteristic peripheral vasculature (Guan et al., 2013) and do not house rhizobia. The detailed structure of early developmental stages of pseudonodules is not well described in the literature. On the contrary, ATIs failed to form pseudonodules on the roots of *L. japonicus* (Kawaguchi et al., 1996; Takanashi et al., 2011) and have only been reported to induce nodule-like structures in one species forming determinate nodules, *Macroptilium atropurpureum* (siratro), albeit with no description of the structure (Relić et al., 1993). This suggests that auxin transport inhibition is a mechanism inducing nodule structures by localizing auxin in the inner cortical region in indeterminate- but likely not determinate-nodule forming species (Kohlen et al., 2017).

Here, we aimed to compare changes in auxin transport and localization during indeterminate and determinate nodule formation. We compared acropetal (toward the root tip) auxin transport in corresponding root segments of *M. truncatula* and *L. japonicus* seedlings. We corroborated these findings with localization of auxin responses during nodulation and with direct quantification of auxin concentrations in these root segments, as we hypothesized that auxin transport affects the available pool of auxin (active and conjugated) at the nodule initiation site. We also tested the ability of ATIs to induce pseudonodules in a number of legume species forming indeterminate and determinate nodules, as well as their ability to inhibit auxin transport and induce auxin responses in the root.

RESULTS

Auxin Transport Regulation during Nodulation Differs between *Medicago truncatula* and *Lotus japonicus*

We were interested to compare auxin transport at the equivalent nodule developmental stages in *M. truncatula* and *L. japonicus* during the early stages of nodulation. To coordinate the time point of measurement with the onset of nodule development, we made root cross sections at different nodule developmental stages (**Figure 1**). In *M. truncatula*, no visible cell divisions were

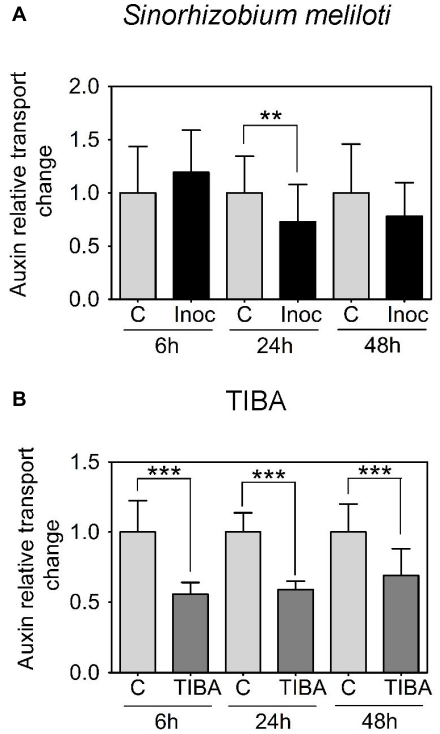

FIGURE 2 | Acropetal auxin transport measurements of *M. truncatula* root segments. **(A)** Relative auxin transport changes were measured in mock or *Sinorhizobium meliloti*-spot inoculated root segments at 6, 24, and 48 h.p.i. **(B)** Relative acropetal auxin transport changes in mock- or TIBA-flood-treated root segments at 6, 24, and 48 h post-treatment. Mann–Whitney *U*-tests and unpaired *t*-tests were used for statistical analyses in **A** and **B**, respectively ($p < 0.05$, n = 15–25 per treatment or time point). Asterisks indicate statistically different auxin relative transport change (**, very significant; *** extremely very significant). Graphs show mean and SD. Abbreviations: C, control; Inoc, inoculated; and TIBA, 2,3,5-triiodobenzoic acid.

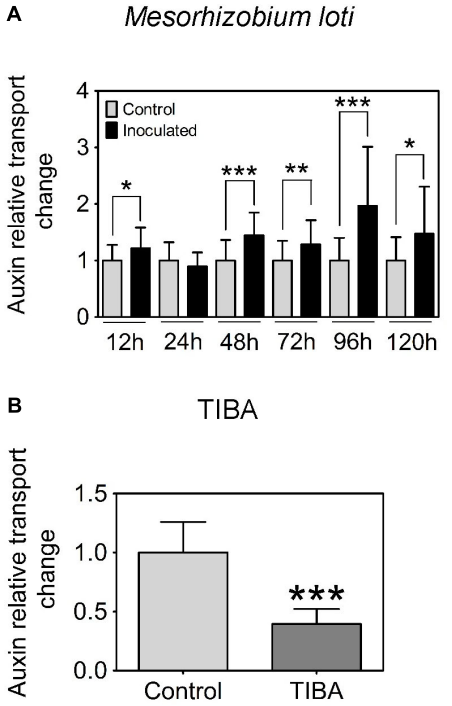

FIGURE 3 | Acropetal auxin transport measurements of *L. japonicus* root segments. **(A)** Relative auxin transport changes were measured in mock or *Mesorhizobium loti*-spot inoculated root segments at 12, 24, 48, 72, 96, and 120 h.p.i. **(B)** Relative auxin transport changes were measured in mock- or TIBA-treated root segments at 48 h post-treatment. Unpaired *t*-tests were used for statistical analyses ($p < 0.05$, n = 25–30 per treatment or time point). Asterisks indicate significant change in relative auxin transport (*, significant; **, very significant; *** extremely very significant). Graphs show mean and SD. Abbreviation: TIBA, 2,3,5-triiodobenzoic acid.

detected at 0 and 6 hours post-inoculation (h.p.i.) (**Figures 1A,B**). We observed the first cortical cell divisions as early as 24 h.p.i. (**Figure 1C**) and more extensive cortical, endodermal, and pericycle divisions at 48 h.p.i. (**Figure 1D**). In *L. japonicus*, no cell divisions were detected at 0, 12, or 24 h.p.i. (**Figures 1E–G**). In one root, we found a single cortical cell division at 48 h.p.i., but not in any other roots. The first visible cell divisions appeared at 72 h.p.i. (**Figure 1I**) and visible nodule primordia at 120 h.p.i. in the majority of roots (**Figure 1K**).

We were interested in auxin transport regulation prior to the formation of visible nodule primordia on the roots. In *M. truncatula*, we measured acropetal auxin transport in the segment just below the inoculation spot at 6, 24, and 48 h.p.i. Auxin transported into the segment below the site of nodule initiation was chosen because if dividing cells inhibit the acropetal export of auxin this would be detectable as a reduced amount of auxin transported into the segment just below these cells. Consistent with our previous findings (Ng et al., 2015), we measured a significant decrease in acropetal auxin transport into the segment below the inoculation site at 24 h.p.i., but not at 6 or 48 h.p.i. (**Figure 2A**).

In *L. japonicus*, visible nodule primordia only formed after 120 h.p.i. under our growth conditions (**Figure 1K**). Hence, we measured auxin transport at 12, 24, 48, 72, 96, and 120 h.p.i. Similar to the findings reported in Pacios-Bras et al. (2003), we found a significant increase in acropetal auxin transport at 48 h.p.i. in the segment below the rhizobia inoculation spot (**Figure 3A**). In addition, acropetal auxin transport also increased significantly at 12, 72, 96, and 120 h.p.i. (**Figure 3A**).

Auxin Transport Inhibitors Induce Pseudonodules on Legumes Forming Indeterminate Nodules

Several studies have reported the ability of certain indeterminate nodule-forming legumes to form nodule-like structures, also termed pseudonodules, in response to ATIs. We wanted to investigate if the predisposition to form pseudonodules in response to ATIs is unequivocally confined to indeterminate-nodule forming legumes. To simulate the transient nature of the acropetal auxin transport inhibition in *M. truncatula*, we performed temporary flooding of selected legume species with the ATIs TIBA and NPA (Rightmyer and Long, 2011). We selected *M. truncatula* and *Trifolium subterraneum* to represent

indeterminate nodule-forming legume species. On the other hand, *L. japonicus*, *Glycine max* (soybean), *Vicia faba* (broad bean), *Vigna unguiculata* (snake bean), and *M. atropurpureum* (siratro) were selected to represent determinate nodule-forming legume species. *Sesbania rostrata* can form indeterminate- or determinate-type nodules, depending on aeration status of the roots (Fernández-López et al., 1998). Selecting this species posed an interesting question as to whether ATIs could induce pseudonodules on this "dual nodule-type" legume.

Using a temporary flooding system, we found that both TIBA and NPA could induce pseudonodules on the roots of *M. truncatula* and *T. subterraneum*. The optimal concentration of TIBA and NPA to induce pseudonodules on *M. truncatula* was 50 μM (**Figure 4A**). At 100 μM, TIBA induced pseudonodules on *M. truncatula* roots at a similar frequency as 50 μM, but a similar concentration of NPA reduced pseudonodules formed on the roots of *M. truncatula* (**Figure 4A**). TIBA, but not NPA, could induce pseudonodule formation at 10 μM on *M. truncatula* roots (**Figure 4A**). For *T. subterraneum*, pseudonodules formed at the highest frequency at 50 and 100 μM TIBA treatment (**Figure 4B**). Pseudonodules were observed on the roots of *T. subterraneum* treated with 1 and 10 μM TIBA, as well as 1, 10, 50, and 100 μM NPA, although pseudonodule numbers were significantly lower (**Figure 4B**). In both legumes, TIBA overall induced significantly more pseudonodules than NPA at the concentrations tested (**Figures 4A,B**; two-way ANOVA, $p < 0.001$). We also tested primary root growth at various concentrations of TIBA and NPA on *M. truncatula* and *L. japonicus* to investigate if they had any adverse effects on root development. At concentrations up to 100 μM TIBA in *M. truncatula* (Supplementary Figure 1A) and 50 μM TIBA in *L. japonicus* (Supplementary Figure 1B), primary root growth was not significantly affected when compared with the control treatment. However, in both legume species, a 10-μM NPA treatment already significantly reduced primary root growth (Supplementary Figures 1A,B), suggesting a stronger pleiotropic effect caused by NPA treatment. We did not observe any pseudonodules forming on the roots of *L. japonicus*, *G. max*, *V. faba*, *V. unguiculata*, or *M. atropurpureum* in response to the temporary flooding with either TIBA or NPA (Supplementary Figure 2; 15–25 plants analyzed per species). Interestingly, a few pseudonodules formed on the roots of *S. rostrata* in response to TIBA or NPA treatment (10 out of 96 plants) at a range of concentrations tested (1, 10, 50, or 100 μM) under non-flooded conditions that lead to indeterminate nodule types (Fernández-López et al., 1998).

The outward appearance of pseudonodules on *M. truncatula* (**Figures 5A,B**), *T. subterraneum* (**Figures 5C,D**), and *S. rostrata* (**Figures 5E,F**) resembled rhizobia-induced nodules. Interestingly, although pseudonodules on *M. truncatula* primarily formed on younger parts of the roots (where rhizobia-induced nodules form), they could also be found on more mature parts of the roots (**Figure 5G**). Cross sections of these structures revealed a more diffuse and randomized nature of cell divisions, as opposed to a more controlled pattern of cell divisions observed in rhizobia-induced nodules. Mature pseudonodules formed on *M. truncatula* (**Figures 6A,B**), *T. subterraneum* (**Figures 6C,D**), and *S. rostrata* (**Figures 6E,F**) all displayed cell divisions in the pericycle, endodermis, and cortex (**Figure 6**). However, pseudonodules were characterized by more extensive pericycle and endodermal cell divisions, rather than the predominantly cortical cell divisions observed in rhizobia-induced nodules.

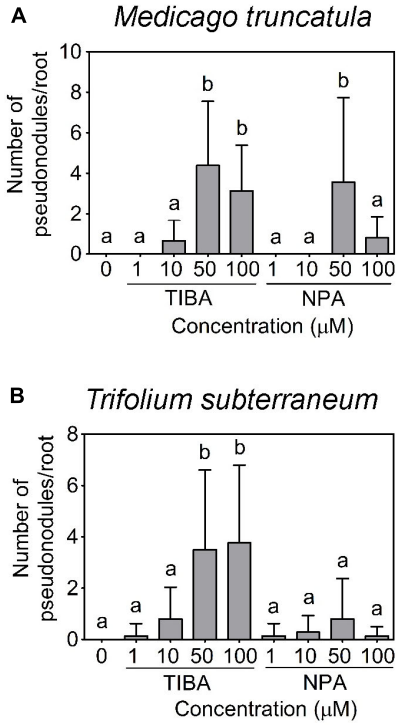

FIGURE 4 | Pseudonodule formation in response to TIBA and NPA treatment at various concentrations. Pseudonodule formation on the roots of **(A)** *M. truncatula* and **(B)** *Trifolium subterraneum* (subclover), in response to TIBA and NPA treatments within the concentration range of 0–100 μM. A two-way ANOVA with a Dunn's multiple comparison post-test were used for statistical analyses. Different lowercase letters indicate statistically different number of pseudonodules per root ($p < 0.05$, n = 20–25 per treatment). Graphs show mean and SD. Abbreviations: TIBA, 2,3,5-triiodobenzoic acid and NPA, 1-*N*-naphthylphthalamic acid.

The legume *S. rostrata* can also form nodules on its stems. We did not observe pseudonodules forming on the stems of *S. rostrata* in response to TIBA or NPA treatment. However, unlike the adventitious root buds found on stems under control treatment (Supplementary Figures 3A,B), we found a higher occurrence of adventitious structures resembling bumps forming on the stems (Supplementary Figures 3D,E,G,H). Cross sections of these structures revealed a thicker layer of tissue with high cell wall autofluorescence (Supplementary Figures 3F,I), visualized under UV light, in comparison to the control (Supplementary Figure 3C).

Previously, we demonstrated that the formation of pseudonodules involved an inhibition of acropetal auxin transport in *M. truncatula* roots (Ng et al., 2015). Thus, we also tested auxin transport regulation in response to TIBA treatment (50 μM) at 6, 24, and 48 h.p.i., similar to the measurements performed for rhizobia inoculation. Unlike the transient nature of acropetal auxin transport inhibition

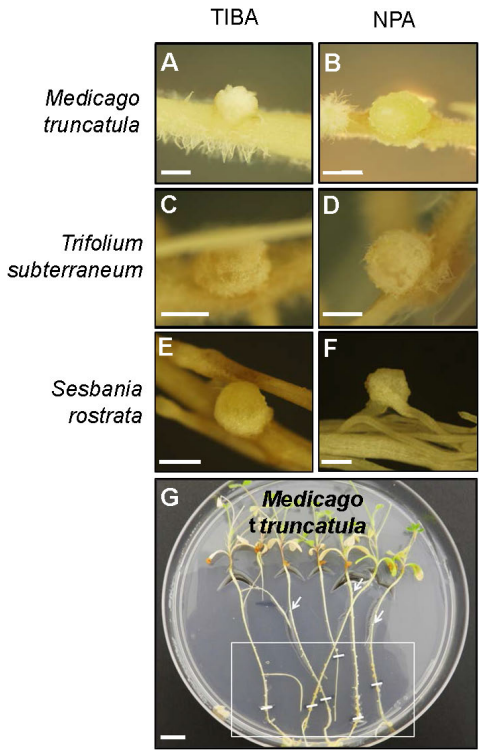

FIGURE 5 | Pseudonodule formation on the roots of legumes in response to TIBA or NPA treatments. Pseudonodules formed on the roots of **(A,B)** *M. truncatula*, **(C,D)** *T. subterraneum* (subclover), and **(E,F)** *Sesbania rostrata*, in response to treatment with either 50 μM TIBA or 50 μM NPA. **(G)** Pseudonodules were formed along the entire roots of *M. truncatula*. The area on the roots encapsulated by the white box indicates the region where the majority of pseudonodules were found on each root. White lines within the box indicate locations of the root tip when the roots were first subjected to TIBA treatment. White arrows indicate pseudonodules found at older parts of the roots. Scale bars represent 1 mm in **(A–F)** and 1 cm in **(G)**. Abbreviations: TIBA, 2,3,5-triiodobenzoic acid and NPA, 1-*N*-naphthylphthalamic acid.

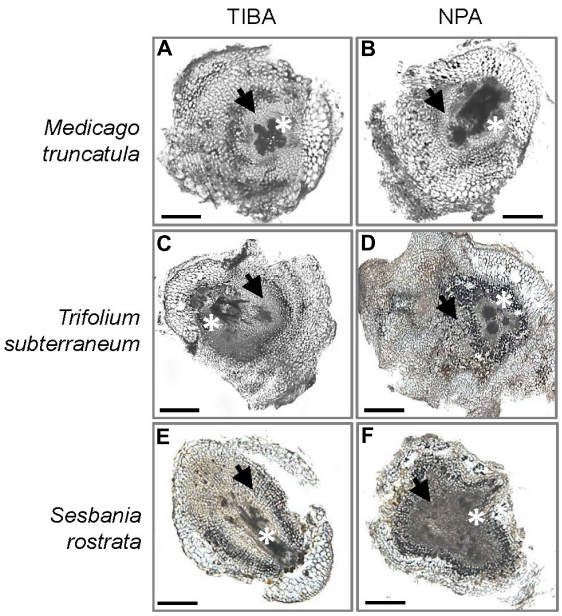

FIGURE 6 | Cross sections of pseudonodules induced by TIBA or NPA treatment. Pseudonodules were induced on the roots of **(A,B)** *M. truncatula*, **(C,D)** *T. subterraneum* (subclover), and **(E,F)** *S. rostrata*. Asterisks indicate location of the primary root vasculature. Arrows indicate pericycle and endodermal cell divisions. Scale bars represent 500 μm. Abbreviations: TIBA, 2,3,5-triiodobenzoic acid and NPA, 1-*N*-naphthylphthalamic acid.

in *M. truncatula* (**Figures 1C**, **2A**), acropetal auxin transport decreased significantly in response to TIBA treatment at 6, 24, and 48 h.p.i. (**Figure 2B**). Although rhizobia inoculation failed to reduce acropetal auxin transport in *L. japonicus*, TIBA treatment also significantly reduced acropetal auxin transport in this legume (**Figure 3B**).

Changes in Auxin Response and Concentration during Nodule Formation in *Medicago truncatula* and *Lotus japonicus*

We localized auxin responses in both *M. truncatula* and *L. japonicus* fully transformed plants carrying the *GH3:GUS* reporter (Pacios-Bras et al., 2003; van Noorden et al., 2007). In *M. truncatula*, auxin responses were enhanced in early nodule primordia at 48 h.p.i. in divided pericycle, endodermis, and inner cortex cells (**Figure 7B** and Supplementary Figure 4). In mature nodules, an auxin response was found in the nodule vasculature and the nodule meristem (**Figure 7C**).

During pseudonodule formation in *M. truncatula*, the first small nodule primordia were found at 7 days following TIBA application, which was slower than formation of equivalent nodule primordia at 48 h after rhizobia inoculation. We found no enhanced *GH3::GUS* expression in the cortex at 48 h after TIBA treatment (Supplementary Figure 5). An increased auxin response was localized in the dividing pericycle, endodermis, and inner cortex cells at the early primordium stage at 7 days after TIBA application, similar to rhizobia-induced nodule primordia (**Figure 7E**). However, in more mature pseudonodules (20 days post-treatment), *GH3::GUS* expression did not resemble that of rhizobia-induced nodules and was confined to pericycle, endodermal, and inner cortical cell layers (**Figure 7F**).

In *L. japonicus*, induction of auxin responses occurred in cortical cells, mainly those surrounding early nodule primordia or those that appeared to have just divided, while primordia themselves showed very low *GH3::GUS* expression (**Figure 7H** and Supplementary Figure 4). We did not detect any changes in auxin response before the onset of cell divisions (**Figures 7A,D,G,J**). In mature *L. japonicus* nodules, auxin responses were restricted to the vasculature (**Figure 7I**). Nodules in *L. japonicus* do not retain an apical meristem, and no apical *GH3::GUS* response was seen. In *L. japonicus* roots treated with TIBA, we detected increased *GH3::GUS* responses first in outer cortical and epidermal cells (5 days post-treatment) and later

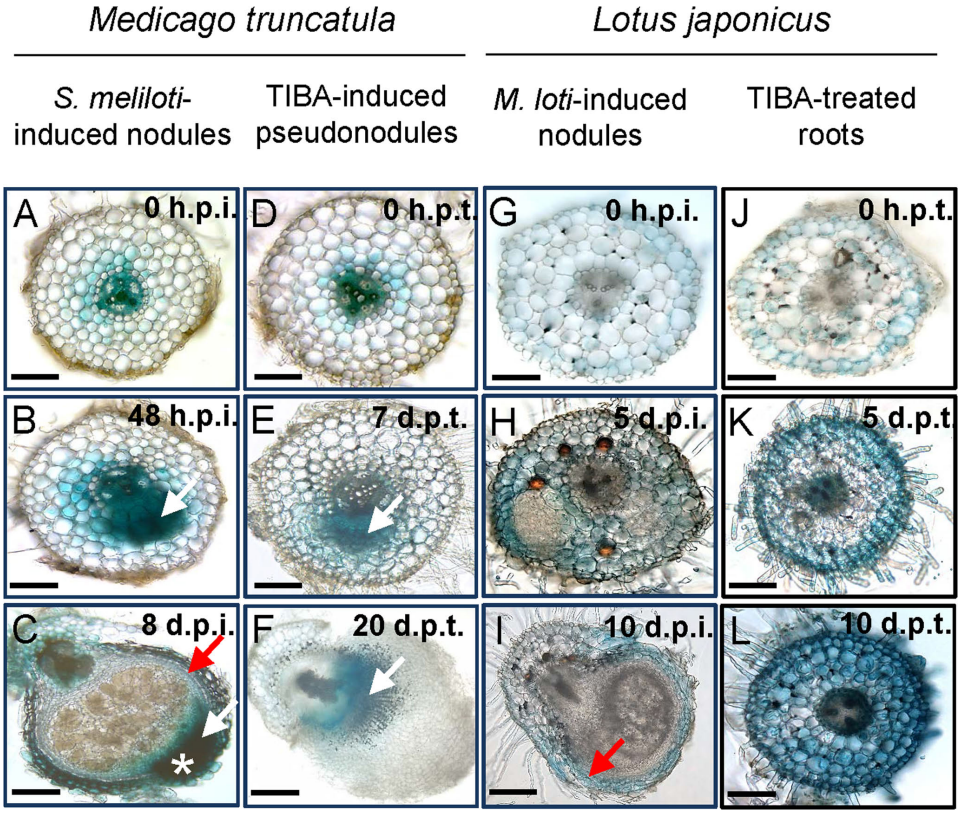

FIGURE 7 | Auxin response as seen by *GH3:GUS* expression in *M. truncatula* and *L. japonicus* roots or nodules. Auxin response in different tissues in **(A–C)** *S. meliloti*-induced nodules on *M. truncatula* roots; **(D–F)** TIBA-induced pseudonodules on *M. truncatula* roots; **(G–I)** *M. loti*-induced nodules on *L. japonicus* roots; and **(J–L)** TIBA-treated roots of *L. japonicus*. The developmental stages are indicated by the time after *S. meliloti*/TIBA/*M. loti* treatment in each case. White arrows indicate auxin response in dividing cells. Red arrow indicates auxin response in the nodule vasculature. White asterisk indicates the location of the nodule meristem, where an enhanced auxin response is observed. Scale bars represent 200 μm. Abbreviations: h.p.i., hours post-inoculation; d.p.i., days post-inoculation; h.p.t., hours post-treatment; and d.p.t., days post-treatment.

in the whole root (10 days post-treatment), but despite serial sectioning of multiple roots, we never detected any divided cells in the cortex (**Figures 7K,L**).

In parallel to the auxin responses, we quantified auxin content in inoculated root segments encompassing the inoculation site. We previously reported increased IAA content in inoculated *M. truncatula* root segments at 24 h.p.i., but not at 6 h.p.i. (Ng et al., 2015). Measurements at 48 h.p.i. in this study showed no significant changes in IAA content (Supplementary Figure 6). However, we found a significant decrease in the concentration of IAA-Ala at 48 h.p.i. that was not found at either 6 or 24 h.p.i. (Ng et al., 2015; Supplementary Figure 6). The auxins PAA, 4-Cl-IAA, and IAA-Val were not detected in any of the samples measured.

In contrast to *M. truncatula*, we measured a temporary decrease in IAA concentration in *L. japonicus* root segments encompassing the nodulation zone at 24 h.p.i. (**Figure 8A**). No IAA changes were detected between control and inoculated *L. japonicus* roots at 48 h.p.i. or 5 days post-inoculation (**Figure 8A**). The concentrations of IBA, IAA-Alanine, IAA-Aspartate, and IAA-Leucine/Isoleucine were not altered by rhizobia inoculation (**Figures 8B–E**). The auxins 4-chloro-IAA, IAA-Phenylalanine, and IAA-Tryptophan were not consistently detected in the root segments (**Figures 8F–H**).

DISCUSSION

In our study, we posed two main questions:

(1) Is acropetal auxin transport inhibition during nodulation restricted to indeterminate nodules, and what are possible reasons for this?
(2) Which other mechanisms could contribute to increased auxin responses in the cortex during nodule initiation?

Is Acropetal Auxin Transport Inhibition during Nodulation Restricted to Indeterminate Nodulation, and What Are Possible Reasons for This?

Consistent with previous results in *M. truncatula*, we observed a transient reduction in acropetal auxin transport following

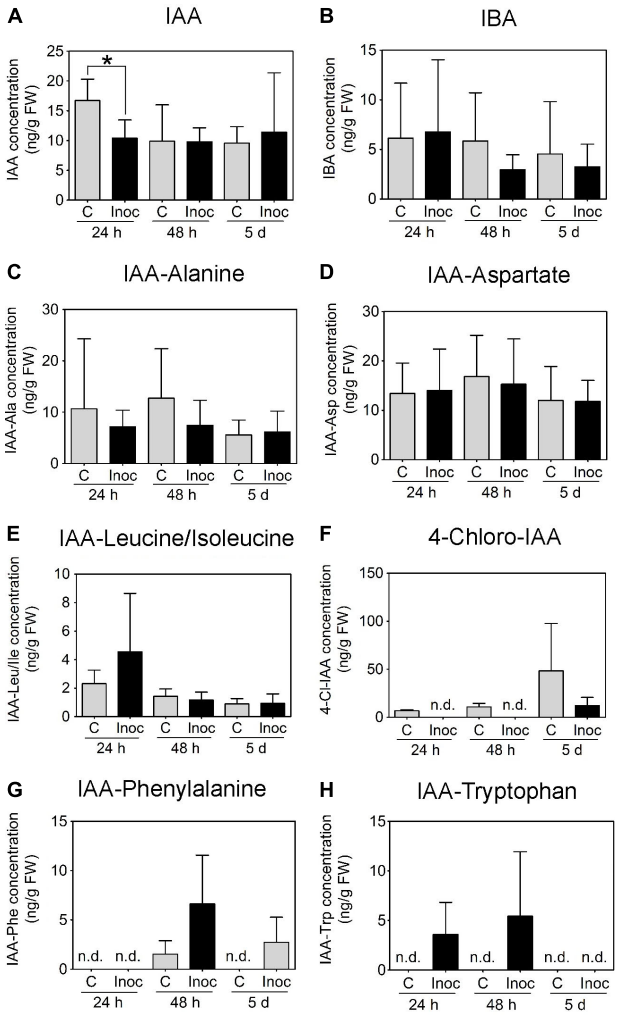

FIGURE 8 | Auxin content in developing *L. japonicus* nodules (4 mm long segments around the inoculation site). Endogenous auxin concentration (ng g^{-1} FW) in *L. japonicus* roots inoculated with *M. loti*- or mock-treated roots was measured at 24 h, 48 h, and 5 days post-inoculation. Auxins detected in *L. japonicus* roots include **(A)** IAA, **(B)** IBA, **(C)** IAA-Ala, **(D)** IAA-Asp, and **(E)** IAA-Leu/Ile. **(F)** 4-Cl-IAA, **(G)** IAA-Phe, and **(H)** IAA-Trp were not consistently detected at all time points. A two-way ANOVA and a Student's *t*-test were used for statistical analyses ($p < 0.05$; $n = 3$–6 per treatment or time point). Asterisk in **(A)** indicates a significant difference in auxin concentration ($p < 0.05$). Graphs show mean and SD. Abbreviations: FW, fresh weight; C, control; Inoc, inoculated; n.d., not detected; IAA, indole-3-acetic acid; and IBA, indole-3-butyric acid.

rhizobia treatment at 24 h.p.i., coinciding with the very earliest cell divisions (Wasson et al., 2006; van Noorden et al., 2006; Plet et al., 2011; Ng et al., 2015). For *L. japonicus*, Pacios-Bras et al. (2003) previously demonstrated an increase in acropetal auxin transport capacity in response to Nod factor treatment at 48 h.p.i., although those experiments were not statistically analyzed. Here, we included two additional features to our measurements: (1) we included additional time points to assess if this increase in auxin transport capacity was of a transient or prolonged nature and correlated with the onset of cell divisions and (2) we measured auxin transport in equivalent segments below the inoculation spot. Crucially, this study provides a direct comparison of two corresponding segments in *M. truncatula* and *L. japonicus*. Unlike the short-term nature of acropetal auxin transport inhibition during indeterminate nodule initiation, we found that an increased auxin transport capacity in *L. japonicus* started at 12 h.p.i., i.e., before the very earliest cortical cell divisions, and continued at 48, 72, 96, and 120 h.p.i., where cell divisions were more extensive.

In *M. truncatula*, knockdown of Mt*PIN4* (ortholog of At*PIN1* mediating acropetal auxin transport; Schnabel and Frugoli, 2004; Kohlen et al., 2017) reduced nodulation (Huo et al., 2006), and transcription of this gene was one of the most highly upregulated by Nod factor treatment (Plet et al., 2011), suggesting that acropetal auxin transport regulation might occur through MtPIN4, although it may involve other auxin transporters. So far it is unknown how the increased acropetal auxin transport in *L. japonicus* is regulated. It would be essential to quantify *PIN* gene expression in *L. japonicus* in the future, and analyze mutants of auxin transporters.

The lack of auxin transport inhibition during *L. japonicus* nodule development was supported by the inability of TIBA or NPA to induce pseudonodules in this species. We observed pseudonodule formation on *M. truncatula*, subclover, and *S. rostrata*, and pseudonodules were also reported in alfalfa and white sweet clover (Hirsch et al., 1989; Wu et al., 1996). Although *S. rostrata* has the capacity to form both nodule types, it typically forms indeterminate-type nodules under non-waterlogging and well-aerated growth conditions (Fernández-López et al., 1998), and our growth system and ATI assays simulated these conditions. Lack of pseudonodule formation on *L. japonicus* in response to ATIs had previously been observed (Takanashi et al., 2011), even though TIBA treatment reduced acropetal auxin transport capacity in *L. japonicus* roots similar to *M. truncatula*. Curiously, gibberellins were able to induce pseudonodules on *L. japonicus*, but not alfalfa roots (Kawaguchi et al., 1996). The mode of action or physiological effects of gibberellins were, however, not examined. Nevertheless, gibberellins are not likely to inhibit acropetal auxin transport because of their failure to induce pseudonodules on alfalfa. In addition to *L. japonicus*, pseudonodules were not found on any of the other examined legume species forming determinate nodules, including *G. max*, *V. faba*, *V. unguiculata*, or *M. atropurpureum*. Pseudonodules had been reported as "few" in response to TIBA or NPA in *M. atropurpureum* (Relić et al., 1993), but no photos were shown in that study and we could not confirm this finding.

Pseudonodules formed in *M. truncatula* in response to TIBA showed *GH3::GUS* expression in the base, but no expression at the pseudonodule "tip," where rhizobia-induced nodules showed strong *GH3::GUS* expression in the nodule meristem. This suggests the lack of a pseudonodule meristem.

Why would ATIs not induce pseudonodules in determinate nodule-forming species? *M. truncatula* roots treated with TIBA formed pseudonodules, and at the earliest stages of their formation, these pseudonodules showed high auxin (*GH3::GUS*)

responses in the pericycle, endodermis, and inner cortex, similar to indeterminate nodule primordia. Modeling has shown that acropetal auxin transport inhibition would produce this pattern of auxin accumulation (Deinum et al., 2012). When we treated *L. japonicus* roots with TIBA, we found increased *GH3::GUS* expression in a different pattern – in the outer cortex, and later on in all cortex cells – but no small primordia were formed. Thus, it is likely that the difference in the tissue types involved in the early cell divisions (pericycle, endodermis, and inner cortex in indeterminate, and outer cortex for determinate nodules) dictates whether auxin transport changes contribute to nodule initiation. It is also possible that cortical responses to auxin differ in indeterminate and determinate nodule-forming species, for example in sensitivity, and this will have to be further explored in the future. For instance, it might be possible that auxin concentrations generated in the cortex in response to ATIs become super-optimal for determinate nodules (Turner et al., 2013).

Which Other Mechanisms Could Contribute to Increased Auxin Responses in the Cortex during Nodule Initiation?

During the earliest stage of nodule initiation, both *M. truncatula* and *L. japonicus* showed increased auxin (*GH3::GUS*) response in the inner or outer/middle cortex, respectively. It is possible that the increased auxin response seen in dividing outer cortical cells in *L. japonicus* is in response to altered sensitivity to auxin. Studies in soybean have demonstrated the role of a number of microRNAs controlling the expression of auxin receptors and response genes that could change sensitivity toward auxin (Mao et al., 2013; Turner et al., 2013). Another mechanism to explain the initial increased auxin response could include auxin synthesis in the cortex, and evidence for the induction of auxin synthesis genes in *L. japonicus* was found previously (Suzaki et al., 2012). However, we did not detect any significant increase in auxin concentration in that area in *L. japonicus* roots. Intriguingly, a reduction in IAA content was measured at 24 h.p.i., although we did not detect any changes in auxin transport or auxin response at that stage. Currently, we cannot explain the significance of this finding; it could be due to increased auxin degradation. In *M. truncatula*, the increased auxin response at the early primordium stage at 48 h.p.i. was not accompanied by increased auxin concentrations, either. This suggests that it is either difficult to detect increased auxin concentrations in small numbers of cells, as 4 mm root segments were harvested for this assay, or that there is no linear relationship between *GH3::GUS* expression and auxin concentration.

Genetic studies on the role of auxin transport carriers during nodulation in *L. japonicus* are lacking. One report highlighted the role of an ABCB-type multidrug resistance protein, LjABCB1, in mature *L. japonicus* nodules, but did not examine its role during early nodule development. The authors proposed that LjABCB1 exports auxin toward infected cells in the nodule, based on the selective localization of the protein at adjacent uninfected cells (Takanashi et al., 2012). Future studies will clearly have to unravel the regulation of various auxin transporters in *L. japonicus* (Kohlen et al., 2017). In addition, it will be necessary to model the changes in acropetal auxin transport in *L. japonicus* computationally, to find out if these observed increases in auxin transport would account for the increased auxin responses in the cortex. Previous modeling has shown that auxin accumulation in the middle/outer cortex could be explained by radial repositioning of PIN proteins (Deinum et al., 2012, 2016).

Apart from the differences between *M. truncatula* and *L. japonicus* in auxin transport at the time of the first cortical cell divisions, we also found differences in auxin responses at the primordia stage. While auxin responses remained high in young nodule primordia of *M. truncatula*, auxin response diminished quickly in *L. japonicus* nodule primordia as reported by other studies (Mathesius et al., 1998; Takanashi et al., 2011; Suzaki et al., 2012; Turner et al., 2013). It is possible that changes in auxin sensitivity in the cortex differentiate the conditions suitable for nodule development in species forming indeterminate and determinate nodules: While reduced auxin sensitivity increased nodule numbers in soybean (Nizampatnam et al., 2015; Wang et al., 2015), a window of higher auxin sensitivity may be required for indeterminate nodule initiation (Mao et al., 2013). However, it was also demonstrated that silencing of the auxin receptor TIR1 in soybean reduced nodulation, suggesting that auxin responses are necessary for determinate nodule formation (Cai et al., 2017). Thus, correct auxin responses in space and time are crucial for nodule development.

In summary, we found no evidence that inhibition of acropetal auxin transport occurs during nodule initiation in *L. japonicus*, and it is unlikely to be a mechanism that creates the correct auxin gradients for other legume species forming determinate nodules because ATIs did not induce any cortical cell divisions in a number of tested species, in contrast to species forming indeterminate nodules. While increased auxin responses occurred in the earliest dividing cortex cells of *L. japonicus*, no significant increase in auxin concentration was measured. In contrast, *M. truncatula* showed more sustained auxin responses in nodule primordia, although increased auxin concentration was only detected at 24 h, preceding nodule primordia. Thus, it is possible that changes in auxin sensitivity in cortical cells, without measurable changes in auxin content, contribute to increased auxin responses.

MATERIALS AND METHODS

Plant Material and Growth Conditions

Plant species used in this study included *M. truncatula* wild-type cultivar Jemalong A17 (South Australian Research and Development Institute, Adelaide, Australia), *L. japonicus* ecotype Gifu B-129 (Biological Resource Center in *Lotus* and *Glycine*, University of Miyazaki, Japan), *T. subterraneum* cv. Karridale (Clean Seeds, Bungendore, Australia), *G. max* cv. Bragg (Prof. Peter Gresshoff, University of Queensland), *S. rostrata* (Prof. Sofie

Goormachtig, Ghent University, Belgium), *M. atropurpureum* (Selected Seeds, Pittsworth, Australia), *V. unguiculate* and *V. faba* cv. Coles Early Dwarf (both Mr. Fothergill's Seeds Pty Ltd., South Windsor, Australia).

Seeds of *M. truncatula, L. japonicus*, *T. subterraneum*, and *M. atropurpureum* were scarified with sand paper, surface-sterilized in 6% (w/v) sodium hypochlorite for 10 min, then washed with sterilized milliQ water five times. Next, *M. truncatula* and *L. japonicus* seeds were imbibed in sterilized milliQ water containing 0.25 mg ml^{-1} of the antibiotic augmentin for 6 h with gentle mixing by rotation to reduce bacterial contamination. Sterilized seeds were washed once with sterilized milliQ water and then plated on Fahråeus (F) medium (Fahraeus, 1957) for *M. truncatula* or 1/4; strength Broughton and Dilworth medium (Broughton and Dilworth, 1971) for *L. japonicus*. For *T. subterraneum* and *M. atropurpureum*, seeds were sown straight onto F plates without the augmentin incubation step. Seeds were incubated at 4°C in the dark for 48 h. Germination of seeds was synchronized by incubating the plates at 25°C for 24–48 h with plates inverted. Seedlings with radicle length of approximately 5–10 mm were transferred onto F plates (*M. truncatula*, *T. subterraneum*, and *M. atropurpureum*) or 1/4; B&D plates (*L. japonicus*). Plates were semi-sealed with Parafilm, placed vertically in a container with a black cardboard interspersed between each plate to shield roots from direct light. Plates were incubated at 25 (*M. truncatula*, *T. subterraneum*, and *M. atropurpureum*) or 20°C (*L. japonicus*), with a 16 h light and 8 h dark period at 150 μmol m^{-2} s^{-1} light intensity.

For soybean, the germination protocol was based on Brechenmacher et al. (2009). Seeds were soaked in 0.1 N HCl for 10 min and then washed with tap water five times. Seeds were then surfaced-sterilized with 6% (w/v) sodium hypochlorite for 15 min and then washed with sterilized milliQ water five times, air dried for 20 min, and subsequently sown on 1/4; B&D plates. Seeds were left at 25°C in the dark for germination over several days. Germinated soybeans were transferred into pots containing autoclaved vermiculite (Grade 3), watered with 1/4; B&D medium, and grown at 16 h light and 8 h dark period at 150 μmol m^{-2} s^{-1} light intensity in a glasshouse.

For *S. rostrata*, the germination protocol was modified from Goethals et al. (1989). Seeds were immersed in 4 M sulfuric acid for 1 h and washed five times with tap water. This was followed by surface sterilization with 6% (w/v) sodium hypochlorite for 15 min and then five washes with sterilized milliQ water. Sterilized seeds were imbibed overnight in sterilized milliQ water. Imbibed seeds were plated onto F plates and left at 25°C in the dark for germination over several days. Germinated seedlings were transferred into glasshouse pots containing autoclaved vermiculite (Grade 3) and watered with F medium twice a week.

Seeds of *V. unguiculata* and *V. faba* were surface-sterilized with 6% (w/v) sodium hypochlorite for 15 min and then washed with sterilized milliQ water five times. Seeds were directly planted into pots containing autoclaved vermiculite (Grade 3) and thinned to one plant per pot after germination. Plants were watered with F medium twice a week and grown in a glasshouse.

Bacterial Strains and Inoculation Conditions

The *S. meliloti* strain A2102, a triple nod mutant for nodD1, nodD2, and nodD3 derived from the WT strain Sm1021, containing the pE65 plasmid encoding a constitutively overexpressed copy of nodD3 (Barnett et al., 2004) was used for all inoculations on *M. truncatula* (kindly provided by Dr. Melanie Barnett and Prof. Sharon Long, Stanford University, Stanford, CA, United States), hereafter referred to as "E65." This strain was used to compare results from this study to that of Ng et al. (2015). We previously established that the E65 strain (Ng et al., 2015) inhibited auxin transport similarly to the wild-type strain 1021 (Wasson et al., 2006). The E65 strain was maintained on Bergensen's Modified Medium (BMM) (Rolfe and Gresshoff, 1988) supplemented with 10 μg ml^{-1} tetracycline and 100 μg ml^{-1} streptomycin (Sigma Chemicals). For *L. japonicus*, inoculation ($OD_{600\ nm} = 0.05$) was performed with *Mesorhizobium loti* strain MAFF303099, maintained on Tryptone-Yeast (TY) medium.

For inoculation of *M. truncatula*, an overnight culture of *S. meliloti* strain E65 in BMM at 28°C was used. The optical density ($OD_{600\ nm}$) of the culture was adjusted to 0.1 for spot-inoculation. Spot-inoculation was performed by placing ∼1 μl of *S. meliloti* culture or BMM, onto the root surface 2 mm above the root tip, corresponding to the nodulation-susceptible zone (Bhuvaneswari et al., 1981). For analyzing *GH3::GUS* expression, spot-inoculation was performed with a glass capillary pulled into a fine tip over a flame and glued to a hypodermic needle.

For spot-inoculation of *L. japonicus*, a liquid culture of *M. loti* in TY medium was incubated for 3 days at 28°C. The $OD_{600\ nm}$ of the cultures was adjusted to 0.05. Spot-inoculation was performed by placing ∼1 μl of rhizobia culture or TY as a negative control, 2 mm above the root tip.

Flood Treatment with Auxin Transport Inhibitors

Seeds were germinated as described above. Seedlings of *M. truncatula*, *L. japonicus*, *T. subterraneum*, and *M. atropurpureum* were treated while growing on agar plates. At 1 week post-transfer onto agar medium, seedlings were treated by flooding, as described in Rightmyer and Long (2011). Diluted solutions of NPA and TIBA (Sigma Chemicals) were made in sterile 50 ml Falcon tubes. Control treatments contained equivalent dilution of methanol (which was used as a solvent for stock solutions). The concentrations of ATIs were chosen because they were previously demonstrated to induce pseudonodules on *M. truncatula* (Rightmyer and Long, 2011). Seedlings were flooded with 20–30 ml of diluted ATIs for 10 s, and then the solution was decanted. Pseudonodules were analyzed 3 weeks after treatment with ATIs.

For plants grown in pots (*G. max*, *S. rostrata*, *V. faba*, *V. unguiculata*, and *M. truncatula* as a positive control for

pot experiments), 50 ml of ATI diluted in growth medium was applied to each pot. This was repeated after 1 week and plants were then left to grow for another 3 weeks before uprooting the plants and analyzing for pseudonodule formation.

Auxin Quantification

Auxin quantification was based on Ng et al. (2015). Commercial auxin standards and a deuterated internal standard were used to determine elution times, collision energies, detection limits, and for absolute quantification. Auxin standards were obtained from OlChemim (IAA-Phenylalanine, IAA-Leucine, IAA-Valine, IAA-Tryptophan, 4-Cl-IAA), Sigma (IAA-Aspartate, IAA-Alanine, IAA-Isoleucine, IAA, IBA, PAA) and Cambridge Isotope Laboratories (indole-2,4,5,6,7-d5-3-acetic acid).

Plant roots were collected at 6, 24, and 48 h.p.i. with rhizobia. Root segments of 4 mm spanning the spot-inoculation site were collected and snap-frozen immediately in liquid nitrogen. A total of 30–40 root segments were collected for each treatment, for each biological replicate. Between 5 and 10 biological replicates were analyzed for each time point and species. The frozen tissue samples were mechanically lysed with stainless steel beads in a Qiagen TissueLyser LT with a pre-cooled tube holder. To each tube 20 μl of the internal standard (1 μg ml^{-1} of 3-[$^2H_5$]indolylacetic acid) followed by 500 μl extraction solvent (methanol:propanol:glacial acetic acid, 20:79:1, v/v/v) were added and auxin extraction was performed in a sonicator bath for 30 min at 4°C. Samples were then centrifuged at 16,000 × *g* for 15 min. The supernatant was transferred to a fresh tube and subsequently dried in a Speedvac centrifuge. Extraction was repeated once, and the supernatant combined with the (dried) supernatant from the first extraction, and subsequently evaporated in a Speedvac centrifuge. Vacuum-dried samples were resuspended with 100% methanol, vortexed for 5 s, and filtered through a Nanosep MF GHP 0.45 μm filter (Pall Life Sciences) by centrifugation at 16,000 × *g* for 1 min. The resuspension step was repeated once. The eluent containing the auxin extracts was transferred to an amber vial and vacuum-dried. Samples were stored at −80°C until analysis. Prior to analysis, samples were taken out from the freezer to equilibrate to room temperature. Each sample was resuspended in 50 μl methanol (Acros Organics):water (60:40, v/v).

Tandem mass spectrometry was performed using an Agilent 6530 Accurate Mass LC–MS Q-TOF (Santa Clara, CA, United States). Samples were subjected to ESI in the Jet Stream interface in both ion positive and negative polarities. Based on optimized LC-ESI-Q-TOF parameters using auxin standards, the auxins IAA, IBA, and IAA-Ala had better sensitivity in the positive mode. The other auxin species were better detected in the negative mode. Optimized conditions in the positive mode were as follows: gas temperature 250°C, drying gas 5 l min^{-1}, nebulizer 30 psig, sheath gas temperature 350°C and flow rate of 11 l min^{-1}, capillary voltage 2500 V, nozzle voltage 500 V, and fragmentor voltage 138 V. Conditions in the negative mode were as follows: gas temperature 300°C, drying gas 9 l min^{-1}, nebulizer 25 psig, sheath gas temperature 350°C and flow rate of 11 l min^{-1}, capillary voltage 3000 V, nozzle voltage 500 V, and fragmentor voltage 140 V. Samples were injected (7 μl) onto an Agilent Zorbax Eclipse 1.8 μm XDB-C18 2.1 × 50 mm column. Solvent A consisted of 0.1% aqueous formic acid and solvent B, 90% methanol/water with 0.1% formic acid. Free auxins and conjugates were eluted with a linear gradient from 10 to 50% solvent B over 8 min, 50–70% solvent B from 8 to 12 min (then held at 70% from 12 to 20 min) at a flow rate of 200 μl min^{-1}. The quadrupole time-of-flight (Q-TOF) was run in targeted MS/MS mode using collision-induced dissociation (CID; N_2 collision gas supplied at 18 psi with *m/z* 1.3 isolation window) where the MS extended dynamic range (2 Hz) was *m/z* 100–1000 with an acquisition rate of 3 spectra s^{-1} and MS/MS at *m/z* 50–1000 at 3 spectra s^{-1}. Data were analyzed using Agilent Technologies MassHunter software (ver. B.5.0).

Histochemistry and Microscopy

Beta-glucuronidase (GUS) staining was performed as described in van Noorden et al. (2007). Sections of 100 mm thickness were made using a Vibratome 1000 (Vibratome Company, St. Louis, MO, United States) and viewed under bright-field optics using a DMLB microscope (Leica Microsystems, Wetzlar, Germany), and images were collected with a mounted CCD camera (RT Slider; Diagnostic Instruments, Sterling Heights, MI, United States).

Auxin Transport Studies

Tritium-labeled indole-3-acetic acid (^{3}H-IAA) solution (7.5 μl of 1 mCi ml^{-1}) (American Radiolabeled Chemicals, St. Louis, MO, United States) was diluted in 20 μl ethanol and mixed with 1.5 ml of melted and cooled 1% agarose at pH 4.8, in a 3 cm diameter Petri dish. The pH was chosen as it is close to the isoelectric point of IAA. Small blocks with dimensions of 2 mm × 2 mm × 2 mm were cut with a scalpel. This standardized the amount of ^{3}H-IAA supplied to plants. Seedlings were pre-treated with rhizobia/ATIs prior to auxin transport study, as described below.

Acropetal auxin transport was performed in relation to the spot-inoculation site. Roots were cut 8 mm from the inoculation spot in the shootward direction (∼12 mm from the root tip). The shoot-containing segment was discarded, and a small ^{3}H-IAA block (2 mm × 2 mm × 2 mm) placed on the cut end of the root-tip containing segment. A Parafilm strip was placed underneath the root segments to prevent diffusion of ^{3}H-IAA from the growth media directly into parts of the root. Samples were incubated vertically for 6 h (*M. truncatula*) or 12 h (*L. japonicus*) in the dark to allow ^{3}H-IAA to diffuse from the agar block through the cut end. The first 4 mm segment touching the ^{3}H-IAA agar block was discarded. The root segments located just below the inoculation site were transferred into individual scintillation vials containing 2 ml scintillation fluid (Perkin-Elmer).

Samples were incubated on an INOVA 2100 Platform Shaker (New Brunswick Scientific) overnight at room temperature. Radioactivity was measured in a scintillation counter (Tri-Carb® Liquid Scintillation Analyzer B2810TR, Perkin-Elmer) over 1 min each. The default settings for tritium decay measurement were used. A vial containing just the scintillation fluid was used as a blank for background subtraction during analysis.

Statistical Analyses

Statistical analyses were carried out with Genstat 15th Edition (VSN International, Hemel Hempstead, United Kingdom) and Prism version 5.02.

AUTHOR CONTRIBUTIONS

JN and UM: conceived, acquired data, analyzed data, and drafted the work.

FUNDING

This project was supported by a grant from the Australian Research Council (DP150102002 to UM).

ACKNOWLEDGMENTS

We thank Prof. Herman Spaink and Prof. Jens Stougaard for kindly providing seeds of the *L. japonicus GH3::GUS*-transformed plants. We also thank Dr. Eva Deinum and Dr. Wouter Kohlen for stimulating discussions during the preparation of this manuscript.

SUPPLEMENTARY MATERIAL

The Supplementary Material for this article can be found online at: https://www.frontiersin.org/articles/10.3389/fpls.2018.00169/full#supplementary-material

REFERENCES

Barnett, M. J., Toman, C. J., Fisher, R. F., and Long, S. R. (2004). A dual-genome symbiosis chip for coordinate study of signal exchange and development in a prokaryote–host interaction. *Proc. Natl. Acad. Sci. U.S.A.* 101, 16636–16641. doi: 10.1073/pnas.0407269101

Benková, E., Michniewicz, M., Sauer, M., Teichmann, T., Seifertová, D., Jürgens, G., et al. (2003). Local, efflux-dependent auxin gradients as a common module for plant organ formation. *Cell* 115, 591–602. doi: 10.1016/s0092-8674(03)00924-3

Bhuvaneswari, T. V., Bhagwat, A. A., and Bauer, W. D. (1981). Transient susceptibility of root cells in four common legumes to nodulation by Rhizobia. *Plant Physiol.* 68, 1144–1149. doi: 10.1104/pp.68.5.1144

Boot, K. J. M., van Brussel, A. A. N., Tak, T., Spaink, H. P., and Kijne, J. W. (1999). Lipochitin oligosaccharides from *Rhizobium leguminosarum* bv. viciae reduce auxin transport capacity in *Vicia sativa* subsp. *nigra* roots. *Mol. Plant Microbe Interact.* 12, 839–844. doi: 10.1094/mpmi.1999.12.10.839

Brechenmacher, L., Lee, J., Sachdev, S., Song, Z., Nguyen, T. H. N., Joshi, T., et al. (2009). Establishment of a protein reference map for soybean root hair cells. *Plant Physiol.* 149, 670–682. doi: 10.1104/pp.108.131649

Broughton, W. J., and Dilworth, M. J. (1971). Control of leghaemoglobin synthesis in snake beans. *Biochem. J.* 125, 1075–1080. doi: 10.1042/bj1251075

Cai, Z., Wang, Y., Zhu, L., Tian, Y., Chen, L., Sun, Z., et al. (2017). GmTIR1/GMAFB3-based auxin perception regulated by miR393 modulates soybean nodulation. *New Phytol.* 215, 672–686. doi: 10.1111/nph.14632

Casimiro, I., Marchant, A., Bhalerao, R. P., Beeckman, T., Dhooge, S., Swarup, R., et al. (2001). Auxin transport promotes Arabidopsis lateral root initiation. *Plant Cell* 13, 843–852. doi: 10.1105/tpc.13.4.843

de Billy, F., Grosjean, C., May, S., Bennett, M., and Cullimore, J. V. (2001). Expression studies on *AUX1*-like genes in *Medicago truncatula* suggest that auxin is required at two steps in early nodule development. *Mol. Plant Microbe Interact.* 14, 267–277. doi: 10.1094/mpmi.2001.14.3.267

Deinum, E. E., Geurts, R., Bisseling, T., and Mulder, B. M. (2012). Modeling a cortical auxin maximum for nodulation: different signatures of potential strategies. *Front. Plant Sci.* 3:96. doi: 10.3389/fpls.2012.00096

Deinum, E. E., Kohlen, W., and Geurts, R. (2016). Quantitative modelling of legume root nodule primordium induction by a diffusive signal of epidermal origin that inhibits auxin efflux. *BMC Plant Biol.* 16:254. doi: 10.1186/s12870-016-0935-9

Fahraeus, G. (1957). The infection of clover root hairs by nodule bacteria studied by a simple glass slide technique. *J. Gen. Microbiol.* 16, 374–381. doi: 10.1099/00221287-16-2-374

Fernández-López, M., Goormachtig, S., Gao, M., D'Haeze, W., van Montagu, M., and Holsters, M. (1998). Ethylene-mediated phenotypic plasticity in root nodule development on *Sesbania rostrata*. *Proc. Natl. Acad. Sci. U.S.A.* 95, 12724–12728. doi: 10.1073/pnas.95.21.12724

Goethals, K., Gao, M., Tomekpe, K., van Montagu, M., and Holsters, M. (1989). Common nodABC genes in Nod locus 1 of *Azorhizobium caulinodans*: nucleotide sequence and plant-inducible expression. *Mol. Gen. Genet.* 219, 289–298. doi: 10.1007/BF00261190

Guan, D., Stacey, N., Liu, C., Wen, J., Mysore, K. S., Torres-Jerez, I., et al. (2013). Rhizobial infection is associated with the development of peripheral vasculature in nodules of *Medicago truncatula*. *Plant Physiol.* 162, 107–115. doi: 10.1104/pp.113.215111

Hirsch, A. M. (1992). Developmental biology of legume nodulation. *New Phytol.* 122, 211–237. doi: 10.1111/j.1469-8137.1992.tb04227.x

Hirsch, A. M., Bhuvaneswari, T. V., Torrey, J. G., and Bisseling, T. (1989). Early nodulin genes are induced in alfalfa root outgrowths elicited by auxin transport inhibitors. *Proc. Natl. Acad. Sci. U.S.A.* 86, 1244–1248. doi: 10.1073/pnas.86.4.1244

Huo, X., Schabel, E., Hughes, K., and Frugoli, J. (2006). RNAi phenotypes and the localization of a protein::GUS fusion imply a role for *Medicago truncatula* PIN genes in nodulation. *J. Plant Growth Regul.* 25, 156–165. doi: 10.1007/s00344-005-0106-y

Kawaguchi, M., Imaizumi-Anraku, H., Fukai, S., and Syono, K. (1996). Unusual branching in the seedlings of *Lotus japonicus*—gibberellins reveal the nitrogen-sensitive cell divisions within the pericycle on roots. *Plant Cell Physiol.* 37, 461–470. doi: 10.1093/oxfordjournals.pcp.a028968

Kohlen, W., Ng, J. L. P., Deinum, E. E., and Mathesius, U. (2017). Auxin transport, metabolism, and signalling during nodule initiation: indeterminate and determinate nodules. *J. Exp. Bot.* 69, 229–244. doi: 10.1093/jxb/erx308

Korasick, D. A., Enders, T. A., and Strader, L. C. (2013). Auxin biosynthesis and storage forms. *J. Exp. Bot.* 64, 2541–2555. doi: 10.1093/jxb/ert080

Kowalczyk, M., and Sandberg, G. (2001). Quantitative analysis of indole-3-Acetic Acid metabolites in Arabidopsis. *Plant Physiol.* 127, 1845–1853. doi: 10.1104/pp.010525

Mao, G., Turner, M., Yu, O., and Subramanian, S. (2013). miR393 and miR164 influence indeterminate but not determinate nodule development. *Plant Signal. Behav.* 8:e26753. doi: 10.4161/psb.26753

Mathesius, U., Schlaman, H. R. M., Spaink, H. P., Sautter, C. O., Rolfe, B. G., and Djordjevic, M. A. (1998). Auxin transport inhibition precedes root nodule formation in white clover roots and is regulated by flavonoids and derivatives of chitin oligosaccharides. *Plant J.* 14, 23–34. doi: 10.1046/j.1365-313X.1998.00090.x

Ng, J. L. P., Hassan, S., Truong, T. T., Hocart, C. H., Laffont, C., Frugier, F., et al. (2015). Flavonoids and auxin transport inhibitors rescue symbiotic nodulation in the *Medicago truncatula* cytokinin perception mutant cre1. *Plant Cell* 27, 2210–2226. doi: 10.1105/tpc.15.00231

Nizampatnam, N. R., Schreier, S. J., Damodaran, S., Adhikari, S., and Subramanian, S. (2015). microRNA160 dictates stage-specific auxin and cytokinin sensitivities and directs soybean nodule development. *Plant J.* 84, 140–153. doi: 10.1111/tpj.12965

Novák, O., Hényková, E., Sairanen, I., Kowalczyk, M., Pospíšil, T., and Ljung, K. (2012). Tissue-specific profiling of the *Arabidopsis thaliana* auxin metabolome. *Plant J.* 72, 523–536. doi: 10.1111/j.1365-313X.2012.05085.x

Overvoorde, P., Fukaki, H., and Beeckman, T. (2010). Auxin control of root development. *Cold Spring Harb. Perspect. Biol.* 2:a001537. doi: 10.1101/cshperspect.a001537

Pacios-Bras, C., Schlaman, H. R. M., Boot, K., Admiraal, P., Langerak, J. M., Stougaard, J., et al. (2003). Auxin distribution in *Lotus japonicus* during root nodule development. *Plant Mol. Biol.* 52, 1169–1180. doi: 10.1023/B:PLAN.0000004308.78057.f5

Plet, J., Wasson, A., Ariel, F., Le Signor, C., Baker, D., Mathesius, U., et al. (2011). MtCRE1-dependent cytokinin signaling integrates bacterial and plant cues to coordinate symbiotic nodule organogenesis in *Medicago truncatula*. *Plant J.* 65, 622–633. doi: 10.1111/j.1365-313X.2010.04447.x

Relić, B., Talmont, F., Kopcinska, J., Golinowski, W., Promé, J., and Broughton, W. J. (1993). Biological activity of *Rhizobium* sp. *NGR*234 Nod-factors on *Macroptilium atropurpureum*. *Mol. Plant Microbe Interact.* 6, 764–774. doi: 10.1094/MPMI-6-764

Rightmyer, A. P., and Long, S. R. (2011). Pseudonodule formation by wild-type and symbiotic mutant *Medicago truncatula* in response to auxin transport inhibitors. *Mol. Plant Microbe Interact.* 24, 1372–1384. doi: 10.1094/mpmi-04-11-0103

Rolfe, B. G., and Gresshoff, P. M. (1988). Genetic analysis of legume nodule initiation. *Annu. Rev. Plant Physiol. Plant Mol. Biol.* 39, 297–319. doi: 10.1146/annurev.pp.39.060188.001501

Roy, S., Robson, F. C., Lilley, J. L. S., Liu, C., Cheng, X., Wen, J., et al. (2017). MtLAX2, a functional homologue of the auxin importer AtAUX1, is required for nodule organogenesis. *Plant Physiol.* 174, 326–338. doi: 10.1104/pp.17.00298

Scanlon, M. J. (2003). The polar auxin transport inhibitor N-1-naphthylphthalamic acid disrupts leaf initiation, Knox protein regulation, and formation of leaf margins in maize. *Plant Physiol.* 133, 597–605. doi: 10.1104/pp.103.026880

Scheres, B., McKhann, H. I., Zalensky, A., Lobler, M., Bisseling, T., and Hirsch, A. M. (1992). The PsENOD12 gene is expressed at two different sites in Afghanistan Pea pseudonodules induced by auxin transport inhibitors. *Plant Physiol.* 100, 1649–1655. doi: 10.1104/pp.100.4.1649

Schnabel, E. L., and Frugoli, J. (2004). The *PIN* and *LAX* families of auxin transport genes in *Medicago truncatula*. *Mol. Genet. Genomics* 272, 420–432. doi: 10.1007/s00438-004-1057-x

Staswick, P. E. (2009). The tryptophan conjugates of jasmonic and indole-3-acetic acids are endogenous auxin inhibitors. *Plant Physiol.* 150, 1310–1321. doi: 10.1104/pp.109.138529

Subramanian, S., Stacey, G., and Yu, O. (2006). Endogenous isoflavones are essential for the establishment of symbiosis between soybean and *Bradyrhizobium japonicum*. *Plant J.* 48, 261–273. doi: 10.1111/j.1365-313X.2006.02874.x

Subramanian, S., Stacey, G., and Yu, O. (2007). Distinct, crucial role of flavonoids during legume nodulation. *Trends Plant Sci.* 12, 282–285. doi: 10.1016/j.tplants.2007.06.006

Suzaki, T., Yano, K., Ito, M., Umehara, Y., Suganuma, N., and Kawaguchi, M. (2012). Positive and negative regulation of cortical cell division during root nodule development in *Lotus japonicus* is accompanied by auxin response. *Development* 139, 3997–4006. doi: 10.1242/dev.084079

Takanashi, K., Sugiyama, A., Sato, S., Tabata, S., and Yazaki, K. (2012). LjABCB1, an ATP-binding cassette protein specifically induced in uninfected cells of *Lotus japonicus* nodules. *J. Plant Physiol.* 169, 322–326. doi: 10.1016/j.jplph.2011.11.008

Takanashi, K., Sugiyama, A., and Yazaki, K. (2011). Involvement of auxin distribution in root nodule development of *Lotus japonicus*. *Planta* 234, 73–81. doi: 10.1007/s00425-011-1385-0

Turner, M., Nizampatnam, N. R., Baron, M., Coppin, S., Damodaran, S., Adhikari, S., et al. (2013). Ectopic expression of miR160 results in auxin hypersensitivity, cytokinin hyposensitivity, and inhibition of symbiotic nodule development in soybean. *Plant Physiol.* 162, 2042–2055. doi: 10.1104/pp.113.220699

van Noorden, G. E., Kerim, T., Goffard, N., Wiblin, R., Pellerone, F. I., Rolfe, B. G., et al. (2007). Overlap of proteome changes in *Medicago truncatula* in response to auxin and *Sinorhizobium meliloti*. *Plant Physiol.* 144, 1115–1131. doi: 10.1104/pp.107.099978

van Noorden, G. E., Ross, J. J., Reid, J. B., Rolfe, B. G., and Mathesius, U. (2006). Defective long-distance auxin transport regulation in the *Medicago truncatula* super numeric nodules mutant. *Plant Physiol.* 140, 1494–1506. doi: 10.1104/pp.105.075879

Wang, Y., Li, K., Chen, L., Zuo, Y., Liu, H., Tian, Y., et al. (2015). MicroRNA167-directed regulation of the auxin response factors GmARF8a and GmARF8b is required for soybean nodulation and lateral root development. *Plant Physiol.* 168, 984–999. doi: 10.1104/pp.15.00265

Wasson, A. P., Pellerone, F. I., and Mathesius, U. (2006). Silencing the flavonoid pathway in *Medicago truncatula* inhibits root nodule formation and prevents auxin transport regulation by Rhizobia. *Plant Cell* 18, 1617–1629. doi: 10.1105/tpc.105.038232

Wu, C., Dickstein, R., Cary, A. J., and Norris, J. H. (1996). The auxin transport inhibitor N-(1-Naphthyl)phthalamic acid elicits pseudonodules on nonnodulating mutants of white sweetclover. *Plant Physiol.* 110, 501–510. doi: 10.1104/pp.110.2.501

Wu, X., and McSteen, P. (2007). The role of auxin transport during inflorescence development in maize (*Zea mays, Poaceae*). *Am. J. Bot.* 94, 1745–1755. doi: 10.3732/ajb.94.11.1745

Conflict of Interest Statement: The authors declare that the research was conducted in the absence of any commercial or financial relationships that could be construed as a potential conflict of interest.

frontiers in Plant Science

METHODS
published: 27 February 2018
doi: 10.3389/fpls.2018.00245

Dual Color Sensors for Simultaneous Analysis of Calcium Signal Dynamics in the Nuclear and Cytoplasmic Compartments of Plant Cells

Audrey Kelner[1†], Nuno Leitão[2†], Mireille Chabaud[1], Myriam Charpentier[2] and Fernanda de Carvalho-Niebel[1*]*

[1] Laboratory of Plant Microbe Interactions, Université de Toulouse, Institut National de la Recherche Agronomique, Centre National de la Recherche Scientifique, Castanet-Tolosan, France, [2] Department of Cell and Developmental Biology, John Innes Centre, Norwich, United Kingdom

OPEN ACCESS

Edited by:
Pascal Ratet,
Centre National de la Recherche Scientifique (CNRS), France

Reviewed by:
Jiahui Wu,
Weill Cornell Medical College, Cornell University, United States
Frantisek Baluska,
University of Bonn, Germany

***Correspondence:**
Myriam Charpentier
myriam.charpentier@jic.ac.uk
Fernanda de Carvalho-Niebel
fernanda.de-carvalho-niebel@inra.fr

[†] These authors have contributed equally to this work.

Specialty section:
This article was submitted to Plant Cell Biology, a section of the journal Frontiers in Plant Science

Received: 17 December 2017
Accepted: 12 February 2018
Published: 27 February 2018

Citation:
Kelner A, Leitão N, Chabaud M, Charpentier M and de Carvalho-Niebel F (2018) Dual Color Sensors for Simultaneous Analysis of Calcium Signal Dynamics in the Nuclear and Cytoplasmic Compartments of Plant Cells. Front. Plant Sci. 9:245. doi: 10.3389/fpls.2018.00245

Spatiotemporal changes in cellular calcium (Ca^{2+}) concentrations are essential for signal transduction in a wide range of plant cellular processes. In legumes, nuclear and perinuclear-localized Ca^{2+} oscillations have emerged as key signatures preceding downstream symbiotic signaling responses. Förster resonance energy transfer (FRET) yellow-based Ca^{2+} cameleon probes have been successfully exploited to measure the spatiotemporal dynamics of symbiotic Ca^{2+} signaling in legumes. Although providing cellular resolution, these sensors were restricted to measuring Ca^{2+} changes in single subcellular compartments. In this study, we have explored the potential of single fluorescent protein-based Ca^{2+} sensors, the GECOs, for multicolor and simultaneous imaging of the spatiotemporal dynamics of cytoplasmic and nuclear Ca^{2+} signaling in root cells. Single and dual fluorescence nuclear and cytoplasmic-localized GECOs expressed in transgenic *Medicago truncatula* roots and *Arabidopsis thaliana* were used to successfully monitor Ca^{2+} responses to microbial biotic and abiotic elicitors. In *M. truncatula*, we demonstrate that GECOs detect symbiosis-related Ca^{2+} spiking variations with higher sensitivity than the yellow FRET-based sensors previously used. Additionally, in both *M. truncatula* and *A. thaliana,* the dual sensor is now able to resolve in a single root cell the coordinated spatiotemporal dynamics of nuclear and cytoplasmic Ca^{2+} signaling *in vivo.* The GECO-based sensors presented here therefore represent powerful tools to monitor Ca^{2+} signaling dynamics in *vivo* in response to different stimuli in multi-subcellular compartments of plant cells.

Keywords: *Medicago truncatula*, *Arabidopsis thaliana*, root symbiosis, root hairs, root elongation zone, calcium, GECO sensors, biotic and abiotic stimuli

INTRODUCTION

Divalent calcium (Ca^{2+}) ions are versatile second messengers regulating many biological processes in eukaryotic and prokaryotic cells (Dodd et al., 2010; Domínguez et al., 2015). In plants, Ca^{2+} mediates developmental and physiological responses to various biotic and abiotic environmental cues (McAinsh and Pittman, 2009; Dodd et al., 2010; Kudla et al., 2010; Stael et al., 2012).

Stimuli-induced Ca^{2+} releases result in transient or repetitive oscillations, distinct in their frequency, amplitude, duration, and spatial distribution. The sensing and decoding of these so-called Ca^{2+} signatures (McAinsh and Pittman, 2009) by Ca^{2+}-binding proteins assure the transduction of the signal to downstream transcriptional and metabolic responses (Galon et al., 2010; Reddy et al., 2011; Whalley and Knight, 2013).

The analysis of Ca^{2+} signatures and their contribution to signaling in different cellular compartments requires tools adapted for monitoring Ca^{2+} dynamics with high spatial and temporal resolution. Bioluminescent aequorin-based probes can successfully quantify variations in Ca^{2+} signaling in plants, but their low light emission limits the spatiotemporal resolution of these responses during imaging (Knight et al., 1991; McCombs and Palmer, 2008). Cellular resolution can be achieved by the use of fluorescent dyes and genetically-encoded Ca^{2+} indicators (GECIs), consisting of fluorescent proteins (FPs) fused to sensor domains. Compared to fluorescent dyes, GECIs have the advantage of being accessible to any cell type and offer the possibility of measuring Ca^{2+} variations in subcellular compartments, by specific targeting of the sensor. The most popular GECI sensors are the ratiometric Förster Resonance Energy Transfer (FRET)-based Yellow Cameleons (YCs) composed of a fluorescent donor-acceptor pair, respectively, CFP and YFP, linked by a calmodulin (CaM) and the CaM-binding peptide of myosin light-chain kinase M13 (Miyawaki et al., 1997; Allen et al., 1999). Upon Ca^{2+} binding to CaM, CaM and M13 interact which triggers protein conformational changes that result in increased FRET between the donor-acceptor pair. More recently, improved FRET-based pairs or hybrid sensors such as BRET (bioluminescent aequorin coupled with a FP) have been engineered and successfully used in plants (Rodriguez-Garcia et al., 2014; Xiong et al., 2014; Bajar et al., 2016).

Targeting FRET-based probes to different subcellular compartments revealed precise Ca^{2+} variations in different organelles, including the nucleus, the endoplasmic reticulum, the chloroplast, peroxisomes, and mitochondria (Iwano et al., 2009; Sieberer et al., 2009; Costa et al., 2010; Krebs et al., 2012; Loro et al., 2012, 2016; Stael et al., 2012; Bonza et al., 2013). The Ca^{2+} dynamics in specific compartments are likely to reflect the differential activation of Ca^{2+} channels and the contribution of diverse intra and extracellular Ca^{2+} stores in the control of specific functions, such as gene transcription (Ranty et al., 2012). A number of stimuli activates Ca^{2+} responses simultaneously in different subcellular compartments (van Der Luit et al., 1999; Wood et al., 2001). As such, in legumes, the perception of diffusible nodulation (Nod) and mycorrhizal (Myc) factors released by nitrogen-fixing bacteria and arbuscular mycorrhiza (AM), fungi respectively, induces calcium oscillations in the nucleus and adjacent cytoplasm (Ehrhardt et al., 1996; Miwa et al., 2006a; Sieberer et al., 2009). Symbiotic calcium spiking was monitored using fluorescent dyes, cytoplasmic FRET-based YC probes (Ehrhardt et al., 1996; Catoira et al., 2000; Wais et al., 2000; Shaw and Long, 2003; Miwa et al., 2006a,b; Kosuta et al., 2008) or nuclear-tagged YFP-FRET probes (Sieberer et al., 2009, 2012; Chabaud et al., 2011; Genre et al., 2013; Sun et al., 2015). Although monitored independently, cytoplasmic and nuclear Ca^{2+} responses were hypothesized to be synchronized based on their relative time period. Nod factors (NF), consisting of lipo-chitooligosaccharides, and AM fungi chitin oligomers (COs), both induce Ca^{2+} spiking, essential for the transduction of downstream symbiotic signaling in the nucleus (Zipfel and Oldroyd, 2017). More recently, major components involved in the generation of Ca^{2+} spiking were identified in legumes. In the model legume *Medicago truncatula,* the potassium channel DMI1 (Ané et al., 2004), the Ca^{2+}-ATPase MCA8 (Capoen et al., 2011), and CNGC15 Ca^{2+} channels (Charpentier et al., 2016), are required for the generation of symbiotic Ca^{2+} oscillations (Granqvist et al., 2012; Charpentier and Oldroyd, 2013; Charpentier et al., 2016). Interestingly, they all locate to both the outer nuclear membrane (ONM) and the inner nuclear membrane (INM) (Capoen et al., 2011; Charpentier et al., 2016). This observation raises the issue of the direction of the observed Ca^{2+} release. Ca^{2+} could be simultaneously released across the INM and the ONM or, sequentially, through the INM or the ONM to the nucleoplasm and cytoplasm, respectively. Thus, simultaneous investigation of nuclear and cytoplasmic Ca^{2+} dynamics is required to gain information on the origin of the specific symbiotic factor-induced nuclear Ca^{2+} signals, and clarify the spatial activation of the ion channels.

Recent studies in animal cells revealed that highly sensitive Ca^{2+} GECI sensors can discriminate stimulus-dependent directional propagation of Ca^{2+} signals (Nakao et al., 2015). These improved GECIs, called GECOs (for GECIs for optical imaging) are circularly permuted single fluorescent intensiometric Ca^{2+}-sensing proteins with a CaM and a M13 peptide domains. Upon Ca^{2+} binding, changes in protein conformation result in a visible increase in its fluorescence intensity (Zhao et al., 2011). GECOs have to date only been targeted to the cytoplasm to study Ca^{2+} signaling in plant cells (Ngo et al., 2014; Keinath et al., 2015; Wang et al., 2015; Tunc-Ozdemir and Jones, 2017; Waadt et al., 2017). However, the available palette of GECO fluorescent protein colors now opens the possibility of concomitantly imaging Ca^{2+}-signaling in different compartments of plant cells (Zhao et al., 2011). Moreover, improved GECO versions were generated through directed evolution and screened for higher intensity signal change upon Ca^{2+} binding, but not yet used in plants (Zhao et al., 2011; Wu et al., 2013).

In this study, we generated dual Ca^{2+} sensors that simultaneously monitor the Ca^{2+} dynamics in the nucleus and cytoplasm, by targeting highly sensitive GECO Ca^{2+} sensors to these subcellular compartments. We demonstrated that the new dual GECO sensors are powerful tools to concomitantly monitor *in vivo* Ca^{2+} dynamics in adjacent nuclear and cytoplasmic compartments of both *M. truncatula* and Arabidopsis roots in response to both biotic and abiotic signals. We unraveled that the symbiotic Nod factor-induced nuclear calcium oscillations preferentially start in the nucleus. Additionally the dual GECO sensor revealed that biotic and abiotic stimuli trigger distinct cytoplasmic and nuclear Ca^{2+} dynamics in *A. thaliana* root cells.

RESULTS

The Highly Sensitive GECO Sensor Enables Real-Time Visualization of Nuclear Ca^{2+} Spiking in *M. truncatula*

In order to evaluate the performance of GECO as a Ca^{2+} sensor for the symbiotic factor-induced nuclear Ca^{2+} oscillations in *M. truncatula*, we designed a compatible binary vector to constitutively express the red fluorescence R-GECO1 (Zhao et al., 2011) in the nucleus of plant cells (Figure S1). This construct, referred to as NR-GECO1, comprises a viral SV40 nuclear localization signal (NLS) fused to the R-GECO1 and driven by the double *CAMV 35S* promoter (*2xp35S*) (Figure S1), and was used together with the previously characterized yellow fluorescence cameleon sensors NUP-YC2.1 (Sieberer et al., 2009) and NLS-YC3.6 (Krebs et al., 2012) to generate *M. truncatula* composite plants via *Agrobacterium rhizogenes*-mediated transformation. Confocal laser scanning microscopy (CLSM) revealed that both the NR-GECO1 and the two cameleon sensors were targeted to the nuclear compartment of *M. truncatula* root cells (Figure S2). NR-GECO1 fluorescence was undetectable in the cytoplasm, and appeared homogeneously distributed within the nucleus (Figure S2A).

Symbiosis-related nuclear Ca^{2+} responses were assessed in the nucleus of growing root hair cells using CLSM (Figure S3). The basal fluorescence signal intensity was recorded for 5–10 min for each sensor before treatment of roots with purified *Sinorhizobium meliloti* NFs (10^{-9} M) (**Figures 1A,C,E**). Following NF application, sustained Ca^{2+} spikes were observed within the nucleus of cells transformed with the three sensors (**Figures 1B,D,F**). They all generated comparable patterns of NF-induced Ca^{2+} spiking, with spike periodicity of about 100–120 s (**Figure 1G**).

To evaluate whether NR-GECO1 was suitable for detecting other Ca^{2+} responses in *M. truncatula*, we challenged *M. truncatula* composite plants and root organ cultures (ROCs) with tetra-chitooligosaccharides (CO4) previously shown to elicit nuclear Ca^{2+} oscillations (Genre et al., 2013; Sun et al., 2015). Similarly to NFs, NR-GECO1 allowed the detection of CO4-induced nuclear Ca^{2+} spiking in both composite plants and ROCs (Figure S4). As previously observed with a cameleon probe (Genre et al., 2013), the NF receptor *nfp* mutant no longer exhibited NF-elicited Ca^{2+} spiking but still displayed CO4-induced Ca^{2+} spiking responses (Figures S4E–G). Taken together, NR-GECO1 can efficiently measure symbiosis-related nuclear Ca^{2+} spiking responses in *M. truncatula* roots.

To investigate sensor performance, we compared the maximum signal change to the basal fluorescence signal (before the spike), by calculating the signal-to-noise ratio (SNR) values for each individual probe. The fractional fluorescence changes (ΔF/F) for NR-GECO1 and the fractional ratio changes (ΔR/R) for the cameleon sensors were measured as described (Figure S3B and Material and Methods), from a high number of individual root hairs. FRET-based probes exhibited rather similar dynamic changes, although NLS-YC3.6 appeared to be

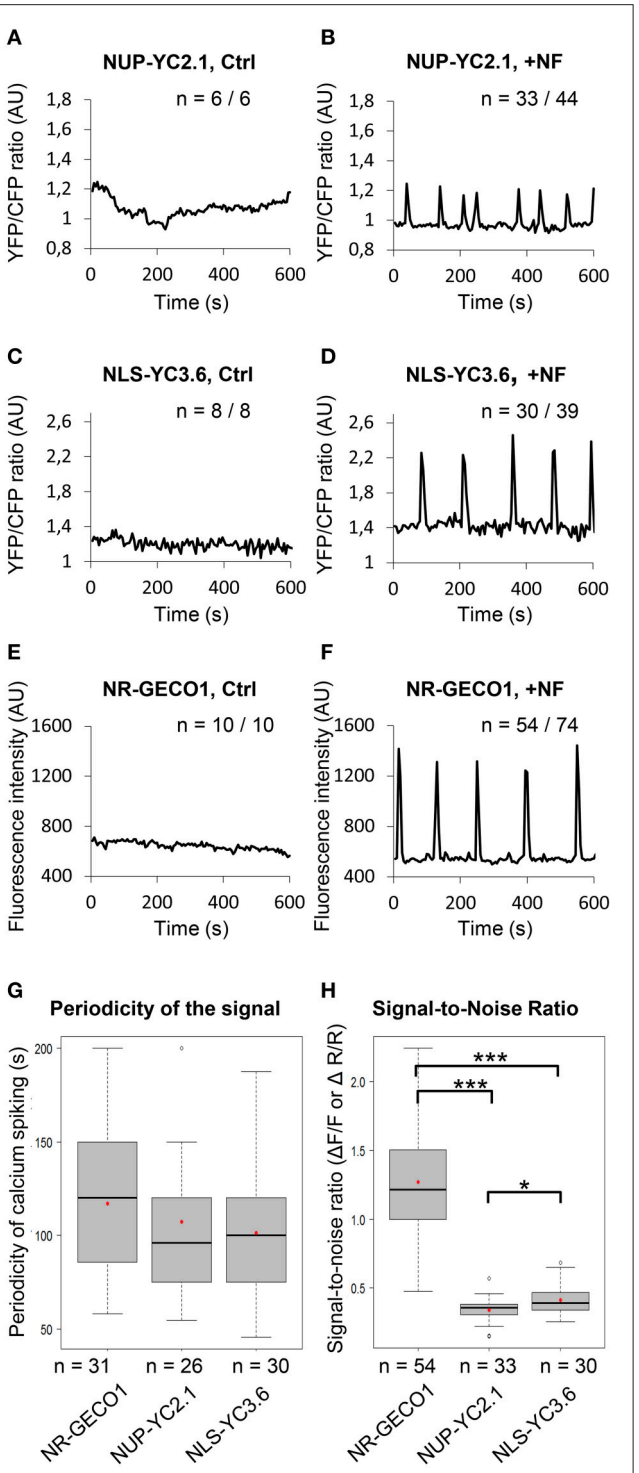

FIGURE 1 | NR-GECO1 displays higher Ca^{2+} signal-to-noise ratio than previously used cameleon sensors. **(A–F)** Representative profiles obtained with the FRET probes NUP-YC2.1 **(A,B)**, NLS-YC3.6 **(C,D),** and the single NR-GECO1 sensor **(E,F)** before (Ctrl) and after Nod Factor (+NF) addition. *n* represents the number of individual root hair cells analyzed from 2 to 3 independent experiments (AU, Arbitrary Units). Note that the y-axis scales are different for each sensor. **(G,H)** Calcium spiking periodicity **(G)** and

(Continued)

FIGURE 1 | signal-to-noise ratio **(H)** was calculated for each individual sensor. *in vivo* Signal-to-noise ratio (SNR) in **(H)** represents signal amplitude changes during calcium spiking and was calculated using fluorescence intensity values (ΔF/F) for NR-GECO1 and YFP/CFP ratio (ΔR/R) values for the cameleon sensors. Box plots represent first and third quartile (horizontal box sides), minimum and maximum (outside whiskers), median (central lines), and mean (solid red circle) values. A one-way ANOVA followed by a Tukey honest significant (HSD) test of the values after a Box-Cox transformation ($\lambda = 0.0606$) did not reveal statistical differences between the three groups ($p > 0.05$) in **(G)**. A Kruskal-Wallis test revealed statistical difference between the groups in **(H)** (*$p < 0.05$ and ***$p < 0.001$).

slightly superior to NUP-YC2.1 with mean SNR values of 0.41 and 0.34, respectively (**Figure 1H**). However, there was a striking difference in the dynamic responses observed between the nuclear NR-GECO1 and the cameleon sensors with a mean SNR value of 1.27 (**Figure 1H**). Thus, NR-GECO1 allows monitoring of NF-induced nuclear Ca^{2+} spiking with a greater sensitivity than the cameleon sensors. Our results confirm the previously described higher sensitivity of the cytoplasmic R-GECO1 in comparison to the YC3.6, in response to the ATP-induced Ca^{2+} signals in *A. thaliana* roots (Keinath et al., 2015). Additionally, using CLSM, NR-GECO1 allowed real time visualization of the Ca^{2+} changes in contrast to the cameleon probe for which the YFP/CFP fluorescent ratio have to be calculated from a pre-selected region of interest (ROI) (Figure S5 and Movies S1, S2). Thus, in comparison to cameleon sensors, NR-GECO1 has a higher dynamic range, which greatly facilitates the rapid monitoring of cell-autonomous dynamics of Ca^{2+} spiking in various *M. truncatula* root hair and non-hair cells.

A Dual GECO Sensor for Simultaneously Monitoring Ca^{2+} Signals in Both Nuclear and Cytoplasmic Compartments of *M. truncatula* Root Cells

Taking advantage of the high sensitivity of GECOs, we generated a dual fluorescence color sensor for imaging Ca^{2+} signal dynamics simultaneously in the cytoplasm and the nuclear compartments of the same root hair cell. We therefore combined the nuclear-tagged red GECO1 and the cytoplasmic green GECO1 in a single construct (Figure S1). In this dual sensor, both the nuclear red and cytoplasmic green GECOs (NRCG-GECO1) are driven by *2xp35S* promoters. CLSM imaging revealed the dual labeling of nuclear and cytoplasmic compartments of *M. truncatula* epidermal cells (**Figure 2A**). In a non-spiking state (**Figure 2A**), the red and green fluorescence proteins are found, respectively, in the nuclear and cytoplasmic regions demonstrating the correct targeting of the GECO to the expected subcellular compartments. However, during a Ca^{2+} spike a merged orange-to-yellow fluorescence signal is observed in the nuclear region, due to the acquisition of increased nuclear R-GECO1 and perinuclear green G-GECO1 fluorescence signals (**Figure 2B**).

Imaging conditions were set up to avoid crossover between fluorescence emissions of the two probes. The excitation of G-GECO1 and R-GECO1 is achieved using an argon 488 nm

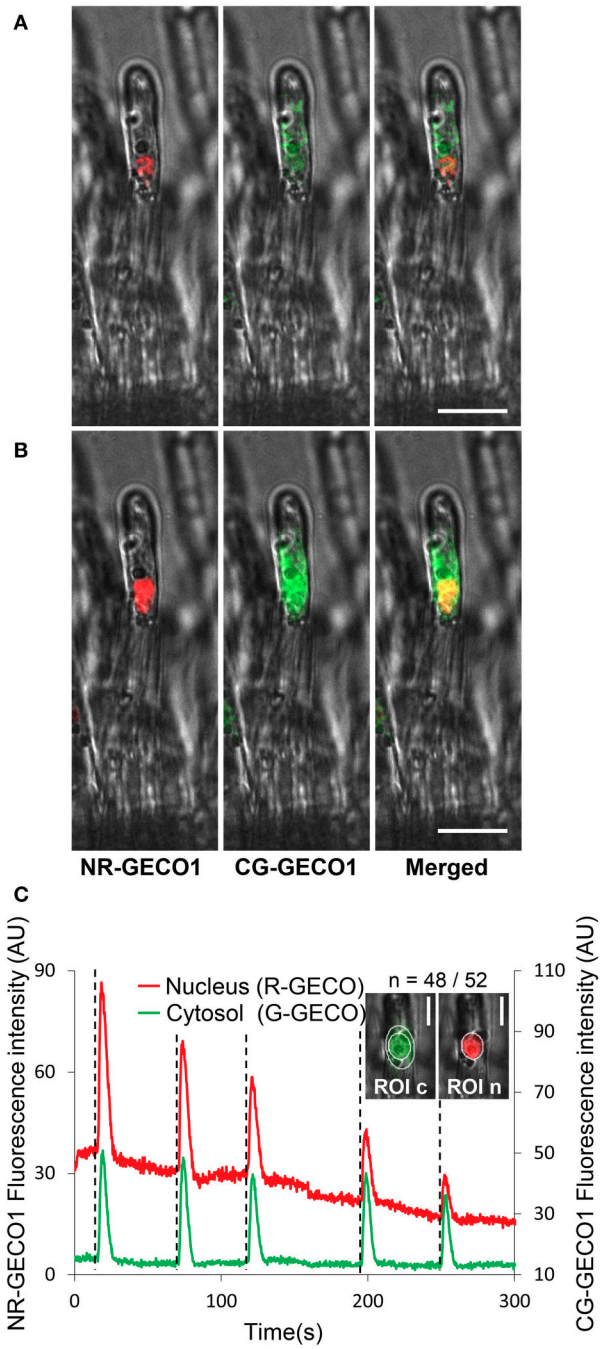

FIGURE 2 | A dual GECO Ca^{2+} sensor targeted to both nuclear and cytoplasmic subcellular compartments reveals coordinated oscillatory Ca^{2+} responses. **(A,B)** Subcellular localization of the dual NRCG-GECO1 sensor in *M. truncatula* root hair cells. Confocal fluorescent images of NRCG-GECO1 sensor before **(A)** and during a spike **(B)** are represented as separated red, green, and merged images with respective bright fields. **(C)** Relative fluorescence intensity traces of NR-GECO1 (red) and CG-GECO1 (green) at 0.25 s intervals from ROIs selected around the nuclear (ROI n) and peri-nuclear cytoplasmic (ROI c) regions of a *M. truncatula* root hair treated with a 10^{-9} M Nod Factor (+NF) solution. Dotted lines mark the initiation of a spike, *n* corresponds to the number of root hairs responding positively/total number of analyzed root hairs. Data were collected from two biological experiments. Scale bars represent 20 μm **(A,B)** and 10 μm **(C)**.

laser and a 561 nm diode, respectively, and emission is detected in the respective fluorescence window ranges of 500–550 and 580–643 nm (Zhao et al., 2011). By using the optimum excitation parameters for G-GECO1 (488 nm excitation, Figure S6A), the green cytoplasmic fluorescence was clearly observed in the expected 500–550 nm emission window in NF-treated *M. truncatula* root hairs. However, a slight bleed-through of the G-GECO1 was observed in the R-GECO1 emission window of 580–643 nm protein. To avoid this, we therefore reduced the fluorescence window emission range for R-GECO1 from 580–643 to 600–643 nm. Importantly, no bleed-through of the R-GECO1 was observed in the G-GECO1 500–550 nm emission window. Thus, the dual NRCG-GECO1 sensor expressed in transformed roots of *M. truncatula* composite plants was able to monitor concomitant nuclear and cytoplasmic Ca^{2+} spiking in an individual NF-treated root hair (**Figure 2C**). Similar coordinated Ca^{2+} responses in the two subcellular compartments were monitored in *M. truncatula* transgenic roots treated with CO4 (Figure S7A). To ensure the specificity of these responses, we used the dual NRCG-GECO1 sensor in the *dmi1* and *dmi3* mutants (Catoira et al., 2000; Arrighi et al., 2006). As expected, coordinated NF-elicited Ca^{2+} spiking was only observed in the *dmi3* mutant (Figure S7). Taken together, the dual NRCG-GECO1 Ca^{2+} sensor targets GECO fluorescent proteins to two subcellular compartments and is suitable for co-imaging of specific Ca^{2+} responses in real time in two distinct subcellular compartments without fluorescence bleed-through.

Ca^{2+} Spiking Preferentially Initiates in the Nucleus of Medicago Root Hairs Responding to Symbiotic Nod Factors

The dual sensor made it possible to simultaneously visualize highly coordinated Ca^{2+} signals in both nuclear and cytoplasmic compartments and therefore resolve the initiation dynamics of the symbiotic factor-induced nuclear Ca^{2+} spiking. To increase temporal resolution, we reduced the image acquisition intervals to below 0.5 s. A qualitative frame-by-frame analysis illustrated the rise in both red and green fluorescence of respective GECOs during a single spike (**Figure 3A**). The selection of regions of interest (ROI) in the nucleoplasm and in different cytoplasmic-associated areas allowed us to precisely follow the progressive rise in fluorescence intensity of the sensors over time (**Figures 3B,C**). In both compartments, the start of a Ca^{2+} spike was recognized by a steep increase in fluorescence intensity to baseline fluorescence levels (**Figures 3B–D**). These analyzes revealed a strong Ca^{2+} rise in the nucleus and in the nuclear periphery, followed by sequential signal propagation toward the root hair tip (**Figures 3B,C**). To further evaluate the dynamics of Ca^{2+} spiking initiation in the perinuclear region, we simultaneously recorded fluorescence data from nuclear NR-GECO1 and cytoplasmic CG-GECO1 from delimited ROI zones (**Figure 3B**) of individual NF-treated root hairs. The precise time for peak initiation (t1) for both GECO probes was compared by calculating the Δ_{t1} value ($CG\text{-}GECO1_{t1}$-$NR\text{-}GECO1_{t1}$) for a large number of individual root hairs (**Figure 4A**). These analyses revealed that the majority of Ca^{2+} spiking (65%) initiated primarily and significantly in the nuclear compartment, while only 2% initiated first in the cytosol. In 30% of the cases, it was not possible to clearly distinguish differences between the Ca^{2+} spiking initiation sites.

To exclude intrinsic differences between the sensors in the targeted compartments we generated a reverse dual sensor expressing R-GECO1 in the cytoplasm and the G-GECO1 in the nucleus (Figures S1, S8). Using the dual NGCR-GECO1 sensor we confirmed the preferential initiation of Ca^{2+} spiking in the nuclear compartment (**Figure 4A**). The time interval (Δ_{t1}) for the initiation of a spike between the nuclear and cytoplasmic compartments was similar for both dual sensors (**Figure 4B**), with median values of 250 ms. Taken together, the dual GECO1 Ca^{2+} sensors generated here allowed us to measure coordinated Ca^{2+} responses in different subcellular compartments of individual cells (Movies S3, S4) and to demonstrate that Ca^{2+} spiking primarily initiates in the nuclear compartment of root hair cells responding to rhizobial Nod factors.

Ca^{2+} Signal Dynamics in Both Nuclear and Cytoplasmic Compartments in *A. thaliana* Root Elongation Zone Cells

To investigate the use of the dual sensor in plant species other than *M. truncatula*, we stably transformed *A. thaliana* with the NRCG-GECO1.2 sensor (Figure S1) comprising improved versions of R-GECO1 and G-GECO1 (Zhao et al., 2011; Wu et al., 2013). Stable transgenic lines were propagated until the T3 generation under hygromycin selection and selected for expression of the dual sensor. CLSM imaging of *A. thaliana* roots demonstrated that CG-GECO1.2 and NR-GECO1.2 localized to the cytoplasmic and nucleoplasmic compartments, respectively (Figure S9). The stable transgenic line is phenotypically like wild type plants, indicating that the constitutive expression of the sensor does not interfere with cellular Ca^{2+} signaling and homeostasis (Figure S9). In *A. thaliana* roots transformed with aequorin or cameleon YC3.6, several studies have reported that biotic and abiotic stimuli induce Ca^{2+} release. As such, chitin, NaCl, ATP, and cold stress have been shown to induce Ca^{2+} release in the root elongation zone (Kiegle et al., 2000; Tanaka et al., 2010; Keinath et al., 2015). However, the subcellular dynamics of these stimuli-induced Ca^{2+} releases is lacking.

To monitor the dynamics of cytoplasmic vs. nucleoplasmic Ca^{2+} release in response to chitooctaose (CO8), NaCl, ATP and cold stress, we focused our study on the root epidermal cells of the elongation zone. Treating 5 day-old roots with CO8 to a final concentration of 10^{-7} M elicited an increase in cytoplasmic Ca^{2+} within 2 min of application in 73% of the plants tested (8/11 plants) (**Figures 5A–C**). Ca^{2+} release was detected only in the cytoplasmic region without any propagation to the nucleoplasm. The Ca^{2+} signature was characterized by a sharp increase followed by progressive smaller oscillations returning to baseline levels over a period of 15 min (**Figure 5B**). The Ca^{2+} signal was not detected after treatment with the buffer control (**Figures 5D–F**). Similarly, ATP to a final concentration of 100 μM induced a specific cytoplasmic Ca^{2+} release 7 min after application (Figure S10).

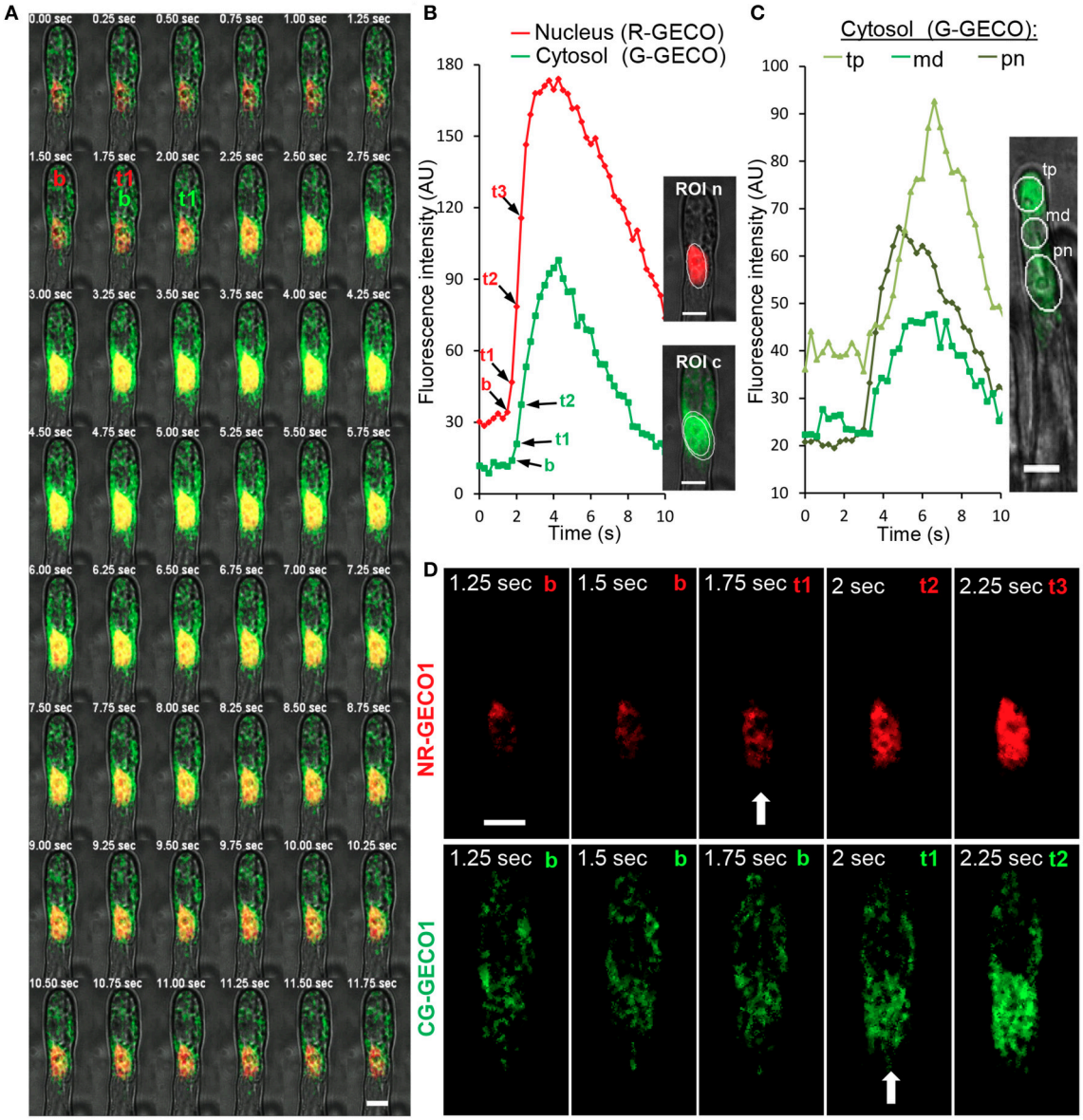

FIGURE 3 | Spatiotemporal dynamics of Ca^{2+} spiking in nuclear and cytoplasmic compartments of a *M. truncatula* root hair responding to NFs. **(A)** A sequential frame-by-frame co-imaging (0.25 s intervals) of nuclear-targeted NR-GECO1 and cytosolic CG-GECO1 revealed coordinated responses during a single Ca^{2+} spike. **(B)** Relative fluorescence intensity traces of NR-GECO1 (red) and CG-GECO1 (green) from ROIs selected around the nuclear (ROI n) and perinuclear cytoplasmic (ROI c) regions. Images on the right represent the maximum projection of respective fluorescence images merged with bright field. **(C)** Relative fluorescence intensity (0.3 s intervals) of CG-GECO1 in selected cytoplasmic regions of interest in the perinuclear (pn), middle (md), or root hair tip (tp) regions during a NF-triggered Ca^{2+} spike. **(D)** Close view of selected fluorescence frames shown in **(A)**. Time points representing baseline fluorescence [b in **(A,B,D)**], the start of the spike [t1 and arrow **(A,B,D)**], and subsequent spike rise time points [t2 and t3 in **(A,B,D)**] are indicated for NR-GECO1 and CG-GECO1. Scale bars represent 10 μm.

The ATP-induced Ca^{2+} signature was similar to the CO8-induced Ca^{2+} release with a sharp peak followed by smaller oscillations, although their frequencies differed (0.6 min^{-1} for CO8 and 1.94 min^{-1} in the case of ATP) (Figure S10). In contrast to CO8 and ATP, which induced a specific cytoplasmic Ca^{2+} response with an oscillatory pattern, NaCl and cold induced Ca^{2+} release in both the cytoplasmic and nucleoplasmic compartments (**Figures 6**, **7**, Movies S5, S6). Each of these stimuli induced a transient Ca^{2+} release first in the cytoplasm followed by a transient Ca^{2+} increase in the nucleoplasm (**Figures 6**, **7**). However, the dynamics of each nucleoplasmic Ca^{2+} increase differ in their amplitudes and timing of activation. Cold shock induced a transient nucleoplasmic Ca^{2+} release 20 to 30 s after the cytoplasmic Ca^{2+} response (**Figure 7**). In contrast, NaCl treatment induced a Ca^{2+} response in the nucleus 2–3 s after cytoplasmic Ca^{2+} release (**Figure 6**).

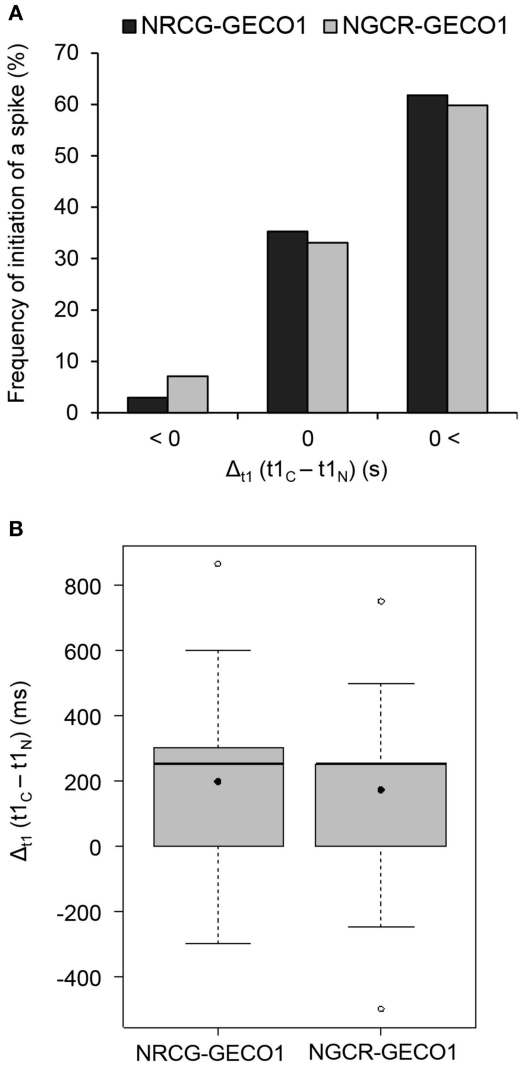

FIGURE 4 | Monitoring NF-elicited Ca^{2+} signaling with dual GECO sensors reveals a preferential Ca^{2+} spike start in the nuclear compartment. Time values corresponding to the start of individual spikes (t1, illustrated in **Figure 3B**) were collected for each sensor and used to calculate the relative delay in the start of a spike. The time interval (Δ_{t1} in s), between peak start measured by sensors, was calculated by subtracting nuclear t1 from cytoplasmic t1-values ($t1_C$-$t1_N$). A Δ_{t1} value below 0 indicates a cytoplasmic-to-nucleus spike start (C→N), a Δ_{t1}-value close to 0 indicates coordinated cytoplasmic and nuclear spike start (C=N), and a positive Δ_{t1}-value indicates a nucleus-to-cytoplasmic spike start (C←N). These analyses were done with $n = 68$ (NRCG-GECO1) and $n = 127$ (NGCR-GECO1) individual spikes from 26 or 24 individual nuclei, respectively. **(A)** Frequency of the individual spikes showing C→N, C=N, and C←N patterns in the dual NRCG-GECO1 (dark gray) and NGCR-GECO1 (light gray) sensors. No significant differences were found between the sensors ($p > 0.05$, chi-square test of goodness-of-fit). Frequency distribution within the different categories (C→N, C=N, and C←N), for each dual sensor, is significantly different and not due to a random distribution (1/3 of observations in each category, $p < 0.001$, chi-square test of goodness-of-fit). **(B)** Time interval between spike start (Δ_{t1} in ms) measured for each dual sensor. Average/median values for NRCG-GECO1 and NGCR-GECO1 of 197/250 and 174/250 ms, respectively, are not significantly different. Box plots represent first and third quartile (horizontal box sides), minimum and maximum (outside whiskers), median (central lines), and mean (solid black circle).

Additionally, the amplitude of NaCl-induced nucleoplasmic Ca^{2+} release is higher than the cytoplasmic Ca^{2+} release, which contrasts with the cold-induced nucleoplasmic Ca^{2+} signal, which is lower than the cytoplasmic Ca^{2+} signal. The differences in timing of activation and amplitude of the Ca^{2+} signals between both compartments strongly suggest that cold and NaCl induce distinct cytoplasmic and nucleoplasmic Ca^{2+} signals. The nucleoplasmic response might be a consequence of the cytoplasmic Ca^{2+} release, or induced independently. All together our results demonstrate that the dual sensor can effectively monitor Ca^{2+} dynamics simultaneously in the cytoplasm and nuclear regions in *A. thaliana* roots cells, and identify various Ca^{2+} signatures generated in response to biotic and abiotic stimuli.

DISCUSSION

Recent years have witnessed powerful advances in genetically-encoded fluorescent Ca^{2+} sensors, notably with the development of single fluorescent protein GECIs, the GECOs (Zhao et al., 2011). These sensors were engineered to emit fluorescence at different wavelengths, thus enabling multicolor and multiparameter imaging in eukaryotic cells (Zhao et al., 2011; Ngo et al., 2014; Odaka et al., 2014; Waadt et al., 2017). Moreover, the GECOs have a higher sensitivity compared to the FRET-based cameleon YC3.6 (Keinath et al., 2015), which we confirmed in response to symbiotic factors in *M. truncatula* roots. The availability of multicolor Ca^{2+} sensors with greater dynamic ranges increases the possibility of exploring Ca^{2+} dynamics at the subcellular level and, notably, the interconnection between Ca^{2+} releases from different compartments. As such, the relation between cytoplasmic and nuclear Ca^{2+} signals, which remains unclear at the cellular level *in planta*, can now be addressed with increased resolution. Thus, we took advantage of the separate fluorescence emission windows of G-GECO (500–550 nm) and R-GECO (600–643 nm) to simultaneously assess Ca^{2+} dynamics in those contiguous cellular compartments. By targeting each of them to either the cytoplasm or the nucleoplasm, we developed the new dual sensors, NRCG-GECO1, NGCR-GECO1, and NRCG-GECO1.2 that allowed the simultaneous monitoring of nuclear and cytoplasmic Ca^{2+} dynamics in *M. truncatula* and *A. thaliana* root cells in response to biotic and abiotic stimuli. Despite the different association rates (K_{on}) of R-GECO and G-GECO (Zhao et al., 2011), these values are in the order of 10^9-10^{15} $M^{-1}{\cdot}s^{-1}$, which means that binding of either sensor to Ca^{2+} occurs faster than image capture. Therefore, any differences observed in the response times between the nucleus and the cytosol are intrinsically biological.

In legume symbioses, nitrogen-fixing rhizobial NF and mycorrhizal factors induce Ca^{2+} oscillations in perinuclear and nuclear compartments. Although the importance of cytoplasmic Ca^{2+}-mediated signal transduction is unknown, nuclear-localized Ca^{2+} is essential to activate a nuclear-localized Ca^{2+} and calmodulin-dependent kinase (CCaMK), that assures downstream transcriptional regulation of endosymbiotic programs (Zipfel and Oldroyd, 2017). Due to the lack of

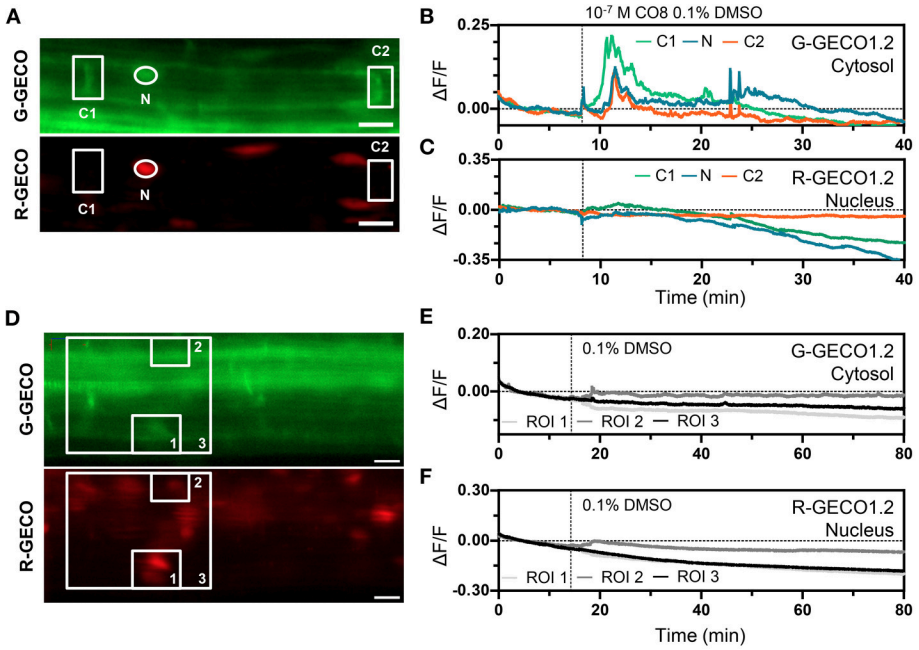

FIGURE 5 | The dual Ca^{2+} sensor reports Ca^{2+} dynamics to CO8. **(A–C)** Representative Ca^{2+} signals induced by 10^{-7} M CO8 in a 5-day-old Arabidopsis root (elongation zone) expressing the dual Ca^{2+} reporter NRCG-GECO1.2 [**(A)**, G-GECO1.2 channel (top); R-GECO1.2 channel (bottom)]. **(B,C)** Normalized fluorescence intensities in the G-GECO1.2 channel **(B)** and the R-GECO1.2 channel **(C)** of the ROIs marked in **(A)** (n = 8/11 plants). **(D,F)** 0.1% DMSO did not induce Ca^{2+} signals in a 5-day-old root (elongation zone) expressing the dual Ca^{2+} reporter NRCG-GECO1.2 [**(D)**, G-GECO1.2 channel (top); R-GECO1.2 channel (bottom)]. **(E,F)** Normalized fluorescence intensities in the G-GECO1.2 channel **(E)** and the R-GECO1.2 channel **(F)** of the ROIs marked in **(D)** (n = 4 plants). Dashed vertical lines mark the moment of CO8 and DMSO application. Scale bars represent 20 μm.

resolution, nuclear Ca^{2+} oscillations appeared synchronized between the nucleoplasm and the adjacent cytoplasmic region (Capoen et al., 2011). Furthermore, the ion channels and pump required to generate the symbiotic factor-induced Ca^{2+} oscillations were reported to localize to both the INM and ONM, although preferential localization of DMI1 to the INM was demonstrated (Capoen et al., 2011; Charpentier et al., 2016). Thus, the nuclear Ca^{2+} oscillations could start simultaneously or specifically from either nuclear membrane (Capoen et al., 2011). Using the NRCG-GECO1 and NGCR-GECO1 sensors, we demonstrated that Ca^{2+} release initiates inside the nucleoplasm in the majority of *M. truncatula* root hair cells elicited by NFs. This result unravels that the ion channels are activated first at the INM. This further suggests that the secondary messenger activating CNGC15 or DMI1 must either diffuse via the nucleopores or be produced inside the nucleus. Several nucleoporin mutants have been shown to be impaired in the generation of the nuclear Ca^{2+} oscillations in a temperature sensitive manner (Kanamori et al., 2006; Saito et al., 2007; Groth et al., 2010). However, their precise roles in this regulation remains unclear. Although the nucleoporins have been proposed to regulate the trafficking of the ion channels to the INM, our results suggest that they might be involved in the trafficking of the secondary messenger or proteins required for the activation of nuclear calcium oscillations.

Our studies further revealed the advantage of the dual GECO sensor to monitor subcellular Ca^{2+} dynamics in adjacent cytoplasm and nucleoplasm compartments of *A. thaliana* cells. By using a stably transformed dual sensor line we compared the dynamics of Ca^{2+} simultaneously in the cytoplasm and nucleoplasm of epidermal cells of the root elongation zone in response to diverse stimuli. We demonstrated that different stimuli (CO8, NaCl, ATP and cold shock) can generate, within the same cell type, diverse Ca^{2+} responses in the cytoplasmic and nucleoplasmic compartments. Notably, CO8 and ATP trigger cytoplasmic-associated oscillatory Ca^{2+} releases that do not diffuse to the nucleoplasm, suggesting that Ca^{2+} buffering proteins or Ca^{2+} uptake mechanisms are rapidly recruited or activated, respectively, to avoid Ca^{2+} diffusion into the nucleus. Interestingly, the ATP-induced Ca^{2+} signals in root cells of the elongation zone differ from a previous study showing dual cytoplasmic and nuclear Ca^{2+} releases (Krebs et al., 2012). This discrepancy might be due to the analysis of distinct root cells displaying specific ATP-induced Ca^{2+} responses, as the same stimulus can elicit different cell type-specific Ca^{2+} signatures (Kiegle et al., 2000). These findings further highlight the importance of monitoring Ca^{2+} dynamics in the same cell type to aptly compare stimuli-induced Ca^{2+} signatures and correlate the Ca^{2+} signature to a biological response. In contrast to CO8 and ATP, cold- and NaCl-induced transient Ca^{2+} signals first in the cytoplasm and then in the nucleoplasm. However, the NaCl- and cold-induced Ca^{2+} signatures in both compartments differ in amplitude and timing of activation, suggesting the involvement of different channels and/or pumps. Notably, the

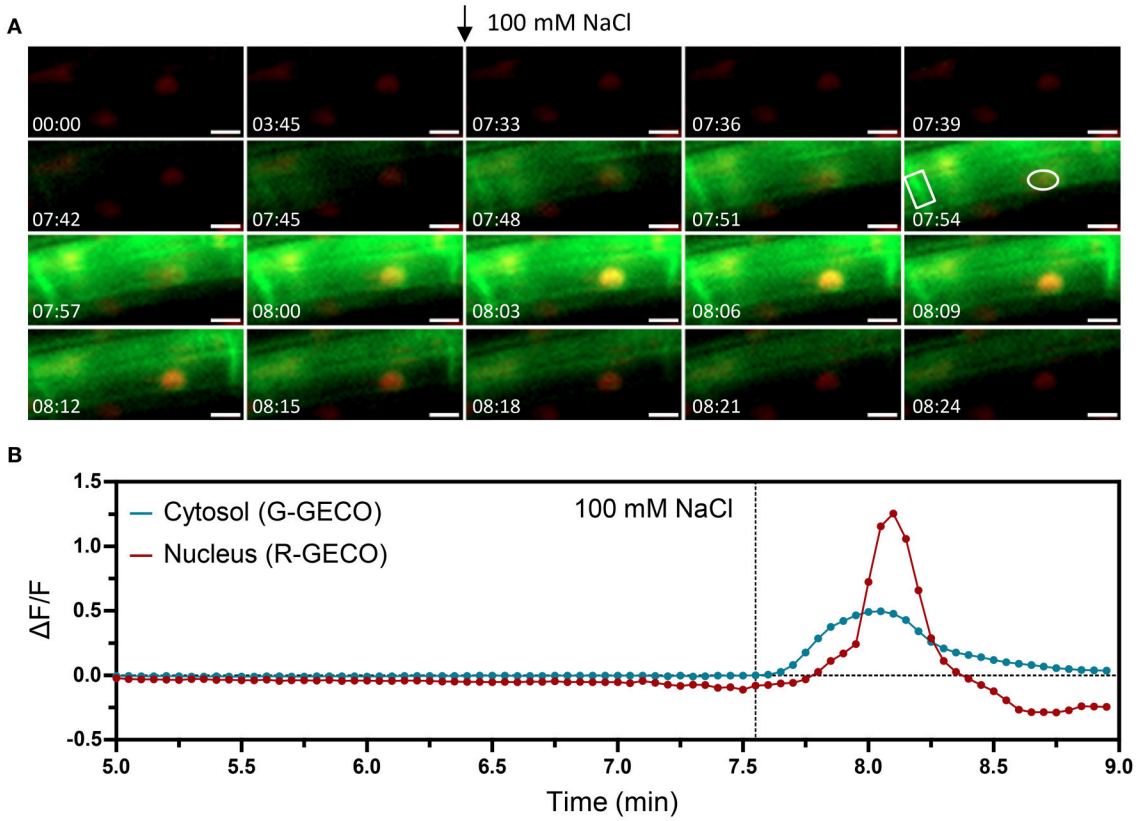

FIGURE 6 | Nuclear and cytosolic Ca^{2+} signals in response to 100 mM NaCl. Ca^{2+} signals induced by salt stress in a 6-day-old Arabidopsis root (elongation zone) expressing the dual Ca^{2+} reporter NRCG-GECO1.2. **(A)** Time-lapse images overlaying the G-GECO1.2 channel (green) and the R-GECO1.2 (red) showing the progression of the salt-induced signal through a cell (timestamps are in minutes and seconds and treatment application is marked with an arrow). **(B)** Normalized fluorescence intensities in the cytosol quantified in the G-GECO1.2 channel (blue) and in the nucleus quantified in the R-GECO1.2 channel (red). The areas quantified are marked in **(A)**. Dashed vertical line marks the moment of treatment with NaCl to a final concentration of 100 mM (n = 7/8 plants). Scale bars represent 10 μm.

NaCl-induced nucleoplasmic Ca^{2+} signal was observed earlier (within 2 s) than the cold-induced Ca^{2+} signal (within 25 s), following the cytoplasmic Ca^{2+} release. Moreover, The NaCl-induced nucleoplasmic Ca^{2+} signal had a higher amplitude than the cytoplasmic Ca^{2+} signal, which contrasts with the cold-induced Ca^{2+} signal, smaller in amplitude. These results support the induction of nuclear Ca^{2+} signals independently of the cytoplasmic Ca^{2+} release, as implied by a recent study regarding the NaCl-induced cytoplasmic/nuclear Ca^{2+} dynamics (Huang et al., 2017). Alternatively, the cytoplasmic Ca^{2+} release might be contributing to the generation of the nuclear Ca^{2+} signal either by diffusion or by triggering a Ca^{2+}-induced Ca^{2+} release mechanism at the nuclear envelope.

In summary, the cytoplasmic and nucleoplasmic dual sensors developed in this work are powerful tools to analyze the subcellular Ca^{2+} dynamics between the cytoplasm and nucleus *in planta*. These sensors will unequivocally be of interest in exploring Ca^{2+}-mediated signaling in response to diverse stimuli in different plant species.

MATERIALS AND METHODS

DNA Constructs

The single and dual GECO Ca^{2+} sensor constructs (Figure S1) were assembled using Golden Gate cloning. All GECO1.0 sensors were cloned under the control of the double cauliflower mosaic virus *35S* promoter (*2xp35S*) and the 35S terminator in the Golden Gate compatible vector *pCambiaCR1 ΔDsRed* (Fliegmann et al., 2016) kindly provided by C. Rosenberg (LIPM). PCR amplification of the individual sequence modules was done using Phusion Taq high fidelity DNA polymerase (New England Biolabs) and respective DNA templates and primer pairs are listed in Table S1. Amplified DNA fragments flanked by *Bsa*I and specific cohesive protruding ends were cloned into pBlueScript II (Agilent) and validated by sequencing before being used in Golden Gate assembly reactions (Engler and Marillonnet, 2014). All level 0 modules used in the dual NRCG-GECO1.2 sensor were synthesized by Life Technologies™ (ThermoFisher Scientific). All assembled Golden Gate binary vectors were verified by PCR, DNA sequencing and restriction digestion before transformation

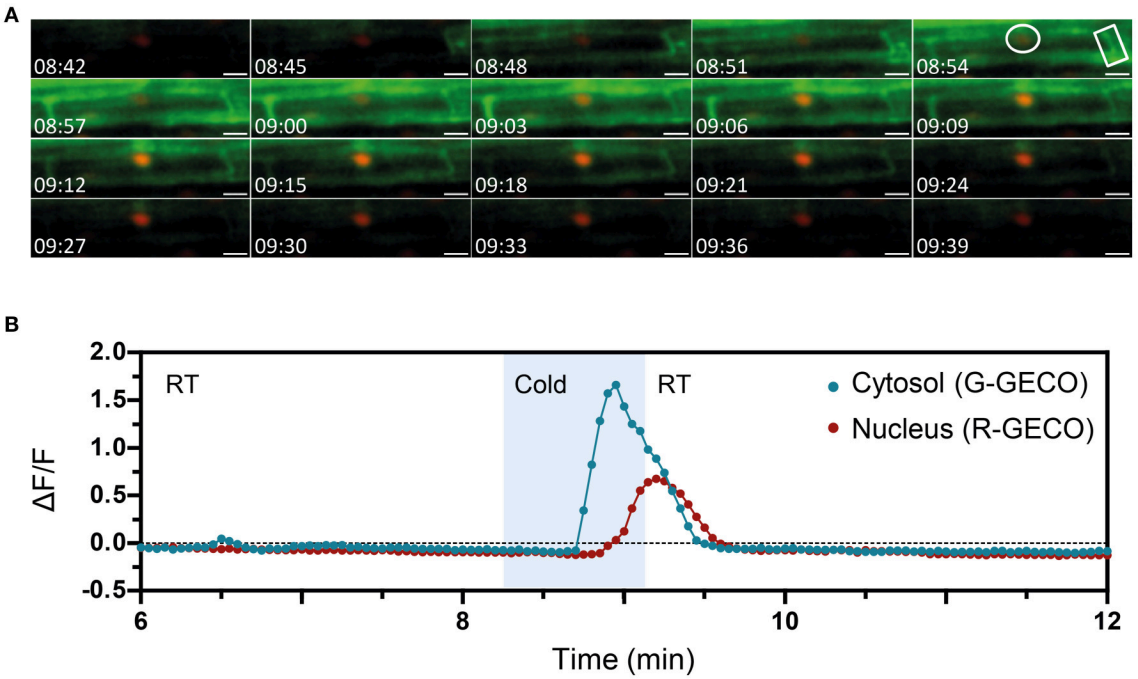

FIGURE 7 | The nuclear and cytosolic Ca^{2+} signals in response to cold are distinct. Ca^{2+} signals induced by cold treatment in a 6-day-old Arabidopsis root (elongation zone) expressing the dual Ca^{2+} reporter NRCG-GECO1.2. **(A)** Time-lapse images overlaying the G-GECO1.2 channel (green) and the R-GECO1.2 (red) showing the progression of the cold-induced signal through a cell (timestamps are in minutes and seconds). Cold was perfused between 08:15 and 09:09. **(B)** Normalized fluorescence intensities in the cytosol quantified in the G-GECO1.2 channel (blue) and in the nucleus quantified in the R-GECO1.2 channel (red). The areas quantified are marked in **(A)**. Area shaded in blue corresponds to the period of cold perfusion ($n = 4$ plants). Scale bars represent 50 μm.

into *Agrobacterium*. The cameleon Ca^{2+} sensors *NUP-YC2.1* and *NLS-YC3.6* used here were previously generated in Sieberer et al. (2009) and Krebs et al. (2012).

Plant Material and Bacterial Strains

Four *M. truncatula* cv Jemalong A17 lines were used in this study: the wild type and the symbiotic mutants *nfp-2* (Arrighi et al., 2006) *dmi1-1* and *dmi3-1* (Catoira et al., 2000; Wais et al., 2000). *M. truncatula* seeds were scarified with sulfuric acid, then surface-sterilized prior to germination and grown on inverted soft Campbel agar plates (http://www.noble.org/medicagohandbook). Arabidopsis seeds were surface-sterilized in 1.5% bleach for 15 min, followed by five washes in sterile water, and then plated in Murashige and Skoog (MS) solid medium (1% sucrose). After 3–5 days at 4°C, plates were moved to a growth cabinet (23°C, 16-h photoperiod, and 300 $\mu mol \cdot m^{-2} \cdot s^{-1}$ light intensity) for germination and growth. The *Escherichia coli* DH5α strain was used for plasmid propagation, the *A. rhizogenes* Arqua1 strain (Quandt et al., 1993) strain for the generation *M. truncatula* composite plants and the *A. tumefaciens* GV3101 (Koncz and Schell, 1986) strain for stable transformation of *A. thaliana*.

Generation and *in Vitro* Culture of *Agrobacterium*-Transformed *M. truncatula* and *A. thaliana*

A. rhizogenes-mediated transformation hairy root transformation of *M. truncatula* was performed as described in Boisson-Dernier et al. (2001) with minor modifications. Germinated seedlings were sectioned ∼3 mm from the root tip and inoculated with a 3–4 μL drop of *A. rhizogenes* bacterial suspension adjusted to an OD_{600nm} of 1 in water. Inoculated seedlings were placed on Fahraeus/agar plates supplemented with 0.5 mM ammonium nitrate and kanamycin ($25 mg.L^{-1}$). Plates were partially sealed with parafilm to allow crucial gas exchanges and placed in a 20°C growth chamber (16-h photoperiod and a light intensity of 70 $\mu E \cdot m^{-2} \cdot s^{-1}$) for 1 week before transferring to 25°C. About 2 weeks-post-inoculation, kanamycin-resistant composite plants were transferred to a beaker containing sterile water supplemented with 200 $mg \cdot L^{-1}$ augmentin (amoxicillin:clavulanic acid [5:1], GlaxoSmithKline), and incubated for at least 30 min, in order to reduce the growth of *A. rhizogenes*. Plants were rinsed twice before being transferred to square plates containing a nitrogen-free modified Fahraeus medium with 0.5% [w/v] phytagel (Sigma-Aldrich) and supplemented with 50 nM 2-amino-ethoxyvinyl-Gly (AVG), adapted for *in vivo* microscopic observations as described in Fournier et al. (2008). Transgenic roots were covered with a sterile, gas-permeable and transparent plastic film (Lumox film, Starsted) that allows the use of water-immersion objectives during imaging. Square plates with composite plants were slightly tilted to encourage the growth of the roots along the plastic film. The lower part of the square plate was wrapped in black plastic to protect the roots from light. *M. truncatula* ROCs expressing the NR-GECO1 sensor were obtained from transgenic composite plants as described by Boisson-Dernier et al. (2001).

ROCs were cultured on M medium (Boisson-Dernier et al., 2001) and propagated vertically until used for microscopy observations.

A. thaliana stable transgenic plants were generated using the floral dip method (Clough and Bent, 1998) and selected in 50 $\mu g \cdot mL^{-1}$ hygromycin B.

Selection and Symbiotic Treatments of *M. truncatula* Transformed Roots

Kanamycin-resistant *A. rhizogenes*-transformed composite plants or ROCs transformed with cameleon or GECO1 constructs were screened for expression of the respective fluorescent sensors using fluorescence stereomicroscopes (Leica MZFLIII and Zeiss axiozoom V16) and a Zeiss Axiophot epifluorescent microscope. Selection of transgenic roots was done using filters adapted to detect yellow/green YFP/GFP (excitation: 470–510 nm; emission: 525–575 nm) or red mApple (excitation: 577–587 nm, emission: 620–680 nm) fluorescent proteins from the different cameleon or GECO1 sensors. Only composite plants with fluorescent transgenic roots were transferred to plates containing nitrogen-free modified 0.5% [w/v] phytagel Fahraeus medium for imaging 3–5 days later. Transgenic roots lying on the medium and covered by a gas-permeable film were treated with 1 to 2 mL of a freshly diluted aqueous solution of purified *S. meliloti* NFs (10^{-9} M) or CO4 (10^{-5} M or 10^{-7} M) that were added to plates between the plastic film and the medium with the help of a micropipette. In the case of ROCs, imaging was performed with excised root sections that were mounted between a slide and a cover slip. Confocal imaging was performed before treatments to assess the background fluorescence levels, and then initiated about 5 min after treatment for a total period of up to 1 h.

Confocal Imaging of Calcium Responses in Transgenic *M. truncatula* and Arabidopsis Roots

The comparison between the nuclear NR-GECO1, the NUP-YC2.1 and the NLS-YC3.6 Yellow Cameleon sensors was performed using a Leica TCS SP2 AOBS confocal laser-scanning microscope equipped with a long-distance 40x water-immersion objective (HCX Apo L 0.80). The 458 nm argon laser was used to excite the CFP of the cameleon sensors (pinhole diameter at 4 Airy units). Fluorescence emission was collected in the 470–500 nm range for CFP and 530–570 nm range for YFP. Images were acquired at 5 s intervals from 5 to 60 min either before or after treatment with a 512 × 512 pixels resolution. The 561 nm diode was used to excite the mApple red fluorescence protein of the NR-GECO1 sensor (pinhole diameter at 3 Airy units) and fluorescence was visualized in the specific 580 to 643 nm emission window. The laser intensity used for the cameleon probes (80% power setting, Sieberer et al., 2009) was reduced to 20% for monitoring Ca^{2+} responses with the NR-GECO1 sensor in order to avoid photo bleaching of the red fluorescence during long acquisitions. Confocal imaging of transgenic roots expressing the dual NRCG-GECO1 and NGCR-GECO1 sensors was done using a beam-splitter Leica TCS SP8 AOBS confocal laser-scanning microscope equipped with a 25x water-immersion objective. The 488 nm argon laser was used to excite the G-GECO1 and the 561 nm diode to excite the R-GECO1. Fluorescent images were recorded simultaneously for NRCG-GECO1 and NGCR-GECO1, using emission windows of 500–550 nm and 600–643 nm for G-GECO1 and R-GECO1 signals, respectively. Fluorescence emission ranges were specifically set for each fluorescent protein in order to avoid overlap between the G-GECO1 and R-GECO1 signals, as detailed in Figure S6. Images were acquired in 200 to 500 ms intervals with a scanning resolution of 512 × 128 pixel. Images were acquired using the Leica confocal software.

The subcellular localization of the GECO1.2 Ca^{2+} reporters was assessed in 6-day-old roots by CLSM using a Zeiss LSM 780 equipped with a 25x/0.8 water objective. G-GECO1.2 was excited at 488 nm and the emitted light was captured between 463 and 500 nm. R-GECO1.2 was excited at 561 nm and emitted fluorescence captured in the 571–640 nm range. For Ca^{2+} imaging, plants were analyzed 5–6 days after germination and carefully mounted in a perfusing (cold treatment) or non-perfusing chamber. Perfusion of cold media was performed using a RC-21BR chamber (Warner Instruments). For ATP, CO8, and NaCl treatments, the elicitors were applied at a 10x concentration to an open chamber made with cover glass and sealed with vacuum grease. After mounting in liquid MS (1% sucrose), samples were incubated at room temperature for at least 15 min before imaging. Ca^{2+} imaging was performed using a Nikon ECLIPSE FN1. The fluorophores were excited at a wavelength of 470 ± 24 nm. Emitted fluorescence was separated by an image splitter and passed through an emission filter of 520 ± 40 nm for G-GECO1.2, and 632 ± 60 nm for R-GECO1.2 (Optosplit, Cairn Research, UK). Images were collected every 2 or 3 s.

Image Analysis

Processing, final cropping, and mounting of the Medicago images were performed using Fiji. The fluorescence, merged images and Supplementary time-lapse movies were obtained after applying a median filter of 2 pixel radius to fluorescence image series. Intensity data was calculated from selected ROI, delimited in individual root hairs within the nuclear region (for nuclear-localized sensors) or tailored in the perinuclear, middle or root hair tip regions (for cytoplasmic sensors). To quantify relative Ca^{2+} spiking amplitudes, the average fluorescence for each ROI was calculated and used to determine the SNR of individual spikes collected from independent roots and biological experiments. The SNR of a given spike measures the difference between the fluorescence baseline and the maximum fluorescence peak value. The SNR values of individual spikes were obtained by calculating the $\Delta F/F$ (F_{max}-F_{min}/F_{min}) or $\Delta R/R$ (R_{max}-R_{min}/R_{min}), in which F_{max} and R_{max} correspond to the maximum fluorescence value or ratio change of a spike and F_{min} and R_{min} correspond to the data point before the onset of a spike.

For image processing of the Arabidopsis data the following steps were conducted using ImageJ 1.48v: background subtraction, registration using MultiStackReg v1.45 (http://bradbusse.net/sciencedownloads.html), and application of a lookup table. Image data were obtained from processed images

using Time Series Analyzer V3_2 (https://imagej.nih.gov/ij/plugins/time-series.html). Normalized datasets ($\Delta F/F$) were calculated as $(F–F_0)/F_0$, where F_0 represent the average of at least 2 min of baseline values (before treatment).

Statistical Analyses

Statistical analyses were performed using R (http://r-project.org). Data were evaluated for normality with the Shapiro-Wilk test and homogeneity of variance with Levenne or Bartlett tests. Parametric (ANOVA) or non-parametric (Kruskal-Wallis) statistical tests were used, respectively, for normally-distributed data and non normally-distributed data. Signal periodicity values of calcium sensors were first transformed into normality using Box-Cox ($\lambda = 0.0606$), before statistical analysis using one-way ANOVA followed by Tukey honest difference (HSD) tests. Statistical analysis of signal-to-baseline ratio was done using the non-parametrical Kruskal-Wallis test. For the dual GECO sensors, statistical analyses of the start of a calcium spike was done using a chi-square test ($p < 0.05$) to (i) compare the frequency of observations in each category to an expected frequency of 1/3 per category if the distribution was random and (ii) to compare the number of observations per category for each sensor grouped in a contingency table.

AUTHOR CONTRIBUTIONS

MyC and FdC-N: conceived the project; AK, NL, MyC, and FdC-N: designed the experiments; AK: performed the *M. truncatula* and NL: the *A. thaliana* experiments; MiC: contributed to the NLS-R-GECO1 in ROCs experiments; AK and NL: prepared the figures; AK, NL, MyC, and FdC-N: wrote the manuscript; MyC and FdC-N: are co-responsible for the work.

ACKNOWLEDGMENTS

We thank David Barker and Joelle Fournier for critical reading of the manuscript, Christian Mazars and Martin Parniske for valuable discussions, Lisa Frances for contributing to the cloning of the R-GECO1 version, Fabienne Maillet for kindly providing purified *S. meliloti* NFs, and Charles Rosemberg for the pCambia Golgen Gate vectors. The CMV-NLS-R-GECO (Addgene plasmid #32447) and CMV-G-GECO1.0 (Addgene plasmid #32462) were generated and provided by Robert Campbell via Addgene, while the YC3.6 construct was kindly provided by Melanie Krebs and Karin Schumacher. AK was supported by a Ph.D. grant of the French Ministry of Education and Research, NL was supported by a Ph.D. studentship from the John Innes Foundation. MyC was supported by BBSRC (BB/P007112/1) and John Innes Centre, and FdC-N lab work was supported by the ANR COME-IN (grant no. ANR-14-CE35-0007-01) and TULIP (grant no. ANR-10-LABX-41) grants.

SUPPLEMENTARY MATERIAL

The Supplementary Material for this article can be found online at: https://www.frontiersin.org/articles/10.3389/fpls.2018.00245/full#supplementary-material

REFERENCES

Allen, G. J., Kwak, J. M., Chu, S. P., Llopis, J., Tsien, R. Y., Harper, J. F., et al. (1999). Cameleon calcium indicator reports cytoplasmic calcium dynamics in Arabidopsis guard cells. *Plant J.* 19, 735–747. doi: 10.1046/j.1365-313x.1999.00574.x

Ané, J. M., Kiss, G. B., Riely, B. K., Penmetsa, R. V., Oldroyd, G. E., Ayax, C., et al. (2004). *Medicago truncatula* DMI1 required for bacterial and fungal symbioses in legumes. *Science* 303, 1364–1367. doi: 10.1126/science.1092986

Arrighi, J. F., Barre, A., Ben Amor, B., Bersoult, A., Soriano, L. C., Mirabella, R. F., et al. (2006). The *Medicago truncatula* lysin [corrected] motif-receptor-like kinase gene family includes NFP and new nodule-expressed genes. *Plant Physiol.* 142, 265–279. doi: 10.1104/pp.106.084657

Bajar, B. T., Wang, E. S., Zhang, S., Lin, M. Z., and Chu, J. (2016). A guide to fluorescent protein FRET Pairs. *Sensors* 16:1488. doi: 10.3390/s16091488

Boisson-Dernier, A., Chabaud, M., Garcia, F., Bécard, G., Rosenberg, C., and Barker, D. G. (2001). *Agrobacterium rhizogenes*-transformed roots of *Medicago truncatula* for the study of nitrogen-fixing and endomycorrhizal symbiotic associations. *Mol. Plant Microbe Interact.* 14, 695–700. doi: 10.1094/MPMI.2001.14.6.695

Bonza, M. C., Loro, G., Behera, S., Wong, A., Kudla, J., and Costa, A. (2013). Analyses of Ca^{2+} accumulation and dynamics in the endoplasmic reticulum of Arabidopsis root cells using a genetically encoded Cameleon sensor. *Plant Physiol.* 163, 1230–1241. doi: 10.1104/pp.113.226050

Capoen, W., Sun, J., Wysham, D., Otegui, M. S., Venkateshwaran, M., Hirsch, S., et al. (2011). Nuclear membranes control symbiotic calcium signaling of legumes. *Proc. Natl. Acad. Sci. U.S.A.* 108, 14348–14353. doi: 10.1073/pnas.1107912108

Catoira, R., Galera, C., de Billy, F., Penmetsa, R. V., Journet, E. P., Maillet, F., et al. (2000). Four genes of *Medicago truncatula* controlling components of a nod factor transduction pathway. *Plant Cell* 12, 1647–1666. doi: 10.1105/tpc.12.9.1647

Chabaud, M., Genre, A., Sieberer, B. J., Faccio, A., Fournier, J., Novero, M., et al. (2011). Arbuscular mycorrhizal hyphopodia and germinated spore exudates trigger Ca^{2+} spiking in the legume and nonlegume root epidermis. *New Phytol.* 189, 347–355. doi: 10.1111/j.1469-8137.2010.03464.x

Charpentier, M., and Oldroyd, G. E. (2013). Nuclear calcium signaling in plants. *Plant Physiol.* 163, 496–503. doi: 10.1104/pp.113.220863

Charpentier, M., Sun, J., Vaz Martins, T., Radhakrishnan, G. V., Findlay, K., Soumpourou, E., et al. (2016). Nuclear-localized cyclic nucleotide-gated channels mediate symbiotic calcium oscillations. *Science* 352, 1102–1105. doi: 10.1126/science.aae0109

Clough, S. J., and Bent, A. F. (1998). Floral dip: a simplified method for Agrobacterium-mediated transformation of *Arabidopsis thaliana*. *Plant J.* 16, 735–743.

Costa, A., Drago, I., Behera, S., Zottini, M., Pizzo, P., Schroeder, J. I., et al. (2010). H_2O_2 in plant peroxisomes: an *in vivo* analysis uncovers a $Ca^{(2+)}$-dependent scavenging system. *Plant J.* 62, 760–772. doi: 10.1111/j.1365-313X.2010.04190.x

Dodd, A. N., Kudla, J., and Sanders, D. (2010). The language of calcium signaling. *Annu. Rev. Plant Biol.* 61, 593–620. doi: 10.1146/annurev-arplant-070109-104628

Domínguez, D. C., Guragain, M., and Patrauchan, M. (2015). Calcium binding proteins and calcium signaling in prokaryotes. *Cell Calcium* 57, 151–165. doi: 10.1016/j.ceca.2014.12.006

Ehrhardt, D. W., Wais, R., and Long, S. R. (1996). Calcium spiking in plant root hairs responding to Rhizobium nodulation signals. *Cell* 85, 673–681. doi: 10.1016/S0092-8674(00)81234-9

Engler, C., and Marillonnet, S. (2014). Golden gate cloning. *Methods Mol. Biol.* 1116, 119–131. doi: 10.1007/978-1-62703-764-8_9

Fliegmann, J., Jauneau, A., Pichereaux, C., Rosenberg, C., Gasciolli, V., Timmers, A. C., et al. (2016). LYR3, a high-affinity LCO-binding protein of *Medicago truncatula*, interacts with LYK3, a key symbiotic receptor. *FEBS Lett.* 590, 1477–1487. doi: 10.1002/1873-3468.12191

Fournier, J., Timmers, A. C., Sieberer, B. J., Jauneau, A., Chabaud, M., and Barker, D. G. (2008). Mechanism of infection thread elongation in root hairs of *Medicago truncatula* and dynamic interplay with associated rhizobial colonization. *Plant Physiol.* 148, 1985–1995. doi: 10.1104/pp.108.125674

Galon, Y., Finkler, A., and Fromm, H. (2010). Calcium-regulated transcription in plants. *Mol. Plant* 3, 653–669. doi: 10.1093/mp/ssq019

Genre, A., Chabaud, M., Balzergue, C., Puech-Pagès, V., Novero, M., Rey, T., et al. (2013). Short-chain chitin oligomers from arbuscular mycorrhizal fungi trigger nuclear Ca^{2+} spiking in *Medicago truncatula* roots and their production is enhanced by strigolactone. *New Phytol.* 198, 190–202. doi: 10.1111/nph.12146

Granqvist, E., Wysham, D., Hazledine, S., Kozlowski, W., Sun, J., Charpentier, M., et al. (2012). Buffering capacity explains signal variation in symbiotic calcium oscillations. *Plant Physiol.* 160, 2300–2310. doi: 10.1104/pp.112.205682

Groth, M., Takeda, N., Perry, J., Uchida, H., Dräxl, S., Brachmann, A., et al. (2010). NENA, a *Lotus japonicus* homolog of Sec13, is required for rhizodermal infection by arbuscular mycorrhiza fungi and rhizobia but dispensable for cortical endosymbiotic development. *Plant Cell* 22, 2509–2526. doi: 10.1105/tpc.109.069807

Huang, F., Luo, J., Ning, T., Cao, W., Jin, X., Zhao, H., et al. (2017). Cytosolic and nucleosolic calcium signaling in response to osmotic and salt stresses are independent of each other in roots of Arabidopsis seedlings. *Front. Plant Sci.* 8:1648. doi: 10.3389/fpls.2017.01648

Iwano, M., Entani, T., Shiba, H., Kakita, M., Nagai, T., Mizuno, H., et al. (2009). Fine-tuning of the cytoplasmic Ca^{2+} concentration is essential for pollen tube growth. *Plant Physiol.* 150, 1322–1334. doi: 10.1104/pp.109.139329

Kanamori, N., Madsen, L. H., Radutoiu, S., Frantescu, M., Quistgaard, E. M., Miwa, H., et al. (2006). A nucleoporin is required for induction of Ca^{2+} spiking in legume nodule development and essential for rhizobial and fungal symbiosis. *Proc. Natl. Acad. Sci. U.S.A.* 103, 359–364. doi: 10.1073/pnas.0508883103

Keinath, N. F., Waadt, R., Brugman, R., Schroeder, J. I., Grossmann, G., Schumacher, K., et al. (2015). Live cell imaging with R-GECO1 sheds light on flg22- and chitin-induced transient $[Ca^{(2+)}]$cyt patterns in Arabidopsis. *Mol. Plant* 8, 1188–1200. doi: 10.1016/j.molp.2015.05.006

Kiegle, E., Moore, C. A., Haseloff, J., Tester, M. A., and Knight, M. R. (2000). Cell-type-specific calcium responses to drought, salt and cold in the Arabidopsis root. *Plant J.* 23, 267–278. doi: 10.1046/j.1365-313x.2000.00786.x

Knight, M. R., Campbell, A. K., Smith, S. M., and Trewavas, A. J. (1991). Transgenic plant aequorin reports the effects of touch and cold-shock and elicitors on cytoplasmic calcium. *Nature* 352, 524–526. doi: 10.1038/352524a0

Koncz, C., and Schell, J. (1986). The promoter of TL-DNA gene 5 controls the tissue-specific expression of chimaeric genes carried by a novel type of Agrobacterium binary vector. *Mol. Gen. Genet.* 204, 383–396. doi: 10.1007/BF00331014

Kosuta, S., Hazledine, S., Sun, J., Miwa, H., Morris, R. J., Downie, J. A., et al. (2008). Differential and chaotic calcium signatures in the symbiosis signaling pathway of legumes. *Proc. Natl. Acad. Sci. U.S.A.* 105, 9823–9828. doi: 10.1073/pnas.0803499105

Krebs, M., Held, K., Binder, A., Hashimoto, K., Den Herder, G., Parniske, M., et al. (2012). FRET-based genetically encoded sensors allow high-resolution live cell imaging of Ca^{2+} dynamics. *Plant J.* 69, 181–92. doi: 10.1111/j.1365-313X.2011.04780.x

Kudla, J., Batistic, O., and Hashimoto, K. (2010). Calcium signals: the lead currency of plant information processing. *Plant Cell* 22, 541–563. doi: 10.1105/tpc.109.072686

Loro, G., Drago, I., Pozzan, T., Schiavo, F. L., Zottini, M., and Costa, A. (2012). Targeting of Cameleons to various subcellular compartments reveals a strict cytoplasmic/mitochondrial Ca^{2+} handling relationship in plant cells. *Plant J.* 71, 1–13. doi: 10.1111/j.1365-313X.2012.04968.x

Loro, G., Wagner, S., Doccula, F. G., Behera, S., Weinl, S., Kudla, J., et al. (2016). Chloroplast-specific *in vivo* Ca^{2+} imaging using yellow cameleon fluorescent protein sensors reveals organelle-autonomous Ca^{2+} signatures in the stroma. *Plant Physiol.* 171, 2317–2330. doi: 10.1104/pp.16.00652

McAinsh, M. R., and Pittman, J. K. (2009). Shaping the calcium signature. *New Phytol.* 181, 275–294. doi: 10.1111/j.1469-8137.2008.02682.x

McCombs, J. E., and Palmer, A. E. (2008). Measuring calcium dynamics in living cells with genetically encodable calcium indicators. *Methods* 46, 152–159. doi: 10.1016/j.ymeth.2008.09.015

Miwa, H., Sun, J., Oldroyd, G. E., and Downie, J. A. (2006a). Analysis of calcium spiking using a cameleon calcium sensor reveals that nodulation gene expression is regulated by calcium spike number and the developmental status of the cell. *Plant J.* 48, 883–894. doi: 10.1111/j.1365-313X.2006.02926.x

Miwa, H., Sun, J., Oldroyd, G. E., and Downie, J. A. (2006b). Analysis of Nod-factor-induced calcium signaling in root hairs of symbiotically defective mutants of *Lotus japonicus*. *Mol. Plant Microbe Interact.* 19, 914–923. doi: 10.1094/MPMI-19-0914

Miyawaki, A., Llopis, J., Heim, R., McCaffery, J. M., Adams, J. A., Ikura, M., et al. (1997). Fluorescent indicators for Ca^{2+} based on green fluorescent proteins and calmodulin. *Nature* 388, 882–887. doi: 10.1038/42264

Nakao, S., Wakabayashi, S., and Nakamura, T. Y. (2015). Stimulus-dependent regulation of nuclear Ca^{2+} signaling in cardiomyocytes: a role of neuronal calcium sensor-1. *PLoS ONE* 10:e0125050. doi: 10.1371/journal.pone.0125050

Ngo, Q. A., Vogler, H., Lituiev, D. S., Nestorova, A., and Grossniklaus, U. (2014). A calcium dialog mediated by the FERONIA signal transduction pathway controls plant sperm delivery. *Dev Cell* 29, 491–500. doi: 10.1016/j.devcel.2014.04.008

Odaka, H., Arai, S., Inoue, T., and Kitaguchi, T. (2014). Genetically-encoded yellow fluorescent cAMP indicator with an expanded dynamic range for dual-color imaging. *PLoS ONE* 9:e100252. doi: 10.1371/journal.pone.0100252

Quandt, H.-J., Pühler, A., and Broer, I. (1993). Transgenic root nodules of *Vicia hirsuta*: a fast and efficient system for the study of gene expression in indeterminate-type nodules. *MPMI* 6, 699–706. doi: 10.1094/MPMI-6-699

Ranty, B., Cotelle, V., Galaud, J. P., and Mazars, C. (2012). Nuclear calcium signaling and its involvement in transcriptional regulation in plants. *Adv. Exp. Med. Biol.* 740, 1123–1143. doi: 10.1007/978-94-007-2888-2_51

Reddy, A. S., Ali, G. S., Celesnik, H., and Day, I. S. (2011). Coping with stresses: roles of calcium- and calcium/calmodulin-regulated gene expression. *Plant Cell* 23, 2010–2032. doi: 10.1105/tpc.111.084988

Rodriguez-Garcia, A., Rojo-Ruiz, J., Navas-Navarro, P., Aulestia, F. J., Gallego-Sandin, S., Garcia-Sancho, J., et al. (2014). GAP, an aequorin-based fluorescent indicator for imaging Ca^{2+} in organelles. *Proc. Natl. Acad. Sci. U.S.A.* 111, 2584–2589. doi: 10.1073/pnas.1316539111

Saito, K., Yoshikawa, M., Yano, K., Miwa, H., Uchida, H., Asamizu, E., et al. (2007). NUCLEOPORIN85 is required for calcium spiking, fungal and bacterial symbioses, and seed production in Lotus japonicus. *Plant Cell* 19, 610–624. doi: 10.1105/tpc.106.046938

Shaw, S. L., and Long, S. R. (2003). Nod factor elicits two separable calcium responses in *Medicago truncatula* root hair cells. *Plant Physiol.* 131, 976–984. doi: 10.1104/pp.005546

Sieberer, B. J., Chabaud, M., Fournier, J., Timmers, A. C., and Barker, D. G. (2012). A switch in Ca^{2+} spiking signature is concomitant with endosymbiotic microbe entry into cortical root cells of *Medicago truncatula*. *Plant J.* 69, 822–830. doi: 10.1111/j.1365-313X.2011.04834.x

Sieberer, B. J., Chabaud, M., Timmers, A. C., Monin, A., Fournier, J., and Barker, D. G. (2009). A nuclear-targeted cameleon demonstrates intranuclear Ca^{2+} spiking in *Medicago truncatula* root hairs in response to rhizobial nodulation factors. *Plant Physiol.* 151, 1197–1206. doi: 10.1104/pp.109.142851

Stael, S., Wurzinger, B., Mair, A., Mehlmer, N., Vothknecht, U. C., and Teige, M. (2012). Plant organellar calcium signalling: an emerging field. *J. Exp. Bot.* 63, 1525–1542. doi: 10.1093/jxb/err394

Sun, J., Miller, J. B., Granqvist, E., Wiley-Kalil, A., Gobbato, E., Maillet, F., et al. (2015). Activation of symbiosis signaling by arbuscular mycorrhizal fungi in legumes and rice. *Plant Cell* 27, 823–838. doi: 10.1105/tpc.114.131326

Tanaka, K., Swanson, S. J., Gilroy, S., and Stacey, G. (2010). Extracellular nucleotides elicit cytosolic free calcium oscillations in Arabidopsis. *Plant Physiol.* 154, 705–719. doi: 10.1104/pp.110.162503

Tunc-Ozdemir, M., and Jones, A. M. (2017). Ligand-induced dynamics of heterotrimeric G protein-coupled receptor-like kinase complexes. *PLoS ONE* 12:e0171854. doi: 10.1371/journal.pone.0171854

van Der Luit, A. H., Olivari, C., Haley, A., Knight, M. R., and Trewavas, A. J. (1999). Distinct calcium signaling pathways regulate calmodulin gene expression in tobacco. *Plant Physiol.* 121, 705–714. doi: 10.1104/pp.121.3.705

Waadt, R., Krebs, M., Kudla, J., and Schumacher, K. (2017). Multiparameter imaging of calcium and abscisic acid and high-resolution quantitative calcium measurements using R-GECO1-mTurquoise in Arabidopsis. *New Phytol.* 216, 303–320. doi: 10.1111/nph.14706

Wais, R. J., Galera, C., Oldroyd, G., Catoira, R., Penmetsa, R. V., Cook, D., et al. (2000). Genetic analysis of calcium spiking responses in nodulation mutants of *Medicago truncatula*. *Proc. Natl. Acad. Sci. U.S.A.* 97, 13407–13412. doi: 10.1073/pnas.230439797

Wang, Y., Dindas, J., Rienmüller, F., Krebs, M., Waadt, R., Schumacher, K., et al. (2015). Cytosolic $Ca^{(2+)}$ Signals enhance the vacuolar ion conductivity of bulging Arabidopsis root hair cells. *Mol. Plant* 8, 1665–1674. doi: 10.1016/j.molp.2015.07.009

Whalley, H. J., and Knight, M. R. (2013). Calcium signatures are decoded by plants to give specific gene responses. *New Phytol.* 197, 690–693. doi: 10.1111/nph.12087

Wood, N. T., Haley, A., Viry-Moussaïd, M., Johnson, C. H., van der Luit, A. H., and Trewavas, A. J. (2001). The calcium rhythms of different cell types oscillate with different circadian phases. *Plant Physiol.* 125, 787–796. doi: 10.1104/pp.125.2.787

Wu, J., Liu, L., Matsuda, T., Zhao, Y., Rebane, A., Drobizhev, M., et al. (2013). Improved orange and red Ca^{2+} indicators and photophysical considerations for optogenetic applications. *ACS Chem. Neurosci.* 4, 963–972. doi: 10.1021/cn400012b

Xiong, T. C., Ronzier, E., Sanchez, F., Corratgé-Faillie, C., Mazars, C., and Thibaud, J. B. (2014). Imaging long distance propagating calcium signals in intact plant leaves with the BRET-based GFP-aequorin reporter. *Front. Plant Sci.* 5:43. doi: 10.3389/fpls.2014.00043

Zhao, Y., Araki, S., Wu, J., Teramoto, T., Chang, Y. F., Nakano, M., et al. (2011). An expanded palette of genetically encoded Ca^{2+} indicators. *Science* 333, 1888–1891. doi: 10.1126/science.1208592.

Zipfel, C., and Oldroyd, G. E. (2017). Plant signalling in symbiosis and immunity. *Nature* 543, 328–336. doi: 10.1038/nature22009

Conflict of Interest Statement: The authors declare that the research was conducted in the absence of any commercial or financial relationships that could be construed as a potential conflict of interest.

frontiers in Plant Science

ORIGINAL RESEARCH
published: 16 November 2017
doi: 10.3389/fpls.2017.01921

W342F Mutation in CCaMK Enhances Its Affinity to Calmodulin But Compromises Its Role in Supporting Root Nodule Symbiosis in *Medicago truncatula*

*Edgard Jauregui[1], Liqun Du[1,2], Cynthia Gleason[3] and B. W. Poovaiah[1]**

[1] Laboratory of Molecular Plant Science, Department of Horticulture, Washington State University, Pullman, WA, United States, [2] College of Life and Environmental Sciences, Hangzhou Normal University, Hangzhou, China, [3] Department of Plant Pathology, Washington State University, Pullman, WA, United States

OPEN ACCESS

Edited by:
Jianping Wang,
University of Florida, United States

Reviewed by:
Muthu Venkateshwaran,
University of Wisconsin–Platteville, United States
Dong Wang,
University of Massachusetts Amherst, United States
Keiko Yoshioka,
University of Toronto, Canada

***Correspondence:**
B. W. Poovaiah
poovaiah@wsu.edu

Specialty section:
This article was submitted to Plant Microbe Interactions, a section of the journal Frontiers in Plant Science

Received: *15 June 2017*
Accepted: *24 October 2017*
Published: *16 November 2017*

Citation:
Jauregui E, Du L, Gleason C and Poovaiah BW (2017) W342F Mutation in CCaMK Enhances Its Affinity to Calmodulin But Compromises Its Role in Supporting Root Nodule Symbiosis in Medicago truncatula. Front. Plant Sci. 8:1921. doi: 10.3389/fpls.2017.01921

The calcium/calmodulin-dependent protein kinase (CCaMK) is regulated by free Ca^{2+} and Ca^{2+}-loaded calmodulin. This dual binding is believed to be involved in its regulation and associated physiological functions, although direct experimental evidence for this is lacking. Here we document that site-directed mutations in the calmodulin-binding domain of CCaMK alters its binding capacity to calmodulin, providing an effective approach to study how calmodulin regulates CCaMK in terms of kinase activity and regulation of rhizobial symbiosis in *Medicago truncatula*. We observed that mutating the tryptophan at position 342 to phenylalanine (W342F) markedly increased the calmodulin-binding capability of the mutant. The mutant CCaMK underwent autophosphorylation and catalyzed substrate phosphorylation in the absence of calcium and calmodulin. When the mutant W342F was expressed in *ccamk-1* roots, the transgenic roots exhibited an altered nodulation phenotype. These results indicate that altering the calmodulin-binding domain of CCaMK could generate a constitutively activated kinase with a negative role in the physiological function of CCaMK.

Keywords: Ca^{2+}/calmodulin-dependent protein kinase, calcium, calmodulin, symbiosis, *Medicago truncatula*

INTRODUCTION

Calcium/calmodulin (Ca^{2+}/CaM)-mediated signaling plays important roles in sensing and transducing environmental stimuli and developmental cues (Du and Poovaiah, 2005; Poovaiah et al., 2013), plant immune responses (Du et al., 2009) and mutualistic plant–microbe interactions (Gleason et al., 2006; Yuan et al., 2017). One important effector protein of this Ca^{2+}/CaM-mediated signaling in plants is the Ca^{2+}/CaM-dependent protein kinase, CCaMK (Patil et al., 1995). CCaMK is nuclear localized and lies downstream of the cellular calcium spiking response that occurs in the symbiosis pathway. After activation by Ca^{2+}/CaM, CCaMK phosphorylates CYCLOPS or IPD3 in *Medicago truncatula*, which are required for symbiosis (Yano et al., 2008).

CCaMK has been well studied not only because of its unique protein structure, but also due to its critical role in the symbiotic interaction between leguminous plants and bacteria and/or fungi (Patil et al., 1995; Ramachandiran et al., 1997; Harper et al., 2004). The protein structure of CCaMK

contains a catalytic domain followed by a CaM-binding/autoinhibitory domain and three EF hand motifs (Sathyanarayanan et al., 2001; Sathyanarayanan and Poovaiah, 2002; Singh and Parniske, 2012). CCaMK is regulated by free Ca^{2+} which binds to the EF hand motifs and Ca^{2+}-loaded CaM, which binds to the autoinhibitory domain (Lévy et al., 2004; Tirichine et al., 2006; Pumplin et al., 2010). This two-step regulatory mechanism allows CCaMK to become active and promote phosphorylation of target proteins that regulate root nodule symbiosis and mycorrhizal arbuscule development (Wang and Poovaiah, 1999; Sathyanarayanan and Poovaiah, 2002; Parniske, 2004). Both regulatory domains are important during symbiotic response (Tirichine et al., 2006; Pumplin et al., 2010). Previous reports demonstrated that expressing only the kinase domain (KD) of this protein or expressing a mutant of the threonine at position 271 (Thr271), located in the KD, resulted in the formation of spontaneous nodules in the absence of bacteria in *Medicago* roots (Sathyanarayanan et al., 2001; Gleason et al., 2006; Tirichine et al., 2006). This indicates that CCaMK's autoinhibitory domain and the EF-hand motifs negatively regulate the kinase activity. Another report has also shown the importance of the EF hand motifs in negative regulation of CCaMK. This study indicated that the EF hand motifs bind free $Ca^{2+}$and keep the CCaMK inactive at basal Ca^{2+} concentrations (Shimoda et al., 2012). Conversely, if free Ca^{2+} is blocked from binding to the EF hand motifs, CCaMK becomes auto-activated (Hayashi et al., 2010; Miller et al., 2013). Recent reports have demonstrated that CCaMK might be regulated by DELLA proteins (Jin et al., 2016) and/or TOR (the target of rapamycin) protein kinase (Nanjareddy et al., 2016) which are essential for symbiotic rhizobial pathway. Furthermore, CCaMK gene is very well conserved among phytozome species (Wang et al., 2015). CCaMKs have been found in peanuts (*Arachis hypogaea*) and tomato (*Solanum lycopersicum*), where it may play roles in the symbiotic pathway (Peng et al., 2017) and/or disease resistance (Wang et al., 2015).

Generally, the key to the activation of the kinase requires the release of the protein's own autoinhibition, which can be accomplished by the binding of CaM to the autoinhibitory/CaM-binding domain (Hayashi et al., 2010; Antolín-Llovera et al., 2012). In 2011, researchers using an auto activated form of CCaMK concluded that CaM-binding is essential for nodulation development during rhizobial symbiosis, but it is not required for fungal symbiosis (Horváth et al., 2011). However, since this auto-activated form could no longer interact with either CaM or free Ca^{2+}, it is critical to study the relevance of the CaM-binding alone during the activation of CCaMK (Takeda et al., 2012). Furthermore, CCaMK protein structure is unique to plants and understanding of its activation and regulation is far from clear. There are reports which have focused in its KD and visinin-like domain and have determined their importance of specific amino acids that regulate its kinase activity in addition to calmodulin and Ca^{2+} binding. Studies on the relationship between calmodulin and Ca^{2+} binding and kinase activity could reveal how this kinase interprets the Ca^{2+} signature during the establishment of plant–microbe symbioses.

In this study, we used a site-directed mutagenesis approach to alter the Calmodulin-binding/autoinhibitory domain of CCaMK in order to observe any variation of the CaM-binding capacity of this protein kinase in the presence of Ca^{2+}. We generated a series of mutations at a critical residue in the autoinhibitory domain (Trp-342) and measured the effects of the mutations on CaM-binding capacity. We found that the mutant W342F has increased CaM-binding capacity, even in the absence of Ca^{2+}. Interestingly, roots expressing W342F developed nodules after rhizobial inoculation, but half of these nodules were smaller than normal and were poorly colonized by bacteria.

MATERIALS AND METHODS

Site-Directed Mutagenesis

Site-directed mutagenesis of CCaMK was performed using a high fidelity KOD DNA polymerase enzyme to construct the desired plasmid with the mutations, following protocol as described (Liu and Naismith, 2008). The mutated CCaMK cds were confirmed by sequencing.

Expression and Purification of CCaMK and Site-Directed Mutants

The full-length of CCaMK and its site-directed mutants were cloned into the bacterial expression system pET28b and transformed into *Escherichia coli* strain BL21 (DE3)/pLysS. The bacteria carrying the above plasmids were grown in LB liquid media containing kanamycin at 37°C until OD_{600} of the culture reached 0.5 units. Once the liquid culture reached this optimal density, 0.5 mM isopropyl β-D-1-thiogalactopyranoside (IPTG) was added to induce the recombinant protein. After 3-h induction, cells were harvested and broken using lysozyme treatment (1 mg/ml) followed by sonication. The recombinant protein was purified with Ni-NTA agarose affinity beads (Qiagen) as described in the manufacturer's manual. The purified proteins were dialyzed against buffer containing 40 mM Tris pH 7.6, 1 mM dithiothreitol (DTT), 1 mM EDTA, and 10% ethylene glycol. Dialyzed proteins were quantified by Bradford assay and stored at −80°C with 15% glycerol.

CaM-Binding Assays

The CaM-2 from *Arabidopsis* conjugated with horseradish peroxidase (CaM-HRP) was used to study the CaM-binding property of CCaMK mutants. The induced proteins of CCaMK and its mutants in pET28b were separated by SDS–PAGE (15%) and transferred onto PVDF membrane. The membrane was blocked in binding buffer (10 mM Tris pH 7.5, 150 mM NaCl, 1 mM $CaCl_2$) containing 5% non-fat dry milk for 1 h at room temperature, then incubated with milk containing binding buffer supplemented with AtCaM2-HRP (1:1000 dilution) for 1 h at room temperature. The membrane was then washed three times in binding buffer for 10 min each. To detect the CaM signal, the BM chemiluminescence Western blotting kit (Roche Applied Science) was used according to instructions from manufacturer.

Autophosphorylation Assays

The autophosphorylation assay was performed in 10 μl reaction mixture using 0.4 μg of CCaMK protein and its mutated versions. The reaction buffer contained 50 mM HEPES pH 7.5, 10 mM magnesium acetate, 1 mM DTT, 10 μM ATP and 0.5 μCi/μl [γ-^{32}P] ATP, in the presence of 5 mM EGTA with or without 1 μM of bovine brain CaM (Sigma); and 0.5 mM of $CaCl_2$ with or without bovine CaM. Samples were incubated at 30°C for 30 min. To stop the reaction, SDS–PAGE sample buffer was added, followed by boiling the samples for 2 min. Samples were separated by a 12.5% SDS–PAGE. Protein gel was then dried and exposed to autoradiography film (Kodak).

Substrate Phosphorylation Assays

All of the *in vitro* kinase assays used 0.4 μg of purified protein in a 10 μl total volume. The buffer contained 50 mM HEPES pH 7.5, 10 mM magnesium acetate, 1 mM DDT, 100 μM ATP, and 0.5 μCi/μl [γ-^{32}P] ATP in the presence of 5 mM EGTA or 0.5 mM $CaCl_2$ or 0.5 mM $CaCl_2$ with 1 μM of bovine brain CaM (Sigma). In order to determine substrate phosphorylation, two micrograms of a bovine myelin basic protein (MBP) was used as substrate. Reactions were stopped by adding SDS–PAGE sample buffer and then boiled for 1 min in water bath. Subsequently, sample reactions were analyzed in SDS–PAGE and gel as dried. The difference of substrate phosphorylation patterns at different conditions was observed by exposing gel to the Kodak autoradiography film.

Hairy Root Transformation

The generation of transgenic roots was performed using a binary vector (pDL28-DPR) containing the native promoter of CCaMK and a red fluorescent protein encoding region from *Discosoma* sp. (DsRed) driven by *Arabidopsis* ubiquitin-10 promoter. The full-length CCaMK and mutant gene (W342F) were digested with SpeI and SalI restriction enzymes and ligated into the binary vector. The verified constructs were transformed into *Agrobacterium rhizogenes* strain K599 to transform the rootless plantlets of wild-type and *ccamk-1* mutant of *M. truncatula* A17. The control groups used in this experiment were wild-type *M. truncatula* explants were transformed with the binary vector without any gene (empty vector). In the other control group, the *ccamk-1* mutant plants were introduced with the empty vector. Our experimental groups were as follows: The third and fourth group used *ccamk-1* plants which were transformed with the binary vector carrying the full-length CCaMK gene and W342F mutant gene, respectively. The seedlings were grown on buffered nodulation medium (BNM) agar plates with Kanamycin selection. After 3 weeks, the plants were screened for transgenic roots by using a Kodak imaging system (Model 4000MM) with corresponding filters for the expression of DsRed fluorescent protein. For the nodulation experiments, the plants with transgenic roots were inoculated with *Sinorhizobium meliloti* 2011 carrying a green fluorescent protein (GFP) reporter gene and transferred to sterilized growth pouches (Mega International). The inoculated seedlings were watered with 1/10 dilution of nitrogen-deprived nutrient media (BNM) and grown under 16/8-h light/dark cycle at 21°C for 28 days. At 28-days post-inoculation, nodules were counted and observed under a Leitz fluorescent stereomicroscope using optical filters for GFP. Green fluorescence verified the presence of living rhizobia inside the developed nodule.

Confocal Microscopy

Selected nodules were analyzed by Zeta 510 Meta confocal microscope in order to determine the location of the bacteria in the nodules formed on the roots of *ccamk-1* complemented with wild-type and mutated version of CCaMK (W342F). Nodules were excised in half and were stained with Calcofluor white, a special fluorescent stain that allows observation of cell walls of tissues due to its binding to cellulose and chitin. For this fluorescent stain, we used excitation filter of 365 nm and emission filter 420 nm in 10× microscope lenses. To determine GFP, we used excitation filter 380 nm and emission filter 480 nm. Merged pictures were obtained and subsequently analyzed.

RESULTS

A W342F Mutation in the CCaMK Autoinhibitory Binding Domain Can Positively Increase Its CaM-Binding Capacity

The CaM-binding domain in CCaMK interacts with CaM, therefore, site-directed mutations were generated in the CaM-binding/autoinhibitory domain to investigate whether the CaM-binding capacity and kinase activity are correlated. Four residues in the calmodulin-binding/autoinhibitory domain were selected: F327, L333, I338, and W342. Mutations in the latter one produced some interesting results. W342 was mutated to five different residues with less mass but similar hydrophobic property (**Figure 1A**). These mutants were tested for CaM-binding capability. The CaM-binding assay showed that one mutant, W342F, exhibited increased CaM-binding capacity as compared to wild-type CCaMK. W342L and W342I showed less binding to CaM in comparison to CCaMK and W342F. The mutant W343V no longer interacted with CaM, however, W342A mutant was able to bind to CaM with a similar capacity as wild-type CCaMK (**Figure 1B**).

Significance of W342F Mutant on Its Kinase Activity

In CCaMK, the binding of CaM to the autoinhibitory domain releases its autoinhibition and activates its kinase activity. Since the W342F mutant showed an increase in CaM-binding ability, we hypothesized that the kinase activity of this mutant could be increased. Therefore, we specifically focused on this potential "gain of function" mutant, and an *in vitro* kinase assay was carried out.

Normally, the autophosphorylation of CCaMK is very low in the absence of Ca^{2+}, and it increases drastically once Ca^{2+} is added to the reaction mixture. Similar to previously published reports, we found that the autophosphorylation of

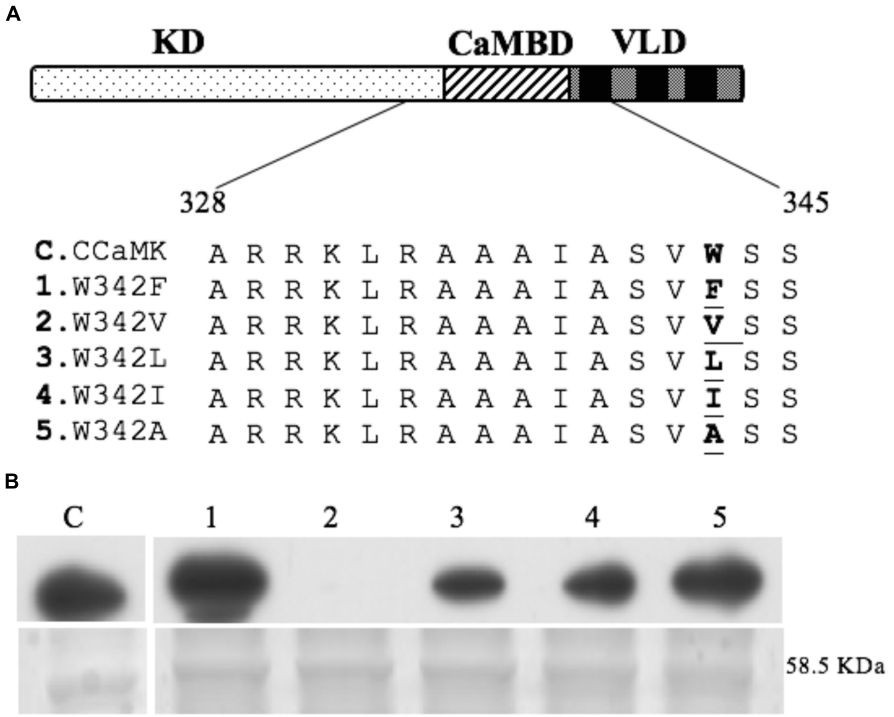

FIGURE 1 | Site-directed mutants and calmodulin-binding assay. Protein structure of CCaMK contains three domains: kinase domain (KD), calmodulin-binding/autoinhibitory domain (CAMBD) and visinin-like domains (VLD). Five mutants were generated by substituting the residue Trp-432 in the calmodulin-binding/autoinhibitory domain of CCaMK **(A)**. For calmodulin-binding assay **(B)**, total proteins from *Escherichia coli* (BL21) expressing the pET28-CCaMK or its mutated versions were separated on SDS–PAGE, transferred to PVDF membrane and incubated with horseradish peroxide (HRP)-conjugated CaM in the presence of Ca^{2+} (1 mM). Upper: Calmodulin binding overlay assay of wild-type and all 5 of the mutants of CCaMK as showed in "**A**"; Lower: Coomassie staining of proteins from *E. coli* (BL21) expressing the pET28-CCaMK or its mutated versions (protein size: 58.5 kDa). The CaM-binding assay was repeated at least 4 times to corroborate the difference.

the wild-type CCaMK was decreased after the addition of CaM (Takezawa et al., 1996; Miller et al., 2013). Interestingly we found the W342F mutant was autophosphorylated even in the absence of Ca^{2+}. The W342F mutant was also autophosphorylated in the presence of CaM and 5 mM EGTA. In the presence of Ca^{2+}, both wildtype CCaMK and the W342F mutant underwent autophosphorylation. However, the autophosphorylation intensity of W342F mutant was reduced in comparison to wild-type CCaMK (**Figure 2A** and Supplementary Figures 1, 2). It seems that the activation of autophosphorylation in W342F mutant is no longer dependent on Ca^{2+}, on the contrary, it responds to the Ca^{2+} signal in an opposing manner as compared to wild-type CCaMK.

We used bovine MBP as substrate to test the substrate phosphorylation activities of CCaMK. These reactions were performed under three different conditions: (1) in the absence of Ca^{2+}, (2) in the presence of Ca^{2+}, and (3) in the presence of Ca^{2+} and CaM. The W342F mutant phosphorylated the substrate in all three conditions, with a slightly increased intensity in the presence of both Ca^{2+} and CaM. Nevertheless, in comparison to CCaMK, this mutant showed a clear reduction in substrate phosphorylation activity even in the presence of Ca^{2+} and CaM (**Figure 2B** and Supplementary Figures 1, 2). Thus, in the W342F mutant substrate phosphorylation is Ca^{2+}-independent and also CaM-independent, and barely responds to Ca^{2+} and CaM inputs.

W342F Negatively Regulates Root Nodule Symbiosis

With the clear indication that the phosphorylation activity of W342F mutant differs from wild-type CCaMK in its biochemical property, we wanted to test the effect of the W342F on nodule formation. The loss-of-function *ccamk-1 Medicago* plants were transformed with W342F or CCaMK by *Agrobacterium rhizogenes* transformation. The transformed roots were inoculated with *S. meliloti* 2011 tagged with a GFP. The *ccamk-1* plants inoculated with *S. meliloti* 2011-GFP did not produce nodules. The *ccamk-1* mutant complemented with wild-type CCaMK produced pink mature nodules at 28-days post-inoculation with *S. meliloti* 2011-GFP. Interestingly, at 28-days post-inoculation, the *ccamk-1* plants transformed with W342F were able to produce nodules, indicating that the W342F mutant can complement the *ccamk-1* plants (**Figures 3**, **4**). The total number of nodules produced on the roots of *ccamk-1* mutant complemented with the W342F mutant (*ccamk-1* + W342F) was comparable to the number of nodules on roots of *ccamk-1* mutant

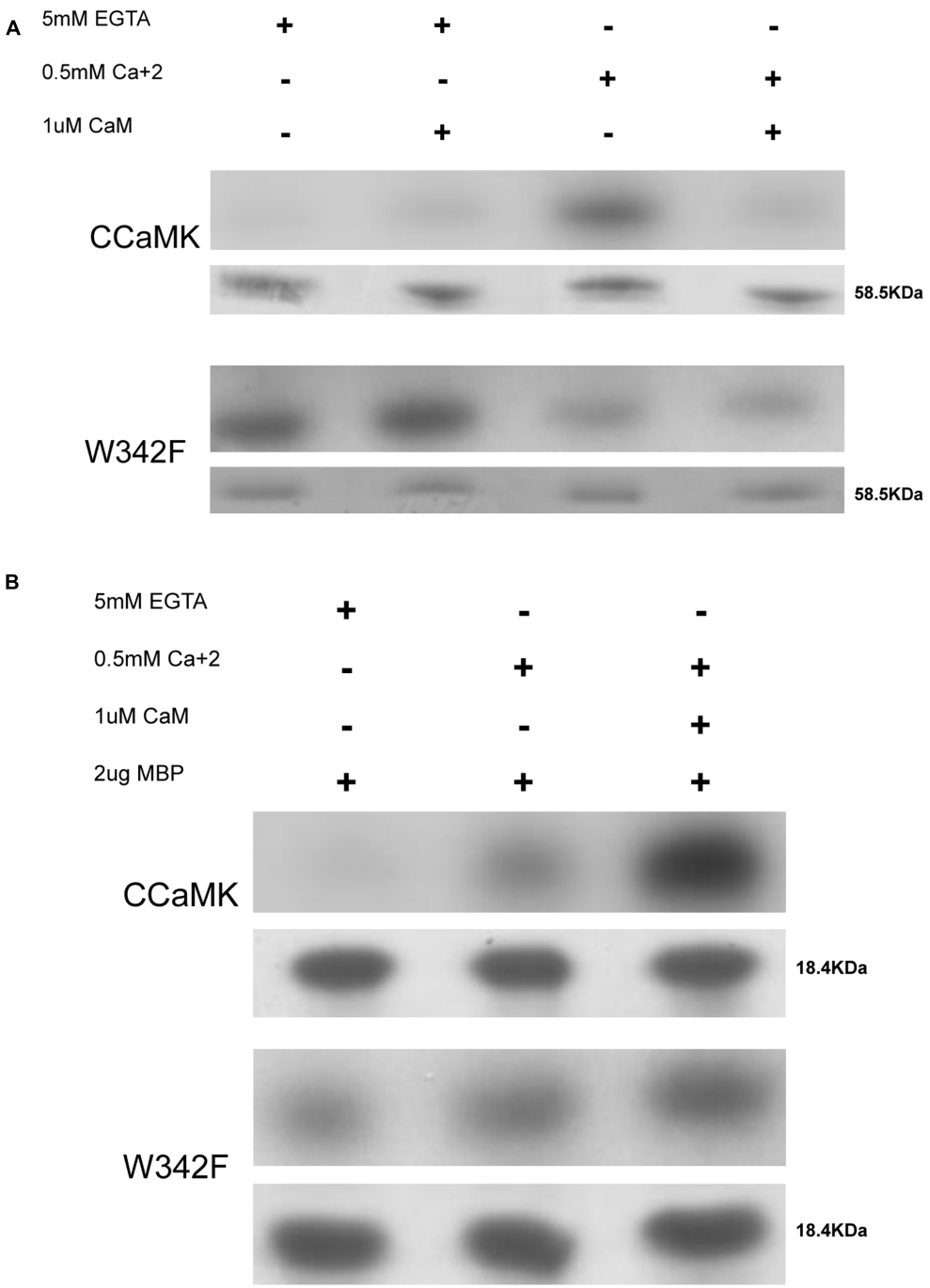

FIGURE 2 | Kinase activity assays of W342F and CCaMK. Autophosphorylation was performed at 30°C for 30 min. **(A)** CCaMK did not significantly phosphorylate itself in the absence of Ca^{2+}. In the presence of Ca^{2+}, CCaMK showed drastically increased autophosphorylation, which remarkably decreased once calmodulin was added. The W342F mutant showed very high levels of autophosphorylation in the absence of Ca^{2+} as compared to CCaMK, indicating that the mutant behaves in a Ca^{2+}-independent manner. Upper: Autoradiograph film demonstrating the autophosphorylation activity of CCaMK and W432F. Lower: Coomassie staining of the purified proteins from *E. coli* (BL21) expressing the pET28-CCaMK and W342F. **(B)** Substrate phosphorylation of CCaMK and W342F. The substrate phosphorylation of CCaMK and W342F was determined in the absence (5 mM EGTA), or presence of Ca^{2+} (0.5 mM $CaCl_2$), or Ca^{2+} and calmodulin together (0.5 mM $CaCl_2$ + 1 μM calmodulin). 2 μg of bovine myelin basic protein (MBP) was used as the substrate. Substrate phosphorylation of W342F in the absence and presence of Ca^{2+} did not follow a similar pattern compared to CCaMK. This mutant displayed a Ca^{2+}- and/or calmodulin-independent substrate phosphorylation capacity, but the maximum level of MBP phosphorylation intensity catalyzed by W342F was remarkably lower than substrate phosphorylation intensity catalyzed by CCaMK in the presence of Ca^{2+} and calmodulin. The kinase activity assays were repeated three times. Upper: Autoradiograph film showing the substrate phosphorylation activity of CCaMK and W432F; Lower: Coomassie staining of MBP substrate (2 μg).

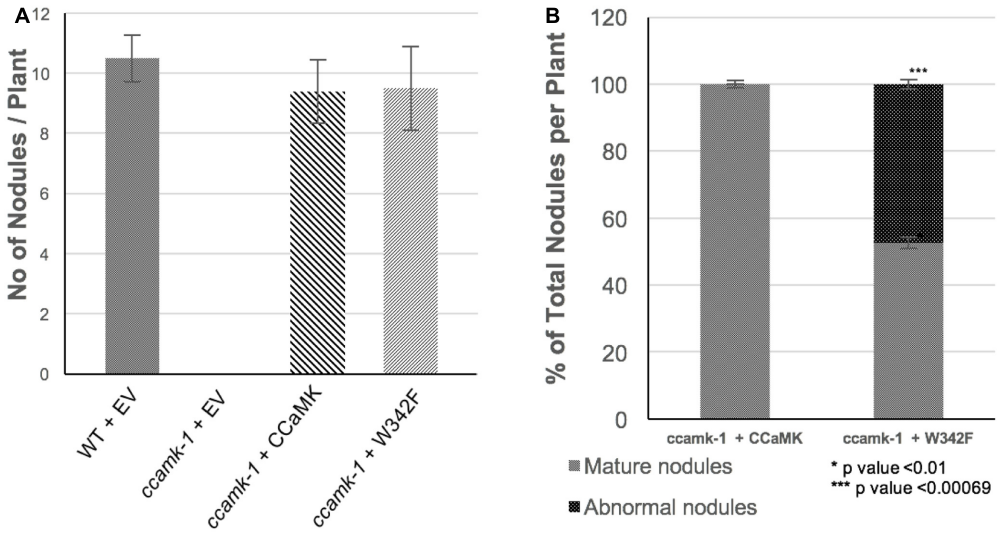

FIGURE 3 | The W342F mutant plants are able to form altered nodules. The roots of *ccamk-1* mutant were transformed with the W342F mutant of CCaMK, roots of WT and *ccamk-1* transformed with empty vector were used as positive and negative controls. **(A)** The number of nodules per plant for each construct was quantitated 28-days after inoculation with *Sinorhizobium meliloti* 2011-Green fluorescent protein (GFP). **(B)** Phenotypic difference of nodule development on *ccamk-1* roots complemented with W342F and CCaMK. W342F mutation resulted in significant increase (*p*-value = 0.00069) in the number of small nodules.

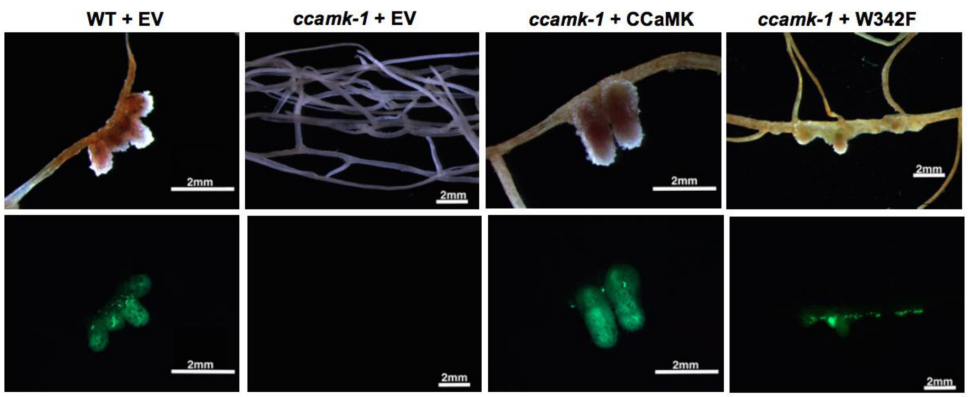

FIGURE 4 | W342F mutation resulted in altered nodule development. Root phenotypes were observed for each construct. Upper: Bright field picture. Lower: GFP fluorescent image of bacteria established in the nodule structure (green color). The W342F mutant complemented *ccamk-1* for root nodule symbiosis.

complemented with wild-type CCaMK (*ccamk-1* + CCaMK) (**Figure 3A**).

Although the total number of nodules was equivalent between *ccamk-1* + CCaMK and *ccamk-1* + W342F plants, the number of mature, pink nodules on the *ccamk-1* + W342F plants roots was significantly less than that on the *ccamk-1* + CCaMK roots (*p*-value = 0.01). The *ccamk-1* + CCaMK roots produced 100% mature, pink nodules after inoculation with rhizobia. Approximately 50% of the nodules on the *ccamk-1* + W342F plants were small abnormal nodules. These small nodules were not observed in the wild-type CCaMK inoculated with rhizobia (*p*-value = 0.00069) (**Figure 3B**). The abnormal nodules were white, indicating poor colonization by rhizobia (**Figure 5A**). Confocal microscopic analysis revealed that GFP-labeled *S. meliloti* 2011 was inside these small nodules but the distribution patterns of the bacteria in the nodule differed from that of the normal mature nodules (**Figure 5B**).

DISCUSSION

Extensive studies have been conducted by using site-directed mutagenesis as a powerful tool to manipulate the coding region of various genes. We took advantage of this well-known strategy to modify a residue on the autoinhibitory/CaM-binding domain in order to alter its well-defined structure and modify the CaM-binding capacity of CCaMK. Altering the CaM-binding capacity of CCaMK should provide a better understanding of the regulation of CCaMK's autoinhibitory domain.

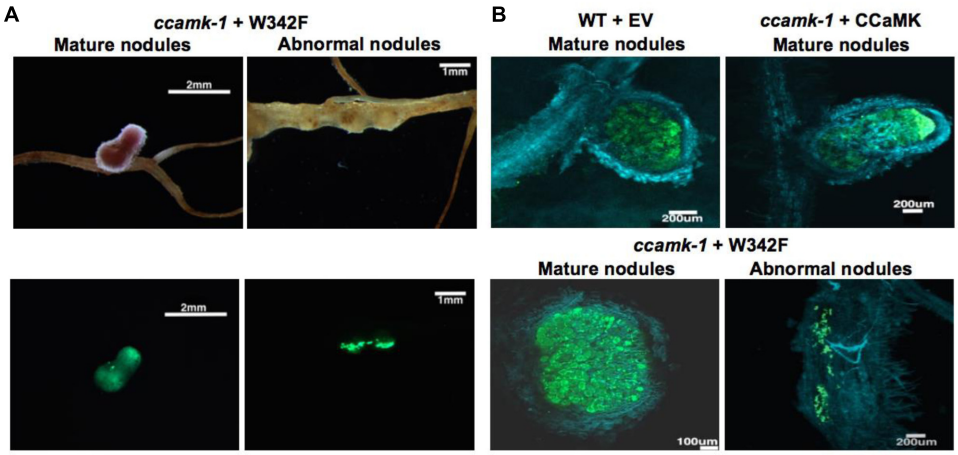

FIGURE 5 | (A) Morphological differences in nodules produced on roots complemented with W342F and CCaMK; **(B)** Confocal microscopic images of mature nodules from roots of wild-type *Medicago truncatula* and *ccamk-1* knockout complemented with CCaMK and W342F mutant. Blue color indicates cell wall tissue stained with Calcofluor white. Green color shows living *S. meliloti* 2011.

The CaM-binding domain contains particular structural features: it forms an α helix with a net positive charge and two hydrophobic anchor residues on one side. These characteristics allow CaM to bind easily in the presence of Ca^{2+} (Yang et al., 2007). Typically, CaM contains two lobes at its N- and C-terminals that are connected by a helix linker, and in the presence of Ca^{2+}, these two lobes will wrap the CaM-binding domain (Tidow and Nissen, 2013). However, there have been reports that some CaM-binding domains showed increased affinity to either of the terminals (Snedden and Fromm, 2001; Liu et al., 2012). This suggests that manipulating the α helix motif can modify its capacity to bind to CaM (Jang et al., 2011; Gifford et al., 2013).

One amino acid in the autoinhibitory/CaM-binding domain of CCaMK (W342) was replaced by amino acids with similar hydrophobicity but smaller masses in order to alter the α helix structure of the CaM-binding domain. Our data showed that reducing the mass of the selected amino acid could alter the capacity of CCaMK to interact with CaM. The mutant W342F showed an increase of CaM-binding in comparison to CCaMK, in addition, mutations W342L and W342I were able to interact with CaM but at lower levels. The mutant W342V did not interact with CaM. Interestingly, W342A mutant was able to bind to CaM similar to wild-type CCaMK even though its mass is relatively lower than that of the valine residue. Therefore, there is no direct correlation between mass of the residue at amino acid 342 and the CCaMK's CaM-binding activity.

W342F mutant had an increase of CaM-binding in comparison to CCaMK. Hence, we postulated that the kinase activity of the mutant could be significantly affected. *In vitro* analysis of CCaMK revealed that autophosphorylation of wild-type CCaMK is Ca^{2+}-dependent, and it is able to phosphorylate its substrate only in the presence of Ca^{2+} and CaM. In this study, we observed that W342F mutant was autophosphorylated and could phosphorylate MBP substrate in the absence of Ca^{2+} and CaM. This strongly suggests that the activity of W342F is Ca^{2+}- and CaM-independent. Even though W342F was able to phosphorylate MBP *in vitro* in the presence of Ca^{2+} and CaM, but the mutant barely responded to Ca^{2+} and CaM stimulation, the intensity of maximum level of MBP phosphorylation was reduced in comparison to that catalyzed by wild-type CCaMK. These results clearly indicate that the CaM-binding domain is critical for the activation of CCaMK. Also, they suggest that CCaMK protein structure may be critical for its regulation because of the possible structural changes when Ca^{2+} and CaM bind. The proximity of W342 to two well-known autophosphorylation sites S343 and S344 might suggest that of Trp-342 could possibly play a role during the autophosphorylation of these two sites (Routray et al., 2013; Jauregui et al., 2017).

Our physiological results demonstrated that the W342F mutation has a negative effect on the nodule morphology, since a significant portion of the nodules observed in the *ccamk-1* + W342F plants were abnormal. These abnormal nodules were smaller and appeared to be infected with fewer rhizobia. This may correlate with the compromised substrate phosphorylation. The W342F mutant exhibited substrate phosphorylation in both the presence and absence of Ca^{2+} and CaM, but the intensity of the phosphorylation was less than that of the wild-type in the presence of Ca^{2+} and CaM. This suggests that even though this mutant could be activated in the absence and presence of Ca^{2+} or CaM, it may not be able to sufficiently phosphorylate the target protein in order to obtain a well-developed, mature nodule in the root. In addition, our mutants did not produce any spontaneous nodules in the absence of bacteria (data not shown). This suggests that enhancing autophosphorylation and substrate phosphorylation in the absence of Ca^{2+} and CaM does not result in an "autoactive" kinase that can stimulate a pathway toward spontaneous nodulation. Therefore, we hypothesize that a threshold of kinase activity must be reached and this could

trigger the production of normal, mature nodules. Since our mutant showed some reduction in the intensity of substrate phosphorylation in presence of Ca^{2+} and CaM, this suggests that phosphorylation may not reach the putative threshold. Hence, the development of many nodules cannot reach the mature stage. Another possibility is that the stability of W342F mutation could be compromised when expressed in the roots.

This study documents that altering the autoinhibitory domain of CCaMK can significant increase the CaM-binding capacity of CCaMK which leads to a negative impact on root nodule development. Understanding of some target proteins of CCaMK involved in the regulation of nodule development might help to understand how CCaMK is involved not only for decoding Ca^{2+} oscillation but also in regulating some down-stream targets of root nodule symbiosis.

AUTHOR CONTRIBUTIONS

EJ conceived the idea for this project in consultation with BP and LD, performed most of the experiments, analyzed results and wrote most of the paper. LD and CG advised, helped in data analysis and supported with further ideas and experiments for the project. BP provided financial support, helped in planning, executing and leading the project. EJ, LD, CG, and BP were involved in manuscript preparation.

FUNDING

This research was supported by the National Science Foundation grant (1021344), and the Washington State University Agricultural Research Center.

ACKNOWLEDGMENTS

The authors thank Prof. R. Geurts for sharing the *Sinorhizobium meliloti* strain. The authors also acknowledge the WSU Franceschi Microscopy and Imaging Center for assistance with the Confocal microscopy. The authors also thank Lorie Mochel for her help in editing.

SUPPLEMENTARY MATERIAL

The Supplementary Material for this article can be found online at: https://www.frontiersin.org/articles/10.3389/fpls.2017.01921/full#supplementary-material

REFERENCES

Antolín-Llovera, M., Ried, M. K., Binder, A., and Parniske, M. (2012). Receptor kinase signaling pathways in plant-microbe interactions. *Annu. Rev. Phytopathol.* 50, 451–473. doi: 10.1146/annurev-phyto-081211-173002

Du, L., Ali, G. S., Simons, K. A., Hou, J., Yang, T., Reddy, A. S. N., et al. (2009). Ca^{2+}/calmodulin regulates salicylic-acid-mediated plant immunity. *Nature* 457, 1154–1158. doi: 10.1038/nature07612

Du, L., and Poovaiah, B. W. (2005). Ca^{2+}/calmodulin is critical for brassinosteroid biosynthesis and plant growth. *Nature* 437, 741–745. doi: 10.1038/nature07612

Gifford, J. L., Jamshidiha, M., Mo, J., Ishida, H., and Vogel, H. J. (2013). Comparing the calcium binding abilities of two soybean calmodulins: towards understanding the divergent nature of plant calmodulins. *Plant Cell* 25, 4512–4524. doi: 10.1105/tpc.113.113183

Gleason, C., Chaudhuri, S., Yang, T., Muñoz, A., Poovaiah, B. W., and Oldroyd, G. E. D. (2006). Nodulation independent of rhizobia induced by a calcium-activated kinase lacking autoinhibition. *Nature* 441, 1149–1152. doi: 10.1038/nature04812

Harper, J. F., Breton, G., and Harmon, A. (2004). Decoding Ca^{2+} signals through plant protein kinases. *Annu. Rev. Plant Biol.* 55, 263–288. doi: 10.1146/annurev.arplant.55.031903.141627

Hayashi, T., Banba, M., Shimoda, Y., Kouchi, H., Hayashi, M., and Imaizumi-Anraku, H. (2010). A dominant function of CCaMK in intracellular accommodation of bacterial and fungal endosymbionts. *Plant J.* 63, 141–154. doi: 10.1111/j.1365-313X.2010.04228.x

Horváth, B., Yeun, L. H., Domonkos, A., Halász, G., Gobbato, E., Ayaydin, F., et al. (2011). *Medicago truncatula* IPD3 is a member of the common symbiotic signaling pathway required for rhizobial and mycorrhizal symbioses. *Mol. Plant. Microbe Interact.* 24, 1345–1358. doi: 10.1094/MPMI-01-11-0015

Jang, D. J., Ban, B., and Lee, J. A. (2011). Characterization of novel calmodulin binding domains within IQ motifs of IQGAP1. *Mol. Cells* 32, 511–518. doi: 10.1007/s10059-011-0109-4

Jauregui, E., Du, L., Gleason, C., and Poovaiah, B. W. (2017). Autophosphorylation of calcium/calmodulin-dependent protein kinase (CCaMK) at S343 or S344 generates an intramolecular interaction blocking the CaM-binding. *Plant Signal. Behav.* 12, e1343779. doi: 10.1080/15592324.2017.1343779

Jin, Y., Liu, H., Luo, D., Yu, N., Dong, W., Wang, C., et al. (2016). DELLA proteins are common components of symbiotic rhizobial and mycorrhizal signaling pathways. *Nat. Commun.* 7:12433. doi: 10.1038/ncomms12433

Lévy, J., Bres, C., Geurts, R., Chalhoul, B., Kulikova, O., Gérard, D., et al. (2004). A putative Ca^{2+} and calmodulin-dependent protein kinase required for bacterial and fungal symbioses. *Science* 303, 1361–1364. doi: 10.1126/science.1093038

Liu, H., and Naismith, J. H. (2008). An efficient one-step site-directed deletion, insertion, single and multiple-site plasmid mutagenesis protocol. *BMC Biotechnol.* 8:91. doi: 10.1186/1472-6750-8-91

Liu, Y., Zheng, X., Mueller, G. A., Sobhany, M., DeRose, E., Zhang, Y., et al. (2012). Crystal structure of calmodulin binding domain of Orai1 in complex with Ca^{2+}/calmodulin displays a unique binding mode. *J. Biol. Chem.* 287, 43030–43041. doi: 10.1074/jbc.M112.380964

Miller, J. B., Pratap, A., Miyahara, A., Zhou, L., Bornemann, S., Morris, R. J., et al. (2013). Calcium/calmodulin-dependent protein kinase is negatively and positively regulated by calcium, providing a mechanism for decoding calcium responses during symbiosis signaling. *Plant Cell* 25, 5053–5066. doi: 10.1105/tpc.113.116921

Nanjareddy, K., Blanco, L., Arthikala, M.-K., Alvarado-Affantranger, X., Quinto, C., Sánchez, F., et al. (2016). A legume TOR protein kinase regulates *rhizobium* symbiosis and is essential for infection and nodule development. *Plant Phys.* 172, 2002–2020. doi: 10.1104/pp.16.00844

Parniske, M. (2004). Molecular genetics of the arbuscular mycorrhizal symbiosis. *Curr. Opin. Plant Biol.* 7, 414–421. doi: 10.1016/j.pbi.2004.05.011

Patil, S., Takezawa, D., and Poovaiah, B. W. (1995). Chimeric plant calcium/calmodulin-dependent protein kinase gene with a neural visinin-like calcium-binding domain. *Proc. Natl. Acad. Sci. U.S.A.* 92, 4897–4901.

Peng, Z., Liu, F., Wang, L., Zhou, H., Paudel, D., Tan, L., et al. (2017). Transcriptome profiles reveal gene regulation of peanut (*Arachis hypogaea* L.) nodulation. *Sci. Rep.* 7:40066. doi: 10.1038/srep40066

Poovaiah, B. W., Du, L., Wang, H., and Yang, T. (2013). Recent advances in calcium/calmodulin-mediated signaling with an emphasis on plant-microbe interactions. *Plant Physiol.* 163, 531–542. doi: 10.1104/pp.113.220780

Pumplin, N., Mondo, S. J., Topp, S., Starker, C. G., Gantt, J. S., and Harrison, M. J. (2010). *Medicago truncatula* Vapyrin is a novel protein required for arbuscular mycorrhizal symbiosis. *Plant J.* 61, 482–494. doi: 10.1111/j.1365-313X.2009.04072.x

Ramachandiran, S., Takezawa, D., Wang, W., and Poovaiah, B. W. (1997). Functional domains of plant chimeric calcium/calmodulin-dependent protein kinase: regulation by autoinhibitory and visinin-like domains. *J. Biochem.* 121, 984–990. doi: 10.1093/oxfordjournals.jbchem.a021684

Routray, P., Miller, J. B., Du, L., Oldroyd, G., and Poovaiah, B. W. (2013). Phosphorylation of S344 in the calmodulin-binding domain negatively affects CCaMK function during bacterial and fungal symbioses. *Plant J.* 76, 287–296. doi: 10.1111/tpj.12288

Sathyanarayanan, P. V., and Poovaiah, B. W. (2002). Autophosphorylation-dependent inactivation of plant chimeric calcium/calmodulin-dependent protein kinase. *Eur. J. Biochem.* 269, 2457–2463. doi: 10.1046/j.1432-1033.2002.02904.x

Sathyanarayanan, P. V., Siems, W. F., Jones, J. P., and Poovaiah, B. W. (2001). Calcium-stimulated autophosphorylation site of plant chimeric calcium/calmodulin-dependent protein kinase. *J. Biol. Chem.* 276, 32940–32947. doi: 10.1074/jbc.M009648200

Shimoda, Y., Han, L., Yamazaki, T., Suzuki, R., Hayashi, M., and Imaizumi-Anraku, H. (2012). Rhizobial and fungal symbioses show different requirements for calmodulin binding to calcium calmodulin-dependent protein kinase in *Lotus japonicus*. *Plant Cell* 24, 304–321. doi: 10.1105/tpc.111.092197

Singh, S., and Parniske, M. (2012). Activation of calcium- and calmodulin-dependent protein kinase (CCaMK), the central regulator of plant root endosymbiosis. *Curr. Opin. Plant Biol.* 15, 444–453. doi: 10.1016/j.pbi.2012.04.002

Snedden, W. A., and Fromm, H. (2001). Calmodulin as a versatile calcium signal transducer in plants. *New Phytol.* 125, 35–66. doi: 10.1046/j.1469-8137.2001.00154.x

Takeda, N., Maekawa, T., and Hayashi, M. (2012). Nuclear-localized and deregulated calcium- and calmodulin-dependent protein kinase activates rhizobial and mycorrhizal responses in *Lotus japonicus*. *Plant Cell* 24, 810–822. doi: 10.1105/tpc.111.091827

Takezawa, D., Ramachandiran, S., Paranjape, V., and Poovaiah, B. W. (1996). Dual regulation of a chimeric plant serine/threonine kinase by calcium and calcium/calmodulin. *J. Biol. Chem.* 271, 8126–8132. doi: 10.1074/jbc.271.14.8126

Tidow, H., and Nissen, P. (2013). Structural diversity of calmodulin binding to its target sites. *FEBS J.* 280, 5551–5565. doi: 10.1111/febs.12296

Tirichine, L., Imaizumi-Anraku, H., Yoshida, S., Murakami, Y., Madsen, L. H., Miwa, H., et al. (2006). Deregulation of a Ca^{2+}/calmodulin-dependent kinase leads to spontaneous nodule development. *Nature* 441, 1153–1156. doi: 10.1038/nature04862

Wang, J.-P., Munyampundu, J.-P., Xu, Y.-P., and Cai, X.-Z. (2015). Phylogeny of plant calcium and calmodulin-dependent protein kinases (CCaMKs) and functional analyses of tomato CCaMK in disease resistance. *Front. Plant Sci.* 6:1075. doi: 10.3389/fpls.2015.01075

Wang, W., and Poovaiah, B. W. (1999). Interaction of plant chimeric calcium/calmodulin-dependent protein kinase with a homolog of eukaryotic elongation factor-1. *J. Biol. Chem.* 274, 12001–12008. doi: 10.1074/jbc.274.17.12001

Yang, T., Du, L., and Poovaiah, B. W. (2007). Concept of redesigning proteins by manipulating calcium/calmodulin-binding domains to engineer plants with altered traits. *Funct. Plant Biol.* 34, 343. doi: 10.1071/FP06293

Yano, K., Yoshida, S., Müller, J., Singh, S., Banba, M., Vickers, K., et al. (2008). CYCLOPS, a mediator of symbiotic intracellular accommodation. *Proc. Natl. Acad. Sci. U.S.A.* 105, 20540–20545. doi: 10.1073/pnas.0806858105

Yuan, P., Jauregui, E., Du, L., Tanaka, K., and Poovaiah, B. W. (2017). Calcium signatures and signaling events orchestrate plant-microbe interactions. *Curr. Opin Plant Biol.* 38, 173–183. doi: 10.1016/j.pbi.2017.06.003

Conflict of Interest Statement: The authors declare that the research was conducted in the absence of any commercial or financial relationships that could be construed as a potential conflict of interest.

frontiers in Plant Science

ORIGINAL RESEARCH
published: 07 September 2017
doi: 10.3389/fpls.2017.01548

The Soybean *Rfg1* Gene Restricts Nodulation by *Sinorhizobium fredii* USDA193

Yinglun Fan[1,2†], Jinge Liu[2†], Shanhua Lyu[1,2], Qi Wang[2], Shengming Yang[2] and Hongyan Zhu[2]*

[1] College of Agriculture, Liaocheng University, Liaocheng, China, [2] Department of Plant and Soil Sciences, University of Kentucky, Lexington, KY, United States

Sinorhizobium fredii is a fast-growing rhizobial species that can establish a nitrogen-fixing symbiosis with a wide range of legume species including soybeans (*Glycine max*). In soybeans, this interaction shows a high level of specificity such that particular *S. fredii* strains nodulate only a limited set of plant genotypes. Here we report the identification of a dominant gene in soybeans that restricts nodulation with *S. fredii* USDA193. Genetic mapping in an F2 population revealed co-segregation of the underlying locus with the previously cloned *Rfg1* gene. The *Rfg1* allele encodes a member of the Toll-interleukin receptor/nucleotide-binding site/leucine-rich repeat class of plant resistance proteins that restricts nodulation by *S. fredii* strains USDA257 and USDA205, and an allelic variant of this gene also restricts nodulation by *Bradyrhizobium japonicum* USDA122. By means of complementation tests and CRISPR/Cas9-mediated gene knockouts, we demonstrate that the *Rfg1* allele also is responsible for resistance to nodulation by *S. fredii* USDA193. Therefore, the *Rfg1* allele likely provides broad-spectrum resistance to nodulation by many *S. fredii* and *B. japonicum* strains in soybeans.

Keywords: soybean, nodulation, nitrogen fixation, rhizobial symbiosis, symbiosis specificity

OPEN ACCESS

Edited by:
Stig U. Andersen, Aarhus University, Denmark

Reviewed by:
Dugald Reid, Aarhus University, Denmark
Erik Limpens, Wageningen University and Research, Netherlands

***Correspondence:**
Hongyan Zhu
hzhu4@uky.edu

† These authors have contributed equally to this work.

Specialty section:
This article was submitted to Plant Microbe Interactions, a section of the journal Frontiers in Plant Science

Received: *01 July 2017*
Accepted: *24 August 2017*
Published: *07 September 2017*

Citation:
Fan Y, Liu J, Lyu S, Wang Q, Yang S and Zhu H (2017) The Soybean Rfg1 Gene Restricts Nodulation by Sinorhizobium fredii USDA193. Front. Plant Sci. 8:1548. doi: 10.3389/fpls.2017.01548

INTRODUCTION

The leguminous plants are able to establish a symbiotic relationship with nitrogen-fixing soil bacteria called rhizobia. The symbiosis is featured by the formation of root nodules where the bacteria in nodule cells can convert atmospheric nitrogen into ammonia and make it available to the plant. This symbiotic partnership has important implications in sustainable agriculture because it reduces the need for nitrogen-based fertilizers.

The legume-rhizobial symbiosis starts with host perception of bacterially derived lipo-chitooligosaccharides known as nodulation (Nod) factors (Oldroyd et al., 2011). Recognition of Nod factors secreted by compatible bacteria induces cell divisions in the root cortex leading to the formation of nodule primordia, and at the same time initiates the infection process that delivers the bacteria into these primordia. Infection of most legumes such as soybeans (*Glycine max*) and alfalfa (*Medicago sativa*) is through root hairs. Bacteria are first entrapped by curled root hairs and multiply to form micro-colonies referred to as infection foci. From these foci, plant-made tubular-like structures, called infection threads, start to develop through local cell wall hydrolysis and invagination of the plant plasma membrane. The infection threads that are colonized by dividing bacteria proceed through the epidermal cell layer into the inner cortex where the nodule primordium has formed. Bacteria are then internalized in an endocytosis-like process

and surrounded by a host membrane, where they differentiate into nitrogen-fixing bacteroides and are confined in organelle-like structures called symbiosomes (Jones et al., 2007; Oldroyd et al., 2011).

While some bacteria can nodulate a wide range of hosts, most bacteria have strict host selectivity. As such, particular rhizobial species or strains nodulate only a narrow group of legume species or genotypes (Broughton et al., 2000; Perret et al., 2000; Wang et al., 2012). Understanding the genetic and molecular basis of this specificity is important for developing strategies to improve the agronomic potential of the root nodule symbiosis in agriculture. It has been reported that plant domestication and breeding processes have led to the reduced ability of the modern cultivars to interact with indigenous soil strains as compared to their wild progenitors (Mutch and Young, 2004; Kiers et al., 2007; Kim et al., 2014). In this case, development of cultivars that are promiscuous with indigenous strains would be beneficial. On the other hand, certain indigenous soil bacteria are highly competitive for nodulation with host legumes but with low nitrogen fixation efficiency. Under this latter scenario, it is desirable to grow plants that can restrict nodulation with low-efficient indigenous strains but nodulate preferentially with the effective inoculant strains (Keyser and Li, 1992; Devine and Kuykendall, 1996).

Establishment of a root nodule symbiosis requires mutual recognition of multiple molecular signals between the symbiotic partners (Jones et al., 2007; Deakin and Broughton, 2009; Oldroyd et al., 2011). Therefore, symbiotic specificity can be regulated by multiple mechanisms at different stages of the nodule development (Perret et al., 2000; Wang et al., 2012, 2017; Liu et al., 2014; Yang et al., 2017). In most legumes, bacterial infection and nodule formation is initiated by host recognition of rhizobial Nod factors (Lerouge et al., 1990; Geurts et al., 1997; Limpens et al., 2003; Radutoiu et al., 2003). Nod factors produced by different bacteria carry specific chemical decorations on the chitin backbone, and this structural diversity has been thought to be a major determinant of nodulation specificity in the legume–rhizobal interaction, particularly at the species level (Bras et al., 2000; Radutoiu et al., 2007). Similar to pathogenic bacteria, symbiotic rhizobia also use conserved microbe-associated molecular patterns (MAMPs) or secreted effectors to facilitate their interaction with the host (D'Haeze and Holsters, 2004; Fauvart and Michiels, 2008; Deakin and Broughton, 2009; Soto et al., 2009; Downie, 2010; Wang et al., 2012; Kawaharada et al., 2015). Accordingly, effector- or MAMP-triggered plant immunity mediated by host receptors also plays an important role in regulating host range of rhizobia (Yang et al., 2010; Wang et al., 2012; Faruque et al., 2015; Kawaharada et al., 2015; Tang et al., 2016).

We have cloned several dominant genes in soybeans (e.g., *Rj2*, *Rfg1*, and *Rj4*) that restrict nodulation with specific rhizobial strains (Yang et al., 2010; Tang et al., 2016). In these cases, symbiosis incompatibility is controlled in a similar manner as 'gene-for-gene' resistance against plant pathogens (Sadowsky et al., 1990; Devine and Kuykendall, 1996). *Rj2* and *Rfg1* are allelic genes, each encoding a typical Toll-interleukin receptor/nucleotide-binding site/leucine-rich repeat (TIR-NBS-LRR) resistance protein that confers resistance to nodulation by specific strains of *Bradyrhizobium japonicum* and *Sinorhizobium fredii*, respectively (Yang et al., 2010), while *Rj4* encodes a thaumatin-like pathogenesis-related protein that restricts nodulation by specific strains of *B. elkanii* (Tang et al., 2016). Moreover, the function of these nodulation-restrictive genes is dependent on the bacterial type III secretion system (Krishnan et al., 2003; Okazaki et al., 2009; Yang et al., 2010; Tsukui et al., 2013; Tsurumaru et al., 2015; Tang et al., 2016; Yasuda et al., 2016). These studies revealed an important role of effector-triggered plant immunity in the regulation of nodulation specificity in soybeans (Wang et al., 2012).

Here we describe the study of symbiotic incompatibility of soybean with *S. fredii* USDA193. A previous report suggested that restriction of nodulation by this strain is associated with the *Rj2* and/or *Rj3* loci (Nakano et al., 1997). Our study revealed a single dominant gene responsible for this incompatibility. Genetic mapping in an F2 population showed co-segregation of the underlying locus with the previously cloned *Rfg1* gene that confers resistance to nodulation by *S. fredii* strains USDA257 and USDA205 (Yang et al., 2010). Through complementation tests and CRISPR/Cas9-mediated gene disruption, we demonstrate that the *Rfg1* allele also is responsible for restricting nodulation by *S. fredii* USDA193. Our study suggests that the *Rfg1* locus is involved in the determination of nodulation specificity with multiple *S. fredii* and *B. japonicum* strains in soybeans.

MATERIALS AND METHODS

Plant Material, Nodulation Assay and Genotyping

The F2 mapping population was derived by crossing the North American cultivar 'Williams 82' with the cultivar 'Peking,' an introduction from China. Peking formed nitrogen-fixing nodules when inoculated with *S. fredii* USDA193 (Nod+) while Williams 82 restricted nodulation by this strain (Nod−) (Keyser et al., 1982). *S. fredii* USDA193, originally isolated from China (Keyser et al., 1982), was obtained from the National *Rhizobium* Germplasm Collection (USDA-ARS, Beltsville, MD, United States). The strain was cultured on YEM agar plates (yeast extract, 1.0 g/L; mannitol, 10.0 g/L; dipotassium phosphate, 0.5 g/L; magnesium sulfate, 0.2 g/L; sodium chloride, 0.1 g/L; calcium carbonate, 1.0 g/L; agar, 15.0 g/L) in the dark at 28°C for 4–5 days, and the bacterial paste was then collected and diluted in sterile water to OD_{600} of 0.1. For nodulation assay, each 1-week-old seedling was flood-inoculated with 10 mL of the bacterial suspension. Plants were grown in sterilized 50/50 Perlite-Turface mix in a growth chamber programmed for 16 h light at 26°C and 8 h dark at 23°C. Nodulation phenotype was assayed 4 weeks post inoculation. Genotyping was conducted by using a CAPS (cleaved amplified polymorphic sequences) marker developed based on a SNP (single nucleotide polymorphism) between the *Rfg1* (Williams 82) and *rfg1* (Peking) alleles. The primer pair used was 5′TGAGAGTACTGGAATGGTGGAG3′ and 5′TTGCTGATCGAACCACTCTG3′, and the restriction enzyme used was *Hpa*I.

Complementation Tests

The Williams 82 allele of *Rfg1* was used for complementation tests. Genomic DNA of the *Rfg1* allele was derived from the BAC clone Gm_WBa0019D20 of Williams 82 (Marek and Shoemaker, 1996) by digestion with *Pst*I and *Bmg*BI. The released 10.9-kb fragment included the 4.9-kb coding region, the 4.0 kb upstream of the start codon containing the promoter and 5′ untranslated region, and the 2.0 kb downstream of the stop codon encompassing the 3′ untranslated region. The DNA fragment was cloned into the binary vector pCAMBIA1305.1 through blunt end cloning. The binary vector was transferred into the Peking genetic background through hairy root transformation as described below. The transgenic roots were identified by GUS-staining because of the presence of a GUS expression cassette in the pCAMBIA1305.1 vector.

CRISPR/Cas9-Mediated Gene Knockout

The CRISPR/Cas9 gene knockout constructs were developed based on the pHSE401 vector described by Xing et al. (2014). Two pairs of oligos were designed to specifically target two different sites within the fourth exon of *Rfg1*. For the first targeted site, we used the oligo pair 5′ATTGATGAGGACTTAAAAAGCTC3′ and 5′AAACGAGCTTTTTAAGTCCTCAT3′. For the second targeted site, we used the oligo pair 5′ATTGACAGTAAGC CTTACTACCT3′ and 5′AAACAGGTAGTAAGGCTTACTGT3′. The underlined sequences represent the targeted positions. The oligo pairs were first annealed to produce a double-stranded fragment with 4-nt 5′ overhangs at both ends, and then ligated into the *Bsa*I-digested pHSE401 vector. The constructs were individually transformed to the Williams 82 (Nod−) background by means of hairy root transformation. To validate the CRISPR/Cas9-mediated gene disruption, the roots that formed nodules were subjected to DNA isolation, PCR amplification, and DNA sequencing. If the initial sequencing suggested the presence of multiple heterogeneous mutant alleles, the PCR product was ligated into pGEM T-Easy Vector System (Promega) and at least 10 colonies were selected for sequencing.

Construction of a Chimeric Gene of *Rfg1* and *Rj2*

The *Rfg1* allele that restricts nodulation by *S. fredii* USDA257 is allelic to *Rj2*, an allele that restricts nodulation by *B. japonicum* USDA122 (Yang et al., 2010). At this locus, there exist three type of alleles in natural populations of soybeans, including the *Rj2 (rfg1*) allele that restricts nodulation with USDA122 but allows nodulation with USDA257, the *rj2* (*Rfg1*) allele that permits nodulation with USDA122 but restricts nodulation with USDA257, and the *rj2* (*rfg1*) allele that nodulates with both strains. These allelic specificities are defined by seven amino-acid substitutions (Yang et al., 2010). However, we did not identify an *Rj2* (*Rfg1*) allele type that prohibits nodulation with both USDA122 and USDA257 in the surveyed soybean lines (Yang et al., 2010). We thus modified the *Rfg1* allele by replacing part of polymorphic sequence of *Rfg1* with the corresponding sequence of the *Rj2* allele, with the expectation to generate a chimeric gene that could lead to restriction of nodulation by both strains. For this purpose, we amplified two overlapping DNA fragments, one that contained the substitutions responsible for the *Rj2* allelic function and another that possessed the substitutions required for the *Rfg1* allelic function. We then used an overlapping PCR strategy to assemble the two DNA templates into a single one. The amplified fragment was then cloned into the *Eco*RI digested genomic construct of *Rfg1* mentioned above using the In-Fusion Advantage PCR Cloning Kits (Clontech). We tested the function of this chimeric allele by transferring it into Peking, a genotype that formed nodules with both USDA122 and USDA257. To avoid redundancy, we will provide a further description of this experiment in the "Results" section.

Hairy Root Transformation

Agrobacterium rhizogenes-mediated hairy root transformation was carried out based on the protocol described by Kereszt et al. (2007). Briefly, bacterial paste of the *A. rhizogenes* strain K599 that contains individual binary vectors was injected into the cotyledonary node of 1-week-old seedlings using a latex free syringe with a thin needle (0.4 mm × 13 mm) (1 ml 27G1/2, Becton, Dickinson & Co.). The infected seedlings were grown in sterile vermiculite and covered with plastic bags in a growth chamber to maintain high humidity. Two to three weeks after inoculation, when hairy roots were well developed at the infection sites, the main roots were removed, and the composite plants were inoculated with rhizobia. Nodulation assays were performed 4 weeks post inoculation.

Microscopic Analysis

Assay for root hair curling followed the method described in Yang et al. (2010). For anatomical analysis of nodules, nitrogen-fixing nodules of Peking and rudimentary nodules of Williams 82 were harvested 4 weeks post inoculation and immediately fixed in 4% paraformaldehyde (w/v) overnight at 4°C. The tissues were then dehydrated in a graded ethanol series followed by a graded series of xylene. After infiltrated in 50/50 Epon-Araldite resin and propylene oxide overnight and then in 75/25 Epon-Araldite resin and propylene oxide for 8 h, the samples were embedded in resin. Embedded tissues were sectioned (10 μm thick) with a microtome, stained with Toluidine Blue, and examined with bright-field optics.

RESULTS

Characterization of the Soybean–*S. fredii* USDA193 Interactions

Sinorhizobium fredii USDA193 formed mature nitrogen-fixing nodules on the roots of Peking (**Figure 1A**) but not on the roots of Williams 82 (**Figure 1B**). Despite being unable to form functional nodules in the Williams 82 background, the bacterial strain could frequently induce the formation of rudimentary nodules, bump-like small cortical proliferations on the roots (**Figure 1B**). In contrast to the infected nodules formed in the compatible interaction (**Figure 1C**), the rudimentary nodules on the roots of Williams 82 were completely devoid of infected

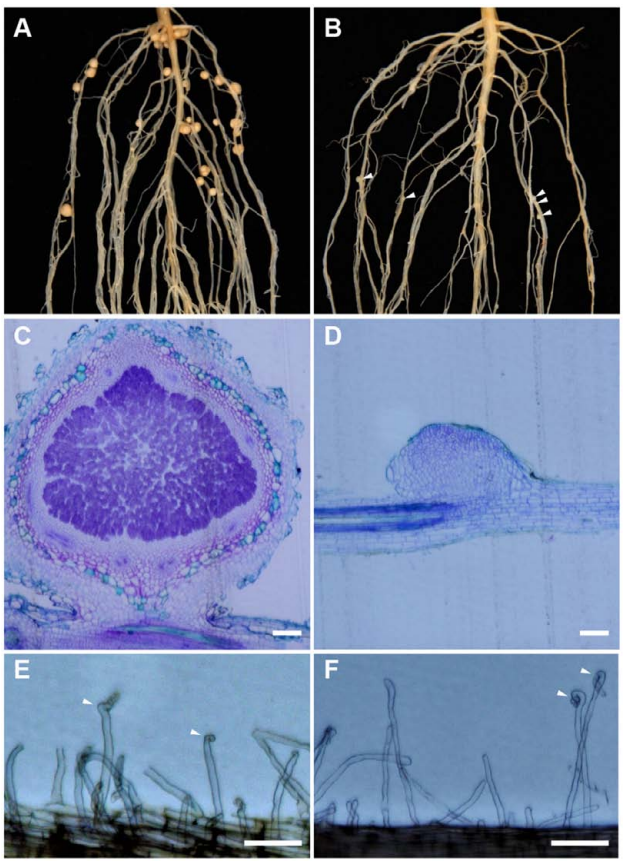

FIGURE 1 | Nodulation specificity associated with *Sinorhizobium fredii* USDA193 in soybean. The bacterial strain formed nitrogen-fixing nodules on Peking **(A)** but only small nodule primordia on Williams 82, as indicated by the arrowheads **(B)**. In the compatible Peking/USDA193 interaction, nodules developed normally and contained bacteria **(C)**, whereas in the incompatible interaction between Williams 82 and USDA193, the nodule primordia did not contain bacteria **(D)**. Bars = 100 μm. However, USDA193 induced root hair curling (indicated by arrowheads) on both Peking **(E)** and Williams 82 **(F)**. Photographs were taken 5 days post inoculation. Bars = 100 μm.

FIGURE 2 | Introduction of the *Rfg1* allele of Williams 82 into Peking led to restriction of nodulation on the transgenic roots by USDA193 (blue), but nodulation was normal on the wild-type roots (white).

bacteria; as such, the cortical cell division ceased at very early stage of the nodule development (**Figure 1D**). The ability to produce rudimentary nodules with USDA193 on the Williams 82 roots suggested that the early responses of Nod factor perception are not affected. Consistent with this inference, root hair curling, a hallmark of Nod factor responses, occurred in both compatible and incompatible interactions (**Figures 1E,F**). Thus, we concluded that the restriction of nodulation by *S. fredii* USDA193 in Williams 82 was not due to a failure in Nod factor perception but caused by the block of bacterial infection.

Restriction of Nodulation with USDA193 Is Controlled by a Single Dominant Gene Mapped to the *Rfg1* Locus

We carried out genetic analysis of the symbiosis incompatibility involving *S. fredii* USDA193 in an F2 population derived from the cross between Williams 82 (Nod-) and Peking (Nod+). From a small population of 122 plants inoculated by USDA193, 95 were Nod− and 27 were Nod+. The segregation statistically fits the 3:1 (Nod− to Nod+) ratio ($\chi^2 = 0.54$, $df = 1$, $P = 0.46$), suggesting that the restriction of nodulation by USDA193 in Williams 82 is controlled by a single dominant gene. The dominant nature of the nodulation-restrictive allele supports our hypothesis that the incompatible interaction between Williams 82 and USDA193 was not due to a failure in Nod factor signaling but resembles 'gene-for-gene' resistance in the plant–pathogen interactions.

Williams 82 and Peking showed the same phenotype when inoculated with *S. fredii* strains USDA257 and USDA193, and we previously reported that the resistance to nodulation with USDA257 in Williams 82 is controlled by the dominant *Rfg1* allele (*Glyma16g33780*) that encodes a TIR-NBS-LRR protein (Yang et al., 2010). We therefore suspected that *Rfg1* possibly also confers resistance to *S. fredii* USDA193. To test this possibility, we started the mapping experiment by using a polymorphic DNA marker developed from *Rfg1*. Consistent with our hypothesis, linkage analysis in the aforementioned F2 population revealed co-segregation between the nodulation phenotypes and the marker

genotypes. Thus, we considered *Rfg1* as a candidate gene that restricts nodulation by *S. fredii* USDA193.

Rfg1 Is Responsible for Resistance to Nodulation by *S. fredii* USDA193

We first tested the *Rfg1* gene by complementation tests using *A. rhizogenes*-mediated hairy root transformation. Because the transformation experiments were performed without selection, the hairy roots induced by *A. rhizogenes* included both transgenic and wild type, which can be readily distinguished by the GUS-staining assay. As shown in **Figure 2**, introduction of the *Rfg1* allele of Williams 82 into the Peking background resulted in complete block of nodule formation on the transgenic roots. From >20 composite transgenic plants that possessed both transgenic and wild-type roots, nodules were formed on the wild-type roots but not on the transgenic roots.

We further used the CRISPR/Cas9-based reverse genetics tool (Doudna and Charpentier, 2014) to knock out the *Rfg1* gene in the Williams 82 background (Nod−). For this purpose, we designed two gRNA vectors that individually target two different sites of the fourth exon (**Figures 3A,B**). The vectors were introduced to *A. rhizogenes* K599 for hairy root transformation, followed by assaying the nodulation capacity of the hairy roots by inoculation with *S. fredii* USDA193. For both vectors, we

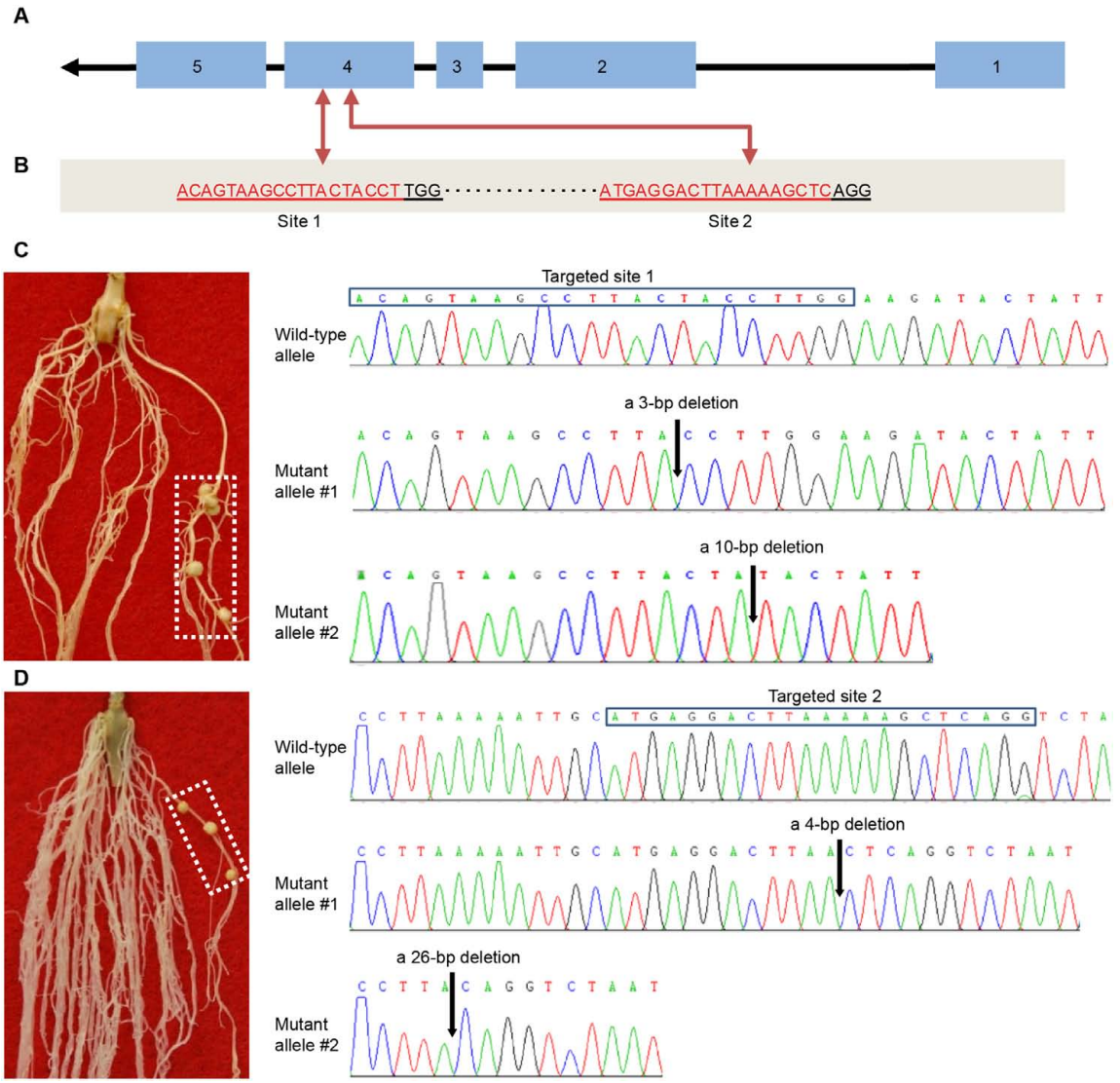

FIGURE 3 | CRISPR/Cas9-mediated knockout of *Rfg1* in the Williams 82 (Nod–) background. **(A)** Gene structure of *Rfg1*. The exons and introns are indicated by boxes and lines, respectively. Arrow indicates the transcription direction. **(B)** Two targeted sites on the fourth exon. The protospacer adjacent motif (PAM) is 'TGG' for the site 1 and 'AGG' for the site 2. **(C)** An example showing that knockout of *Rfg1* at the site 1 led to the formation of root nodules on a transgenic root (boxed). Sequence analysis revealed that this root contained two mutant alleles, one with a 3-bp deletion and another with a 10-bp deletion (indicated by arrows). **(D)** An example showing that knockout of *Rfg1* at the site 2 also resulted in the formation of root nodules on a transgenic root (boxed). Sequence analysis of the DNA from this root identified two mutant alleles, one with a 4-bp deletion and another with a 26-bp deletion (indicated by arrows).

obtained >30 putative transgenic roots from more than 50 independent plants that formed mature nitrogen-fixing nodules. DNA sequencing validated the targeted gene disruption in these roots and these roots did not contain the wild-type allele. Two examples are illustrated in **Figures 3C,D**. **Figure 3C** shows that a transgenic root forming nodules resulted from the knockout of *Rfg1* at the site 1, and sequence analysis revealed two mutant alleles, one with a 3-bp deletion and another with a 10-bp deletion. **Figure 3D** represents an example showing that knockout of *Rfg1* at the site 2 also led to the formation of root nodules on a transgenic root; sequence analysis identified two mutant alleles, one with a 4-bp deletion and another with a 26-bp deletion when compared with the wild-type allele. Taken together, we conclude that *Rfg1* is responsible for nodulation restriction by *S. fredii* USDA193 in Williams 82.

Functional Analysis of a Chimeric Gene of *Rfg1* and *Rj2*

Rfg1 and *Rj2* are allelic genes, each encoding a TIR-NBS-LRR protein of 1052 amino acids (Yang et al., 2010). A survey of a group of soybean lines identified three types of naturally occurring alleles, namely *Rj2 (rfg1)*, *rj2* (*Rfg1*), and *rj2* (*rfg1*) (Yang et al., 2010). The *Rj2 (rfg1)* allele restricts nodulation with USDA122 but not with USDA257; the *rj2* (*Rfg1*) allele restricts nodulation with USDA257 but not with USDA122; and the *rj2* (*rfg1*) allele allows nodulation with both strains. These allelic specificities are determined by seven amino acid substitutions occurring around the C-terminus of the NBS domain and the sixth LRR repeat (**Figures 4A,B**). Comparing between Rj2 (rfg1) and rj2 (rfg1) and between rj2 (Rfg1), and rj2 (rfg1) suggests that E452 and I490 are required for the *Rj2*-mediated nodulation restriction against USDA122, while E731, N736, S743, D756, and S758 are essential for *Rfg1*-mediated resistance against USDA257 and USDA193. If this inference is true, then the chimeric gene of *Rj2* and *Rfg1*, called *Rj2* (*Rfg1*), encoding a protein with E452, I490, E731, N736, S743, D756, and S758, would prevent nodulation with both strains. We generated multiple transgenic roots (from >100 independent plants) expressing the chimeric gene in Peking that carries an *rj2* (*rfg1*) allele and forms nodules with USDA257, USDA193, and USDA122. In consistence with our hypothesis, the transgenic roots restrict nodulation with both USDA257 (**Figure 4C**), USDA193 (**Figure 4D**), and USDA122 (**Figure 4E**). The transgenic roots retained their ability to nodulate with *B. japonicum* USDA110, a strain that nodulates both *Rj2* and *Rfg1* genotypes (**Figure 4F**).

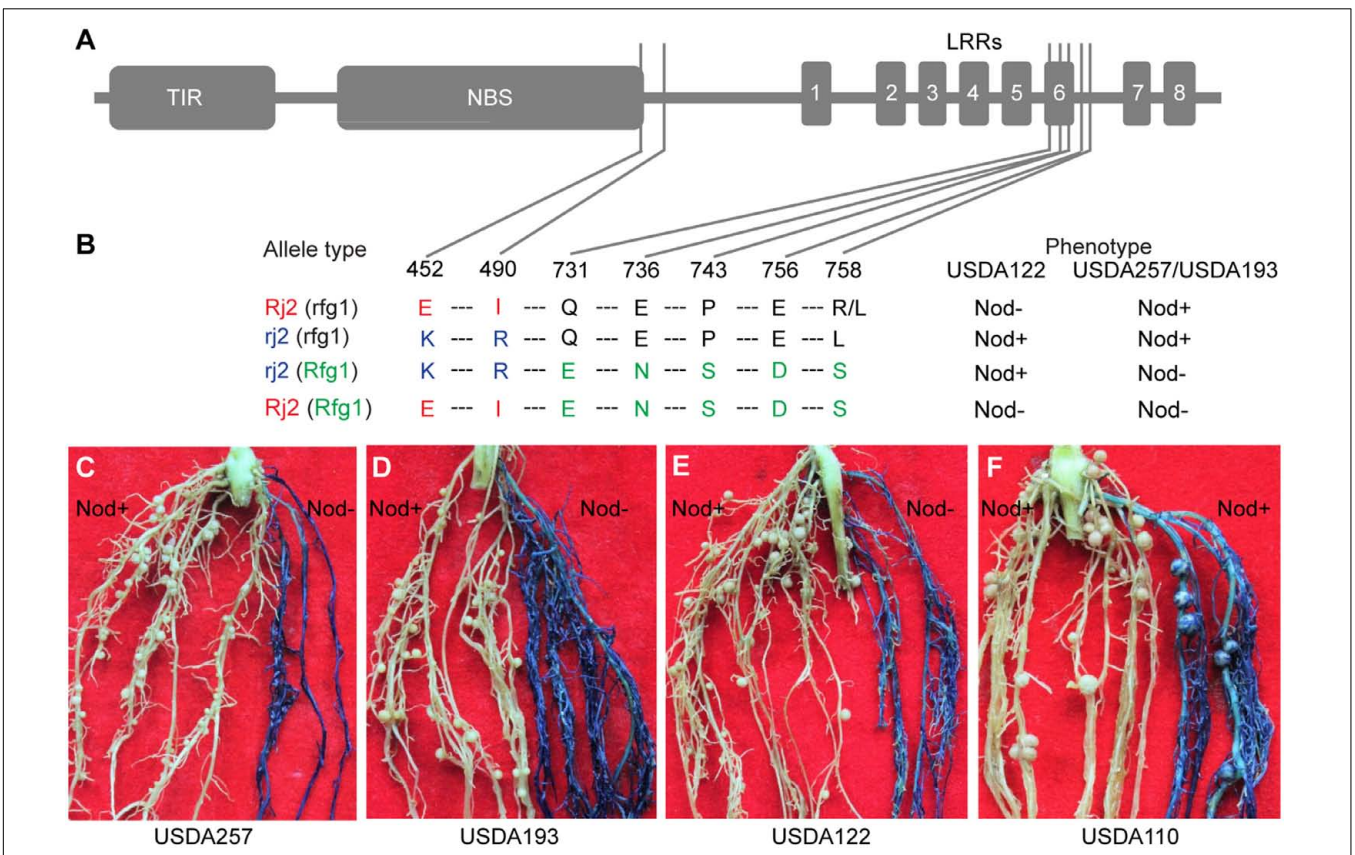

FIGURE 4 | Functional analysis of a chimeric gene of *Rfg1* and *Rj2*. **(A,B)** Domain structure of the TIR-NBS-LRR protein **(A)** showing the seven substitution sites and amino acid polymorphisms that distinguish between the Rj2 (rfg1), rj2 (rfg1), and rj2 (Rfg1) protein isoforms **(B)**. Rj2 (Rfg1) represents a protein isoform resulting from expressing the chimeric gene. **(C–F)** Transgenic roots expressing the chimeric gene (blue) in the Peking background restricted nodulation by USDA257 **(C)**, USDA193 **(D)**, and USDA122 **(E)** but allowed nodulation with *B. japonicum* USDA110 **(F)**. In all cases, the nodulation was normal on the non-transgenic roots (white).

DISCUSSION

Previous studies showed that the soybean *Rfg1* gene restricts nodulation with the fast-growing *S. fredii* strains USDA257 and USDA205 (Devine and Kuykendall, 1996; Yang et al., 2010). The *Rfg1*-mediated resistance to USDA257 was dependent on the bacterial type III secretion system and presumably resulted from the effector-triggered plant immunity, even though the cognate effector(s) has not yet been identified (Krishnan et al., 2003; Yang et al., 2010). In this paper, we demonstrate that the soybean *Rfg1* allele also conditions nodulation restriction with *S. fredii* USDA193, suggesting that *Rfg1* likely provide broad-spectrum resistance against a proportion of *S. fredii* strains (Keyser et al., 1982).

The soybean *Rj2/Rfg1* locus confers nodulation specificity toward many naturally occurring *B. japonicum* and *B. fredii* strains (Caldwell, 1966; Devine and Kuykendall, 1994; Trese, 1995; Yang et al., 2010). A survey of 847 soybean genotypes from Asian countries revealed an *Rj2* allele frequency of 0.02, mainly originated from southeast China (Devine and Breithaupt, 1981). In contrast, the *Rfg1* allele occurred with a much higher frequency of 0.44 in a similar population consisting of 285 plant introductions from Asian countries (Devine, 1985). The distribution of the *Rfg1* (0.44) and *rfg1* (0.56) allele frequencies suggests that these alleles has not been subjected to strong natural selection. However, a screen of 197 soybean lines from the Midwestern United States revealed an *Rfg1* allele frequency of 0.83, suggesting that the compatibility with *S. fredii* strains may be eroded during the breeding process, likely due to the narrow genetic basis of germplasms used in the soybean breeding programs (Balatti and Pueppke, 1992). The diversification of the *Rfg1* and *rfg1* alleles appears to predate that of the *Rj2* and *rj2* alleles. The *Rj2* (*rfg1*) allele likely have derived from the *rj2 (rfg1)* allele through gain-of-function mutations. The *rj2 (rfg1)* allelic form is most promiscuous, conferring an unrestricted nodulation phenotype with many strains that are restricted by the *Rj2* or *Rfg1* alleles. Therefore, the *rj2 (rfg1)* genotype should be prioritized in soybean breeding programs if the goal is to ensure the cultivar to be able to nodulate with indigenous bacterial strains.

The polymorphic *Rj2*/*Rfg1* locus encodes a TIR-NB-LRR gene with three allelic variants that show differing specificities to yet unknown bacterial effectors. E452 and I490 in or near the C-terminal NBS domain of Rj2 are required for the recognition of the cognate effector from *B. japonicum* USDA122, while E731, N736, S743, D756, and S758 in the LRR domain of Rfg1 are essential for the recognition of the corresponding effectors secreted by USDA257 and USDA193. This situation is similar to the previous studies showing that both TIR, NBS, and LRR domains could be involved in the determination of resistance specificity (Ellis et al., 1999; Dodds et al., 2001; Mondragón-Palomino et al., 2002; Ellis et al., 2007). The chimeric *Rj2(Rfg1)* allele composed of E452, I490, E731, N736, S743, D756, and S758 could recognize corresponding effectors of all these strains. Such an allele could exist in natural population if intragenic recombination events occur between the *Rj2(rfg1)* and *rj2(Rfg1)* alleles. It is possible that these polymorphic sites play a role in direct effector binding or intra- or intermolecular interactions in protein complexes during recognition and signaling. Further analysis of the mechanisms underlying the recognitions mediated by the *Rj2/Rfg1* locus awaits the identification of the cognate bacterial effectors.

AUTHOR CONTRIBUTIONS

YF, JL, SL, and HZ: conception and design of the work. YF, JL, QW, SY, and SL: performed the work and analyzed data. HZ wrote the paper.

FUNDING

This work was supported by the Kentucky Soybean Promotion Board to HZ and by the National Natural Science Foundation of China (grant number 31271751) to SL and YF. YF and SL received support from the Shandong Provincial Education Association of China to study at University of Kentucky.

ACKNOWLEDGMENTS

We thank Patrick Elia (US Department of Agriculture-Agricultural Research Service, Beltsville, MD, United States) for providing the rhizobial strains and Dr. Qijun Chen (China Agricultural University, Beijing, China) for providing the CRISPR/Cas9 binary vectors.

REFERENCES

Balatti, P. A., and Pueppke, S. G. (1992). Identification of North American soybean lines that form nitrogen-fixing nodules with *Rhizobium fredii* USDA257. *Can. J. Plant Sci.* 72, 49–55. doi: 10.4141/cjps92-006

Bras, C. P., Jordá, M. A., Wijfjes, A. H., Harteveld, M., Stuurman, N., Thomas-Oates, J. E., et al. (2000). A *Lotus japonicus* nodulation system based on heterologous expression of the fucosyl transferase NodZ and the acetyl transferase NoIL in *Rhizobium leguminosarum*. *Mol. Plant Microbe Interact.* 13, 475–479. doi: 10.1094/MPMI.2000.13.4.475

Broughton, W. J., Jabbouri, S., and Perret, X. (2000). Keys to symbiotic harmony. *J. Bacteriol.* 182, 5641–5652. doi: 10.1128/JB.182.20.5641-5652.2000

Caldwell, B. E. (1966). Inheritance of a strain specific ineffective nodulation in soybeans. *Crop Sci.* 6, 427–428. doi: 10.2135/cropsci1966.0011183X000600050010x

Deakin, W. J., and Broughton, W. J. (2009). Symbiotic use of pathogenic strategies: rhizobial protein secretion systems. *Nat. Rev. Microbiol.* 7, 312–320. doi: 10.1038/nrmicro2091

Devine, T. E. (1985). Nodulation of soybean plant introduction lines with the fast-growing rhizobial strain USDA 205. *Crop Sci.* 25, 354–356. doi: 10.2135/cropsci1985.0011183X002500020037x

Devine, T. E., and Breithaupt, B. H. (1981). *Frequencies of Nodulation Response Alleles, Rj2 and Rj4, in Soybean Plant Introductions and Breeding Lines*. Washington, DC: USDA.

Devine, T. E., and Kuykendall, L. D. (1994). Genetic allelism and linkage tests of a soybean gene, *Rfg1*, a soybean gene controlling nodulation with fast-growing *Rhizobium fredii* strain 205. *Plant Soil* 158, 47–51. doi: 10.1007/BF00007916

Devine, T. E., and Kuykendall, L. D. (1996). Host genetic control of symbiosis in soybean (*Glycine max* L.). *Plant Soil* 186, 173–187. doi: 10.1007/BF00035072

D'Haeze, W., and Holsters, M. (2004). Surface polysaccharides enable bacteria to evade plant immunity. *Trends Microbiol.* 12, 555–561. doi: 10.1016/j.tim.2004.10.009

Dodds, P. N., Lawrence, G. J., and Ellis, J. G. (2001). Six amino acid changes confined to the leucine-rich repeat beta-strand/beta-turn motif determine the difference between the P and P2 rust resistance specificities in flax. *Plant Cell* 13, 163–178. doi: 10.1105/tpc.13.1.163

Doudna, J. A., and Charpentier, E. (2014). Genome editing. The new frontier of genome engineering with CRISPR-Cas9. *Science* 346:1258096. doi: 10.1126/science.1258096

Downie, J. A. (2010). The roles of extracellular proteins, polysaccharides and signals in the interactions of rhizobia with legume roots. *FEMS Microbiol. Rev.* 34, 150–170. doi: 10.1111/j.1574-6976.2009.00205.x

Ellis, J. G., Dodds, P. N., and Lawrence, G. J. (2007). Flax rust resistance gene specificity is based on direct resistance-avirulence protein interactions. *Annu. Rev. Phytopathol.* 45, 289–306. doi: 10.1146/annurev.phyto.45.062806.094331

Ellis, J. G., Lawrence, G. J., Luck, J. E., and Dodds, P. N. (1999). Identification of regions in alleles of the flax rust resistance gene L that determine differences in gene-for-gene specificity. *Plant Cell* 11, 495–506. doi: 10.1105/tpc.11.3.495

Faruque, O. M., Miwa, H., Yasuda, M., Fujii, Y., Kaneko, T., Sato, S., et al. (2015). Identification of *Bradyrhizobium elkanii* genes involved in incompatibility with soybean plants carrying the *Rj4* allele. *Appl. Environ. Microbiol.* 81, 6710–6717. doi: 10.1128/AEM.01942-15

Fauvart, M., and Michiels, J. (2008). Rhizobial secreted proteins as determinants of host specificity in the rhizobium-legume symbiosis. *FEMS Microbiol. Lett.* 285, 1–9. doi: 10.1111/j.1574-6968.2008.01254.x

Geurts, R., Heidstra, R., Hadri, A. E., Downie, J. A., Franssen, H., Van Kammen, A., et al. (1997). *Sym2* of pea is involved in a nodulation factor-perception mechanism that controls the infection process in the epidermis. *Plant Physiol.* 115, 351–359. doi: 10.1104/pp.115.2.351

Jones, K. M., Kobayashi, H., Davies, B. W., Taga, M. E., and Walker, G. C. (2007). How rhizobial symbionts invade plants: the *Sinorhizobium-Medicago* model. *Nat. Rev. Microbiol.* 5, 619–633. doi: 10.1038/nrmicro1705

Kawaharada, Y., Kelly, S., Nielsen, M. W., Hjuler, C. T., Gysel, K., Muszyñski, A., et al. (2015). Receptor-mediated exopolysaccharide perception controls bacterial infection. *Nature* 523, 308–312. doi: 10.1038/nature14611

Kereszt, A., Li, D., Indrasumunar, A., Nguyen, C. D., Nontachaiyapoom, S., Kinkema, M., et al. (2007). *Agrobacterium rhizogenes*-mediated transformation of soybean to study root biology. *Nat. Protoc.* 2, 948–952. doi: 10.1038/nprot.2007.141

Keyser, H. H., Bohlool, B. B., Hu, T. S., and Weber, D. F. (1982). Fast-growing rhizobia isolated from root nodules of soybean. *Science* 215, 1631–1632. doi: 10.1126/science.215.4540.1631

Keyser, H. H., and Li, F. (1992). Potential for increasing biological nitrogen fixation in soybeans. *Plant Soil* 141, 119–135. doi: 10.1007/BF00011313

Kiers, E. T., Hutton, M. G., and Denison, R. F. (2007). Human selection and the relaxation of legume defences against ineffective rhizobia. *Proc. Biol. Sci.* 274, 3119–3126. doi: 10.1098/rspb.2007.1187

Kim, D. H., Kaashyap, M., Rathore, A., Das, R. R., Parupalli, S., Upadhyaya, H. D., et al. (2014). Phylogenetic diversity of *Mesorhizobium* in chickpea. *J. Biosci.* 39, 513–517. doi: 10.1007/s12038-014-9429-9

Krishnan, H. B., Lorio, J., Kim, W. S., Jiang, G., Kim, K. Y., DeBoer, M., et al. (2003). Extracellular proteins involved in soybean cultivar-specific nodulation are associated with pilus-like surface appendages and exported by a type III protein secretion system in *Sinorhizobium fredii* USDA257. *Mol. Plant Microbe Interact.* 16, 617–625. doi: 10.1094/MPMI.2003.16.7.617

Lerouge, P., Roche, P., Faucher, C., Maillet, F., Truchet, G., Promé, J. C., et al. (1990). Symbiotic host-specificity of *Rhizobium meliloti* is determined by a sulphated and acylated glucosamine oligosaccharide signal. *Nature* 344, 781–784. doi: 10.1038/344781a0

Limpens, E., Franken, C., Smit, P., Willemse, J., Bisseling, T., and Geurts, R. (2003). LysM domain receptor kinases regulating rhizobial Nod factor-induced infection. *Science* 302, 630–633. doi: 10.1126/science.1090074

Liu, J., Yang, S., Zheng, Q., and Zhu, H. (2014). Identification of a dominant gene in *Medicago truncatula* that restricts nodulation by *Sinorhizobium meliloti* strain Rm41. *BMC Plant Biol.* 14:167. doi: 10.1186/1471-2229-14-167

Marek, L. F., and Shoemaker, R. C. (1996). Construction and size characterization of a bacterial artificial chromosomal (BAC) library from soybean. *Soybean Genet. Newslett.* 23, 126–129.

Mondragón-Palomino, M., Meyers, B. C., Michelmore, R. W., and Gaut, B. S. (2002). Patterns of positive selection in the complete NBS-LRR gene family of *Arabidopsis thaliana*. *Genome Res.* 12, 1305–1315. doi: 10.1101/gr.159402

Mutch, L. A., and Young, J. P. (2004). Diversity and specificity of *Rhizobium leguminosarum* biovar viciae on wild and cultivated legumes. *Mol. Ecol.* 13, 2435–2444. doi: 10.1111/j.1365-294X.2004.02259.x

Nakano, Y., Yamakawa, T., Ikeda, M., and Ishizuka, J. (1997). Nodulation of *Rj*-soybean varieties with *Rhizobium fredii* USDA 193 under limited supply of nutrients. *Soil Sci. Plant Nutri.* 43, 929–932. doi: 10.1080/00380768.1997.10414659

Okazaki, S., Zehner, S., Hempel, J., Lang, K., and Göttfert, M. (2009). Genetic organization and functional analysis of the type III secretion system of *Bradyrhizobium elkanii*. *FEMS Microbiol. Lett.* 295, 88–95. doi: 10.1111/j.1574-6968.2009.01593.x

Oldroyd, G. E., Murray, J. D., Poole, P. S., and Downie, J. A. (2011). The rules of engagement in the legume-rhizobial symbiosis. *Annu. Rev. Genet.* 45, 119–144. doi: 10.1146/annurev-genet-110410-132549

Perret, X., Staehelin, C., and Broughton, W. J. (2000). Molecular basis of symbiotic promiscuity. *Microbiol. Mol. Biol. Rev.* 64, 180–201. doi: 10.1128/MMBR.64.1.180-201.2000

Radutoiu, S., Madsen, L. H., Madsen, E. B., Felle, H. H., Umehara, Y., Gronlund, M., et al. (2003). Plant recognition of symbiotic bacteria requires two LysM receptor-like kinases. *Nature* 425, 585–592. doi: 10.1038/nature02039

Radutoiu, S., Madsen, L. H., Madsen, E. B., Jurkiewicz, A., Fukai, E., Quistgaard, E. M., et al. (2007). LysM domains mediate lipochitin-oligosaccharide recognition and *Nfr* genes extend the symbiotic host range. *EMBO J.* 26, 3923–3935. doi: 10.1038/sj.emboj.7601826

Sadowsky, M. J., Cregan, P. B., Rodriguez-Quinones, F., and Keyser, H. H. (1990). Microbial influence on gene-for-gene interactions in legume-*Rhizobium* symbioses. *Plant Soil* 129, 53–60. doi: 10.1007/BF00011691

Soto, M. J., Dominguez-Ferreras, A., Perez-Mendoza, D., Sanjuan, J., and Olivares, J. (2009). Mutualism versus pathogenesis: the give-and-take in plant-bacteria interactions. *Cell Microbiol.* 11, 381–388. doi: 10.1111/j.1462-5822.2008.01282.x

Tang, F., Yang, S., Liu, J., and Zhu, H. (2016). *Rj4*, a gene controlling nodulation specificity in soybeans, encodes a thaumatin-like protein but not the one previously reported. *Plant Physiol.* 170, 26–32. doi: 10.1104/pp.15.01661

Trese, A. T. (1995). A single dominant gene in McCall soybean prevents effective nodulation with *Rhizobium fredii* USDA257. *Euphytica* 81, 279–282. doi: 10.1007/BF00025618

Tsukui, T., Eda, S., Kaneko, T., Sato, S., Okazaki, S., Kakizaki-Chiba, K., et al. (2013). The type III secretion system of *Bradyrhizobium japonicum* USDA122 mediates symbiotic incompatibility with *Rj2* soybean plants. *Appl. Environ. Microbiol.* 79, 1048–1051. doi: 10.1128/AEM.03297-12

Tsurumaru, H., Hashimoto, S., Okizaki, K., Kanesaki, Y., Yoshikawa, H., and Yamakawa, T. (2015). A putative type III secretion system effector encoded by the MA20_12780 gene in *Bradyrhizobium japonicum* Is-34 causes incompatibility with *Rj4* genotype soybeans. *Appl. Environ. Microbiol.* 81, 5812–5819. doi: 10.1128/AEM.00823-15

Wang, D., Yang, S., Tang, F., and Zhu, H. (2012). Symbiosis specificity in the legume-rhizobial mutualism. *Cell Microbiol.* 14, 334–342. doi: 10.1111/j.1462-5822.2011.01736.x

Wang, Q., Yang, S., Liu, J., Terecskei, K., Ábrahám, E., Gombár, A., et al. (2017). Host-secreted antimicrobial peptide enforces symbiotic selectivity in *Medicago truncatula*. *Proc. Natl. Acad. Sci. U.S.A.* 114, 6854–6859. doi: 10.1073/pnas.1700715114

Xing, H. L., Dong, L., Wang, Z. P., Zhang, H. Y., Han, C. Y., Liu, B., et al. (2014). A CRISPR/Cas9 toolkit for multiplex genome editing in plants. *BMC Plant Biol.* 14:327. doi: 10.1186/s12870-014-0327-y

Yang, S., Tang, F., Gao, M., Krishnan, H. B., and Zhu, H. (2010). *R* gene-controlled host specificity in the legume-rhizobia symbiosis. *Proc. Natl. Acad. Sci. U.S.A.* 107, 18735–18740. doi: 10.1073/pnas.1011957107

Yang, S., Wang, Q., Fedorova, E., Liu, J., Qin, Q., Zheng, Q., et al. (2017). Microsymbiont discrimination mediated by a host-secreted peptide in *Medicago truncatula*. *Proc. Natl. Acad. Sci. U.S.A.* 114, 6848–6853. doi: 10.1073/pnas.1700460114

Yasuda, M., Miwa, H., Masuda, S., Takebayashi, Y., Sakakibara, H., and Okazaki, S. (2016). Effector-triggered immunity determines host genotype-specific incompatibility in legume-*Rhizobium* symbiosis. *Plant Cell Physiol.* 57, 1791–1800. doi: 10.1093/pcp/pcw104

Conflict of Interest Statement: The authors declare that the research was conducted in the absence of any commercial or financial relationships that could be construed as a potential conflict of interest.

The reviewer DR and handling Editor declared their shared affiliation, and the handling Editor states that the process nevertheless met the standards of a fair and objective review.

Advantages of publishing in Frontiers

OPEN ACCESS
Articles are free to read for greatest visibility and readership

FAST PUBLICATION
Around 90 days from submission to decision

HIGH QUALITY PEER-REVIEW
Rigorous, collaborative, and constructive peer-review

TRANSPARENT PEER-REVIEW
Editors and reviewers acknowledged by name on published articles

Frontiers
Avenue du Tribunal-Fédéral 34
1005 Lausanne | Switzerland

Visit us: www.frontiersin.org
Contact us: info@frontiersin.org | +41 21 510 17 00

REPRODUCIBILITY OF RESEARCH
Support open data and methods to enhance research reproducibility

DIGITAL PUBLISHING
Articles designed for optimal readership across devices

FOLLOW US
@frontiersin

IMPACT METRICS
Advanced article metrics track visibility across digital media

EXTENSIVE PROMOTION
Marketing and promotion of impactful research

LOOP RESEARCH NETWORK
Our network increases your article's readership